REPORT DOCUMENTATION PAGE

Form Approved
OMB No. 0704-0188

PLEASE DO NOT RETURN YOUR FORM TO THE ABOVE ADDRESS.

1. REPORT DATE *(DD-MM-YYYY)*	2. REPORT TYPE	3. DATES COVERED *(From - To)*
2008-05-31	Final	03/01/07-05/31/08

4. TITLE AND SUBTITLE

Workshop to Critically Examine Potential Spintronics Applications of Wide Gap Semiconductor such as ZnO Based Nanostructures and their Status

5a. CONTRACT NUMBER

5b. GRANT NUMBER

FA9550-07-1-0172

5c. PROGRAM ELEMENT NUMBER

6. AUTHOR(S)

Hadis Morkoc, Ph.D.

5d. PROJECT NUMBER

5e. TASK NUMBER

5f. WORK UNIT NUMBER

7. PERFORMING ORGANIZATION NAME(S) AND ADDRESS(ES)

Virginia Commonwealth University
School of Engineering
Box 843068
Richmond, VA 23284-3068

8. PERFORMING ORGANIZATION REPORT NUMBER

Final Technical; Index 542067

9. SPONSORING/MONITORING AGENCY NAME(S) AND ADDRESS(ES)

ONR REG ADMIN ATLANTA-N66020
100 Alabama St SW, Suite 4R15
Atlanta, GA 30303-3104

10. SPONSOR/MONITOR'S ACRONYM(S)

11. SPONSOR/MONITOR'S REPORT NUMBER(S)

AFRL-OSR-VA-TR-2012-0713

12. DISTRIBUTION/AVAILABILITY STATEMENT

Approved for Public Release; distribution is unlimited

13. SUPPLEMENTARY NOTES

14. ABSTRACT

A meeting attended by selected experts October 18-20 2007 at Virginia Crossing, Resort
1000 Virginia Center Pkwy just outside of Richmond VA to openly discuss Challenges facing ZnO and GaN: Facts and Myths. The scene setting presentations were followed by shorter presentations with open flow of information and questions. Among the topics discussed were bulk GaN and ZnO, defects, p-type doping, particularly for ZnO, promising heterostructures and devices based on ZnO, ferromagnetism in GaN and ZnO, doping of high mole fraction AlGaN and InGaN, particularly p-type, light extraction and efficiency in GaN based LEDs, degradation mechanisms in GaN based lasers, degradation mechanisms in GaN based HFETs and potential measures to enhance lifetime and performance, negative differential resistance in GaN based heterostructures, and intersubband transitions. This report provides an incisive treatise of these topics with attention being paid to problem areas, possible solutions and what can be expected.

15. SUBJECT TERMS

GaN, ZnO, p-type doping, HFET and laser reliability, ferromagnetism, defects, LED efficiency droop, ZnO devices

16. SECURITY CLASSIFICATION OF:			17. LIMITATION OF ABSTRACT	18. NUMBER OF PAGES	19a. NAME OF RESPONSIBLE PERSON
a. REPORT	b. ABSTRACT	c. THIS PAGE			Hadis Morkoc
Unclassified	Unclassifed	Unclassified	SAR		19b. TELEPHONE NUMBER *(Include area code)* 804-827-3765

Reset

Standard Form 298 (Rev. 8/98)
Prescribed by ANSI Std. Z39.18

Challenges facing ZnO and GaN: Facts and Myths

Virginia Crossing Resort October 18-19, 2007
Glen Allen, VA 23059

Submitted to

Donald J Silversmith, Ph.D., MBA
Program Manager, Physics and Electronics Directorate
Air Force Office of Scientific Research (AFOSR/NE)
Air Force Research Laboratory
Suite 325/Room 3112
875 North Randolph St.
Arlington (Ballston), VA 22203-1768
(703) 588-1780
FAX: (703) 696-8481
E-mail: donald.silversmith@afosr.af.mil

Submitted by

Hadis Morkoç
Virginia Commonwealth University
School of Engineering
P. O. Box 843068
Richmond, VA 23284-3068
TEL: (804) 827-3765
E mail:hmorkoc@vcu.edu

Table of content

I. Bulk GaN

I.1. Introduction

To use the already overused word "paradigm buster", GaN was for quite sometime considered as a paradigm buster in the sense that surprisingly high performance optical and electrical devices have been possible in this material grown on foreign substrates with lattice and thermal expansion coefficient mismatch and in some cases stacking mismatch with ensuing high concentration of defects. As long as the progress was being made and the performance of the devices improved the motto seemed to hold. However, as the demand for performance continually increased, issues about the lifetime and efficiency of devices surfaced which goes counter to earlier assertions the GaN can handle defects. One now wonders if the paradigm buster is really appropriate even for GaN realizing that defects do matter. It may soon seem that all the roads must go through bulk GaN substrates which naturally is the ultimate approach to obtain the best quality layers.

Because much of the point defects in GaN and related materials are directly or indirectly caused by extended defects and the extended defects are caused mainly by the lattice mismatch, the question arises as to what can be done in the way of obtaining bulk GaN substrates. While there have been efforts to produce bulk GaN by the ammono-thermal method as well as the high pressure method, the substrate size has been limited. The freestanding HVPE templates represent a good intermediate step, but liftoff is challenging for large area wafers without breakage. The make or break issue is whether commercially viable high quality bulk GaN substrates can be prepared. Further, high resistivity GaN bulk substrates, conducting for optical devices and high resistivity for FETs, can be produced. The workshop participants were tasked to address the core of the aforementioned issues. There seems to be a consensus that solution growth, as in the case of all the other bulk semiconductor growth, is the most promising method for producing bulk GaN. In line with this notion, the presentations focused on the solution growth. Below a review of the presentations at the workshop as well as what is pertinent and available in the literature.

At the workshop, an overview of ammonothermal growth, which requires high pressures, was given by M. Alexander. This was followed by growth of GaN, by again the ammonothermal method, by T. Fukuda and F. Orioto. These segued into a "solution GaN seeded growth at near atmospheric pressure" by B. Feigelson followed by a succinct review of the sublimation growth of bulk GaN and AlN by J. Edgar. Finally, the rapid growth HVPE approach for producing pseudo-bulk GaN was discussed by A. Usikov.

I.2. Challenges

Due to the high covalency of GaN [binding energy of the gallium nitrogen bond E ~ 9.12 eV/ atom] the decomposition pressure (P_M) at the melting point (T_F ~ 2500 ^oC)[1] is extremely high (~ 4.5 GPa).[2] For pressures below P_M, gallium nitride does not melt but decomposes. At atmospheric pressure for example, gallium nitride is stable up to 1200 K

and it can be stabilized at higher temperatures by increased pressure.[2] Consequently, the standard techniques of crystal growth generally used for obtaining semiconductor wafers (Bridgman, Czochralski, Verneuil) cannot be employed for GaN. The congruent melting of gallium nitride has only been achieved very recently by Utsumi *et al*.[3] This technique does not lead at this time to large crystals (<100 mm), limited by the extreme experimental conditions (6 GPa, 2200 ^{o}C) which in turn places a roadblock for transitioning this method to production. Due to the gallium nitride decomposition, only few methods have been developed for GaN bulk crystals. Below is a brief overview of experimental techniques that are in development for producing bulk GaN substrates.

I.3. Brief review of growth techniques

I.3.1. High-pressure nitrogen solution growth

Relatively large GaN crystals (platelets with a surface area exceeding now 100 mm^2) have been obtained through the high pressure nitrogen solution growth method, under development for some 15 years in Warsaw (Poland).[4] High nitrogen pressure and high temperature conditions (1–2 GPa and 1400–1500 ^{o}C also for increasing the solid solubility of N in the Ga melt) are required for converting metallic gallium into gallium nitride. At the present time, the high-pressure nitrogen solution growth is the most developed technique for growing "truly" bulk GaN despite its shortcomings primarily in terms of the size of the crystals.

The resulting crystals have been characterized for their structural, mainly by X-ray diffraction (XRD) and TEM, and electrical and optical properties. Furthomore, these high pressure produced crystals have also been used for epitaxy and device fabrication, providing other measures of their quality. The FWHM of (0004) XRD rocking curves is about 20–30 arcsec for crystals up to 3 mm and up to 40–50 arcsec for the 12 mm ones. The crystalline quality has been evaluated more precisely with the determination of the lattice parameters for the entire crystal volume.[5] For crystals exceeding 2 mm, the parameters *a* and *c* were slightly larger (0.01%) for the $(0001)_{Ga}$ face than those for the $(000\text{-}1)_{N}$ face. This difference corresponds to a curvature of the plates, whose radius was determined to be 1.5 m. The divergence in this parameter probably originates from the greater growth rate on the N face in Ga rich conditions, inducing an increase of point defects (Ga antisites, N vacancies, Ga interstitials). The most probable point defects in these crystals are gallium vacancies due to their low formation energy even in gallium rich crystallization conditions.[6] The dislocation density does not exceed 2 x 10^2 cm^{-2} in crystals.[7,8,9]

Unintentionally doped crystals, however, exhibit high n-type conductivity with a free electron concentration of 5 x 10^{19} cm^{-3}, and a mobility of about 60 cm^2 V^{-1} s^{-1}.[10] These electrons are thought to probably originate from the oxygen atoms substituting for nitrogen. A high oxygen concentration (about 10^{18}–10^{19} cm^{-3}) was indeed evident in secondary ion mass spectrometry (SIMS) characterizations. Moreover, unlike nitrogen the dissociation of the oxygen molecule on the surface of the gallium solution is a process

without energy barrier that favors its incorporation into gallium nitride during the crystal growth.[11]

Disadvantages of high-pressure nitrogen solution growth:

-First of all, the growth environment requires the control of the severe oxygen contamination because the synthesis of gallium oxide is a predominant problem.
-Too demanding experimental conditions (pressure and temperature) limit the transitioning of the process to large scale (pressure of 1–2 GPa associated with the temperature of 1500 °C can be reached only with a very limited and expensive apparatus). Any increase of size, in order to obtain larger crystals, requires substantial efforts for the control of the experimental conditions, the reliability of the devices, and consequently their price.

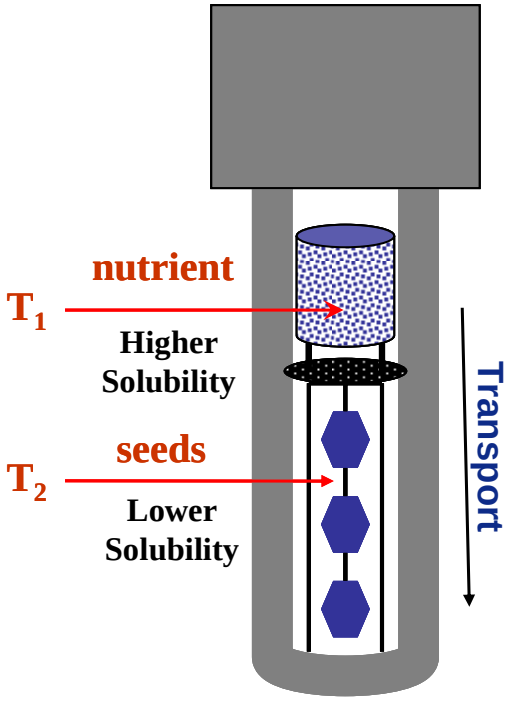

Figure 1. Schematic of autoclave for ammonothermal growth of GaN (courtesy of M.N. Alexander of Air Force Research Laboratory, Sensors Directorate).

I.3.2. Ammonothermal growth

Ammonothermal growth belongs to the group of solvothermal growth techniques, which encompass a separate class of technologies which are capable of producing nano to macro-size single-crystalline solid state matter under elevated pressure and temperature regimes. The basic principle is the use of a liquid polar solvent (water in hydrothermal *e.g.* for ZnO and ammonia, NH_3, in ammonothermal, *e.g.*, for GaN, growth), which forms metastable products with the solute (nutrient). Mineralizers are frequently used which are even essential to increase the solubility of the nutrient(s). Schematic of autoclave for ammonothermal growth of GaN is shown in Figure 1. **Merits of the solvothermal growth technology comprise:** (a) operation near the thermodynamic equilibrium (very low temperature gradient) with the ability to generate high crystallinity; (b) large amount of crystalline material can be obtained over a long process time, thus enabling a high throughput; (c) no need for expensive equipment to acquire and maintain vacuum technology; (d) environmentally

benign conditions for production and capability for recycling of the solution; (e) over 60 years in use for diverse mass-produced crystals such as the low-temperature modification of quartz (SiO_2). ZnO is the first semiconductor crystal, which can be grown on industrial scale by the solvothermal method for the purpose of wafer production. Details of the ammonothermal growth of GaN are discussed in a recent review paper by Fukuda and Ehrentraut.[12]

Some specifics for solvothermal growth of SiO_2, ZnO, and GaN

SiO_2 (hydrothermal):
Temperature of 400°C;
Pressure < 1000atm;
Water solvent;
KOH and NaOH mineralizer;
Lasca precursor.

Characteristics of the process: easy to handle solvent; moderate pressure; under mass production.

ZnO (hydrothermal):
Temperature of 400°C;
Pressure < 1000atm;
Water solvent;
KOH and LiOH mineralizer;
Lasca precursor.

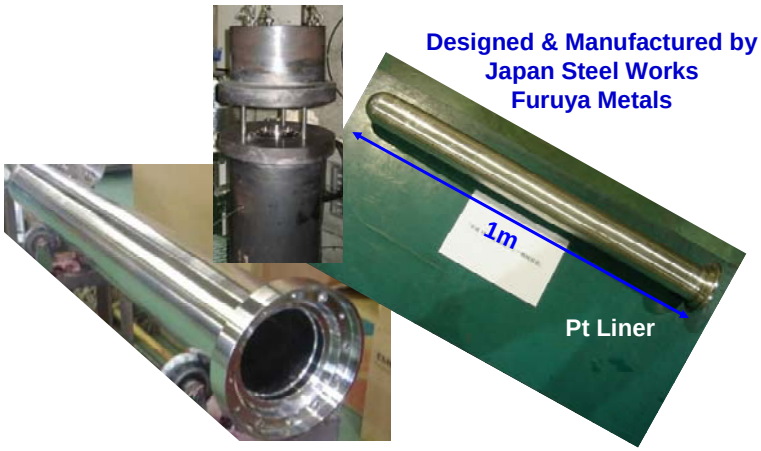

Figure 2. Autoclave for GaN ammonothermal growth (courtesy of T. Fukuda of Tohoku University).

GaN (ammonothermal):
Temperature of 400-550°C;
Pressure < 1500atm;
Liquid NH_3 solvent;
NH_4Cl and NH_4I mineralizer;
Ga and GaN powder precursor;
Characteristics of the process: difficult to handle solvent; insufficient information about GaN solubility; difficult to control high pressure (< 1500atm).

Key point 1 for successful ammonothermal growth of GaN is corrosive resistant autoclave (Pt liner, see Figure 2).

Key point 2 is the knowledge of solubility curve of GaN in ammonia

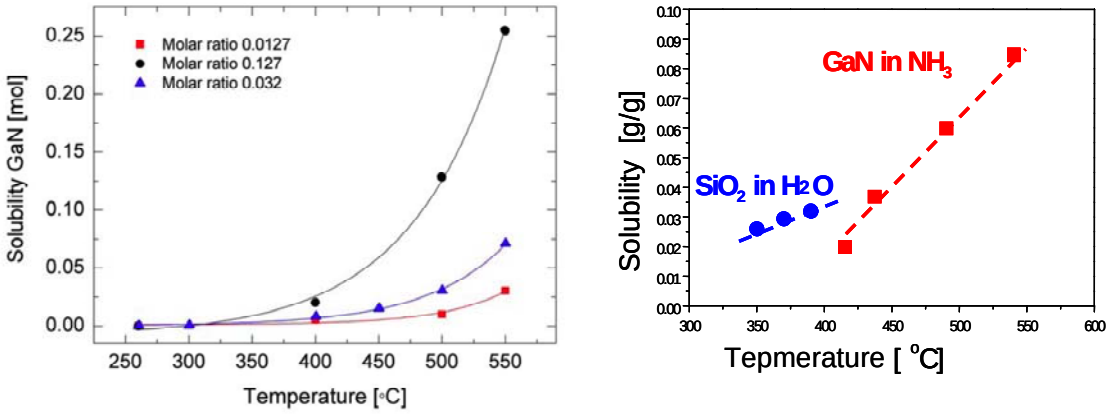

Figure 3. Solubility of GaN for three different molar ratios of GaN and NH_4Cl measured using Pt cell (courtesy of T. Fukuda of Tohoku University).

Very recently, Ehrentraut *et al.*[13] have reported solubility of GaN in NH_4Cl-containing supercritical ammonia. As seen in Figure 3, the gradient of the solubility curve is "positive" for acidic mineralizers (basic mineralizers show "negative" gradient[14]), and the gradient value is close to that for quartz. Therefore, controllable growth particularly for large size crystals over a long period of growth time is possible. Moreover, improved supersaturation has yielded ammonothermal GaN of high optical quality comparable to HVPE-grown GaN.[13]

The ammonothermal crystal growth (solvothermal process using NH_3 as solvent) has not allowed the preparation of large GaN crystals as of now yet and published data about the material quality are very limited. However, the technique has some merits for the preparation of "truly" bulk crystals with appropriate size and crystalline quality. Figure 4 shows the price per cm^2 for various single crystals as a function of growth rate. As obviously seen in the figure, the ammonothermal growth of GaN can potentially provide competitive price particularly in the case of mass production.

Robert Dwiliñski of the company Ammono Ltd. (ul. Czerwonego Krzyza 2/31 00-377, Warsaw, Poland; E-mail: "dwilinski at ammono.com.pl) has presented a picture of a one inch diameter GaN wafer produced by the ammonothermal technique at the International Workshop on Bulk Nitride Semiconductors held in Brazil, in September 2007.[15]

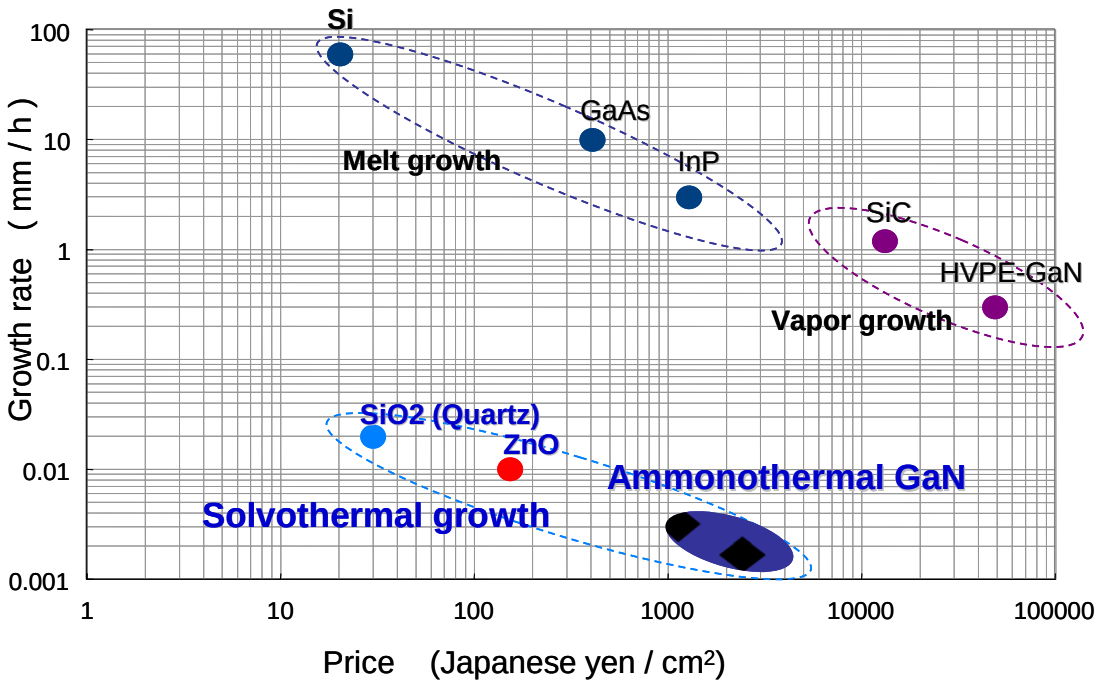

Figure 4. Crystal growth rate in comparison to the normalized estimated price for a wafer. The scalability of the solvothermal method results in a drastic price drop for ammonothermal GaN in comparison to HVPE GaN (after Fukuda and Ehrentraut[12]).

Potential advantages of ammonothermal growth:

-Truly bulk, truly freestanding crystals for substrates

- Can be performed at very low temperatures and accessible pressures (the same range as the one involved in the α-quartz crystal growth, a process developed in industrial productin scale already[16]). Low temperature, together with low-temperature-gradient growth, should yield low point defect density.

-Low dislocation density is possible (< 10 cm^{-2} in best quartz)

-Chemical equilibrium growth (sometimes disadvantageous)

-Spatially uniform intentional doping is possible

-Spatially uniform alloying is possible (e.g., AlGaN grown at AFRL-Hanscom)

-Faceted growth is possible – e.g., to facilitate attainment of non-polar substrates

-Process should be scalable to economical high-volume production (analogous to ~10,000 kg of quartz produced annually)

Challenges facing ammonothermal growth

-More thorough characterization of the material grown by ammonothermal method is needed (electrical/optical, structural, residual impurities *etc.*)

-What is known about ammonothermal autoclave technology is not sufficient. One of the main questions that can be raised is whether corrosion would limit the autoclave lifetime and size! Current experiments are pushing the autoclave

technology to its limits as higher growth temperatures and pressures would be more than just desirable.

-Fundamental and incisive NH_3–based phase diagram efforts would help (little has been published since the 1930s).

-It is about time for serious epi-on-ammono and device-on-ammono research. Free exchange of ideas would stimulate all areas.

I.3.1. Flux method

The Na flux method has been introduced in Sendai (Japan) in mid 1990s by Shimada and co-workers.[17] However, this technique leads to smaller GaN crystals as compared to high-pressure nitrogen solution growth. The method is characterized by lower pressure and temperature conditions (5–10 MPa, 700–800^{o}C) in which sodium acting as a catalyst for the dissociation of nitrogen molecules is employed. The range of salts used has later been expanded to include Na, Li, Li_3N or Ca_3N_2 for this flux based growth method reliant on solutions with Ga.[18,19,20] Flux methods use elemental Ga, gaseous nitrogen and either elemental alkali metal or alkali metal nitrides to increase the reactivity and solubility of nitrogen in Ga (recall that the natural solubility of N in Ga is rather limited which otherwise necessitates the use of high temperatures and pressures employed in the high pressure method). In the flux methods, the gaseous nitrogen reacts with the flux/elemental gallium combination to saturate the solution and cause for the crystal to form. A variant of this method with is dubbed "seeded GaN growth from Na flux" appears to show some potential.[21,22] However, the low solubility of nitrogen in the solution limits the growth rate.

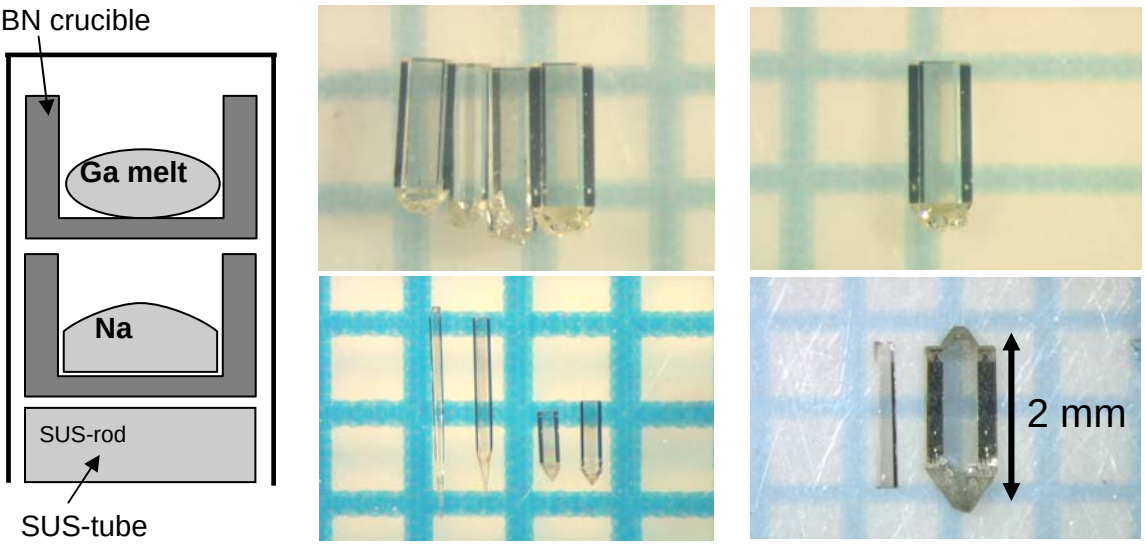

Figure 5. Schematic of the Na flux method and GaN single crystals prepared by using this technique (courtesy of F. Orito of MC Research & Innovation Center, Mitsubishi Chemical Corporation).

An important point is that the high quality GaN single crystals grown by the Na flux method with Na vapor (see Figure 5) can be used as seeds for ammonothermal method.[23]

The flux method is realized at rather moderate temperatures and pressures. Therefore, it should not be absolutely impossible to use this method in large scale. However, sodium, used in the flux method, is very reactive and must be handled under controlled conditions. Moreover, Na has to be of very high purity or else the size and the crystalline quality advantages of the resulting crystals are largely diminished.

I.3.4. Solution GaN seeded growth at near atmospheric pressure

Growth of GaN and BN crystals from molten solution with Ga-free solvent was reported very recently.[24,25] The solvent in this case is prepared by adding solid Li_3N to a mixture of alkali and alkaline earth fluorides (the schematic of the technique is shown in Figure 6). This technique is being developed so far only at the Naval Research Laboratories (NRL) at the present time and very little is known about the material characteristics and technique limitations.

The following advantages of the solution technique can be noted:

-Low defect bulk material requires near equilibrium crystal growth conditions.

-Growth on a seed approach is amenable for commercial production of large, high quality substrates.

-Growth at moderate temperatures and pressures made possible by this method is desirable for scalability, low substrate cost for industrial production.

At the present time, the small size crystals of very high crystal quality are available. Full width at half maximum of (0004) rocking curve is 16 arcsec. Two orders

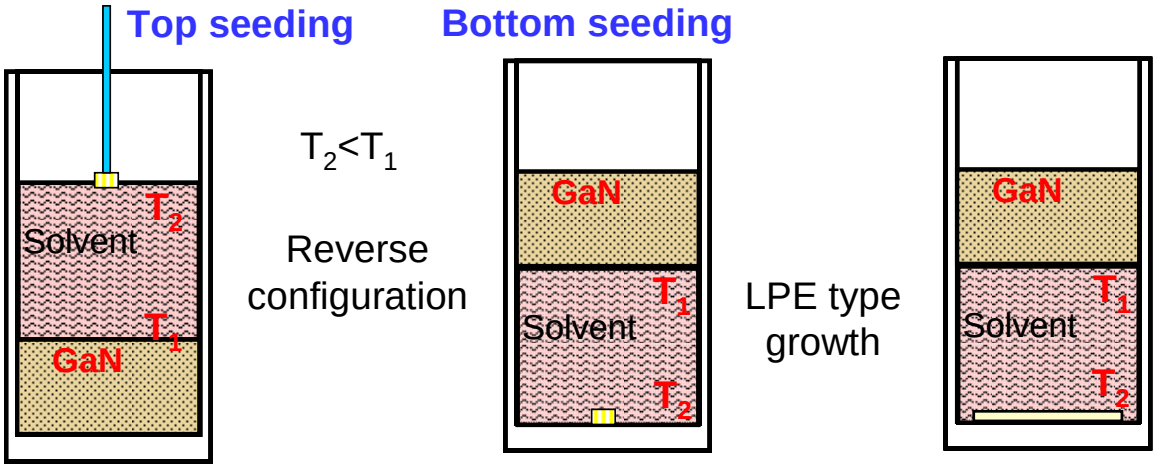

Figure 6. Schematic of GaN solution growth (courtesy of B.N. Feigelson of Naval Research Laboratory).

of magnitude reduction of the (0002) XRD diffraction peak was observed for the homoepitaxial layers grown on bulk GaN, *e.g* FWHM= 34.561 arcsec on the Ga-face, and FWHM= 34.612 arcsec on the N-face. As for the status of this solution growth method:

1. Seeded solution temperature gradient growth of bulk GaN at moderate temperatures (~800°C) and pressure (<3 bar) has been demonstrated.
2. Top and bottom seeding growth configurations are in the process of being explored.
3. The characteristics of the solution growth process and results allow the projection that this is a production compatible bulk GaN seeded solution growth process and that is suitable and scalable for bulk GaN with 2" or larger diameter substrates at low cost with high quality
4. Growth reactor improvements, however, are needed and planned, such as crucible rotation mechanism for stirring the solution and a new heating system to control temperature gradients well.

I.3.5. Sublimation growth of AlN

Advantages of AlN bulk crystals grown by sublimation

Sublimation growth, one kind of physical vapor transport growth of crystals, has several advantages over the melt growth in that it provides lower growth temperatures, morphological stability, and relatively easy implementation (the schematic of AlN sublimation growth is shown in Figure 7). This method cannot be applied to GaN due to too high

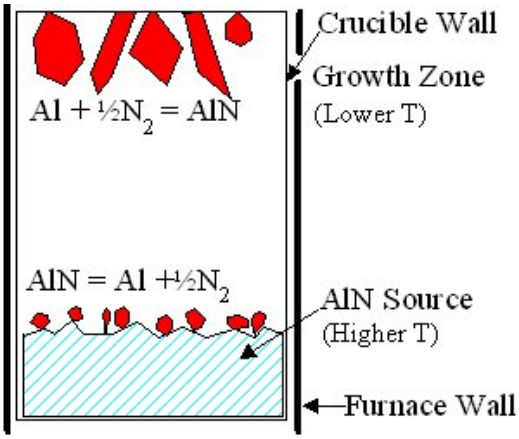

Figure 7. Schematic of growth system (courtesy of J.C. Edgar of Kansas State University).

vapor pressure of N over Ga, but application to AlN is possible and has been exploited many decades ago[26] owing to merits of AlN on its own before the recent advent of GaN. We should mention, however, that due to the high reactivity of aluminum vapor at high sublimation

temperatures of aluminum nitride, some serious problems still remain to be addressed such as the need for high-purity AlN source and inert crucible for AlN growth (Further details about sublimation growth can be found elsewhere[27]).

Sublimation process advantages:

-Viable low-pressure growth process.
-Truly high growth rates (>500 μm/h).
-Nonpolar substrates are feasible.

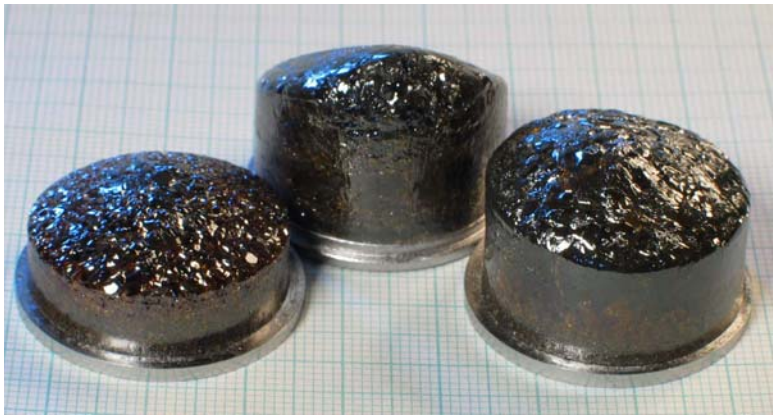

Figure 8. Boules, 25 mm in diameter, and 20 mm long, c-axis aligned in the growth direction (courtesy of J.C. Edgar of Kansas State University).

AlN material advantages:

-High thermal conductivity (~3.2 W/cm·K).
-High electrical resistivity (~$8x10^{10}$ Ω·cm).
-UV transparent (to λ ~200 nm).

Status of bulk AlN

-High crystal quality of the material featured by FWHM of XRD rocking curves of <10 arcsec and low dislocation density of < 1000 cm^{-2}.[28]
-Crystal IS, Inc., (Green Island, NY) has recently reported 2" diameter c-plane substrates with ~1000 dislocations/cm^2.[29]
-Several devices on AlN reported include a 300 nm UV-LED with 4-5 times higher CW output power than similar devices on sapphire, and 370 nm UV LD.
-The Fox Group (Deer Park, NY) sells 15 mm diameter c-plane AlN, and has prepared 2" diameter wafers.
-Fairfield Crystals, Inc. (Fairfield, CT) has produced 6 mm diameter single crystals that are several millimeters thick.

Despite the recent progress, **the following major challenges for bulk AlN** need to be overcome:

-High stress and cracking of the AlN crystals.
-Seeded growth and/or crystal expansion.
-Compatibility/durability of the crucible and furnace fixture materials.
-High residual impurity concentrations.
-Sub-bandgap UV absorption.

We should hasten to state that the high thermal conductivity does not automatically justify giving up the lattice matching available with GaN substrate whose thermal conductivity of 2.3 W/(cm K) is in fact formidable. Staying true to cardinal rule of lattice matching, AlN substrate could prove to be just what might be needed for large mole fraction AlGaN growth for a variety of deep UV applications. Crystal IS has reported very recently etch pit densities of 1.8 x 10^5 cm^{-2} for $Al_{0.5}Ga_{0.}5$ and <1 x 10^6 cm^{-2} for 2-μm-thick epilayers GaN on AlN substrates.[29] Returning to GaN, the lattice mismatch induced defects associated with GaN on AlN is too high a price to pay for what could be construed as an incremental increase in thermal conductivity. The high crystalline quality materials, such GaN on GaN, can withstand higher temperatures without degrading thus paving the way for a more efficient heat flux removal. However, in applications such as back illuminated deep UV detectors, transparency of the substrate is an important virtue and AlN could find a niche application there. To reiterate use of AlN for GaN based emitters and power amplifiers is highly unattractive as compared to lattice matched GaN substrates.

I.3.6. Hydride vapor-phase epitaxy

The hydride vapor-phase epitaxy (HVPE) is presently the sole technology capable of growing reasonably thick GaN layers of relatively high optical and structural quality GaN[30] at reasonable growth rates. Łucznik et al.[31] reported the growth of 2-mm-thick GaN single crystals on high pressure grown GaN seeds at growth rates of 100–500 μm/h along the crystallographic c-axis. Kyma Technologies, Inc. has produced 10-mm-thick GaN boules with this method and even explored non polar orientations cut from these boules. A limitation of the HVPE technique is the problem of dislocation generation and control of parasitic nucleation, particularly for layers exceeding about 100 μm in thickness.[31] Another issue for HVPE-grown GaN that seems be persisting is that there seems to be an achievable minimum in the dislocation densities of ~10^5 cm^{-2}. It is very likely that there will always remain enough stress in the wafers, since they originate on sapphire or GaAs substrates, to introduce dislocations!

Current status of HVPE technology

Substrate applications:

Bulk substrates: GaN, demonstrated.
AlN, demonstrated.

Freestanding: GaN, small volume production (2-inch) GaN for blue LD production;
AlN, demonstrated (2-inch);
AlGaN, demonstrated (20 mm).

Template substrates: GaN, small volume production (2-inch) of blue LEDs;
Demonstrated (3-, 4-, and 6-inch);
AlN, small volume production (2-, 3-, 4- inch) of HFETs;
Demonstrated (6- inch);
AlGaN, pilot production (2-inch) of UV LEDs;
Demonstrated (3- and 4- inch);
InN, demonstrated, sampling (2-inch);
InGaN, demonstrates, sampling (2-inch).

Device applications: 360 nm and 420 nm LEDs, small volume production
300 – 350 nm LEDs, demonstrated
AlGaN/GaN HFETs, demonstrated

HVPE technology is rather mature, and n- and p-type doping is established. Recently, efforts have been focused on developing semi-insulating GaN for high-power/high-frequency devices.[32, 33] HVPE- templates are used in industrial-scale production of GaN-based devices.

I.4. Conclusions

The most developed techniques now is the HVPE growth, which has already found indispensable uses in device production, in particular laser diodes due to extreme demand placed on the material quality by this device. However, HVPE is not "truly" bulk growth of freestanding material. The HVPE-grown templates suffer from such obvious problems as the residual strain owing to the thermal mismatch between the substrate and grown material. As such the actual substrate size is really much smaller than the developmental reports might lead one to believe. This and the cost are, perhaps, the reasons why efforts are underway to develop alternative techniques.

The current state of the affairs is such that any technique for growth of "truly" bulk GaN would have to be competitive with the HVPE growth of bulk GaN in the near future. High-temperature solution growth, ammonothermal, solution seeded, and sublimation growth techniques (limited to the growth on AlN) show some promise for production of bulk crystals. Although all these aforementioned methods are at the development stage, single crystals of high structural perfection have been demonstrated. However, several important questions must be answered in order to assess the potential of each of the above-discussed techniques for mass production:

-Long-term reliability of the hardware for the growth apparatus, especially in the case of the ammonothermal technique employing high pressure and highly aggressive liquid

ammonia media is imperative. This problem becomes even more challenging for high temperature solution growth (P= 1-2 GPa and T = 1400 – 1500 ^{o}C) making this technique less likely for mass-production.

-Concentration of residual impurities (primarily oxygen) is of concern. Generally, the data on residual impurity compositions are insufficient. Furthermore, the cost for mass production must be reasonable, and the development of doping technology must be pursued and conquered.

II. Bulk ZnO

II.1. Introduction

Unlike GaN, ZnO has seen reasonable success, even early on, with growth of what could be genuinely considered bulk ZnO. Various approaches such as the hydrothermal method, the melt grown method, and the vapor transport method have been utilized to produce bulk ZnO material. Although somewhat slow, the hydrothermal method is viewed as a scalable process for production of large area and large quantities of ZnO. However, the hydrothermally grown ZnO is contaminated from nutrients such as Li, K, etc., which have detrimental effects on the epitaxial films grown on hydrothermal-ZnO wafers. In this debate the participants were asked to speak to the critical issues that are faced by bulk ZnO and efforts that are underway to tackle them and potentially conquer them. Below is a summary of the present status of the bulk ZnO.

Growth of bulk ZnO crystals is mainly carried out by using variations of the three primary methods: hydrothermal,[34,35,36] seeded vapor transport (sublimation),[37,38,39] and melt growth.[40,41] Because of its high vapor pressure, growth of ZnO from the melt is difficult, and growth by vapor-phase deposition is difficult to control. The crystal growth is driven by a small amount of supersaturation of the solution during hydrothermal reaction.

II.2.Brief review of growth techniques

II.2.1. Pressurized melt grown ZnO

The melt growth process employs a modified Bridgman configuration producing very good quality crystals with low defect density and relatively high growth rates (1–5 mm/h) as compared to competing techniques. This approach utilizes a patented method of melting and crystallizing materials with high melting point (above ~1450 ^{o}C), a volatile component in the structure, or thermodynamic instabilities at or near the material's melting point (decomposes into atomic components) at atmospheric pressure. The vessel is a high pressure induction melting apparatus, wherein the melt is contained in a water-cooled crucible (a rough schematic is depicted in Figure 9). Zinc oxide powder is used as the starting material. Melting is accomplished by radio frequency (rf) induction heating. The rf energy produces joule heating until the ZnO is molten at about 1900 °C. Once the molten state is attained, the crucible is slowly lowered away from the heated zone to allow crystallization of the melt.

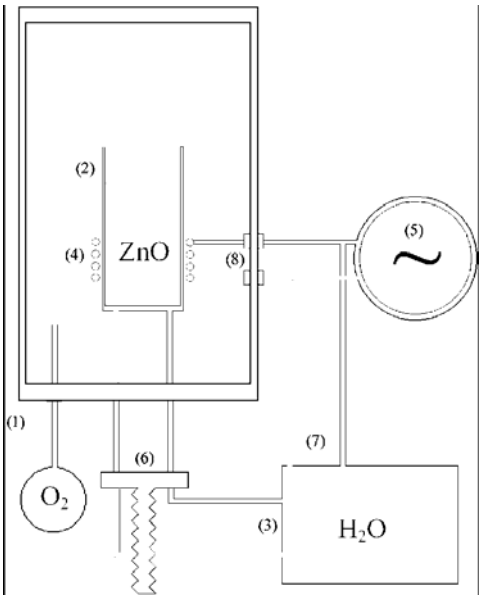

Figure 9. A schematic illustration of the ZnO crystal growth apparatus (after J. Nause and B. Nemeth[41])

The pressurized melt growth offers the following advantages: High purity, commercially viable growth rates (1–5 mm/h), with multiple orientations (*c, a* or *m*-plane) made possible by three dimensional nature of the growth, and *in situ* doping control (semi-insulating or n^+). The material properties of the pressurized melt grown ZnO can be characterized as relatively low defect density (etch-pit density is ~10^4 cm^{-2}), x-ray full width at half maximum (FWHM) of about 49 arc sec for the (0002) x-ray rocking curve[41], room-temperature electron concentration and mobility of 5 x 10^{17} cm^{-3} and 131 $cm^2/(Vs)$[41], respectively, very high optical quality with defect-related PL constitutes ~ 0.1% of the total radiative recombination (the caveat here is the this form of characterization depends very much on the excitation intensity with higher intensities favoring the bandedge related emission), and approximately 85% quantum efficiency of the exciton emission

The method, however, has some undesirable characteristics as well, among which is the low angle grain boundaries. Crystals without grain boundaries show x-ray rocking curves narrower than 50 arcsec. Furthermore, the residual impurity concentration is high which must be reduced.

The current status of the method can be summed as follows: Only a limited amount of 50-mm material is available for growth due to small angle boundaries. On the positive column, the growth vessel can be scaled so that substrates at a diameter of 75 mm or larger could be obtained. In terms of the impurities, the level in the earlier material was about 19.7 ppm with primary impurities being Al, Si, Fe, Cd, and Pb, all of which come from metallic Zn used in the preparation of the ZnO source material. The improved powder source impurity levels are at Cd (4ppm), Fe (2 ppm), Pb (5 ppm), with all others being below detection limit. In terms of the resultant ZnO crystal chemical purity, the impurity levels were Cd (2 ppm), Fe (2 ppm), and Pb (4 ppm). The analysis for Ca showed 1 ppm both in the powder source and the crystalline material that resulted.[42]

II.2.2. Seeded Chemical Vapor Transport (SCVT) growth of ZnO by ZN Technology

In the chemical vapor transport method, the reaction takes place in a nearly closed horizontal tube. Pure ZnO powder used as the ZnO source is placed at the hot end (hot zone) of the tube which is kept at about 1150 °C. The material is transported to the cooler end of the tube, maintained at about 1100 °C, with H_2 carrier gas. The carrier gas is necessary because the vapor pressures of O and Zn are quite low over ZnO at these temperatures. At the cooler end, ZnO is formed by the reverse reaction, assisted by a single-crystal seed. To maintain the proper stoichiometry, a small amount of water vapor is added. A growth time in the range of 150–200 h leads to 2-in.-diameter crystals with about 1 cm in thickness from which the wafers can be sliced and polished as shown in Figure 10.

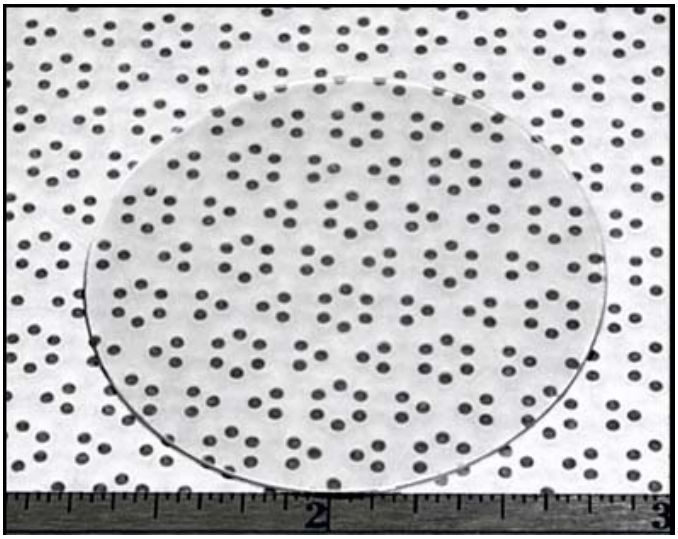

Figure 10. Water-clear SCVT-grown ZnO wafer with CMP finish on both faces (courtesy of J.J. Song of ZN Technology).

The Material characteristics of Seeded Chemical Vapor Transport can be succinctly described as follows: Basically, 2-inch-diameter ZnO wafer can be, and has been, produced with high spatial uniformity (<1% from CL measurements). Furthermore, room-temperature Hall free-electron concentration and mobility in unintentionally doped material are about $6x10^{16}$ cm^{-3} and 205 $cm^2/(V\ s)$, respectively. Finally, very high optical quality has been achieved providing that the surface of wafers is prepared well. The chemical impurity analysis for a few wafers growth by this technique is tabulated in Table 1.

Table 1. Impurity analysis of ZnO crystals grown by SCVT (Courtesy of J.J. Song of ZN Technology, Inc.).

- Boron and aluminum only suspected n-type dopants detected (red)
- Nitrogen and sodium as only possible p-type dopants detected (blue)
- The major impurity consistently present is silicon (from the quartz ampoule)
- Elements not shown in the table have not been detected down to their respective detection limits

	Sample A	Sample B	Sample C
	ppma	ppma	ppma
B	0.012	0.012	0.028
C	0.040	0.004	0.091
N	0.028	0.180	1.200
Na	0.015	ND	ND
Al	0.009	0.007	0.020
Si	0.330	0.280	0.660
Ti	0.001	ND	ND
Sn	ND	0.077	ND
Pb	0.002	ND	ND

Just as in other methods, the seeded chemical vapor transport technique also comes with some disadvantages. To cite a few, the wafers have grain boundaries and the low growth rate is problematic which would undoubtedly result in high cost for wafers

II.2.3. Hydrothermally-grown ZnO Crystals

As alluded to above, the hydrothermal method lends itself for mass production. Figure 11 shows a schematic hydrothermal growth system. The hydrothermal method uses ZnO single-crystal seeds suspended by Pt wire, and sintered ZnO strings together with a KOH and LiOH aqueous solution are used as a nutrient. The seeds and the particular nutrient used are placed into a Pt crucible. This crucible is sealed by welding and placed in an autoclave. The autoclave is then placed into a two-zone vertical furnace. ZnO is transferred from the nutrient in the higher-temperature zone to the seeds in the lower-temperature zone. The seeds grow to bulk ingots about 10 mm in size after 2 weeks.

Typical growth conditions employed are as follows: The seed temperature, T_1 is typically 345 ^{o}C, the nutrient temperature, T_2 is typically 355 ^{o}C (nutrient), and the pressure in the vessel is about 1- 2 kbars. Generally, about 70-85% of the volume can be filled. As for the nutrients, LiOH/KOH solvent has been used. Depending on the particulars, the growth runs last some :20-50 days.

The potential advantages of the hydrothermal ZnO are that it is truly a bulk growth method and , truly free-standing wafers up to 3 inch in diameter have been produced. Furthermore, high crystal quality is made available because the material experiences no thermal stress during growth. Continuing on with other attributes of the hydrothermal grown ZnO, low dislocation density is possible (< 10 cm^{-2} in quartz), the growth takes place in chemical equilibrium growth (sometimes disadvantageous), spatially uniform alloys of ZnO are possible (e.g., ZnMgO grown at AFRL-Hanscom). intentional doping

of the bulk material with (e.g., Al, In, N, Co as demonstrated at AFRL-Hanscom) is possible, very high laser hardness was demonstrated in AFRL-Hanscom crystals (even with ~10^{18} electrons/cm^3), faceted growth for non-polar material is possible, and finally, hardware required for growth is essentially the same as that for quartz growth which is very mature.

As touched upon above, mass production with the hydrothermal method by employing large autoclaves is a reality. The process is scalable to economical high volume production and ZnO growth rates of ~½ that of the quartz growth rate (10,000 kg/year of quartz are produced) have

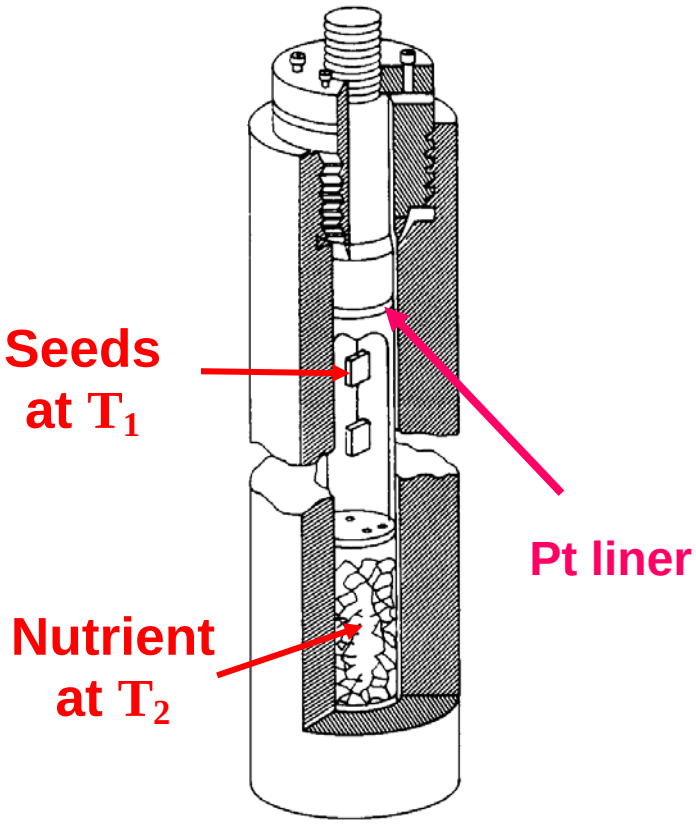

Figure 11. Schematic of autoclave for hydrothermal growth (courtesy of M.N. Alexander of Air Force Research Laboratory, Sensors Directorate).

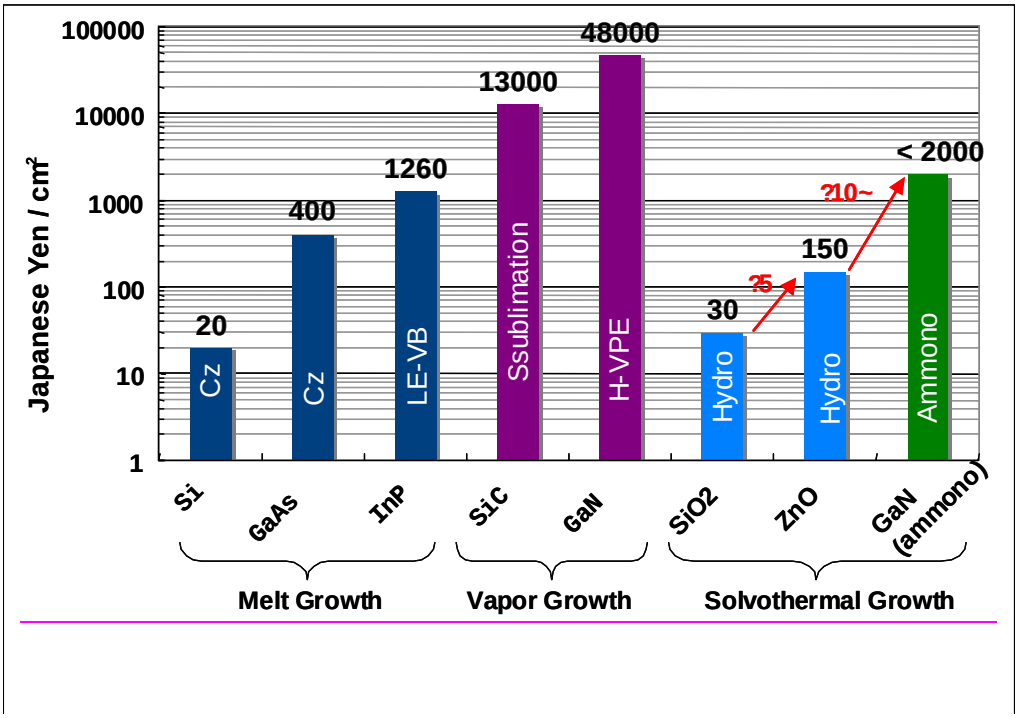

Figure 12. Normalized prices for wafers from semiconductors grown from the melt, the vapor, and from the high-pressure solution. The price for ammonothermal GaN is an estimate. (After reference 43).

been demonstrates. Figure 12 compares the price per cm^{-2} for single crystals grown by various techniques. It is obvious from the chat that the hydrothermal techniques is very cost efficient despite the low growth rates.[43]

Bulk Hydrothermal ZnO Status: Successes

Going beyond the method itself and focusing on the accomplishments made possible by this method, excellent ~ 7.5 cm diameter c-axis single crystal substrates have been grown (Tokyo Denpa). 2.5 cm diameter c-axis single crystal substrates are routinely grown at AFRL-Hanscom albeit for research purposes only. Structurally excellent large single crystals are grown by the Fukuda group in Sendai. The FWHM value of the (0002) x-ray diffraction rocking curves is about 20 arc. sec.[44] It should also be added that unintentionally doped ZnO grown by the hydrothermal technique is highly resistive (n-type): $n \approx 1x10^{14}$ cm^{-3}, $\mu_n \approx 200$ cm^2/Vs.[44] The crystals with dislocation etch pit densities < 500 cm^{-2} can be obtained on a routine basis. The vacancy concentrations currently are about ~ 10^{16} cm^{-3} as determined by positron annihilation which points to some needed improvement. Doping with N, which can be a p-type impurity, to levels of ~ 10^{18} cm^{-3} has been demonstrated (AFRL-Hanscom, so have indium and aluminum doping (again n-type). Extending the method further, alloys of ZnO such as ZnMgO with up to 5.5% Mg have been demonstrated (AFRL-Hanscom)

Bulk Hydrothermal ZnO Status: "Challenges" and Opportunities

The hydrothermal method also faces some challenges. Among them is the quality control of ZnO as "semiconductor crystal" which is more demanding than would be for other applications. Not specific to the hydrothermal method, a stable and well-characterized p-doping with high hole concentration is needed. The impurity levels need to be lowered further. As seen from Figure 13, the main impurities in hydrothermal ZnO are Si, Cd, and Li. The source of Si and Cd are the mineralizer and raw material, respectively; and their concentrations can be reduced by using higher purity starting materials. The main challenge, however, is how to reduce the Li concentration caused by the aqueous solution of LiOH which is used as a mineralizer.[34] The segregation, in the c+ and c– directions which manifests itself as piling up of unintentional impurities near seed is another issiue. Continuing on with challenges faced the vacancy concentrations must be reduced further.

While on the topic, let us also touch upon the challenges that are commonly faced by all the ZnO growth methods. Growth of non-c-axis crystals might need to be explored as polarization charge in structures based on the polar c-plane in GaN is beginning to be viewed as problem rather that an advantage. The situation would be worse in ZnO which might call for non-polar surfaces to be made available. Learning from the GaN technology, this is best done with growth of the bulk material along the c-direction and slicing it along the m-plane for example. This approach eliminates problems induced by the low formation energy of basal stacking faults. We should also mention that the lack of mid-gap donor/acceptors would frustrate efforts to obtain high resistivity wafers (may not be an intractable problem for high purity crystals because the band gap is large). To reiterate, Mg and Cd alloying and doping need to be improved considerably. Finally, the effects of impurities on the growth kinetics with respect to. the morphology are not well understood which need further investigations.

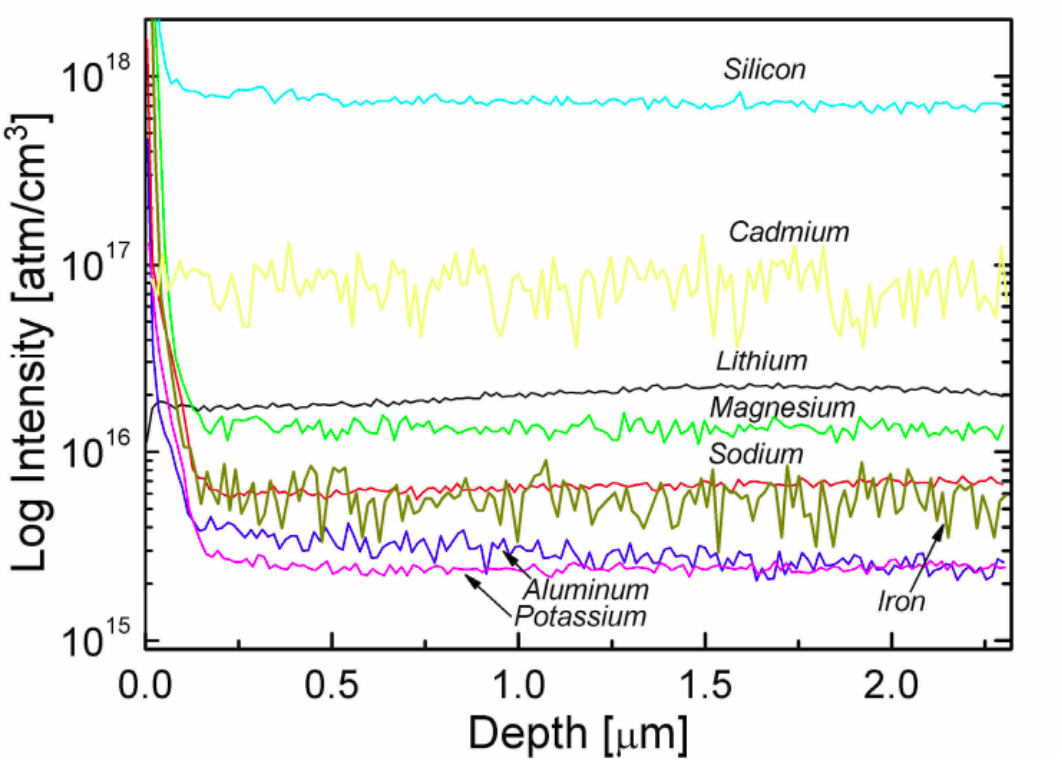

Figure 13. Results of secondary ion mass-spectroscopy of hydrothermal ZnO (courtesy of T. Fukuda of Tohoku University).

II.3.Conclusions

It can be successfully argued that bulk ZnO is a reality. ZnO wafers manufactured by different vendors employing different technologies are commercially available. Table 2 illustrates the current status of the three main growth techniques used for bulk ZnO growth. At the present time, the hydrothermal growth of ZnO is the most mature technology. The hydrothermal material shows the best crystal quality, among the methods discussed, and low concentration of impurities, with an exception of Li (see Table 2). As has been shown by the large volume quartz crystal production, the hydrothermal technique is scaleable for mass production. The main challenge for the hydrothermal method is to produce Li-free ZnO. In addition, doping and alloying technologies need to be improved. The competing technologies (pressurized melt growth and seeded chemical vapor transport) are at the developmental stage. The near term goal for the competing growth methods is to resolve the problem of grain boundaries. Pressurized melt growth also suffers from high concentration of residual impurities. Although SCVT provides the lowest concentration of residual impurities, cost reduction is challenging for this techniques owing to low growth rate.

Table 2. Comparison of ZnO quality grown by different methods (T. Fukuda of Tohoku University, summary of the data reported at ZnO workshop[45]).

Nominal specification						
Maker	Fabrication	2"?	Grades?	Rocking curve (arc.sec)	Contaminants (ppm)	Source
Cermet	Melt Growth	Yes	Research (low) & Production (high)	42	Total < 10 Cd (2), Fe(2), Pb(4), Ca(1)	Ref. [42]
Tokyo Denpa	Hydrothermal	Yes	Single Crystal	18	Total < 13 Li(<12), Fe(<0.5), Al(<0.4), K(<0.2)	Ref. [46]
Eagle Picher	SCVT	Yes	3 grades: I, II, III	<100	Total = 3.2 Si (0.7), N(0.7), B(0.5), Ga(0.5)	Ref. [45]
ZN Technology	SCVT	Yes	?	32 (1 cm x 1cm)	Total < 0.56 Si(<0.3), N(<0.2)	Ref. [45]

III. Point Defects

III.1. Introduction

Characteristically, defects represent one of those areas of semiconductors which are synonymous with controversy, and GaN and ZnO did not escape this axiom, as the measurement techniques are not able to precisely correlate electrical or optical manifestation of defects to their origin. It is therefore highly appropriate to refer to the topic as "Not so well understood point defects in GaN and ZnO". While numerous assignments of the defect-related luminescence bands can be found in literature, only few of them can be construed as trustworthy. Over the years the nitrogen and oxygen vacancies were believed to be dominant shallow donors in GaN and ZnO, respectively. Now it is becoming increasingly clear that these vacancies are formed in noticeable concentrations only after electron irradiation. Another vital myth has to do with green emission observed in ZnO. Nearly up to the present time the green luminescence band in ZnO has been commonly attributed to transitions from oxygen vacancies to the valence band. However, it is relatively easy to point out that such transitions are highly unlikely in n-type ZnO. Problems in the identification of point defects are discussed from theoretical and experimental points of view. The summary given below is based on the presentations delivered by Drs. C. Van de Walle and M. Reshchikov as well as reports available in the literature.

III.2. Point defects in GaN and ZnO from the theoretical standpoint

Point defects encompass aberrations from the ideal crystal in the form of native defects such as vacancies, interstitials and antisites, and extrinsic defects such as impurities and defect complexes with impurities. The likelihood of presence of point defects, and if so their concentration, depends on their formation energies. In thermodynamic equilibrium the concentration of a point defect is given by

$$c = N_{sites} \exp\left(-\frac{E_f}{kT}\right),$$

Equation 1

where E_f is the formation energy and N_{sites} is the number of sites the defect can be incorporated.

It follows that the defects with high formation energy will be formed in low concentrations and the defects with low E_f may be abundant. The formation energies of native defects in GaN [47,48,49,50] and ZnO [51,52,53,54] have been calculated by several groups, and the results generally agree. We should mention that the calculations are performed for an otherwise ideal crystal structures with no defects other than the one under investigation. In reality deviations from this ideality such as extended defects, other point defects and strain could serve to alter the results of these calculations. Nevertheless, calculations for ideal structures give us an insight as to how likely it is for a native defect to form. Analyses of the formation energy for the native defects in GaN and ZnO (Figure 14) show that the dominant native defects in GaN and ZnO should be vacancies: cation vacancies in *p*-type material (when the Fermi level is close to the valence band) and anion vacancies in *n*-type material (when the Fermi level is close to the conduction band). Note that some of the native defects (with the formation energy of several eV), according to Eq. (1.1), have extremely low probability to form during growth.

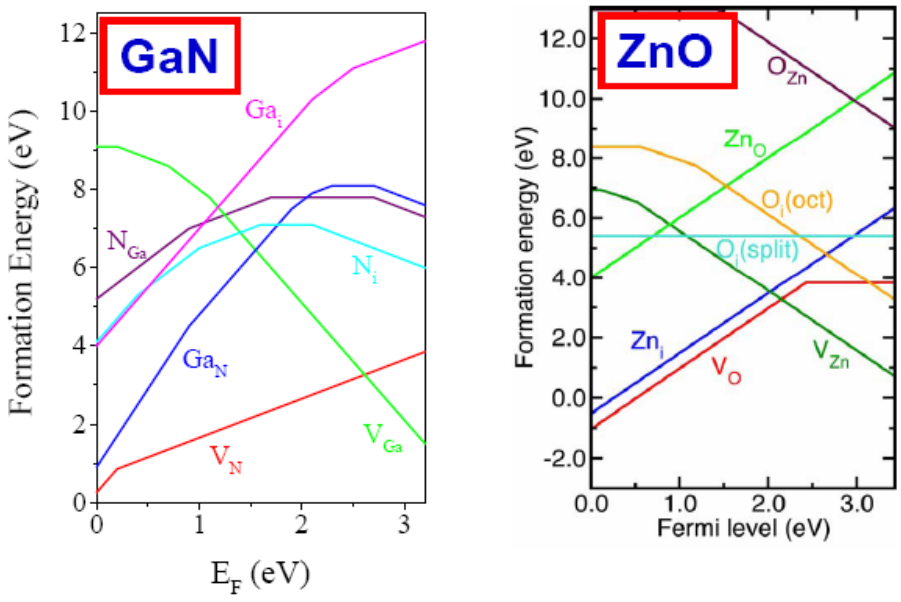

Figure 14. Formation energies of native defects in GaN and ZnO as a function of the Fermi level (courtesy of C.G. Van de Walle of University of California at Santa-Barbara).

First principles calculations based on the density functional theory (DFT) within the local density approximation (LDA) are able to predict not only the probability of the defect formation but also the energy levels of the defects in different charge states. The defect energy levels in these calculations can be found as the Fermi-level position for which the formation energies of charge states q_1 and q_2 are equal. The energy levels for the main native defects in GaN and ZnO are shown in Figure 15.

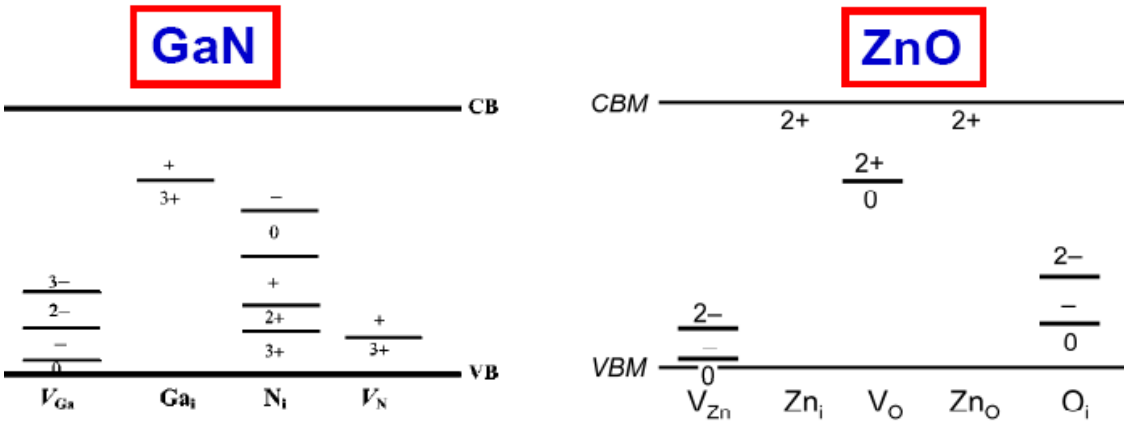

Figure 15. Defect transition levels for native defects in GaN and ZnO (courtesy of C.G. Van de Walle of University of California at Santa-Barbara).

.

A transition level corresponds to position of the zero-phonon line in the case of defect-related photoluminescence (PL) or PL excitation, which is close to the thermal ionization energy in experiments such as PL and deep-level transient spectroscopy (DLTS). As alluded to in the abstract, the main native defects expected in GaN and ZnO are reviewed below.

The calculations indicate that the nitrogen vacancy, V_N, in GaN and the O vacancy, V_O, in ZnO have very high formation energies in *n*-type GaN and ZnO, respectively. Thus, these defects cannot be the shallow donors responsible for *n*-type conductivity of undoped GaN and ZnO, contrary to the conventional wisdom dominated the GaN and ZnO communities for decades. Moreover, V_O in ZnO is a deep donor, not a shallow one. Because of high formation energies of the anion vacancies in *n*-type material (the Fermi level close to the conduction band), these defects should not present in the as-grown GaN and ZnO, but can *e.g.* be formed after electron irradiation. We should hasten to indicate, however, that the N some calculations point to the possibility of N vacancies even in n-type GaN. In contrast, the anion vacancies can be formed abundantly in *p*-type material and may be the main cause of the self-compensation when attempting to achieve p-type doping.

Oxygen vacancies in ZnO received a special attention in the presentation of Dr. Van de Walle. V_O in ZnO is a deep donor with two stable states (V_O^0 and V_O^{2+}). Its metastable state (V_O^+) can be observed in transitions involving optical excitation. V_O is a so-called negative-U center implying that the 2+/+ level lies above +/0 level. According to Van de Walle, V_O is not formed in the as-grown ZnO but can be produced by electron irradiation. Electron paramagnetic resonance (EPR) studies indeed revealed the presence of V_O in electron irradiated ZnO with g = 1.99.[55,56,57] Transitions involving V_O^+ can be seen as a broad red band peaking at about 600 nm, as concluded from optically detected EPR.[57] This result is in excellent agreement with the first-principles calculations for V_O.[51]

According to the first-principles calculations we can expect that broad photoluminescence (PL) bands in GaN and ZnO are related to transitions involving vacancies. In particular, the omnipresent yellow luminescence (YL) band observed in *n*-type GaN is most likely due to the transitions from the conduction band (or from shallow donors at cryogenic temperatures) to the 3-/2- level of V_{Ga} or 2-/- level of the $V_{Ga}O_N$ complex. The blue luminescence (BL) band in *p*-type GaN has been proposed to involve V_N. The green luminescence (GL) band in ZnO is assumed to be due to transitions from the conduction band (or shallow donors) to the 2-/- level of V_{Zn}, in analogy with GaN. Note that impurities such as Cu in ZnO can also be responsible for the broad PL bands. For a detailed discussion see references [58] and [59].

First-principles calculations also provide information on the ability of point defects to diffuse at a given temperature, which underscores the mobility of point defects. The estimated annealing temperatures and the energy migration barriers for the native defect motion in ZnO are listed in Table 3.

Table 3. Estimated annealing temperatures for vacancies and interstitials in ZnO

	E_b (eV)	T annealing (K)
Zn_i^{2+}	0.57	219
V_{Zn}^{2-}	1.40	539
V_O^{2+}	1.70	655
V_O^{0}	2.36	909
O_i(split)	1.40	539
O_i(oct)	1.10	424

As follows from Table 3, zinc interstitials are mobile at temperatures well below room temperature, resulting in the formation of complexes. Estimated annealing temperatures for defect motion provided in Table 3 are consistent with the experimental results.[51]

Since the native defects in GaN and ZnO cannot explain the n-type conductivity in these materials, participation by impurities introduced unintentionally during growth as shallow donors has been invoked to account for the observations. In GaN the dominant shallow donors are O_N and Si_{Ga}. In ZnO the situation is much less clear. There are multiple experimental results indicating that hydrogen is involved in the formation of the shallow donor states in ZnO. However, it appears that a single type of hydrogen-related defect cannot explain the wide dispersion in the reported experimental data. The first-principles calculations predict formation of at least two types of the H-related shallow donors. Interstitial H has low formation energy which is consistent with observed solubility and electron concentration in as-grown ZnO.[60] As mentioned, this acts as a shallow donor. Above 500°C, however, the interstitial H is unstable, which can explain the observed persistent conductivity. However, the observed dependence of the electron conductivity on oxygen pressure cannot be explained by the presence of interstitial H. However, the substitutional hydrogen (H_O), also with low formation energy and acting as a shallow donor, is more stable and can explain the observed dependence of the conductivity on oxygen partial pressure.[61] Hydrogen can be introduced as an unintentional donor in vapor-phase transport, hydrothermal growth, MOCVD (sources, carrier gas), MBE (residual gas), laser ablation, and sputtering in H_2 atmosphere, or during annealing in forming gas.

Among the main challenges facing the theorists are as follows:

a) More sophisticated computational techniques are needed to deal with the "band gap problem".
b) Reliable experimental results are needed for identification of defects and defect-related transitions that can be compared with theory (PL, optically detected EPR, positron annihilation spectroscopy, and DLTS).
c) Surfaces are very crucial in determining the properties of GaN and ZnO. In particular, a significant surface conductivity has been observed in ZnO.[62,63] It is,

therefore, natural to expect various theories mentioned do take surfaces into account.

III.3. Point defects in GaN and ZnO from the experimental standpoint

Photoluminescence (PL) is a powerful tool to study point defects in wide-bandgap semiconductors. Typically point defects with deep levels are responsible for the broad, and often structureless bands in the PL spectrum. A common misconception is that the PL bands are broad because of many energy levels in the band gap due to "imperfections" or interaction of defects. In fact the main reason is the strong electron-phonon coupling, i.e. in addition to a photon, a number of phonons is also emitted during recombination of electrons and holes bound to defects. Another common misconception is that PL provides only qualitative data (relative concentrations of defects) but not quantitative. In fact, quantitative methods have been developed, and one can find not only the concentrations of point defects but also the absolute internal quantum efficiency, carrier capture cross-sections, charge states, excited states, etc.[64]

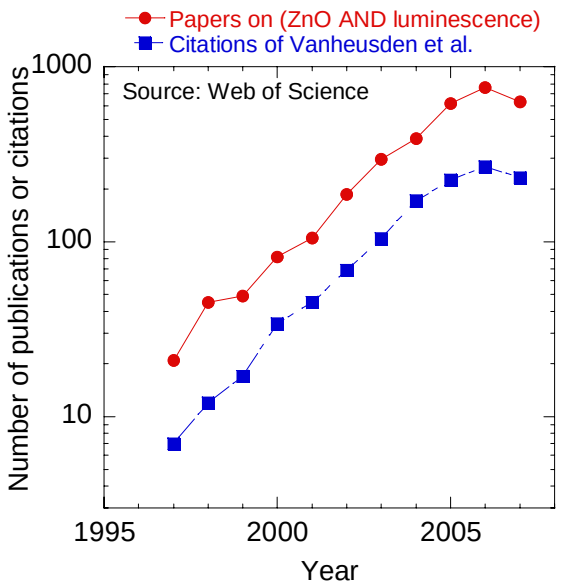

Figure 16. Number of publications mentioning luminescence in ZnO in comparison with number of citations of works by Vanheusden et al on the origin of the green band in ZnO (courtesy of M.A. Reshchikov of Virginia Commonwealth University).

Despite much activity and many reports, sadly very little is really known about point defects in GaN and ZnO. A lot of the commonly believed information is questionable if not false. A case in point is the oxygen vacancy in ZnO. Just about in one every three publications dealing with luminescence in ZnO the green PL band in ZnO has attributed this band to V_O, namely to transitions from the deep donor level associated with V_O to the valence band, following the report by Vanheusden et al.,[65] see the chart in Figure 16. This identification, which is not correct, is based on the erroneous assignment of the EPR signal with g = 1.96 to oxygen vacancy. It is well established that V_O is responsible for the EPR signal with g=1.995, whereas the g = 1.96 signal belongs to the shallow donor.[55,56,57] Moreover, a transition from a donor state to the valence band is very unlikely in an *n*-type semiconductor, which is what all the available ZnO is. The origin of the green band in ZnO is not very clear either. Note that several (at least five) broad bands related to different point defects can be distinguished in undoped high-quality ZnO.[66] One of these bands is clearly related to an internal transition associated with the

Cu_{Zn} acceptor whose ground state is close to the conduction band.[67] The origin of other defects (presumably deep acceptors) remains unknown.

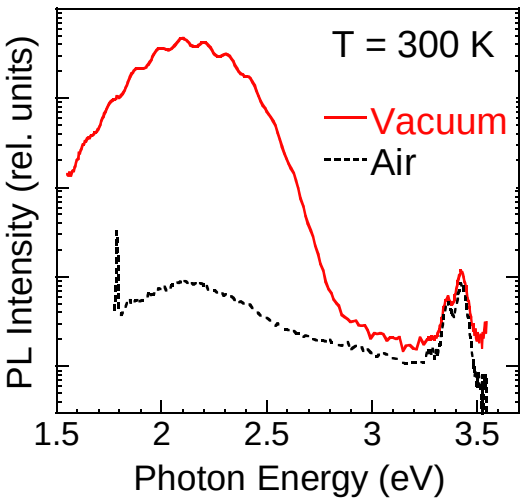

Figure 17. PL spectrum in C-doped GaN measured in air ambient and in vacuum (courtesy of M.A. Reshchikov of Virginia Commonwealth University).

The identity of defect(s) responsible for the broad yellow band in GaN also remained very controversial for decades. The most commonly accepted assignment is that the YL band is caused by transitions from the conduction band (or shallow donors at low temperatures) to a deep acceptor, the deep acceptor being the V_{Ga}-related defect.[47] Recent experiments demonstrated that at least in high-purity freestanding GaN templates the green and yellow bands are caused by transitions from the conduction band to two charge states of the $V_{Ga}O_N$ complex.[68] The frequently proposed assumption that carbon is responsible for the YL band in GaN which appears to be incorrect since in intentionally C-doped GaN no correlation between the YL-related defects and concentration of carbon could be found.[69]

Another very common myth is that room-temperature PL spectrum can provide information about the presence of point defects in GaN or ZnO. Figure 17 demonstrates that the YL band in GaN can be very weak or very strong depending on the ambient at room temperature. This fact again indicates that the surface plays a tremendous role in the electrical and optical properties of these wide-bandgap semiconductors.[70,71,] There is a significant band bending near the surface due to surface states.[72,7374] Among the causes of surface of surface charging in GaN and apparently ZnO is adsorption of ions and molecules from air which appears to be the dominant effect. Unfortunately, the importance of the surface effects is not adequately understood by majority of researchers in GaN and ZnO communities.

Although numerous assignments of the broad PL bands have appeared in the literature, only a handful can be considered as reliable. Among these bands are the yellow and green bands in freestanding GaN templates which are unambiguously assigned to the two charge states of the $V_{Ga}O_N$ complex.,[68] the blue band with a characteristic fine structure and the zero-phonon line at 3.10 eV which is attributed to Zn_{Ga} acceptor in GaN,[64] the green band with a fine structure and the zero-phonon line at 2.859 eV which is attributed

to Cu_{Zn} acceptor in ZnO,[67] and the Gaussian-shaped orange band peaking at 1.96 eV at low temperatures which is attributed to Li_{Zn} in ZnO.[75] However, majority of the PL bands in these materials remain unidentified not only in the strict sense but even the types of transitions are not always established. The state of the affairs in terms of defect analysis obviously calls for more in depth and incisive investigations, not bountiful and superficial reports which end up obscuring the problem rather than illuminating it.

IV. Ferromagnetism in GaN and ZnO related materials

IV.1. Preface

Both GaN and ZnO have seen arguably more than sufficient number of papers reporting ferromagnetism, in some cases all the way up to a Curie temperature of 900 K. Magnetization measurements using a SQUID magnetometer have been the primary method of analysis to reach these conclusions. If true, spin based devices are assumed to follow. More stringent measurements, however, such as magnetic circular dichroism which probes the Zeeman splitting have not been able to confirm these claims although magnetic ion doped semiconductors such as GaAs, InGaAs, and ZnTe have passed this test. Magnetotransport measurements which can be done in GaAs and InGaN agree with magnetization measurements. However, both ZnO and GaN doped with magnetic ions are high resistivity preventing magnetotransport measurement from being made. In this debate we heard a tutorial talk from an expert how spin has been and can be used not just for storage but also in some novel devices. This was followed by another tutorial talk on fundamentals of magnetic ion doped semiconductors. Further, this was followed by yet another tutorial talk on magnetic circular dichroism (MCD) measurements, again by a noted expert in the field. Finally, other theoretical contributions such as those by Dr. S. Wei, particularly why Gd is able to produce Bohr magnetons in the thousands are discussed.

IV.2. Introduction

Diluted magnetic semiconductors (DMSs), or sometimes referred to as semimagnetic semiconductors, are semiconducting materials in which a fraction of the host cations is substitutionally replaced by magnetic ions. Much of the attention on DMS materials is due to their potential applications in what is dubbed the "spintronics" devices, which exploit the spin in magnetic materials along with charge of electrons in semiconductors. Transition metals (TMs) that have partially filled *d* states (Sc, Ti, V, Cr, Mn, Fe, Co, and Ni; Cu has a completely filled d shell, however, acts as magnetic impurity in Cu^{2+} charge state) and rare earth elements that have partially filled *f* states (e.g. Eu, Gd, Er) have been used as magnetic ions in DMS. The partially filled *d* states or *f* states contain unpaired electrons, in terms of their spin, which are responsible for exhibiting magnetic behavior. There are many mechanisms that could be responsible for magnetic ordering. In DMS materials the delocalized conduction band electrons and valence band holes interact with the localized magnetic moments associated with the magnetic atoms. Generally, when 3*d* transition metal ions are substituted for the cations of the host, the resultant electronic structure is influenced by strong hybridization of the 3*d* orbitals of the magnetic ion with mainly the *p* orbitals of the neighboring host anions. This hybridization gives rise to the strong magnetic interaction between the localized 3*d* spins and the carriers in the host valence band.[76] Due to the application induced necessity that the DMS materials must exhibit ferromagnetism with a critical temperature above room temperature in order to

have practical applications in spintronics devices, that temperature, i.e., the Curie temperature (*TC*), is naturally deemed to be the bottleneck issue.

GaN and ZnO have attracted intense attention in the search for high T_C ferromagnetic DMS materials since Dietl *et al.*[77] predicted that GaN- and ZnO-based DMSs could exhibit ferromagnetism above room temperature upon doping with transition elements such as Mn (on the order of 5% or more) in *p*-type (on the order of 10^{20} cm^{-3}) materials. This conclusion in simple terms is in part due to the strong *p-d* hybridization, which involves the valence band in the host, owing to small nearest neighbor distance and small spin dephasing *spin-orbit* interaction. Even though the common wisdom indicates for the hole exchange to be dominant, Sato *et al.*[78] predicted that the ferromagnetic state $Co^{2+}(d^7)$ in Co-doped ZnO could be stabilized by *s-d* hybridization, pointing to the possibility that high- Curie-temperature ferromagnetic materials could be realized in *n*-type ZnO as well. Das *et al.*[79] showed by first-principles calculations that Cr-doped GaN can be ferromagnetic regardless whether the host GaN is of the form of bulk crystal or clusters. These types of predictions set off a flurry of intensive activity, including experimental, for transition metal doped GaN and ZnO as potential DMS materials with applications in spintronics.

IV.3. Brief overview of existing theories

In dilute magnetic semiconductors a sizable portion of atoms (as much as 36% of Mn in ZnO) is randomly substituted by transition-metal elements, giving rise to localized magnetic moments in the semiconductor matrix. The presence of magnetic ions affects the free carrier behavior through the *sp-d* exchange interaction between the localized magnetic moments and the spins of the itinerant carriers.[76] TM elements have valence electrons corresponding to the 4*s* orbital, and have partially filled 3*d* shells, thus the name 3*d* transition metals (i.e. Mn with the shell structure of $1s^2\ 2s^2\ 2p^6\ 3s^2\ 3p^6\ 3d^5\ 4s^2$). Both GaN and ZnO are of wurtzite structure, which is formed by tetrahedral (s-p^3) bonding. Generally, 3*d* transition-metal ions substitute for the cations of the host semiconductors, i.e., Zn sites in ZnO and Ga sites in GaN. In ZnO, the particular transition-metal element, for example, Mn, contributes its $4s^2$ electrons to the s-p^3 bonding, and can therefore substitutionally replace the Zn in the tetrahedral bonding to form a TM^{2+} charge state. In GaN, being a trivalent type, the bonding configuration requires 3 electrons which can be satisfied with the transition-metal elements contributing three electrons and form $TM^{3+}(3d^4$ for Mn) charge states. However, depending on the position of the Fermi level, which is generally near the conduction band in GaN, the third electron appears to be acquired from a donor site resulting in a large binding energy without leaving any corresponding hole in the valence band. This means that both $TM^{2+}(3d^5$ for Mn) and $TM^{3+}(3d^4$ for Mn) states might be possible and co-exist in GaN.

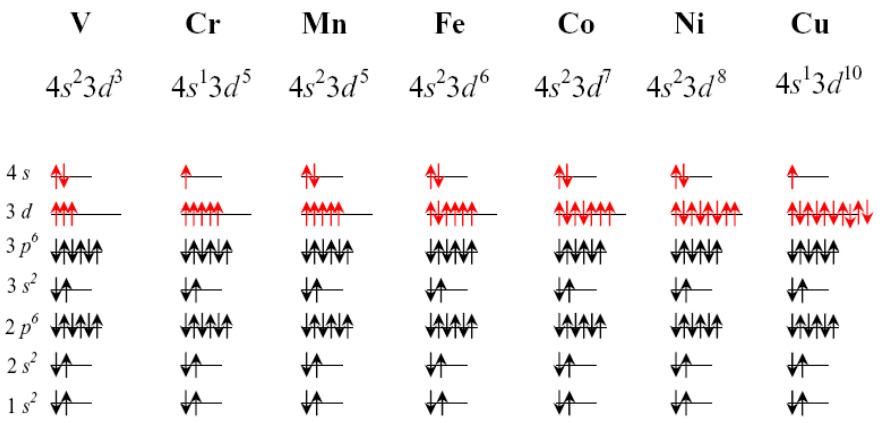

Figure 18. Electronic configuration of the 3*d*-states and 4*s*-states of transition metal elements (from V to Cu) (after Liu *et al*.[80]

The 3*d* band of the Mn^{2+} ion is exactly half-filled with 5 electrons among the 10 available states, with an energy gap between the up-spin (↑) occupied states and empty down-spin (↓) states. For other transition metals, such as Fe, Co, and Ni, one of the bands is usually partially filled (up or down) as shown in Figure 18. The TM-*d* bands of the transition metal hybridize with the host valence bands (O-*p* bands in ZnO and N-*p* bands in GaN) to form the tetrahedral bonding. This hybridization gives rise to an exchange interaction between the localized 3*d* spins and the carriers in the host valence band. In this simple picture, the *s*–like conduction band does not mix with the TM-*d* bands, but it is still influenced by the magnetic ion.

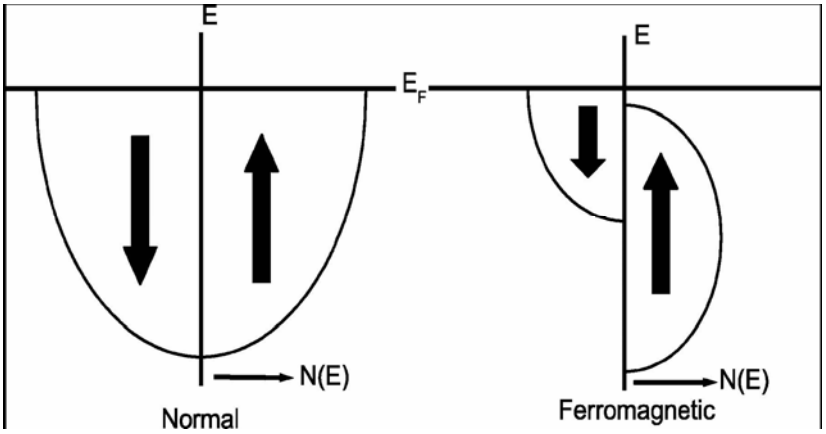

Figure 19. A schematic representation of the density of electronic states available to electrons in a normal metal and in a ferromagnetic metal whose majority spin states are completely filled. E is the electron energy; EF is the Fermi level; and N(E) is density of states (After Prinz [81]).

The important characteristic of a ferromagnetic material is the spontaneous magnetization below the Curie temperature, also referred to as the critical temperature. As shown in Figure 19 the *d* band in ferromagnetic materials is divided into spin-up and spin-down sub-bands,[81] which are displaced in energy with respect to one another, so that the spin-up band is filled first, and the spin-down states contain the remaining, if any, electrons. The difference in the numbers of spin-up and spin-down electrons gives rise to the observed spontaneous magnetic moment. In order to have any practical application in functional devices, it would be desirable to have a Curie temperature well above room temperature. Further, for some device applications it is also desirable to have the ferromagnetism to be due to carrier-induced ferromagnetism, so that the magnetic properties of the DMS can be manipulated by external means such as through manipulation of the hole concentration. A better understanding of the underlying mechanismsin GaN and ZnO, similar to that in GaAs, will certainly provide the much needed guidance for material design.

In a nutshell, the mechanisms pertinent to magnetism are direct super-exchange (which is antiferromagnetic), indirect super-exchange (could be ferromagnetic), carrier-mediated exchange (ferromagnetic) including the much celebrated double exchange mechanism, and bound magnetic polarons, to cite a few.

In the Zener model, the direct interaction between *d* shells of the adjacent Mn atoms (*super-exchange*) leads to an antiferromagnetic configuration of the *d* shell spins because the Mn-*d* shell is half-filled. On the other hand, the indirect coupling of spins through the conduction electrons tends to align the spins of the incomplete *d* shells in a ferromagnetic manner. Accordingly, the mean-field approach assumes that ferromagnetism occurs through interactions between the local moments of the Mn atoms mediated by free holes

in the material. The spin-spin coupling is also assumed to be a long-range interaction, allowing the use of a mean-field approximation.

Early attempts to understand the magnetic behavior of DMS systems are based on models in which the local magnetic moments are assumed to interact with each other via Ruderman-Kittel-Kasuya-Yoshida type (RKKY) interactions. The basic idea behind the RKKY interaction is based on the exchange coupling between the magnetic ion and the conduction band electrons. It should be mentioned that *s* and *d* wavefunctions are orthogonal and would not lead to any interaction in a perfect one electron system. The conduction electron is magnetized in the vicinity of the magnetic ion, with the polarization decaying with distance from the magnetic ion in an oscillatory fashion. This oscillation causes an indirect superexchange interaction (RKKY) between the two magnetic ions on the nearest or the next nearest magnetic neighbors. This coupling may result in a parallel (ferromagnetic) or an anti-parallel (antiferromagnetic) setting of the moments depending on the separation of the interacting atoms. The RKKY interaction between Mn spins via delocalized carriers has been used to explain the ferromagnetism observed in PbSnMnTe[82] However, if the carriers come from Mn-*d* states and are localized, i.e. far from being free-electron-like, the RKKY interaction may not be realistic.

The mean-field Zener model, proposed by Dietl *et al*.,[77] has been successful in explaining the transition temperatures observed for *p*-(Ga,Mn)As and (Zn,Mn)Te, and is based on the original model of Zener[83] and the RKKY interaction. As compared to the RKKY interaction, the mean-field Zener model takes into account the anisotropy of the carrier-mediated exchange interaction associated with the spin-orbit coupling in the host material. In the process it reveals the important effect of the spin-orbit coupling in the valence band in determining the magnitude of the T_C and the direction of the easy axis in *p*-type ferromagnetic semiconductors. Based on this model, it was predicted that TM-doped *p*-type GaN and ZnO, as shown in Figure 20, are the most promising candidates for ferromagnetic DMS with a high Curie temperature. However, these temperature values are predicated on the incorporation of some 5% transition metal element and hole concentrations of above 10^{20} cm^{-3}, which in fact may never be attainable. Sato and Katayama-Yoshida[84] performed first principles calculations of the electronic structures of TM-doped ZnO and proposed the double exchange mechanism to be responsible for the carrier-induced ferromagnetism. The double exchange mechanism has been successfully used to explain the ferromagnetism observed in (In,Mn)As.[85] In the double exchange mechanism originally proposed by Zener[86] magnetic ions in different charge states couple with each other by virtual hopping of the 'extra' electron from one ion to the other. In the DMS material, if neighboring TM magnetic moments are in the same direction the TM-*d* band is widened by the hybridization between the up-spin states. Therefore, in the ferromagnetic configuration the band energy can be lowered by introducing carriers in the *d* band. In these cases, the 3*d* electron in the *partially* occupied 3*d*-orbitals of the TM is allowed to hop to the 3*d*-orbitals of the neighboring TM, if neighboring TM ions have parallel magnetic moments. As a result, the *d*-electron lowers its kinetic energy by hopping in the ferromagnetic state. This is the so-called double exchange mechanism. However, more recent calculations he electronic structures of ZnO-based dilute magnetic semiconductors performed by Katayama-Yoshida group within the self-interaction-

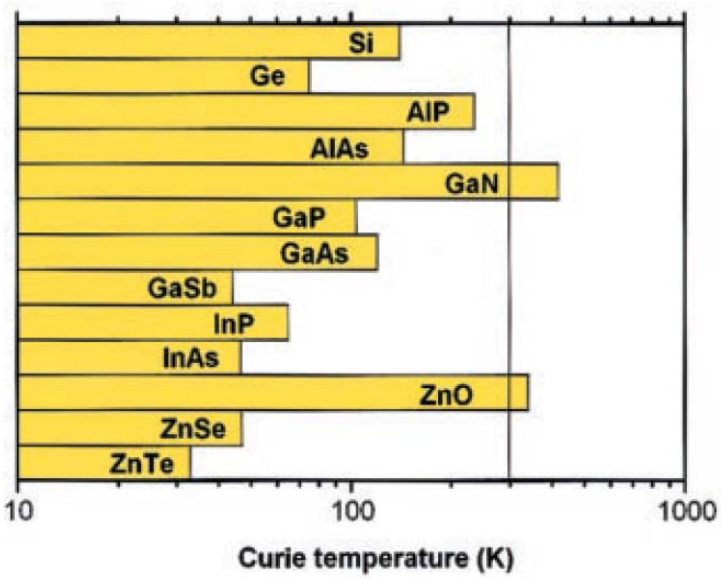

Figure 20. Theoretically predicted Curie temperatures as function of band gap in DMSs with a hole concentration of 3.5 x 10^{20}/cm^3 containing 5% Mn (After Dietl *et al.*[77]).

corrected local density approximation have shown that strong double exchange interaction is not expecting to work, except for (Zn,V)O.[87]

To summarize the theories used for description of DMS can be classified as follows:

-RKKY: Indirect exchange coupling of magnetic moments over relatively large distance via band electrons due to the Coulomb exchange. It becomes efficient when a high concentration of free carriers is present such as in metals for which it was developed.

-Direct super-exchange: Direct coupling of magnetic ions through overlap of magnetic orbitals.

-Indirect super-exchange Spins of two magnetic ions are correlated due to the exchange interaction between each of the two ions and the valence *p*-band.

-Double exchange: Couples magnetic ions in different charge state by virtual hopping of the 'extra' electron from one ion to the other through interaction with *p*-orbitals.

The first principles calculations predict that ZnO doped with transition metals V, Cr. Fe, Co, and Ni[88] show ferromagnetism for concentrations from 5 to 25%, whereas the Mn-doped ZnO shows spin glass state at ground state because of the exact half-filled d^5 state of Mn ions.[84] For comparison, V^{2+}, Cr^{2+}, Fe^{2+}, Co^{2+}, and Ni^{2+} have d^3, d^4, d^6, d^7, and d^8 electronic configurations, respectively, as illustrated in Fig.1.

In addition to the models mentioned above, an alternative model considers whether the ferromagnetic ordering of the Mn moments could originate from carriers (holes) that are present in the material but localized at the transition-metal impurity.[89,90,91, 92, 93,94,95,96] Furthermore, ferromagnetism in DMS has been accounted for by the formation of bound

magnetic polarons (BMPs).[89,90] The BMPs are formed by the alignment of the spins of many transition-metal ions with those of the much lower number of weakly bound carriers such as excitons within a polaron radius. The localized holes of the polarons act on the transition-metal impurities surrounding them, thus producing an effective magnetic field and aligning all spins. As temperature decreases the interaction distance (boundary) grows. Neighboring magnetic polarons overlap and interact via magnetic impurities forming correlated clusters of polarons. One observes a ferromagnetic transition when the size of such clusters is equal to the size of the sample.

IV.4. Experimental studies

IV.4.1. GaN-based DMSs

A number of approaches have been explored to synthesize single-phase (Ga,Mn)N, among which are ion implantation,[97] epitaxial growth[98,99,100,101,102,103] CVD growth of Mn-doped GaN nanowires,[104] and diffusion of Mn into GaN templates.[105] In many of these reports the observed ferromagnetic behavior above room temperature for (Ga,Mn)N have been attributed to spin-charge double exchange interaction. On the other hand, there are also studies,[97,106,107] which acknowledge the possible presence of secondary phases due to the low solubility of magnetic ions in GaN such as ferromagnetic Ga-Mn and ferromagnetic Mn-N alloys, as being responsible for the observations of ferromagnetism. Depending on the various preparation techniques of (Ga,Mn)N, these precipitates might in fact be the major contributors to the total magnetic moment of the samples investigated. Besides Mn-doped GaN, there are also reports on the doping with other transition metal ions in III-nitride materials, such as Mn-doped AlN,[108] Cr-doped GaN,[109,110,111] Cr-doped AlN,[109,112,113] Co-doped GaN,[114] Fe-implanted *p*-type GaN,[115] Gd-doped GaN,[116,117] and Vanadium (V) -doped GaN.[114] The solubility of TM elements in GaN is about 10% to form single phase solid solution. Generally the results obtained for these TMs are as conflicting as those for Mn-doped GaN. Cr-doped GaN was predicted to have the most stable ferromagnetic state in transition metal-doped GaN by Sato *et al.*[118] and Das *et al.*[79] using first principles calculations. Prior to the above-mentioned theoretical work, Cr-doped GaN single crystals[110] and thin films[111] have been grown and studied for their magnetic properties. Single crystal (Ga,Cr)N samples fabricated by adding Cr to GaN single crystal by flux method showed ferromagnetic T_C at 280 K, whereas the thin films grown by ECR MBE were reported to display ferromagnetic behavior with a Curie temperature higher than 400 K. Utilizing another magnetic metal, Shon *et al.*[115] reported implantation of Fe^+ ions into *p*-type GaN which gave rise to ferromagnetism based on their observations of apparent ferromagnetic hysteresis loops in individual measurements performed at 10 and 300 K. Ferromagnetism was confirmed by temperature-dependent magnetization measurements which yielded persistent ferromagnetism above 350 K. Vanadium, on the other hand, when implanted into *p*-type GaN films at doses of 3×10^{16} and 5×10^{16} cm^{-2}, has been found experimentally[114] to be paramagnetic up to 300 K, contradicting the theoretical

prediction[118] that V-doped GaN has ferromagnetic states even without any additional carrier doping treatment.

Gd-doped GaN is a peculiar system among other GaN-based DMSs, because the ferromagnetic order has been reported for the material containing as low as 10^{16} to 10^{17} cm^{-3} Gd[116,117,119] that rules out the possible presence of magnetic precipitates in sufficient amount. The case of (Ga,Gd)N looks to be especially promising for spin-manipulation based applications, because this material exhibits colossal magnetic moment per Gd ion (up to 4000 μ_B).[116] Such a high magnetization as well as the nature of ferromagnetic ordering in this material has been explained[120] in the framework of band coupling model suggesting the polarization of GaN matrix developed by Dalpian *et al.*[121] The results obtained by Dalpian and Wei[120] based on *ab initio* calculations suggest the GaGdN alloy to be antiferromagnetic. However, the picture changes with donors present in that the donor electrons mediate antiferromagnetically ordered Gd ions (due to now allowed interaction) stabilizing ferromagnetic ordering of the material. GaN doped with *f*-shell Gd drastically differs from GaN doped with *d*-shell TMs in terms of the exchange splitting at the energy band extrema. While *d* levels can couple mostly to the valence band maximum (i.e., free holes are needed to stabilize ferromagnetic phase), *f* levels can couple both to the valence band maximum and conduction band minimum. Anomalous Hall effect measurements seem to be the next natural step to confirm the theoretical explanation of colossal magnetic moment in (Ga,Gd)N through electron-mediated exchange.

IV.4.2. ZnO-based DMSs

For spin applications involving the ZnO family, the solubility of transition metal (TM) elements, especially Mn and Co, can reach up to 35 %. As already mentioned, ZnO too has received a great deal of attention, since ferromagnetism above room temperature was also predicted for Mn-doped ZnO-based DMSs in *p*-type (on the order of 10^{20} cm^{-3}) material[122] as well as for Co-doped ZnO in *n*-type ZnO[123]. However, magnetic properties of ZnO doped with variety of 3*d*-TMs resulted in conflicting experimental results (see the review by Liu *et al.*[80]). (Zn,Co)O[124], (Zn,Ni)O[125,126], (Zn,Sn)O[127], and (Zn,Mn)O[124,128,129] were found to be paramagnetic, while others reported ferromagnetism in (Zn,Co)O[130,131,132], (Zn,V)O[133,134], and (Zn,Mn)O.[135] Che Mofor *et al.*[136] have reported paramagnetic behavior of (Zn,Mn)O doped to moderate Mn concentrations, whereas the material containing about 19 % Mn showed a weak ferromagnetism which was attributed to Mn-rich clusters observed by TEM. Several recent studies on (Zn,Mn)O and (Zn,Co)O showed that any magnetic ordering is strongly method specific[130,135,137] and appears to be sensitive to chemical ordering of the TM ions and defects such as vacancies and interstitials.

IV.4.3. Limitations of conventional techniques and magneto-optical measurements

Most of the reports discuss observation of ferromagnetism or ferromagnetic-like behavior with apparent Curie temperatures near or above room temperature in TM-doped GaN and ZnO primarily in the context of magnetic hysteresis measurements performed by superconducting quantum interference device (SQUID) magnetometer in combination with x-ray diffraction (XRD) that may be insufficient for revealing the origin of ferromagnetic ordering. Many of compounds involving TMs and host elements of ZnO and GaN are ferromagnetic (see the review by Liu *et al.*[80]); however, conventional XRD cannot reveal second phase inclusions at the nm scale. Impurity-defect complexes may be another source of ferromagnetic order observed in DMSs using SQUID measurements. While some studies suggest a defect-mediated exchange involving oxygen vacancies[138], no direct observations of impurity-defect complexes in TM-doped have been reported in literature. At the moment, very little is known about complex-related magnetic ordering. The problem demands for much deeper theoretical and experimental microscopic studies. It should be kept in mind that SQUID measurements are very sensitive in that any clustering or second phase of magnetic ions would appear in magnetization, and X-ray and TEM measurements are too insensitive to detect them, leaving optical and magneto-transport measurements as the critical steps to be taken when possible.

New insight into the problem of the origin of ferromagnetism in TM-doped wide gap semiconductors GaN and ZnO is provided by studies of spinodal decomposition in these materials (a brief review by Dietl[139] describes the current status of the problem), illustrating the complexity of the problem. This particular argument for DMS considers phase separation or spinodal decomposition into regions with low and high concentration of magnetic constituents, and FM or AFM regions with high concentration determine the magnetic properties (through high blocking temperature).[140,141,142] For instance, even though it was proven by MCD measurements that (ZnCr)Te is intrinsicly ferromagnet,[143,144] Koroda *et al.* [142] have demonstrated recently spinodal decomposition in (Zn,Cr)Te co-doped with iodine as well as in the films grown under Zn-rich conditions, while the films co-doped with nitrogen or grown under Te-rich conditions have been homogeneous. The associated magnetooptical and magnetotransport properties of such a material were dominated by the formation of Cr-rich (Zn,Cr)Te metallic nanocrystals embedded in the Cr-poor (Zn,Cr)Te matrix. The formation of Ga–Mn secondary phases in (Ga,Fe)N has been suggested on the basis of spatial correlation of Ga and Mn detected by fluorescence mapping using synchrotron radiation microprobe (see Figure 21a).[145] The presence of ferromagnetic signatures was linked to the formation of Fe-rich nanocrystals in (Ga,Fe)N, as evidenced by TEM and EDS studies (Figure 21b).[146]

Several approaches to the control over the spinodal decomposition have been demonstrated. For instance, strain was observed to promote the decomposition.[147] Also, spinodal decomposition was blocked because of Coulomb repulsion when TM was charged, where the charge state of TMs can be controlled by co-doping with shallow impurities.[140,148] These studies provide the tools allowing one to utilize the spinodal

decomposition for fabricating structures with new functionalities through self-organized assembling of magnetic nanocrystals.

The interpretation of Hall effect measurements, a straightforward method that usually proves carrier mediated ferromagnetism via the detection of the anomalous Hall effect, is challenging for ZnO-based DMSs, because heavily doped ZnO ($3.2x10^{18}$ to $1.3x10^{20}$ cm^{-3}) exhibits a negative magnetoresistance due to *s–d* exchange coupling without any

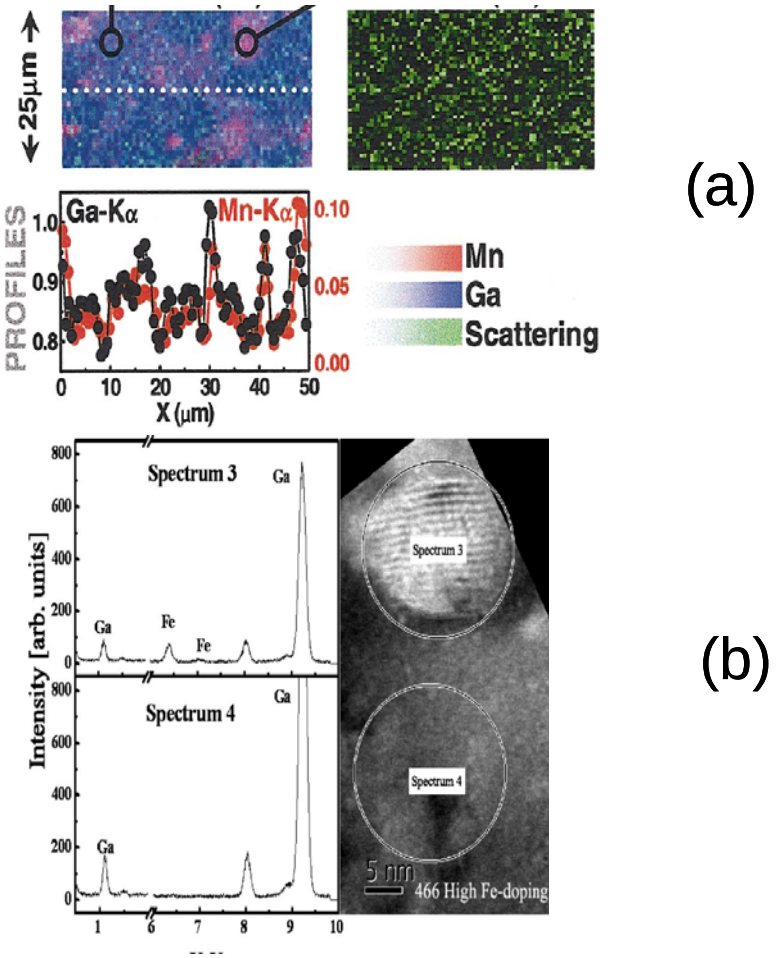

Figure 21. Microscopics images illustrating spinodal decomposition in (a) (Ga,Mn)N[145] and (b) (Ga,Fe)N.[146] (a) Red, blue, and green correspond to the Mn K_α, Ga K_α fluorescence line, and inelastic (Compton) scattering signal, respectively. Ga (in black) and Mn (in red) profiles along the white scan line are shown in the lower part. (b) EDS spectra for sample (left panel) taken around the precipitate (right panel) showing that the concentration of Fe is significantly enhanced in the region of the precipitate.

doping with TMs.[149] Another source of misinterpretation of the Hall data is an apparentanomalous Hall effect in a ferromagnetic metal/semiconductor structure due to the stray field.[150]

Moving to the optical techniques, magneto-optical spectroscopy probes the magnetooptical signal as a function of photon energy, and can be used to probe the magnetic properties of the DMS materials only. The magneto-optical effect in dilute magnetic semiconductors is directly related to the interaction between the *d*-electrons of the transition metal ions and the *s,p* electrons of the host semiconductor. Therefore, it is possible to separate intrinsic and extrinsic contributions. Particularly, MCD spectroscopy is useful for thin film studies because the effect of substrate on the spectrum is negligible contrary to magnetization measurement. Magnetic field applied to DMS results in spin-dependent Zeeman splitting of energy bands (Figure 22). The MCD signal is enhanced at the absorption edge of DMS host semiconductor in addition to other critical points,[151,152,153,154] which comes about as a result of carrier-mediated exchange interaction between the localized spins. When the MCD signal is proportional to the applied magnetic field one can surmise paramagnetic behavior. Ando *et al.*[151, 155] discussed the advantages of magneto-optical spectroscopy for characterizing. DMSs. MCD can be used to detect the difference in optical absorption or reflection for left and right circularly polarized light in the presence of a magnetic field parallel to the light propagation direction. It is well known that an external magnetic field causes Zeeman splitting of the atomic energy levels. In DMS, the magnetic field effect on the *s,p*-band electrons is amplified by the magnetic moment of the transition metal ion through the *s,p-d* exchange interaction causing enhanced splitting of the band structure. A strong MCD signal indicates a strong *s,p-d* exchange interaction, and the polarity (positive or negative) of the MCD signal at the critical point (CP) energies can be used to interpret the polarity of the exchange constant. To make the point clear the schematic band splitting of $Cd_{1-x}Mn_xTe$ at the Γ point, which has been studied in detail (the picture is not perfectly clear yet in GaN or ZnO), is shown in Figure 23.[155] Each material has its own set of CP energies reflecting its electronic band structure. The CP of the band structure will clearly show up in the MCD spectrum, which provides a fingerprint for each material. This allows the identification of the material that is responsible for the observed MCD signal.

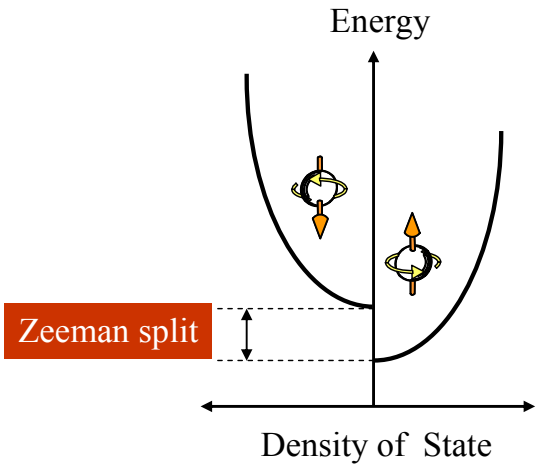

Figure 22. Schematic of Zeeman splitting (courtesy of K. Ando of National Institute of Advanced Industrial Science and Technology, Japan).

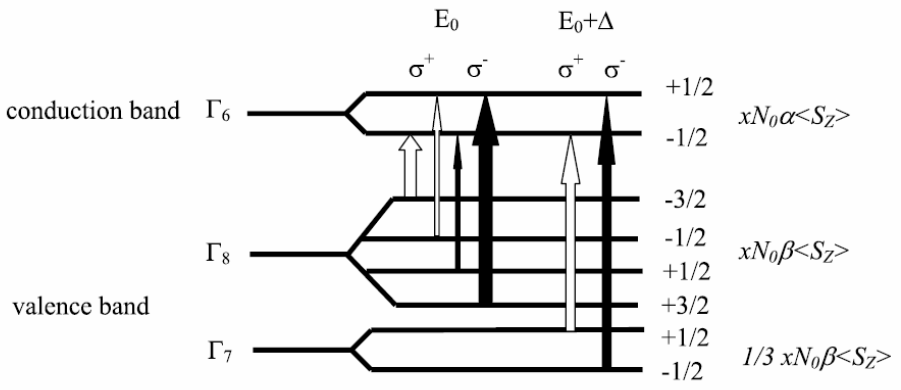

Figure 23. The schematic band splitting of $Cd_{1-x}Mn_x$ Te at the Γ point. Here x is the concentration of magnetic ions, and $\langle S_Z \rangle$ is the average component of the spin of the magnetic ion along the external field in the z direction. $N_0\alpha$ is the s-d exchange constant, and $N_0\beta$ is the p-d exchange constant. σ^+ represents the right circular polarization, and σ^- represents the left circular polarization (after Ando *et al.*[153]).

Intrinsic ferromagnetism in $In_{1-x}Mn_x$ As[156], $Ga_{1-x}Mn_xAs$[154], and $Zn_{1-x}Cr_xTe$[143,144] has been confirmed to be DMS-like by using MCD spectroscopy. To investigate the magneto-optical properties of ZnO, Ando *et al.*[151,152] measured the MCD spectra in films alloyed with Sc, Ti, V, Cr, Mn, Fe, Co, Ni, and Cu using pulsed laser deposition. Figure 24 shows the MCD spectra of (0001) oriented (Zn,TM)O films. The high quality of the ZnO film grown on a lattice-matched $ScAlMgO_4$ substrate led to a small but clear MCD structure at the band gap 3.4 eV. Other films were grown on lattice-mismatched Al_2O_3 substrates. ZnO films doped with Mn, Fe, Co, Ni and Cu show clear MCD structures near 3.4 eV. Therefore, the authors argued that these TM-doped ZnO are DMSs. The films alloyed with Sc, Ti, V, and Cr did not show any noticeable magneto-optical effect and could therefore be deemed as antiferromagnetic. The magnetic field and temperature dependence of the MCD spectra for the DMS films show that all these films are paramagnetic.

Employing MCD spectroscopy Ando[157] showed the presence of s,p-d exchange interaction in a room-temperature ferromagnetic (Ga,Mn)N film. Furthermore, both the magnetic field dependence and the temperature dependence of the MCD intensity confirmed that the $Ga_{1-x}Mn_xN$ sample measured was a paramagnetic diluted magnetic semiconductor and it was thus postulated that the ferromagnetism of the sample arose from some unidentified material which may not be detectable by X-ray diffraction.

However, as was discussed above, the properties of TM-doped ZnO and GaN depend crucially of material quality, which is, most likely, the main source of conflicting reports claiming the presence or absence of ferromagnetism in these materials. In contrast to

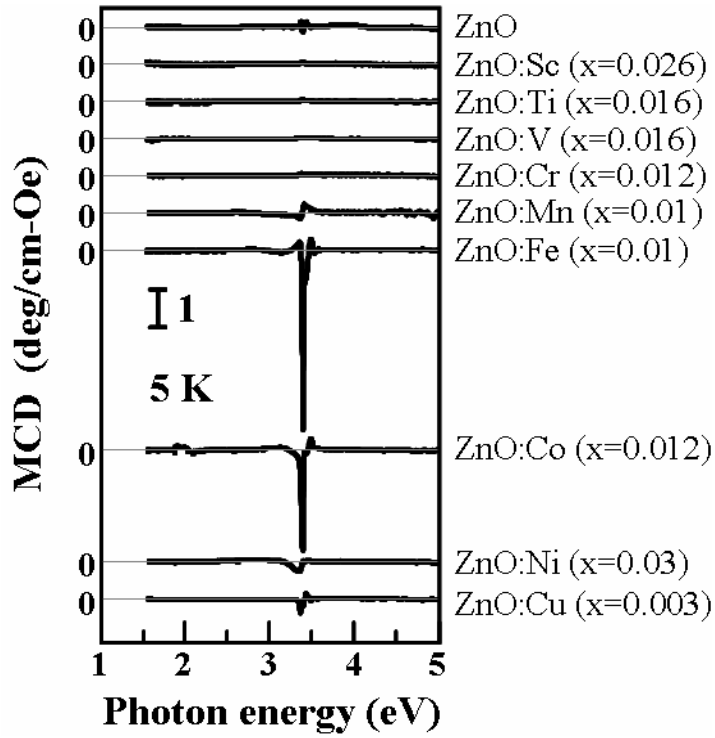

Figure 24. Transmission MCD spectra of ZnO and ZnO:TM (after Ando et al.[151,152]).

early reposrts, recent magneto-optical measurements performed on high-quality (Zn,Co)O[158], (Ga,Mn)N[159], and (Ga,Fe)N[160] point to strong ferromagnetic ordering in these materials.

Characterization of the *s,p-d e*xchange interaction has been one of the main topics for the II–VI based DMSs. The confirmation of the *s,p-d* exchange interaction is the most important task to be carried out when the synthesis of new true DMS materials are attempted.

IV.5. Spin-injection from GaN- and ZnO-based DMSs

Many proposed device applications of DMSs demand injection of spin-polarized carriers into the active device region (spin light emitting diodes (LED), spin field effect transistor,[161] *etc.*). One rather straightforward way to measure the degree of spin polarization of free carriers is to measure the degree of circular polarization of light emitted from a spin LED. However, the situation in wurtzite materials is quite different from that in zinc-blend materials. Early experiments have shown the absence of spin polarization in electroluminescence and the photoluminescence (PL) from InGaN/GaN spin LEDs, which was suggested to result from fast spin relaxation.[162,163]

The degree of circular polarization depends on the oscillator strengths of transitions involving heavy hole (HH) and light hole (LH) valence band states and the spin

coherence time. Therefore, these quantities should be measured before further characterization. In order to measure the spin coherence time and to estimate the spin

polarized carrier injection efficiency from the electroluminescence data, the selection rules and the valence band structure in wurtzite structures must be understood. The valence band in wurtzite materials is split into three bands (A, B, and C) due to crystal field and spin-orbit coupling. The spin degeneracy of these three bands and the conduction band is lifted in the presence of a magnetic field resulting in small symmetric Zeeman splittings, as shown in Figure 25 near the Γ point.[164] The allowed transitions following the selection rules $\Delta L_z=\pm 1$ (in $\sigma^{\pm}$ polarization, respectively) are indicated by the arrows (σ^+ right, σ^- left circular polarization). Initial evaluation of spin coherence in a spin LED may be done optically. A net spin polarization of the photoexcited carriers can only be achieved when optical excitation ensures preferential spin orientation. Whether or not circular polarization can be observed in wurtzite semiconductors where the spin-orbit coupling is small is still being debated. Some experimental results suggest that it might be unlikely in GaN-based light emitting diodes.[163] Even if it were the case for GaN, the ZnO system has some differences as will be discussed below and it has not been subjected to much experimental research.

The degree of circular light polarization is defined by $\boldsymbol{P_{circ}=[I(\sigma^+)-I(\sigma^-)]/[I(\sigma^+)+I(\sigma^-)]}$, where $I(\sigma^{\pm})$ is the intensity of the $\sigma^{\pm}$ polarized light. The degree of spin polarization in terms of the spin populations ($n\uparrow\downarrow$) is $\boldsymbol{P_{spin}=[n(\uparrow)-n(\downarrow)]/[n(\uparrow)+n(\downarrow)]}$. Therefore, the relationship between P_{spin} and P_{circ} is needed. For strong spin–orbit interaction as in GaAs (Δ_{so}=340 meV), this is easily obtained even for bulk samples with degenerate HH and LH states, as the optical transitions involving the HH states are 3 times stronger than those involving the LH states (therefore, $P_{spin} = 0.5\ P_{circ}$). For wurtzite materials, however, where the spin-orbit coupling is much weaker [Δ_{so}(GaN) = 4 meV, Δ_{so}(ZnO) = 4 meV], the strength of these transitions for these valence bands (i.e. A and B bands) are suggested to be comparable.[163, 165, 166, 167] Therefore, one complication here is the possible cancellation of the PL polarization due to a spectral overlap of the radiative transitions involving A and B bands with opposite polarization when both the heavy and light hole valence band states are populated, governed by their densities of states, owing to small A-B splitting. Note that these results should only be

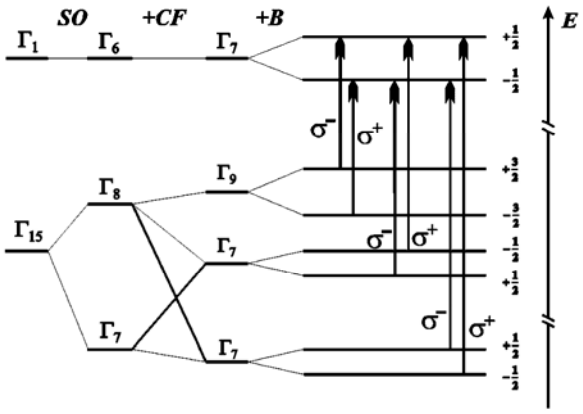

Figure 25. Breaking symmetry scheme of the conduction and valence bands in wurtzite phase. The allowed transitions are marked by arrows (after R. Stepniewski *et al.*[164]).

considered for now only as preliminary data, because even the intrinsic ferromagnetism in GaMnN is still under question. The degree of free-carrier spin polarization in TM-doped GaN and ZnO has not been measured yet as well.

IV.6. Applications

In today's networked world information is carried by charge carriers, stored by localized magnetic moments, and transmitted increasingly by light beams. However, there is a growing recognition that devices exploiting spins as information carriers — so-called spintronic devices — could provide such advantages as nonvolatility, increased data processing speed, decreased electric power consumption, and increased integration densities compared to conventional semiconductor devices. By now, there have been various proposed devices exploiting spin manipulation such as the spin field effect transistor (FET) proposed by Das and Datta,[161] spin light emitting diodes (LEDs), spin resonant tunneling device, optical switches operating at terahertz frequency, modulators, encoders, decoders, and quantum bits for quantum computation and communication.

At the moment, magnetic random access memory (MRAM) based on magnetic tunnel junctions (MTJ) are the only commercial devices exploiting spin manipulation (Figure 26, reference [168]). MRAM is based on the difference in tunnel currents between the two ferromagnetic materials separated by a thin dielectric layer for parallel and antiparallel magnetizations. The 4 Mb MRAM chips targeted to replace SRAMs were marketed by Freescale Semiconductor in July 2006.The problem here is that SRAM technology is huge and in place already.

MRAM provides the following advantages:
-Nonvolatility: (> 10 years);
-Fast read, write, erase, access times (30 nsec);
-Durable: > 10^{15} read, write, and erase cycles;
-Radiation hardness.

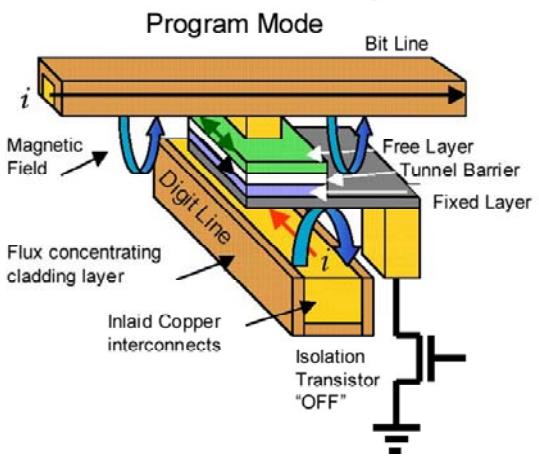

Figure 26. MTJ based MRAM (courtesy of M. Johnson of Naval Research Laboratory).

Most promising candidate for next generation MRAM is based on MTJs with MgO barriers. [169 , 170] As illustrated in Figure 27 (reference [171]), the magnitude of MTJ signal in the structures with MgO barriers can reach tunnel magnetoresistance (TMR) ratios of few hundreds of percents.

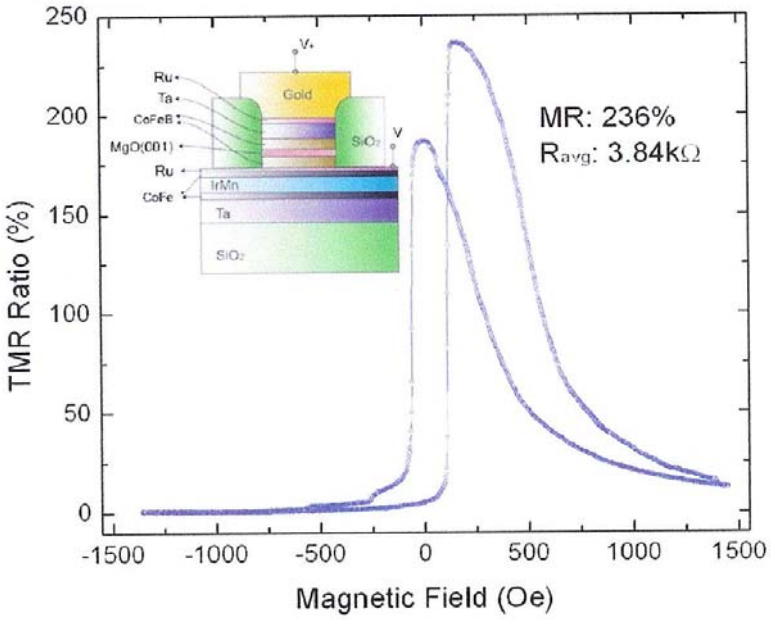

Figure 27. TMR curve of a typical MTJ with a 1.6-nm-thick barrier after annealing at 425 °C. The inset shows the schematic cross section of the fabricated MTJ (after Weifeng Shen *et al*.[171]).

IV.7. Conclusions

Above room temperature ferromagnetism in GaN and ZnO would lead to the use of these materials in devices exploiting not only the electron charge but also the electron spin. There have been many reports of ferromagnetic behavior in magnetic ion doped GaN and ZnO, many indicating well above room temperature Curie temperatures. SQUID magnetometry, which is too sensitive, has been the main measurement technique to identify ferromagnetism. Optical measurements have not been all that much consistent with magnetization measurements, opening the door to many questions. At the present time, much more still has to be done to understand the phenomena observed in wide gap semiconductors GaN and ZnO doped with TMs.

On the theoretical side, the results from different theoretical approaches do not agree well with experimental data. Presumably, no single model is capable of explaining the properties of a wide class of purportedly dilute magnetic semiconductors including ZnO and GaN with their many variants. Additionally, the information about microstructure of DMSs is insufficient and lack important detail. In this vein, extended X-ray absorption fine structure and scanning transmission microscopy studies of DMS can shed light on

the detailed microscopic structure of the lattice, which is more complicated than assumed in at least some of the theoretical approaches reported and discussed here.

On the experimental side it is still not sufficiently clear if the uniformly doped hosts or some other phases or even defect-impurity complexes are responsible for the observed magnetic hysteresis in magnetization measurements. Invoking the other techniques, e.g. MCD measurements, can shed some light on the intrinsic or extrinsic nature of magnetic ordering in these materials. Again, the state-of-the-art techniques for structural investigations can give a better insight into the phase composition as well as the nature of defect-impurity complexes. Conclusive demonstration of injection of spin-polarized carriers from GaN- and ZnO-based structures is an imperative step towards device applications. One more important issue that must be resolved theoretically and confirmed experimentally is the existence of carrier-mediated ferromagnetic exchange in these materials, which is the most desirable exchange mechanism for devices exploiting spin polarized carriers.

V. Reliability of GaN-based field effect transistors

V.1. A primer into microwave GaN heterojunction field effect transistors (HFET) status

- GaN FETs vigorously pursued in industry for commercial and military applications.

- Primary commercial applications (2-4 GHz): WiMax , wireless base station.
  - Nitronex, RFMD, Cree, Eudyna.
- Primary military applications: S- and X-band radar, wide bandwidth jammers and decoys (through MMW), low-noise amplifiers.
  - Raytheon, Cree, TriQuint, HRL, BAE, Northrop-Grumman.
- Performance attractive for both military and commercial applications.
- Some think that insertion is just around the corner.
  - BUT
  - Reliability remains a major technical hurdle.
    - Notable improvements in reliability, but lacking consistency.

The dark side of GaN HFETs II

- DC based MTTF data are ~10^6 at 140 ^{O}C but do not necessarily hold up at RF stress wherein the gate is swung between reverse and forward bias.

- Some devices perform reasonably well in RF, but others even from the same wafer do not. No predictability as to the longevity??

- High electric fields, much higher than faced in GaAs HFETs, together with coupled phenomena of electric field (polarization), temperature, and mechanical strain exacerbate the situation causing catastrophic failure through defect generation.

- Field plate used to reduce the electric field near the drain side of the gate limits device operation to RF communications band.

- GaN on SiC is prone to cracking, even if avoided after growth, cracks appear during repeated bias stress (thermal cycling).[1]

- IV characteristics show electron trapping at the surface, in AlGaN bulk, GaN buffer and as such are biased dependent and show frequency dispersion.

[1] Y. Nanishi, "degradation issues in GaN HFETs", ZnO/GaN workshop Oct.17-18, 2007, Richmond VA USA

- Gate current causes extension of the gate depleting the drain side of the channel with long time constants and causing gate lag.

- The RF power and efficiency are not as high as can be expected from DC I-V characteristics

- Strong electron and phonon coupling leads to hot phonon populations, velocity degradation, difficulty to remove heat.

- Metal, contact and Schottky, phase change after extended high power operation is potentially disastrous

- High defect concentration and associated inhomogeneities cause permanent degradation due to defect generation, exacerbated by strain, polarization, temperature coupling at the drain side of the gate

What is needed

- Understanding of the failure mechanisms at the fundamental semiconductor level, including gate leakage, rapid RF degradation, and inconsistency

- Understanding velocity limitation and heat removal bottlenecks, and defect generation during stress.

- Devising structures to address the above mentioned fundamental problems

- Understanding of the inter-metallurgy and metallurgy semiconductor interdiffusion and phase change

- Devising models that would be predictive of the device longevity.

V.2. Introduction

The exciting news is that the GaN-based FET devices have come a long way and are already exceeding the performances of the mature GaAs-based technologies in power. It is expected that the GaN-based FETs will play major roles in the high power, high frequency military and commercial arenas for microwave and millimeter wave transmitters and receivers for communications and radar devices, but not before serious reliability issues are addressed.[172] High frequency operation, however, also requires that the need for field plates, which spreads the electric field, is obviated without losing ground on the drain voltage front. Commercial devices operative in the communication band, about 2 GHz, are already available that boast quite impressive performances. The show-stopper is that the reliability of the devices, however, still remains to be adequately addressed in that the reports of longevity are inconsistent with researchers still seeking to

understand the trapping and degradation mechanisms. This is affront to the backdrops of some of the commercial players radiating the message that all is well, although not all devices even from the same wafer show similar longevity and RF stress takes more of a toll than the standard 3 temperature extrapolation-based predictions of the lifetime. It is a fact that we do not fully understand the degradation mechanisms from which these materials suffer. If we hope to make consistent, reliable predictions of device lifetimes, particularly when the devices are being pushed to RF operation near their limits, more work will need to be done in characterizing the long term stability of the devices, and quite clearly new physical models for the failure mechanisms will have to be developed.

Peak performance wise, GaN is doing well, and is poised to command the (now GaAs dominated) commercial market in high power, high frequency applications. The clincher, however, is the lifetime and just as important if not more its predictability on a reliable basis. As a specific example for peak performance, the NPT35050A HFET (a GaN on Si technology available from Nitronex)[173], designed for 3.3-3.8GHz WiMAX applications boasts a typical OFDM performance at V_{DD}=28V, I_{DQ}=750mA of >50W P_{3dB} @ 3.5GHz, drain efficiency ~18% at 6W, with gain 12dB @6W. Also, a number of industry standard (JEDEC) reliability tests such as DC and RF HTOL and ESD tests have been passed by this device, as well as MIL standard technological tests for vibration, shock, moisture resistance, etc. (See Reference [174]). RF drift has been reduced to nearly no change in 500hrs operation. 3-temperature (3T) DC lifetime tests fit well to Arhenius-type behavior with 2.0eV activation energy (E_A). (See Section III.B.) This measurement translates into 10^7 hr lifetime for devices at 150°C. This is further validated (by predicting) that E_A at 200°C (10^7 hr) is valid to 215°C—providing some confidence in the Arhenius E_A and thus lifetime figures quoted. However, 3T fits are not satisfactory above 310°C and are not consistent with RF stress tests available in GaN HFETs in general, not to mention the all too important predictably of the 3T test itself. Therefore, it is imperative that some yet to be uncovered mechanism, likely affecting unpredictability of lifetime as well as vast variation among HFETs even on the same wafer be uncovered. The causes of reversible and catastrophic failure mechanisms under RF stress and at higher temperatures would need to be explored. We should mention that polarizability of GaN, which was touted initially as being a blessing, temperature and mechanical strain are coupled. In addition, the strong electron-phonon coupling leading to a hot phonon population to be built up which degrades carrier velocity and heat dissipation are serious issues that must be dealt with. The very high fields which GaN is supposed to withstand, give rise to a hot region by the gate edge on the drain side, causing local strain and parametric changes in properties of GaN and also couples with local defects to create more defects leading to hard failure. Below, we discuss the performance of GaN based HFETs, known mechanisms in effect affecting failure, and what the future holds.

Furthermore, some of the best devices from the laboratories in terms of total power in one package as well as cutoff frequencies are given in Figure 28.

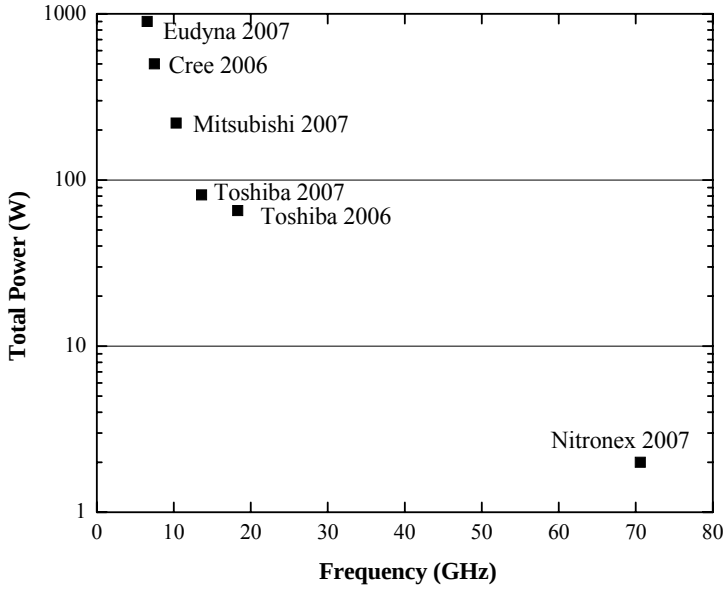

(a)

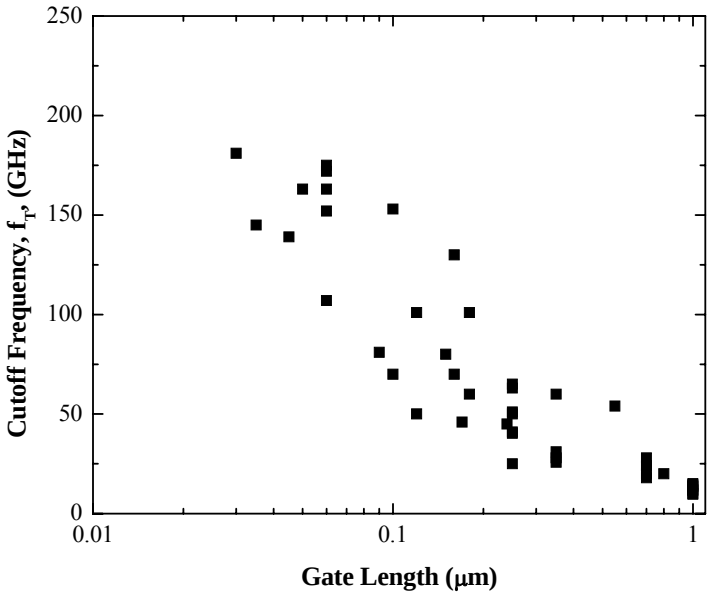

(b)

Figure 28. (a) Demonstrated total power achieved by GaN-based HFETs from various laboratories. (b) Demonstrated cutoff frequencies, f_T.

But, can we really predict 10^7 hour lifetimes (>1100 years), predicted from innocent 3 temperature failure data, for real devices? Most probably not! There are high fields present in the GaN-based devices (made possible by the high breakdown field of

the material, ~5x10^6 vs. ~4x10^5 Vcm^{-1} for GaAs-based devices). The same high field induced strong piezoelectric response of the GaN system means that we must rethink our traditional GaAs-based reliability predictors. The typical GaAs-based approach to characterize failure is depicted schematically in Figure 29. Depending on the failure rate *vs*. operating time, there are three regimes of failure termed infant, random, and wear-out. Some devices suffer what is called the early (infant) failure, occurring earlier than usual for a device and addressed commercially by a "burn in" procedure to ensure that devices that will suffer from such failure do so in the factory rather than in the customer's hands. This is followed by random failure, which generally occurs at a relatively constant rate over the lifetime of a device. And finally, devices enter the realm of wear-out failure, altogether leading to a bathtub-shaped dependence on time. Ideally, it would be desirable to eliminate the infant and random failures and reduce the wear-out failure rate to the extent possible.

The genesis of the reliability problem is generally rather difficult to comprehend unless the specific failure mechanism is illuminated. Typically, there are both reversible and sudden or gradual catastrophic (nonreversible) failure mechanisms simultaneously at play. Reversible degradation, such as that caused by non-regenerative point defects capturing electrons temporarily is characterized by recoveries with time constants congruent with the dominating trap/defect. The catastrophic failure mechanisms can be attributed to defect generation and metallurgy/mechanical (strain induced) failure. Schemes to ascertain the existence and importance as well as methods to retard the appearance of these various degradation phenomena, ultimately giving rise to failure, will be addressed in Sections II and III.

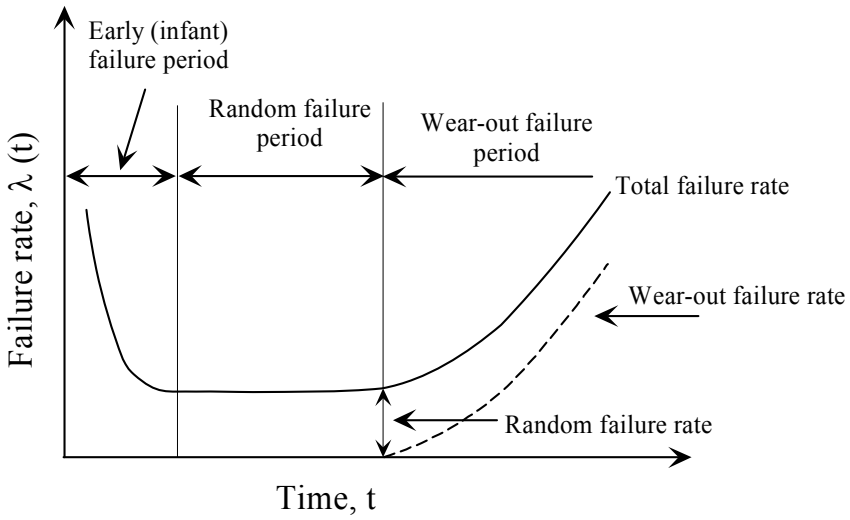

Figure 29. A schematic representation of three failure regions, namely infant failure experience very early on, random failure period, and wear our failure. Courtesy of A. Christou. (after Christou [175])

The notion that the operation and reliability of the GaN system requires additional consideration over the existing GaAs-based predictors is further evidenced by the fact that oftentimes DC measurements do not accurately predict RF performances, and that DC accelerated life testing does not correlate with RF degradation. The questions that must be addressed in order to bring the GaN-based devices to maturity, particularly bringing the reliability to a reasonable and predictable point are: What are the mechanisms responsible for the root causes of failure? How can we observe, characterize, and contain/eliminate these mechanisms? How do we translate these physical phenomena into statistical distributions in order to make predictions at production scales? *Specifically: What is the nature and origin of the high density of traps on the AlGaN surface? How can we control the interface roughness and additionally achieve high Al concentrations in the barrier? Can we accurately simulate the devices with their strongly coupled piezoelectric, strain, electric field, and pyroelectric effects? What types of radiation are most strongly affecting the GaN crystals for space applications?*

Inconsistencies in lifetime will continue to plague the GaN system unless properly addressed. To give a flavor of the wide variance between devices even on the same wafer, in one particular test of RF stressing (V_{drain}=30V, I_{DQ}=100mA/mm, f=4GHz), gate lag reduced by 0-20%, P_{out} changed by 0dB to >-2dB after 24hr stress, and threshold voltages changed by 0 to 0.5V.[176] The question to be begged here is whether we are in fact creating defects during stressing and how can be avoid doing so? Looking at cross sectional TEM images of a degraded device (see Figure 30), the interface of AlGaN/GaN clearly shows some modification at the gate edge (in interfacial oxide layer and in the AlGaN crystal).[173,176] But what kind of dependence on temperature does this modification have? Is it related to the increase in gate current that is seen in many degraded devices? Is it mitigated by preexisting defects in the GaN channel material? The point is that across the same wafer, one can find devices with both reasonably long and short lifetimes. It does seem that DC stress does not degrade RF performance nearly to the extent that RF stress does. Furthermore, transients are typically unchanged after this degrading RF stress, which points to a mechanism relating degradation to the increased gate leakage after the RF stress.

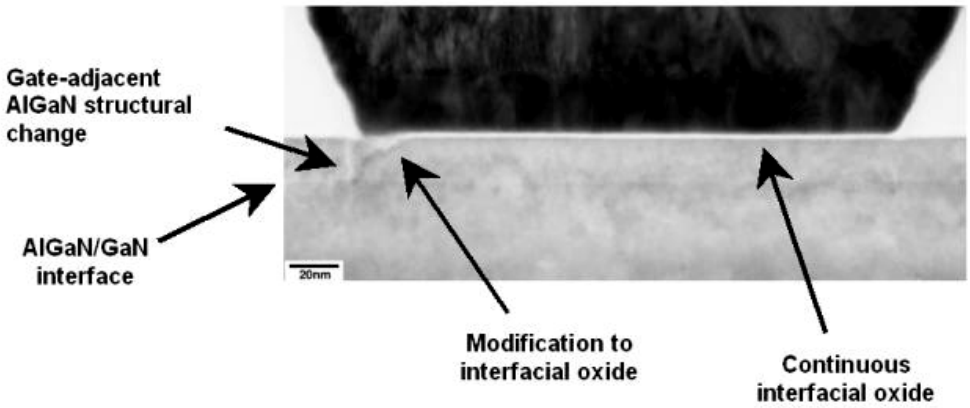

Figure 30. Cross-sectional TEM of a degraded AlGaN/GaN FET illustrating some sort of modification in the crystal structure at the AlGaN/GaN interface as well as in the interfacial oxide layer at the drain side of the gate. (after Binari *et al.*[176]).

V.3. Degradation and Reliability

V.3.1. Terms

Let us quickly define the terms that we will use in describing trapping and degradation phenomena, which are believed to be truly at the heart of the reliability of the devices. Trapping mechanisms are still not completely understood, although a great deal of work has been dedicated to determining its causes and eliminating its effects. The terms that will be discussed are current collapse, gate lag, drain lag, frequency dispersion, power/current drift, and power/current slump. Trapping can occur in the GaN buffer layer, at the heterointerface, in the AlGaN barrier layer, or on the surface, and there is not a one-to-one correlation between types of traps and observable effects.

In reviewing the GaAs literature (where most trapping phenomena have been observed before, giving us a good starting point for assessment of trapping in GaN) the term ***current collapse*** refers to the reduction in drain current that occurs after the application of a high drain bias. This phenomenon is reproducible and recoverable and occurs due to hot carriers being injected to and trapped in the barrier layer as a result of being accelerated in the region of high electric field (real space transfer).[177]

The ***gate lag*** and ***drain lag*** correspond to time delays in the drain current when the gate voltage or the drain voltage is suddenly changed, respectively. The phenomenon of gate lag is related to traps on the surface of the AlGaN barrier layer, and thus efforts to reduce it using passivating layers (silicon nitride and other dielectrics have been undertaken and the lifetime/reliability of these passivating layers are of course related to the overall reliability of the HFET device, but this is a whole other story), annealing, or various surface treatments have been successful. The drain lag has been attributed to traps located spatially in the buffer layer, which would require better quality buffer layers and/or insertion of a barrier, but surface treatments have also been shown to reduce the drain lag, so there is at least some portion of the drain lag that is associated with the surface traps. In either case, at RF frequencies, the overall movement of charge and transients associated with this movement is the issue at hand as we consider lag effects.

Devices with significant gate lag typically also suffer from ***transconductance dispersion***, wherein the transconductance measured at DC does not coincide with that measured at high frequency—at high frequencies the traps beyond the exponential decay associated with transit time and feedback capacitance charging time. This is one type of ***frequency dispersion***, another being ***output conductance dispersion,*** or ***output resistance dispersion***, which can be correlated with the drain lag.

Kinks have been observed in the drain current vs. drain voltage for HFET devices, particularly evident at low temperatures.[178] The phenomenon can be attributed to additional carriers being generated by impact ionization. The holes generated in the process tend to reduce the total charge (say, on the surface) by electrons that results in

virtual gating (and thus current collapse). It was therefore predicted and experimentally shown that this effect does in fact compete with the room-temperature dominating current collapse and results in increased drain currents at low (<200K) temperatures.[179]

Finally ***current drift*** or ***power drift*** or ***slump*** refer to decreases in time of current or power, either recoverable (***drift***) or nonrecoverable (***slump***). Drifts are manifestations of the above mentioned trapping (lag) phenomena, while slumps can be considered to be related to the hot phonon/hot electron/high field-induced defect generation and related degradation. While these terms and phenomena are general and more the "macro" effects of the underlying physical phenomena, they are nonetheless useful in discussing the overall utility of a device in a real application.

V.3.2. Materials Issues

V.3.2.1. Crystal Quality

It would be prudent to mention first that a great deal of the issues related to degradation and to experimental device performances not being as high as they should be in principle is related to the GaN or AlGaN material quality which is aggravated by the piezoelectric nature of the material. Traps in both the barrier and buffer layers as well as at the heterointerface are sites at which electrons can reside, resulting in virtual gating, current reduction, and frequency dispersion as traps have some charging and discharging time constants associated with them. Dislocations, even when they are fully coordinated owing to high piezoelectricity, are known to both collect traps and form other complexes, and are also known to be effective leakage sites for reverse-biased GaN Schottky contacts.

That being said, it is interesting to note that despite the desire to reduce the threading dislocation density to improve the Schottky performance, it has been shown that thinner GaN buffer layers result in lower current (measured simply as current through a pair of ohmic contacts) and higher breakdown fields, despite the increase in the density of threading dislocations.[180] Additionally, in thinning the GaN thicknesses, the Schottky behavior as well as Hall data looks unchanged in AlGaN/GaN heterostructures. The reduction in current can be attributed to the fact that the threading dislocations are acting to compensate the unintentionally doped GaN (as acceptor states tend to localize along the TD).

An additional point to be made regarding the quality of the crystal is that of the interface roughness at the AlGaN/GaN interface. While the desire to increase the sheet carrier concentration in order to attain very high currents can be achieved by increasing the mole fraction of Al in the barrier layer, as this increase in Al concentration exceeds 30%, sheet resistance increases (due to alloy scattering or interface roughness or both). Additionally, the gate leakage tends to increase as Al concentrations exceed 30%.[181] In order to achieve high sheet densities while at that the same time eliminating the need to

move to large AlN mole fractions in the AlGaN barrier layer, groups are investigating the use of (lattice-matched) InAlN barrier layers.[182]

Thin AlN spacer layers between the AlGaN and GaN have been effective in improving mobility and electron velocity values in the 2DEG at the AlGaN/GaN interface by reducing the alloy scattering and reducing the ionized impurity scattering. However, it has been indicated that gate contacts are unstable after application of stress gate forward currents more than 5mA/mm in devices with an AlN spacer layer. Comparing HFET structures with and without AlN barriers, it was found that a HFET without an AlN barrier structure was more stable, even when stressed to high forward currents more than 100mA/mm.[183,184] The issue at hand here could be oxidation of the AlN, hot electron degradation, and/or relatively high strain, during stressing, resulting in poorer reliability in devices employing AlN layers. We should mention that Al-containing alloys have been shown to be notorious for causing lifetime degradation in electrical and optical devices and Al-free layers have been developed to combat this.

Eventually, GaN substrates would be needed for longevity. In addition, the point is that semi-insulating or at least high resistivity buffer layers are also required for high frequency applications. Therefore, the buffer layers must be compensated by one mechanism or another. Typically Fe doping is used and thus its stability and/or the effect of the deep levels created would be an issue to contend with. More importantly, all of the issues comprising of dislocation density and of Schottky gate leakage, of strain and of sheet charge density, of Al mole fraction in the barrier and AlN use in the spacer layer, must be addressed in tandem and inevitably some compromises will have to be made.

V.3.2.2. Surfaces

The reliability problem in GaN HFETs has been generally attributed by the practitioners to surface processing and passivation because significant performance variations are observed as these steps are altered. For example, it has been shown that a basic mechanism involving quantum mechanical tunneling of electrons from the gate electrode on the drain side to the surface of the semiconductor exists, particularly when subjected to high terminal voltages.[185,186] Electrons leaking from the gate electrode to the surface of the semiconductor have been shown to affect the reliability.[187]

When a high drain bias voltage is applied, imperative for high power operation, and the HFET is driven with a large RF input signal, the peak voltage at the drain can attain a magnitude essentially twice the magnitude of the DC bias voltage in class A operation. Simulations indicate that the magnitude of the electric field at the edge of the gate electrode on the drain side can easily exceed 6-8 MV/cm, which is sufficient to produce quantum mechanical electron tunneling at the gate terminal. The electrons that tunnel from the gate electrode can (*i*) accumulate on the surface of the semiconductor next to the gate on the drain side (can be modified by surface passivation), (*ii*) move along the surface by a trap-to-trap hopping mechanism, creating a gate-to-drain leakage current, or (*iii*) if the energy of the electrons is sufficiently high, avalanche ionization

could occur on the surface. If ionization does end up occurring and band structure permitting, light might be observed emanating from the gate edge. Light emission from the gate edge is often observed in the large-signal operation of GaAs MESFETs, but so far has not been observed in AlGaN/GaN HFETs.
When the electrons accumulate on the surface of the semiconductor near the gate between it and the drain, a "virtual gate" effect is created causing an effective lateral extension of the gate toward the drain. As the electron tunneling proceeds, the density of electrons on the semiconductor surface increases. The electrons so accumulated on the surface create an electrostatic charge that causes a partial depletion of the conducting channel electrons, thereby causing a reduction in the channel current, and a corresponding decrease in the RF output power. Electron tunneling continues as long as the device is operating. Therefore, the degradation is a function of time, which creates a reliability problem. The shift in the forward turn-on voltage and the magnitude of the reverse current are affected by the degree of electron tunneling experienced by the gate. This process is reversible in that when the bias is removed and sufficient time allowed for equilibrium to be reached, the original operating characteristics would be restored.

The current conduction characteristics evolve as improved device design, surface processing, and passivation are implemented. It is possible to modify and reduce the tunnel leakage *e.g.* by use of an optimized field-plate HFET design. However, the field plate, while effective in reducing the electric field by spreading it out, degrades high frequency performance by increasing the gate-drain capacitance. A better solution seems to lie in reducing if not eliminating the current conduction paths such as surface state and bulk defects in the barrier as well as improving the layer quality and optimizing device design for a better robustness.

There are two current paths for gate leakage, as shown in Figure 31. The main path is surface leakage with electrons flowing along the AlGaN surface to the drain contact. The other source of leakage is the gate/channel leakage wherein electrons flow through the barrier to the channel below. In any case, electron conduction occurs by a trap-to-trap hopping mechanism which is inherently very slow, where both thermionic emission and tunneling are likely involved.

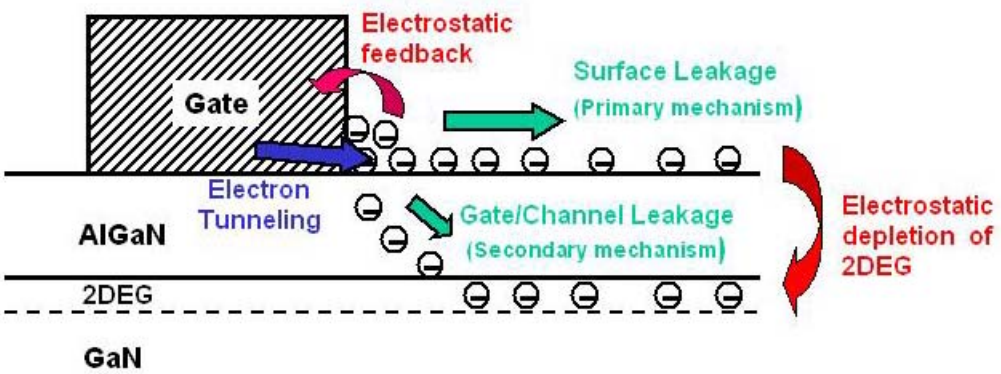

Figure 31. Schematic of the mechanisms of gate leakage. (After Bilbro [188]).

Some theoretical calculations have been conducted to describe the factors affecting tunneling of electrons out of the gate. It has been reported that there are five factors: *i*) the gate edge roughness; *ii*) net charge at the AlGaN/passivation interface; *iii*) dielectric constant of the medium above the HEMT surface; *iv*) nontriangular potential barrier; and *v*) negligible angular tunneling from the gate edge.[189] However, there have been no experimental results proving these attributions.

In one simulation effort that was undertaken to better understand the surface effects of GaN-based devices, devices utilizing a surface into which electrons can tunnel from the gate have been used to generate good agreements to experimental values of drain current (V_{ds}/I_{ds} family of curves) as well as gate leakage (V_{ds}/I_g family of curves). The model is physically understood as electrons tunneling from the gate to the surface, then hopping along surface states. This phenomenon results in leakage current (along the surface), although at some critical field a conducting channel into the AlGaN barrier layer is formed.[188] Both of these phenomena would give rise to a virtual gate, resulting in reduced current and in transient analysis would give rise to lags mentioned above. Considering electrostatic feedback (electrons returning to the gate due to electronic attraction to image charges), transient responses of I_{ds} and I_{gs} could also be predicted.[188]

Although the gate leakage can be attributed to both current conduction along the surface and the vertical transport through the barrier to the channel at the heterointerface, it is still not well understood which mechanism is the most important. For GaN Schottky contacts, screw dislocations have been shown to increase the reverse current by 300-500 times while only resulting in a 6 fold increase results from edge-types.[181] However, in these experiments, the spacing between Schottky and ohmic contacts is large enough that the lateral field (along the surface) is not nearly as large as it is in an HFET device where the gate-drain separation is much shorter. More studies are necessary to determine whether the dislocations are really that important in the HFET devices.

V.3.3. **Metallurgical Issues**

In addition to degradation inherent to semiconductor, be it permanent or temporary, the metal-semiconductor diffusion, phase change in metal stacks, and electromigration within the metal are sources of potential permanent degradation. Electromigration of the gate electrode metal, impurity activation, and contact diffusion effects are reasonably well understood particularly in conjunction with, e.g. GaAs based devices. However, GaN based devices push the metallization technology to its limit causing some metallurgical changes particularly under prolonged high current operation. Exacerbating the Schottky barriers is the presence of electric high field and gate leakage current (small gate cross section leads to high current densities). The Ti/Al based contacts on GaN are reasonably stable against oxidation and cracking when Al is sealed with Ni/Au[190] but nut sufficiently stable for prolonged operation. However, Ti/Au seal over Ti/Al become rough after annealing with bad line definition, which leads to current filamentation and therefore premature breakdown. Mo/Au and Pt/Au seals have also been used with limited or no success leaving Ni/Au seal as the preferred choice. Ultimately though, an n^+ top layer atop the AlGaN barrier would need to be used to not only reduce

the contact resistance but also ensure uniform current distribution. This would necessitate selective dry etching methods for gate recessing, which have already been explored for this purpose to some extent.[191,192]

The reliability investigations of GaN FETs have been relatively less developed in comparison to the GaAs counterparts. As in the case of GaAs and in fact to a larger extent due to large current levels/fields involved. As a result both the gate and drain/source metallurgy undergoes change including phase change. Degradation of this kind is progressive and not reversible. Therefore, this process must be understood well and incorporated into the physics based reliability model. As in the case of GaAs based FETs, the extent of electromigration is dependent on factors such as conductor-line properties and any inhomogeneities as well as structural features of the conductor layout. Naturally, electromigration must be studied noting that the magnitude of defect transfer depends superlinearly on current density, which poses a formidable challenge for GaN based FETs. High temperatures, particularly applicable to gate and drain metallization, cause mass transport facilitated by short distance diffusion associated with defects, such as dislocations, grain boundaries, interphase boundaries, and/or external surfaces. It is therefore imperative that we study and understand fully the mechanisms for electromigration and impart that knowledge into the reliability model.

V.3.4. Physical Issues-High Field Effects: Hot Electrons and Hot Phonons

Hot phonons are intimately related to reliability of the GaN-based FET devices in that the generation of large quantities of hot phonons will inevitably lead to the generation of defects. Obviously, one would like to minimize if not fully eliminate the quantity of defects in devices, and when defects are being generated during the operation of a device, the reliability of the device is clearly in question. In order to understand why the hot phonons are a source of reliability concern, one must first recall that the phonon is merely the quantum of motion, and when one considers that the distribution function for hot phonons in the channel of an FET is such that the occupation of said phonons is extremely dense, in a relatively narrow portion of k-space, the concern of the generation of large atomic vibrations and subsequent new crystal defects is clear. Figure 32 shows the distribution function for hot phonons in a highly doped GaN sample at high fields, which is applicable to the conditions found in a 2DEG at the AlGaN/GaN interface (in fact, it could be argued that this is a somewhat conservative statement since the "bulk" density in a 2DEG could be over 10^{20} cm^{-3} and that the effects of the hot phonons are exacerbated in an AlGaN/GaN system over a GaN system, see below).

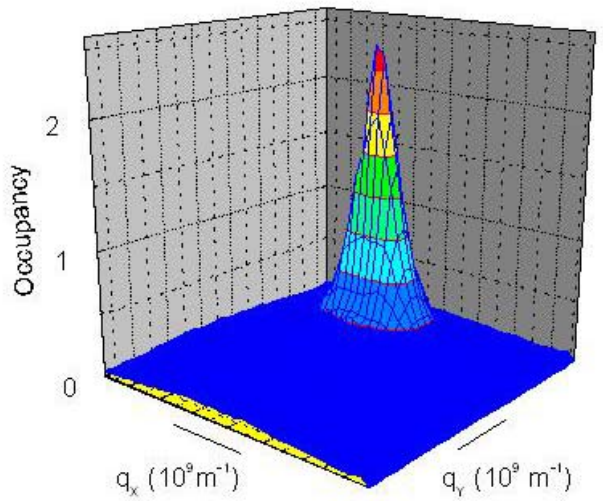

Figure 32. Distribution of hot phonon states for highly doped GaN at high fields (n=10^{18} cm^{-3}, E=50kV/cm). The lattice temperature is 300K. (Matulionis [193]).

With respect to the HFETs, it is important to consider that even though the channel portion of the FET may primarily reside in the lower bandgap GaN layer, the effects of the hot phonons are important to consider and even are exacerbated in the AlGaN/GaN system over the bulk GaN system as demonstrated in Figure 33. The figure shows the amount of power per electron that can be dissipated for a given electron energy. Temperature on the x-axis is the noise temperature, in the regime where the noise temperature can be translated into kinetic energy of the electron.

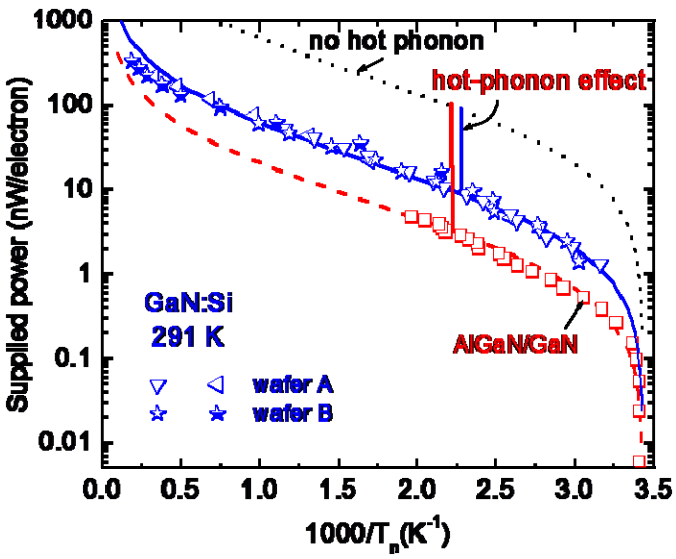

Figure 33: The hot phonon effect is 3-4 times stronger in the AlGaN/GaN system than in bulk GaN. (after Liberis *et al.* [194]).

In short, the hot electrons and hot phonons generated in high electric fields could cause new defects to form, and this is furthermore exacerbated by inhomogeneities and electromechanical coupling in a piezoelectric material such as AlGaN or GaN. Existing defects and the defects so generated due to hot phonons/electrons have a G-R noise signature which can be monitored rather well with low frequency noise measurements as has been applied to GaAs-based and GaN-based FETs previously.[195, 196, 197] Strong electron-phonon coupling in GaN afforded by the ionic nature, leads to efficient phonon generation (perhaps as high as some 30 times stronger as compared to GaAs), which in turn leads to an increased hot phonon population as the LO phonon decay mechanism (to longitudinal acoustic phonons) cannot keep up with the generation. The hot phonons are capable of generating point defects, particularly in the vicinity of point defects already formed during growth and in high local fields (piezo nature coupled with inhomogeneities). This causes drift and degradation in device performance, which is not incorporated in many garden variety statistical models that are often applied to GaN. The hot phonon decay mechanisms are not well developed in GaN.

The upper limit of the hot phonon temperature is really determined by device failure. Much higher hot phonon temperatures are attained in modified heterojunction designs. These designs eventually should provide high phonon and electron temperatures to be reached before failure as well as short phonon lifetimes. However, the hot phonon and hot electron, particularly the former, induced generation of point defects is a problem which can be mitigated by high quality layers which eventually would have to be on high resistivity freestanding GaN or high resistivity GaN when it is available. Fe-doping is capable of providing stable high resistivity. It should also be stated that use of expensive SiC substrates for the high thermal conductivity may not be even be well justified over using GaN substrates as the bottleneck for power dissipation appears to be LO phonons decaying into LA phonons anyway. Only after such decay occurs does the thermal conductivity come into the picture.

V.3.5. Other Issues

Various methods and materials for passivating FET devices have been employed with varying degrees of success. While the reliability of the passivant itself is an issue (as for example, a Si_3N_4 passivation layer deteriorates with time) that is still to be resolved, different passivants and surface treatments will have different results on the performance of the device. Typically, a passivant tends to increase the sheet carrier density as the (negative) charges on the surface which tend to deplete the underlying channel are essentially moved away from the surface, or as the AlGaN surface tends to relatively become positively charged.[198] Additionally, passivation has been shown to reduce the RF current slump as well as increase the breakdown voltages of devices.[199] Although the use of the passivant would tend to point the blame of poor performance at the surfaces of the devices, one must be careful and consider that, for example, in any deposition scheme that utilizes hydrogen either as a carrier or a precursor (such as SiH_4 in Si_3N_4 deposition), H can diffuse into the AlGaN and even into the GaN and “passivate” the deep levels in

the underlying epitaxial layers.[200] In short, all aspects of processing must be considering when attempting to describe the physical phenomena occurring in the devices, and everything must be optimized in tandem in order to achieve success.

Although not a fundamental issue like the material quality or metallurgy, the issue of long term stability most likely warrants an entirely separate section since it is particularly evident in the GaN devices. In one study, after 1 month, in a device with Al concentration of 29%, the sheet resistance increased by ~7 times, sheet density decreased by ~33%, and the mobility decreased by ~5 times. AFM imaging showed cracks on the AlGaN surface that were not present in the as grown samples; however, by storing the devices in N_2 instead of air, resistance and carrier density slightly increased, and mobility decreased by ~33%. This degradation was attributed to O diffusion into surface (~25nm by SIMS).[201] Similar results were found by another group when studying other samples grown by both MOCVD and MBE with varying growth conditions, concentrations.[202] Although a cap layer and gate recess would likely alleviate some of this degradation, considering the depth to which the O diffuses as evidenced by the SIMS analysis, the development and application of some sort of hermetic barrier in packaging will obviously be desirable for long-term usage of GaN-based devices.

V.4. Degradation and Reliability Measurements

Methods that are important for characterization of the FET devices span structural, optical, and electrical types of techniques. In the end, all of the techniques have to be considered in parallel, and comparisons against simulation results must be done in order to achieve a real understanding of the degradation physics.

V.4.1. Degradation: Trapping and Reversible Effects

V.4.1.1. Structural

TEM measurements are useful to quantify defects that are generated particularly at interfaces, during the growth of layers on foreign substrates, and comparisons after thermal, DC, or RF stresses can yield some insight into the generation of such defects (For example see Figure 30)

V.4.1.2. Electrical

The defect related anomalies surrounding GaN HFETs must be addressed if the goal is to attain long operating lifetimes under realistic conditions. Fortuitously, much work in understanding the trapping that affects the devices both in the throughout the crystal structure as well as on the surface through electrical and optical measurements has been done.

Current collapse has been observed in GaN-based devices[203,204] as shown in Figure 34, albeit the effect is not attributable to the DX center as in the GaAs case.[205] The collapse seen in GaN can be recovered or avoided through the heating or illumination of the sample.[206]

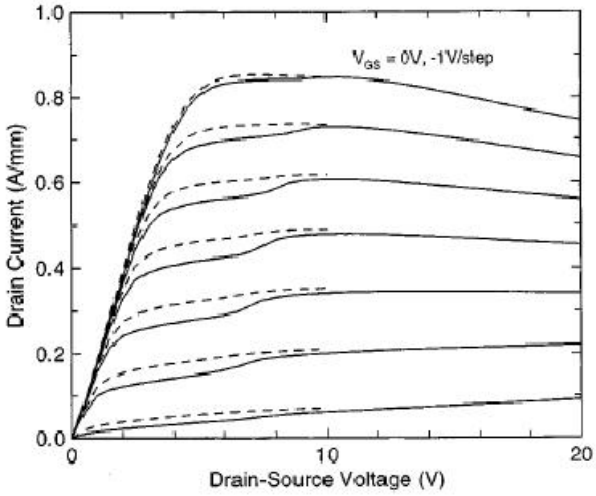

Figure 34. Current collapse in a GaN MESFET. Dotted lines show the current when the drain bias is limited to 10V. With high drain biases (solid lines), I_d is suppressed, termed current collapse. (after Binari *et al.*[204]).

A manifestation of the traps both on the surface as well as in the underlying AlGaN barrier or GaN buffer layers is that the pulsed IV measurements do not coincide with the DC measurements. These measurements can be used essentially as predictor of how well the device will perform under large signal operation[207], but are also of utility in determining trap levels in the semiconductor or on the surfaces. As briefly mentioned above, the gate lag is characterized by a slow transient to DC value of the drain current after sudden application of an increased potential to the gate (i.e. pinchoff to open channel condition). Figure 35 shows a measurement of the gate lag as well as its manifestation in the pulsed gate IV measurement.[208] This would have a profound effect on the RF performance of the devices in question. The drain lag, meanwhile, is characterized by a similar but opposite response to a sudden application of increased potential to the drain of a device (i.e. off-state to on-state). Figure 36 shows the measurement of the drain lag as well as its manifestation in the pulsed drain IV measurement.[208]

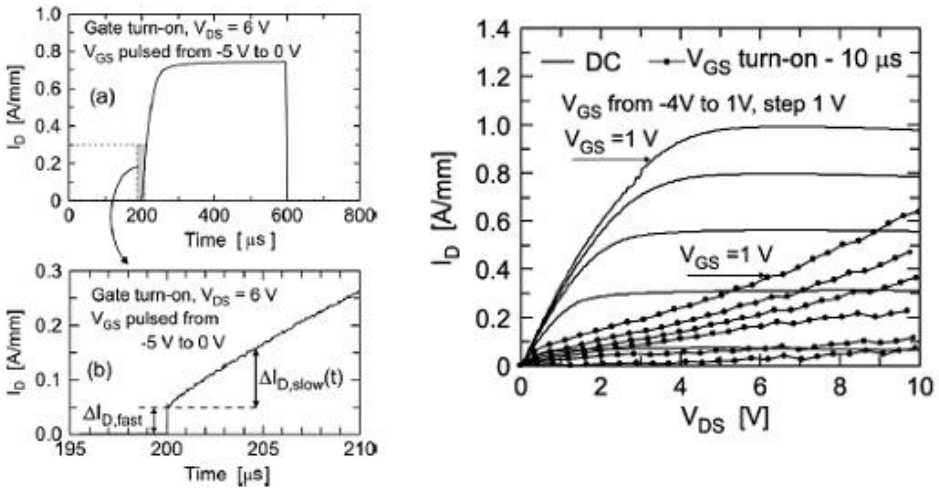

Figure 35. (Left) Measurement of gate lag. The drain current does not immediately respond to a pulsed gate. (Right) Manifestation of gate lag in a pulsed IV measurement. Drain current only reaches a fraction of its DC value during the pulse, resulting in markedly lower current in the pulsed IV curve. (after Meneghesso *et al.*[208]).

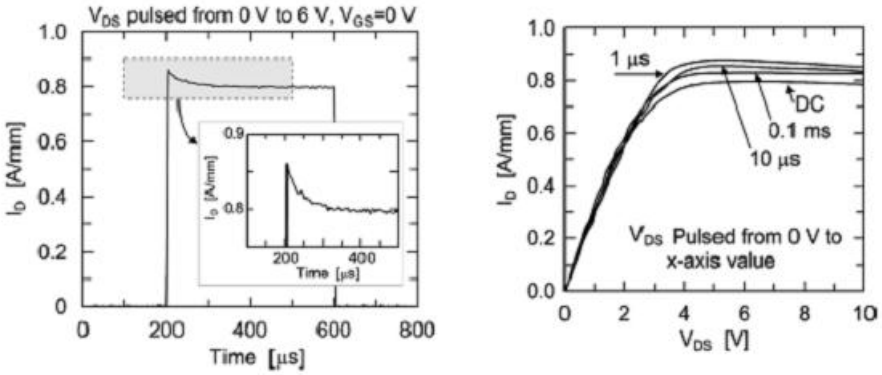

Figure 36. (Left) Measurement of drain lag. The drain current has an immediate overshoot (over DC value) in current to a pulsed drain. (Right) Manifestation of drain lag in a pulsed IV measurement. Drain current exceeds its DC value during the pulse. (after Meneghesso *et al.*[208]).

As the crystal quality is improving, we are approaching the quantum limit at which intrinsic 1/f noise can be studied apart from other sources of noise. New physical descriptions of the 1/f noise that express both the conventional quantum 1/f noise as well as the coherent 1/f noise (arising out of a state of the collective motion of the carriers and expressed by the magnetic energy per unit length) have been developed and efforts to correlate this noise to device lifetimes look promising.[209] For example, thermally stressing the devices (which would tend to reduce the lifetime of the devices) to only 440K resulted in an increase in 1/f noise of 4 orders of magnitude, demonstrating the potential sensitivity of the technique.

V.4.1.3. Optical

DLTS measurements are a powerful method to ascertain deep trap levels, their concentration, and capture cross sections. [210] Optical DLTS (ODLTS), and photoionization studies have been useful in determining point defects, some of which have been responsible for the trapping mechanisms and current collapse discussed above.[211] By carefully analyzing the wavelength dependence on the recovery of the current, one can estimate the depth of the trapping centers that are responsible for the current collapse. Two traps at 1.8 and 2.85 eV below the conduction band with densities of mid-10^{11} cm^{-3} were identified by Klein *et al.*[212], and they interestingly coincided with traps previously attributed to persistent photoconductivity in GaN samples. Furthermore, evidence of more severe current collapse occurring in layers grown at lower pressures (and thus with higher levels of carbon incorporation)[213] add credence to the growing consensus that current collapse can be attributed to electron traps in the GaN buffer layer.

As mentioned above the "hot" phonons [defined as non-equilibrium LO phonons launched by non-equilibrium (hot) electrons] scattering is extremely important at high field and absolutely must be taken into account when one considers the performance of a GaN-based FET device. At the heart of the issue is the point that for a given electron temperature, the energy relaxation time and thus the energy dissipation rates of the (hot) electrons are an order of magnitude less than in the case where the hot phonons were not generated. [214] Monte Carlo simulations agree with femtosecond laser experiments performed by Sun.[215] Furthermore, Monte Carlo simulations of carrier velocity with and without hot phonons (and with different hot phonon lifetimes, and therefore, with different velocities - velocity lower for longer lifetimes). Using pump-probe Raman, lifetime was measured to be ~3ps in bulk GaN at RT.[216]

V.4.1.4. Thermal

Measurements to assess the temperature of a device may be predictors of lifetimes. IR and microRaman thermal mapping techniques have been used to deduce temperatures of the devices with micrometer spatial resolution. IR measurements on TLM structures were also used to measure temperature but microRaman showed even higher temperatures. Finite element analysis (FEA) method was then used to model the FET (using a pure thermal as opposed to an electrothermal model), and the linewidth and shift of the micro-Raman signal correlated to FEA results, but underestimated (stokes-antistokes method also correlates with the linewidth method). 2D electric field corrections have been shown to improve fits.[217] Finally, an Arhenius Plot yielded the mean time to failure and the authors' claim is that by putting the same power into a device at DC, RF failure can be "measured" using DC biases. These techniques yield lifetimes better than 1000 hrs. Again, the fundamental question is what the failure mechanism is and particularly in the case of the thermal measurements, what is the temperature that is most important in predicting failure? Is it in fact the highest temperature, at the drain side of the gate where electric fields are at their highest, that is most important? Can these methods scale to large wafers? Does the 3-temperature RF prediction agree with the 3-temperature DC prediction?

V.4.2. Reliability Measurements

A typical procedure to ascertain lifetimes of various types of devices is the accelerated life test. Accelerated life testing is typically performed at three different but elevated temperatures in which cumulative failure rates are recorded and the mean time to failure (MTTF) for each of the three temperatures is established. The test is therefore referred to as the three temperature (3T) life test. The failure is defined as *e.g.* reduction in the drain current by 10%. The MTTF figures so determined are then converted to a single Arrhenius plot wherein the MTTF values are plotted in a log scale as a function of inverse temperature. Extrapolation to a given temperature then determines the expected MTTF for an HFET operating at that temperature, more applicably the channel temperature, which is always higher than the case temperature. The example given in the introduction yielding a lifetime of 10^7 hrs at 150°C is shown in Figure 37 as a demonstration

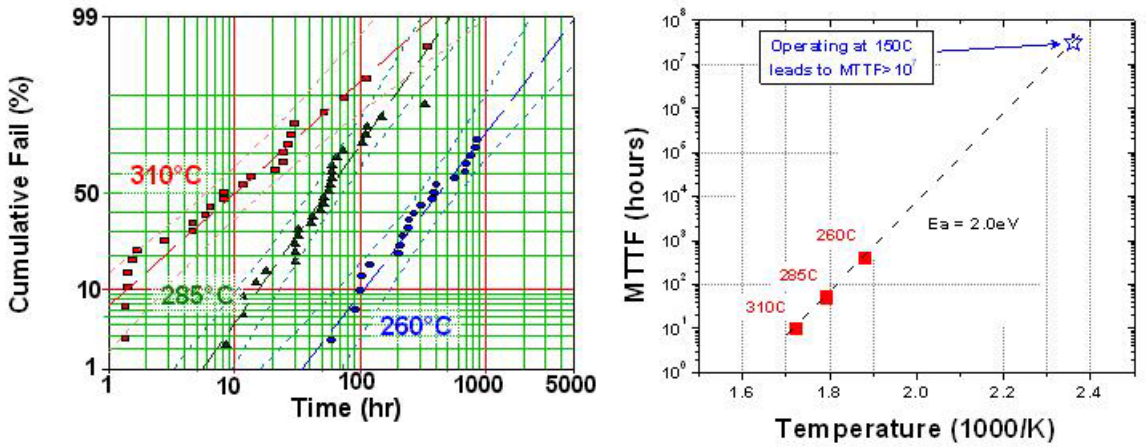

Figure 37. (Left) Three temperature (3T) lifetime test data showing the cumulative failure rates *vs*. time obtained at 3 different temperatures, namely 180, 285, and 310 °C. The σ values for 180 and 285 °C are approximately 1 but that at 310 °C is 1.5 which might imply contribution by infant failure. (Right) Arrhenius plot of the mean time to failure determined at three different temperatures 180, 285, and 310 °C which lead to an activation energy of about 2 eV and an extrapolated MMTF value greater than 10^7 hours at 150°C (courtesy of Dr. A. Hanson of Nitronex).

This method, however, provides a limited test and does not consider RF biasing and pulsed operation wherein the gate voltage is swung in the forward direction among others. Another aggravating factor is that it is difficult to measure the peak junction temperature particularly when a field plate is used which obstructs optical access to the semiconductor. In addition, the junction temperature at the heterointerface should be measured as opposed to the surface temperature. For the above-mentioned reasons, it is prudent to perform a series of tests as outlined in the following paragraph augmented by various RF, pulsed, and the combination thereof measurements. The infant mortality and

failures of similar manifestation must also be investigated which is discussed later on in this section.

Critical issues for accelerated life testing are that they are intended to provide estimates of device reliability in a time much shorter than that required to produce a significant number of failures under normal operating conditions. To be successful, the tests must stress the largest possible number of devices in a controlled manner without introducing artifacts (i.e., unrealistic failure modes). The accelerated tests normally adopted, which must definitely be augmented by RF and pulsed IV tests, and the various combination thereof as they among others stress the gate by pushing to forward operating mode during part of the RF swing, in particular for power HFETs are:[218]

(a) **High temperature storage test** (HTS). Unbiased samples are stored at different temperatures, in order to accelerate thermally-activated failure mechanisms, such as interdiffusion processes, occurring at the metal/semiconductor and semiconductor/ semiconductor interfaces.

(b) **High temperature operating-life test** (HTOL or HTOT). Samples are stored at different temperatures and biased in conditions similar to those experienced by the device during normal operations, aiming at studying the combined effects of thermal and electrical stresses. This approach in the form of the 3T plot is used to determine the MTTF Arrhenius plot, which is very limited and does not really represent by itself the real operating conditions of the device.

(c) **High forward gate current test** (HFGC). The gate Schottky diode is forward biased in order to investigate the effects of high current densities (at high temperatures).

(d) **High temperature reverse bias test** (HTRB). The gate Schottky diode is reverse biased close to breakdown voltage to observe the cumulative effects of high electric fields and temperatures.

(e) **Temperature humidity bias test** (THB) and **highly accelerated stress test** (HAST). Samples are biased in a high temperature and high relative humidity environment. To increase both temperature and relative humidity, a pressure cooker is employed in the HAST test. Usually the gate diode is reverse biased to analyze the effects of humidity directly on the chip and the protection capability of the passivation layers and of plastic packages.

Sometimes the accelerating factors are not kept constant during the test but are increased at defined times, giving rise to the so-called "step stress" test, which can be either thermal or electrical. The purpose of this test is twofold: *(i)* it can give very quick information on the limiting conditions for the investigated technology, *(ii)* step stresses are used (with carefully defined time intervals) to obtain reliability predictions.

A clear advantage of RF life tests over the abovementioned tests is that the devices operate very close to the actual system working conditions, so that reliability predictions can be more accurate and representative. In particular, for high power devices, large RF signals can drive the devices in electrical conditions not experienced during DC life testing. However, it is not easy to control RF working conditions during life testing, so

that it is possible to introduce spurious failure mechanisms due to overstress, input/output impedance mismatching, in particular at high temperature, etc. Moreover, the same failure mechanisms enhanced by RF life testing, such as electromigration caused by forward gate conduction or degradation due to operation close to gate-drain breakdown, can be induced by proper DC tests such as HFGC or HTRB, which can be performed under well-controlled conditions.

For parameter monitoring, it is generally preferable to measure both DC and RF parameters, in spite of the fact that in some cases a clear correlation was found between DC and RF degradations. In the case of DC parameters it is, however, recommended not to limit the characterization to classical transistor parameters [drain saturation current (I_{dss}), pinch-off voltage (V_p), transconductance (g_m), etc.] but also include the measurement of other parameters, such as parasitic resistances, gate diode characteristics etc. which can help to correctly identify the actual failure mechanisms.

In the thermal characterization methods, accurate evaluation of the channel temperature of devices under test is needed to correctly accelerate the different failure mechanisms and to evaluate their activation energy. The channel temperature (T_{ch}) of an electronic device is conventionally described as the sum of the case temperature (T_{case}) and of the product of the power dissipation (P_D) by the thermal resistance (R_{th}), i.e., $T_{ch} = T_{case} + P_D R_{th}$. To evaluate R_{th} of microwave MESFETs, the electrical method based on the current-voltage forward IV characteristics of the gate Schottky barrier diode is widely used because it enables T_{ch} (ΔV_{gs}) to be evaluated through a calibration curve, so that R_{th} is then obtained from the knowledge of T_{ch} (ΔV_{gs}), T_{case} and P_D. It should be noted that also R_{th} is itself a function of the temperature.

In operating conditions, or during accelerated life tests, however, the power dissipated in the active device areas leads to a non-uniform increase of the device temperature. T_{ch} (ΔV_{gs}) is therefore an unknown weighted average of the temperature distribution on the device and can be very inaccurate, in particular if a small area of high temperature exists within the structure. The actual temperature distribution on the chip can be measured by liquid crystal techniques or directly observed by means of high lateral resolution infrared (IR) thermography (IR near field optical microscopy and μ-Raman spectroscopy mapping can also be used), which allows one to detect the thermal gradients caused by local differences in the heat dissipation or by structural inhomogeneities.

V.5. Summary

A complete understanding of the "sudden failure"' problem [219] requires the development of a model that can simulate the mechanical stress, coupled with pyroelectric and polarization effects, on the lattice resulting from high electric fields. Defects consisting of screw dislocations, misfit defects, cracks, and point defects that are certain to be generated under high field and elevated temperatures can be introduced. The lifetime of semiconductor devices is strongly related to the densities of dislocations or point defects. It is known that in GaAs-based devices the moderate dislocation density (~

10^4 cm^{-2}) can affect the operating life of the devices. Since in GaN-based structures the dislocation density is several orders of magnitude higher (~ 10^8 cm^{-2}), the degradation rate can be related to the presence of extremely high dislocation densities and simple and complex point defects associated with them.

In short, despite extensive device developments motivated by increased power performance, there is still work to be done before the devices can be deemed sufficiently reliable. Although some lifetimes look reasonable at a drain bias of 28V, the research now needs to focus on the identification of the processes involved. Among them are gate leakage, high field effects potentially causing metal diffusion and causing defect generation, and degrading crystal quality, particularly at the AlGaN/GaN interface in conjunction with hot electrons and phonons, and imbricated thermal and mechanical strain issues. Research on methods to suppress the hot phonon phenomena by developing structures to enhance the power dissipation per electron and finally pushing forward towards an understanding of the mechanisms of failure, through design of test structures which allow us to probe the intertwined effects of high field, hot electrons and hot phonons, and piezoelectric and spontaneous strains from one another in an effort to determine the real physics of failures is also needed.

VI. ZnO and GaN-based lasers

VI.1. Introduction

The lasers pushed the GaN technology early on to attain low defect density material. The approach was to use thick HVPE layers (which may also involve epitaxial lateral overgrowth - ELO) and a series of buffer layers, again using ELO to reduce the defect concentration. These efforts led to edge emitting lasers which are at the heart of Blu-Ray DVD technology advanced by Sony with a good deal of help by Sony's control and or influence on the content. However, as in the case of other semiconductor laser technologies before GaN, the question is whether surface emitting lasers and in particular a special form of them, polariton lasers, can be developed. Surface emitting lasers are very demanding in terms of reduced threshold and dense two-dimensional integration, but their realization using GaN- and ZnO-based active regions faces major challenges related to reflector stack fabrication and current confinement, to cite a few. Polariton lasers are slightly more demanding due to their much lower thresholds. The participants were posed to deal with fundamental question in this field: What are the driving forces and also the current roadblocks for vertical cavity electrical injection lasers? Will they be used for pumps in lighting? What are the prospects for polariton lasers? What are the prospects for ZnO lasers such as edge emitters? Are random lasers a reality of hoax? Below, we give a summary to the field and its status as well as the views presented at the workshop.

VI.2. Edge-emitting lasers

Edge-emitting lasers where the light propagates within the wafer plane of the chip and is reflected or coupled out at a cleaved edge are widely used forms of semiconductor lasers. Their resonator lengths are typically between a few hundred μm to a few mm, which is sufficient for achieving high gain. However, the optical loss is rather high. In the edge-emitting lasers, the laser beam is guided in a double heterostructure which forms a waveguide. This structure can restrict the generated carriers to a narrow region and provide high efficiency. Depending on the waveguide properties, it can provide a high-beam quality but poor output power, or a high output power but with poor beam quality. The laser output also has a large divergence from the cleaved edge forming an elliptical beam profile. This results in a poor coupling efficiency, and therefore, edge emitting lasers require expensive packaging techniques such as micro-lenses or beam guides.

Soon after the first report of the blue laser diode (LD),[220] GaN-based LDs became commercially available and are currently used in Blu-Ray DVD technologies for optical storage and recording and reading, in projection TVs, and laser printers. GaN-based LDs which use InGaN or AlInGaN alloys show good performance with lifetimes in excess of 10,000 hours. However, device reliability is still a main concern in the industry. The device lifetime depends on the dislocation density. In the early stages, huge amount of threading dislocations (10^9-10^{10} cm^{-2}) were present due to the lattice-mismatch between

GaN and sapphire substrates. Having semiconductor lasers lasting even long enough in the laboratory to be measured with this high dislocation density is a tribute to the low dislocation mobility in GaN, some 14 times smaller than that in GaAs for example. Nevertheless, even with relatively small mobility dislocations are a lifetime killer and efforts have been underway to reduce them. One obvious method, of course, which was not available early on, is to use GaN substrates which are now standard substrates for GaN-based LDs. As a result, less than 1×10^{-6} cm^{-2} dislocation densities were achieved. To realize long-lived and high power GaN-based LDs, it is also important to reduce planar defects and the associated dislocations which may be formed at the interfaces of InGaN quantum wells (QWs).

The formation of In-In bonds at the interface between the InGaN QW and the barrier layers, which result in inversion domains, has to be suppressed using either AlGaN alloy or GaN as barrier layers instead of InGaN. [221] There are still compositional inhomogeneities and the notorious V-shape defects introduced in the MQW, whose origin lies with dislocations extending to the quantum well region.[222] These V-shaped defects have been reported to take the form of an open hexagonal, inverted pyramid with {1011} sidewalls.[223] Other defects not emanating from the dislocations and running upwards towards epi-surface have been observed in conjunction with quantum well laser structures. These defects have combined the planar defect and the dislocation nature which provides the impetus for Tomiya *et al*.[221] to call them "multiple defects". While the exact size of these multiple defects depends on several parameters including the growth conditions, they can range from 50 nm to 200 nm, as shown in Figure 38. Defects on the order of 4-6 are generated from the boundary of edges of each planar defect. Weak beam $(11\bar{2}0)$ dark field images of these planar defects indicate they consist of columnar sub-grains that are twisted slightly with respect to each another. Furthermore, they are also twisted in relation to the surrounding normal matrix. This twisting creates the *a*-type dislocations from the boundaries of the planar defects. High resolution lattice images indicate that these planar defects are formed at the interface between the quantum well region and the barrier layers. Conversion beam electron diffraction studies indicated the polarity to be opposite of the surrounding matrix which means that they represent inversion domains.

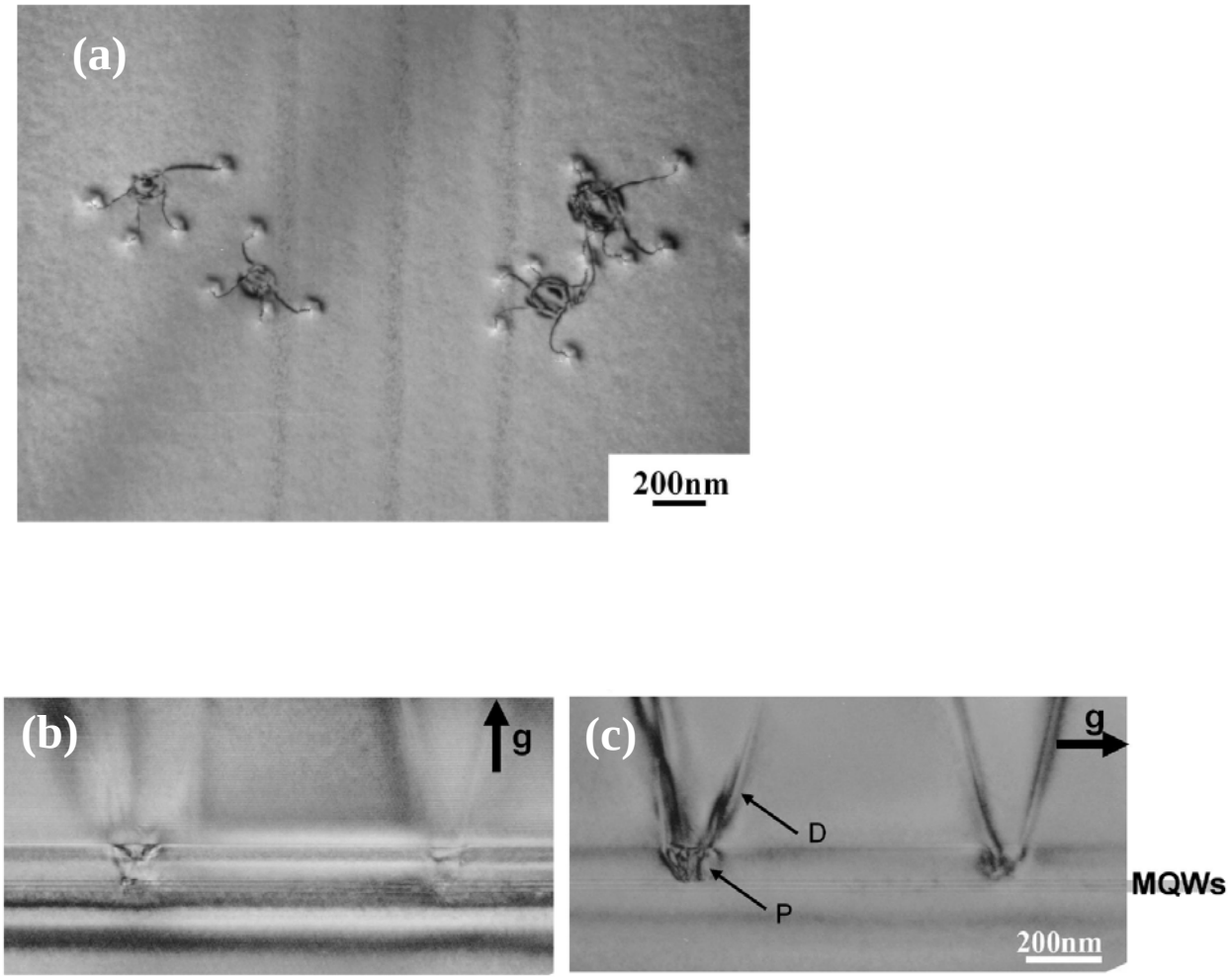

Figure 38. Plan view image of multiple defects (a), and cross sectional TEM $<1\bar{1}00>$ images of the multiple defects with g = 0002 (b) and g = $\bar{1}\bar{1}20$ where the planar defects observed in the quantum well region are indicated by P and the dislocation nucleating from these planar defects are depicted by D (c). (Courtesy of S. Tomiya of Sony Corporation).

Let us now delve into the formation mechanism of these planar defects. The presence of In rich precipitates observed in the vicinity of multiple defects mitigate the planar defect formation, as shown in Figure 39. Recall that the stacking sequence of the closed packed (0001) plane of the wurtzite structure is a-A-b-B-a-A-b-B-. If this stacking sequence along *c*-axis is a-A-b-B-a-A-b-B-B-b-A-a-B-b it would represent inversion domains (IDs). Since the In-rich precipitates nucleate near the multiple defects, excess B-B bonds are thought to be In-In. Therefore, Tomiya *et al.*,[221] speculate that the ID defects form due to excess In-In bonds at the interface between the quantum wells and the barrier layers. The need to suppress the formation of metal-metal bonds, particularly at the interface between the quantum well region and the barrier is obvious.

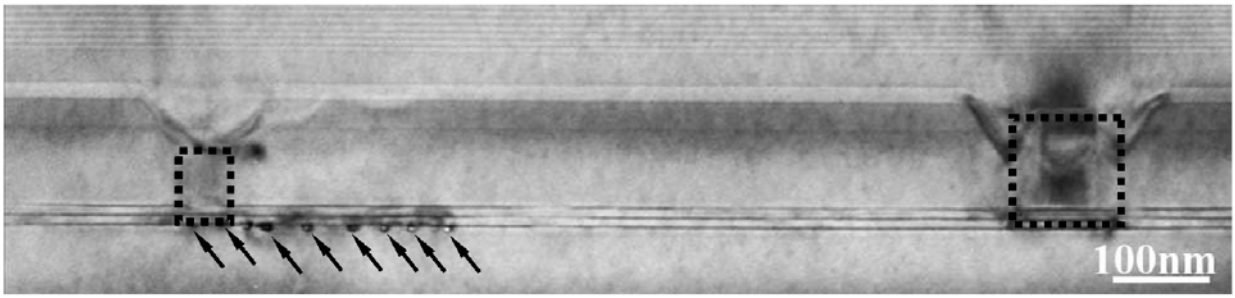

Figure 39. Cross sectional bright field TEM image of the multiple defects where the arrows point to the In-rich precipitates. Note that the planar defects and the dislocations are out of contrast. Furthermore, the planar defects are indicated by the dotted lines. (Courtesy of S. Tomiya of Sony Corporation).

As a result of the measures such as using GaN substrates and improved growth conditions the defect levels are reduced and the laser degradation is now taking a route similar to other semiconductors before GaN and focusing on intrinsic degradation of the material such as production of non radiative recombination centers and dark line defects, and laser facet damage. Pertinent to power extraction from edge emitting lasers one facet, which is called the back facet is coated with high reflection coating to prevent light emission which is wasted. The other facet, the front facet, might be coated with an antireflection coating to the extent desired for power extraction. To increase power extraction, which is termed as edge loss, the laser cavity length can also be shorter which requires higher levels of pumping per unit area and thus sets the stage for degradation.

The role of dislocations deserves further elaboration in that while their mobility is low, dislocations, even the fully coordinated ones, introduce states within the bandgap. The low dislocation mobility can be used to argue against degradation related to the dislocation multiplication and glide, in general referred to as dark line defects (DLD).[224,225] However, dislocations introduce inhomogeneous local strain which in turn could, under severe demanding device operation, pave the way for generation and then multiplication of non radiative point defects. Mg dopant used for p-type AlGaN and GaN would not only diffuse, but could also be responsible for non radiative recombination centers and or at least making the generation of non radiative recombination centers more plausible. Although not yet fully identified, diffusion of Mg and native defects could be responsible for laser degradation.[226,227] There is evidence that degradation in GaN based lasers is a thermally activated process with a characteristic activation energy of 0.32 eV – 0.81 eV. [228,229,230]

Occurrence of sudden failure with reduction of cavity length in high power GaN-based laser diodes is a serious issue related to device reliability, as shown in Figure 40 (a). These failures are in part caused by excess heating of the front facet which has its origin in increasing capture cross section of nonradiative recombination centers by the diffusion of point defects/impurities (such as Mg dopants) during laser operation. Employing a current injection-free region near the facet, typically called the Non Injected Facet (NIF), by as long as 45 μm, obtained by simply absence of the *p*-electrode metals near the laser

facet, significantly reduces the catastrophic optical damage[221, 231] and increases the lifetime, as shown in Figure 40 (b), which is estimated to be more than 10,000 hours under 0.75 W (reduced to 0.65 W after 700 hrs under 6.2 kA/cm^2 drive current) CW operation at room temperature.[221]

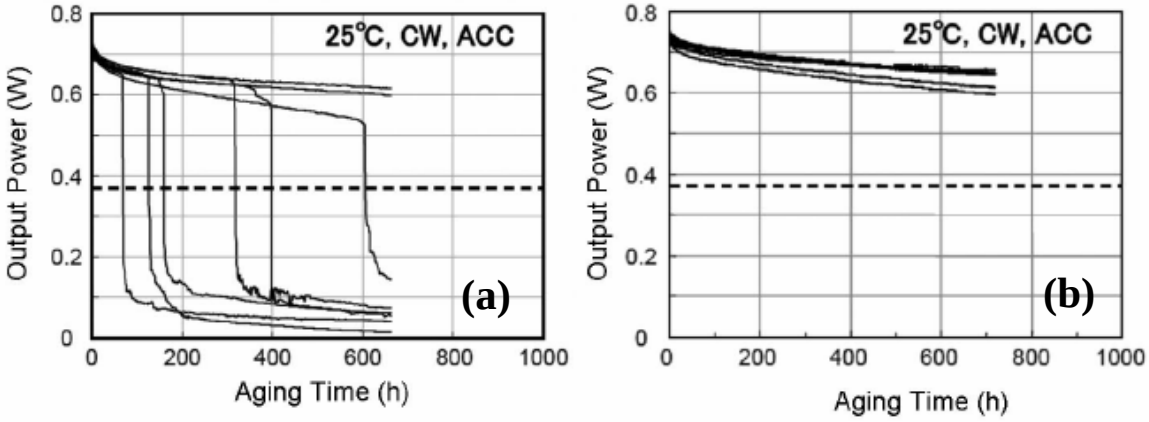

Figure 40. Aging test results of (a) laser diodes with conventional structure and (b) with current injection-free structure (Courtesy of S. Tomiya of Sony Corporation).

The premature degradation has also been attributed to the photon-mitigated carbon deposition on the dielectric stack on the front facet.[230] The deposited carbon is thought to have its origin in residual organic materials with C-H bonds. When the residual carbon contamination has been successfully removed by plasma cleaning just before cap-welding, the improved lifetime of the plasma cleaned laser diode packed with argon gas exceeded 2,000 h under 90 mW cw-operation at 60 °C.[230] Kim *et al.*[230] undertook an extensive study of facet damage, as mentioned caused by C contamination, by employing field emission SEM (FESEM) and field emission Auger electron spectroscopy (FEAES) to examine the front facet after aging, as shown in Figure 41 for two tested LDs, where the dotted lines outline the laser ridge for guide to the eye. During the aging tests, the cw output power of two LDs, LD1 and LD2, were kept at 40 mW and the current increase rate was observed to be much larger LD1, where the damage was more drastic. The FESEM image of LD1 shows extensive damage to the antireflection (AR) facet, the emitting surface (see top row in Figure 41). The oval shaped damage developed during aging resembles the near field emission pattern whose center is just below the ridge bottom.

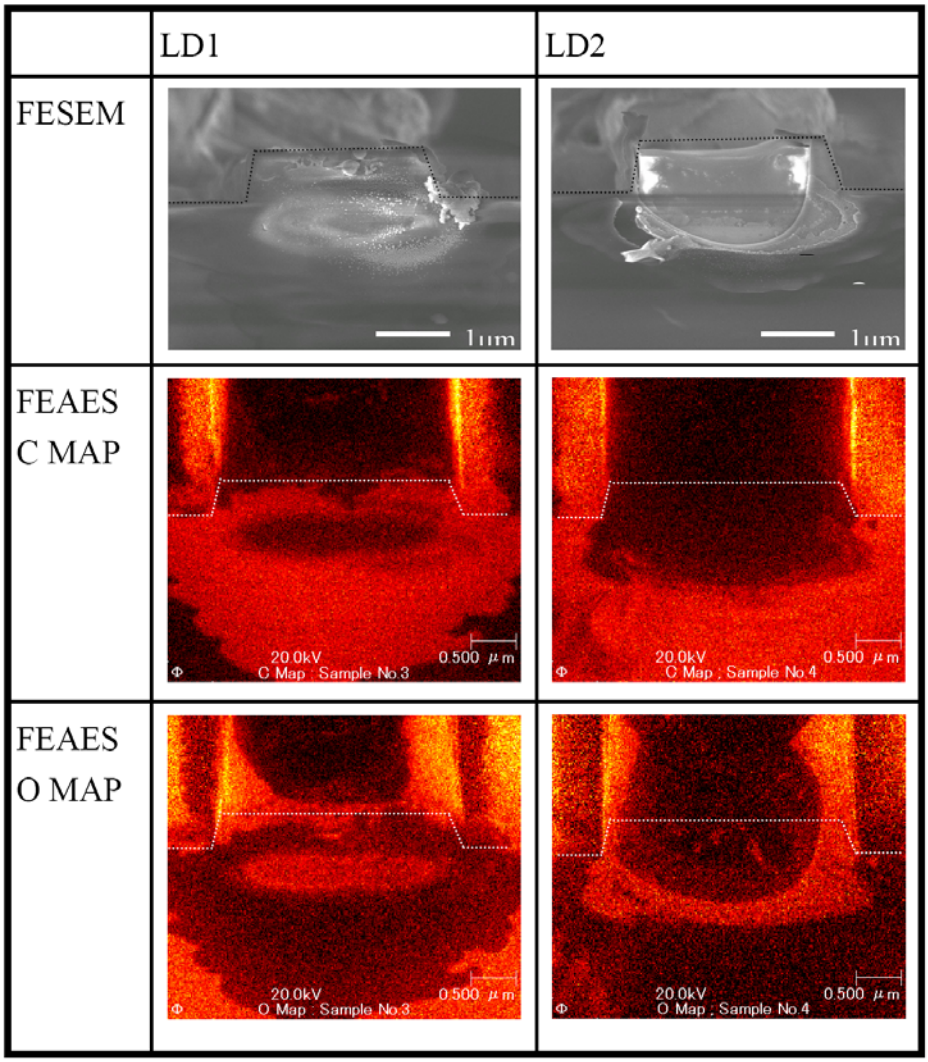

Figure 41. Field emission SEM (FESEM) and field emission Auger electron spectroscopy (FEAES) images based on carbon and oxygen mapping for two LD samples, LD1 and LD2 (courtesy of C. C. Kim of L.G. Electronics).

The FEAES scans undertaken by Kim *et al.*[230] indicated that the damage is caused by the presence of C which covered the dielectric facet coating whose shape is similar to that of the near field pattern as shown in Figure 41 (middle row). Therefore, it is fair to conclude that C deposit induced by the emitted laser light during the aging test caused increased absorption of photons. Interestingly C deposited less in the core area of the oval shaped damage where the optical density of the emitted light is higher than in the areas near the circumference. In addition, the FESEM image of LD2 in Figure 41 showed layer peeling, similar to that observed by Marona *et al.*[231] On the exposed surfaces GaN, oxide, and carbon can be seen. Where the GaN is seen, the oxide and the carbon layers peeled of, and thus C and O elements were not detected in the FEAES analysis. The peeling of the carbon layer is associated with the recovery of the optical properties. LD2 sample showed

the partial recovery around 100 h during the life time test. The results indicate that the initial degradation due to the carbon deposition is partially recovered in LD2 by peeling off of the carbon layer. The results lead to the conclusion that the premature degradation during the early stages of life tests is due to the photon-induced carbon build up on the light emitting facet.

As already mentioned, the use of the carbon removing process resulted in great improvement in the lifetime of the LDs. The mean time to failure using automatic power control (APC) mode life testing under pulse-wave operation (pulse width = 2ns, duty = 50%) of 160 mW was estimated as 2,240 h and 980 h at 60 °C and 70 °C, respectively. The failure here was defined as a 30% increase in operating current.

In order to delineate degradation caused by facet damage and non radiative processes, Marona *et al*.[231] undertook a study in which the operation current and emitted optical power, being the most sensitive from the point of view of the lifetime of the device, were both systematically varied. The threshold current and voltage, differential efficiency and its characteristic temperature T_0 were monitored with the conclusion that facet and near facet degradation, bulk degradation and quite rarely, contact degradation (attributed to processing flaws) occurred. In large percentage of devices, high temperature near the facets was noted accompanied by the SiO_2/TiO_2 coating delamination or large catastrophic degradation within the stripe area adjacent to the facet, the optical origin of which is now deemed high photon density related as this type of damage occurs also after testing the device just below the lasing threshold, consistent with other observations.[232]

Returning to the Non Injected Facet (NIF), the unpumped region of the waveguide should, in principle, increase the optical loss and thus the threshold current.[231] However, the threshold current was not noted to significantly increase, in part because of the compensating effect of decreasing pumped area and pertinent to reliability possibly reduced heating and resultant minimization of defect generation. Inclusion of a non-pumped region certainly reduces the temperature of the near facet region. Temperature reduction could aid in facet damage as well as reducing the temperature induced degradation of the semiconductor. In most cases the degradation was found to manifest itself mainly by an increase in the threshold current through a square root dependence on aging time, suggestive of the diffusion process being responsible for the damage.[221,231] The diffusion mitigated failure process maybe driven by current itself, current induced increase of the junction temperature, and optical field or by all these factors together. One of the best tests is to perform aging test below and above lasing threshold to delineate the effect of optical field from other processes. Doing so led to the conclusion that the optical field does not influence the degradation rate. [231] Optical field being out of the way, performing measurements of the degradation rate as a function of the operating current could shed light on the effect of current and related heat. The time derivative of the evolution of the threshold current density can be used as a measure of the degradation rate. A strong, nearly exponential, dependence of the so defined degradation speed on the operation current has been observed.[231] The results can be interpreted by assuming a normal Joule heating which can be described as:

$$D = C\exp\left[\frac{-E_A}{l\left(T_{RT}+\alpha_1 I\right)}\right] \text{ or } D = C\exp\left[\frac{-E_A}{l\left(T_{RT}+\alpha_2 P\right)}\right]$$

Equation 2

where D is degradation rate, C the pre-exponential constant, E_A the characteristic activation energy of the degradation process, T_{RT} is room temperature, P is the power dissipation, I is the current, α_2 is a constant connected with thermal resistance which is on the order of 12 K/W (α_1 is similar to α_2 in that it is tied to current as opposed to the power). Fitting Equation 2 to the experimental data, an α_1 coefficient of 200 K/A and an activation energy E_A of 0.42 eV have been deduced.[231] The good fitting lends support that the current-induced increase of the junction temperature is indeed one of the driving forces for the degradation.

Let us now turn our attention to aging-related increase of the non radiative recombination in the active area and increase of the leakage current. Here the "leakage" is used, as in any optical device, to represent the component of the current flowing through the device but not contributing to radiative recombination. For example carriers escaping the quantum wells before recombination fall into this category. To delineate which process plays a more important role in degradation, a series of experiments, namely cathodoluminescence should be performed for observing spots of non radiative recombination in the active region, and the characteristic temperature T_0 in the threshold equation:

$$J_{th} = J_0 \exp\left(T / T_0\right)$$

Equation 3

Basically, the CL signal of aged devices showed a decrease between 5 – 30 % as compared to virgin control devices. The obtained results might be susceptible to substantially large errors due to *e.g.* the compositional inhomogeneities. Nevertheless, the decrease of CL intensity (never increase) statistically confirms the appearance of nonradiative centers in the active area of these devices. The contrast changes in the CL images are typically uniformly distributed over the entire stripe area which represents a notable deviation from that observed in the GaAs/AlGaAs lasers[224,225] in which the degradation is manifested through the appearance of black dots or lines (dark lines) in the CL microphotographs. However, in interpreting the aforementioned differences one should keep in mind the relatively much shorter minority carrier diffusion length in InGaN which may have a bearing in the resulting CL images.

Correlation of the slope efficiency (the slope of the I-L curve) to the threshold current is also illuminating, see Figure 42. A positive correlation would indicate the increase of non radiative recombination as the main cause of degradation. A strong correlation has been observed in some cases, but in other cases no such correlation has been noted.[231] A perplexing behaviour can be explained by the formation of a parallel

path, or leakage current, for the current flow. Due to the formation of the parallel path with the aging time increasingly larger portion of the current flows without participating in the radiative process meaning without feeding the lasing processes. As mentioned this effect may be also treated in the context of current leakage (vertical, lateral or facet related). The fact that the slope efficiency in some cases remains constant during aging, and in some cases is nearly proportional to the change of the threshold current indicates that both mechanisms (leakage, and non radiative recombination) are indeed contributories to varying degrees to this process.

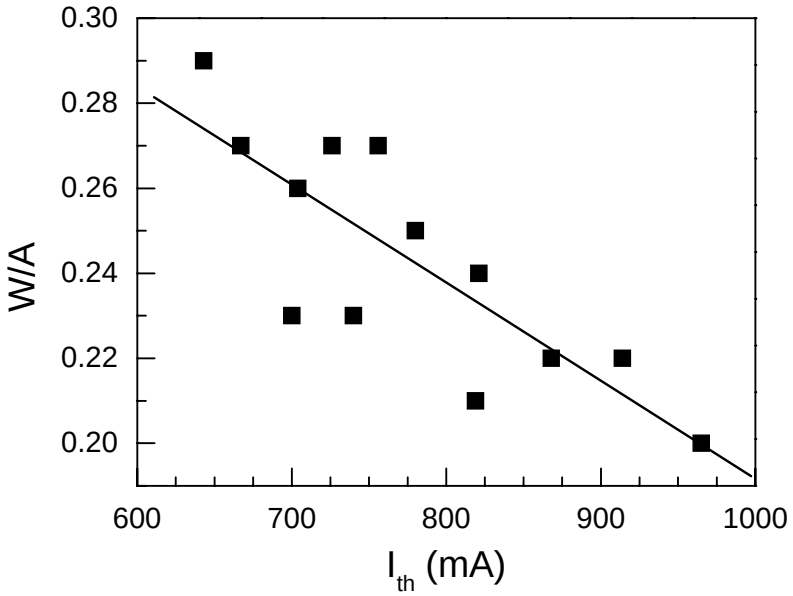

Figure 42. Correlation between slope efficiency (W/A) and threshold current (I_{th}) after aging (courtesy of P. Perlin of Institute of High Pressure Physics, Poland).

Leakage current is typically reflected in the magnitude of the characteristic temperature, T_0 expressed in Equation 3. A higher leakage current would imply a lower value of T_0. In nitride based semiconductor lasers, the typical reported values of T_0 are between 80 K and 235 K,[229,233] but there are also reports of anomalous values of T_0,[234] including negative values.[235] The negative value[235] has been attributed either to the anomalous temperature dependence of the carrier capture rates or the increasing temperature facilitating a relatively more homogeneous hole distribution through the multiple quantum wells. The holes, having an effective relative mass of 2, need additional thermal energy to better overcome the barriers. The characteristic temperature measured before, during, and after the aging procedure[231] is shown Figure 43. The initial value of T_0 = 274K increased by a factor of 4 after 45 h aging. For room temperature aging the threshold current changed significantly, but for higher temperature aging (~ 80 °C) the increase is relatively small. The higher temperature behavior can be explained by the

formation or increase of a thermal barrier for holes. The barrier can be the quantum barriers or *e.g.* that introduced by electron blocking layer in the valence band. It might be prudent to consider that the large value of the T_0 parameter does not necessarily imply a good confinement of carriers within QWs.

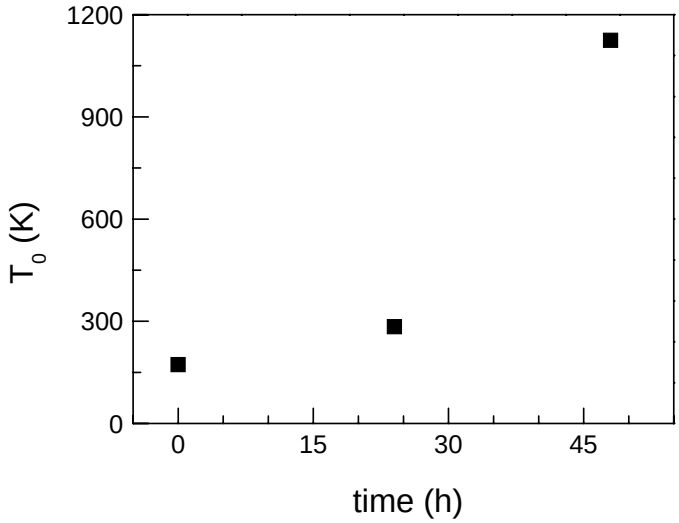

Figure 43. Characteristic temperature of laser diodes (T_0) as a function of aging time (courtesy of P. Perlin of Institute of High Pressure Physics, Poland).

To summarize, in terms of the materials issues affecting the laser reliability, it now appears that the degradation is related to multiple defects formed at the interface between the quantum wells and barrier, and generation of non radiative recombination centers within the quantum wells. Furthermore, the facet damage which occurs can be mitigated some by introducing a non injection stripe near the front facet. The material/device designs which include mainly the electron leakage (facilitated in part by large effective mass of holes) and processing details to either prevent or remove C deposits on the facets.

VI.3. Surface emitting lasers

Another type of semiconductor lasers, vertical cavity surface emitting lasers (VCSELs), has many potential advantages over the edge-emitting variety. The laser beam in VCSELs propagates in the direction perpendicular to the wafer surface. The cavity layer with a thickness of only several wavelengths is sandwiched between two distributed Brag reflectors (DBRs). Because the gain region is short in vertical cavity devices, the reflectivities of the top and bottom DBRs are required to be more than 90 %, in order to overcome optical losses for lasing. In fact, the bottom DBR should be almost 100 % reflective while the top one is made to have a slightly smaller reflectivity depending on the desired optical power extraction. To provide the high reflectivity, a large number of stacked semiconductor layers is necessary as generally the refractive index mismatch between the two compatible semiconductors forming the DBR is rather small. The most important advantage of the VCSELs is that they may be integrated as two dimensional

arrays on the wafer level that would provide high-density optical storage with significantly reduced read-out time and high speed/high-resolution laser printing/scanning technology. Additionally, VCSELs exhibit completely circular field patterns as opposed to the elliptical beam profile with an aspect ratio of 4 between the vertical and horizontal modes in the edge-emitting lasers, making light coupling relatively easier.

Research on III-Nitride semiconductors has now shifted towards further improvements of the materials quality and device performance, including all too important packaging, and the development of new devices such as resonant cavity LEDs and VCSELs. With increasing efficiencies and output power levels, LEDs are now seriously considered for solid-state lighting due to reduced power consumption, high durability, and lower maintenance costs, not to mention reduced carbon footprint on the environment.[236] The standard approach to obtain white light for indoor applications is to use either a blue LED (or LD) to pump two dies or the cumbersome three primary color LEDs. However, the latter approach cannot meet the color rendering index requirements of the international commission on illumination (CIE) [236] when conventional LEDs are used, as blue and particularly green nitride LEDs have broad emission and their emission wavelengths are injection dependent. As for lasers, GaN-based VCSELs are expected to outperform the conventional edge-emitting laser diodes in terms of power consumption, manufacturing costs, and lifetime, particularly considering the difficulties associated with cleaved cavity facets in this material system. When the cavity size is of the order of the emission wavelength, the spontaneous emission rate can be controlled and the lasing threshold can be reduced due to the large optical gain arising from the giant joint density of states in wide bandgap materials. The gain characteristics of the edge-emitting InGaN/GaN quantum well laser diodes suggest that room temperature operation of nitride VCSELs is possible. However, despite significant efforts over the past decade, lasing in GaN-based electrically injected VCSELs is not available, though possible under optical pumping.

Recently, blue-violet lasing action at ~422 nm under optical pumping in an electrical injection ready VCSELs was reported.[237] A low average threshold power density of 50 W/cm^2 was achieved in a crack-free planar hybrid $5\lambda/2$ GaN microcavity containing three InGaN quantum wells with a bottom lattice-matched AlInN/GaN DBR and a top dielectric (SiO_2/Si_3N_4) DBR. The VCSEL structures were grown by MOCVD and the cavity region had both *n*- and *p*-type regions as well as an AlGaN electron blocking layer on the *p* side making such a planar design in all points identical to that of a real structure ready to be processed to fabricate mesas and deposit electrical contacts. A spontaneous emission coupling factor $\beta \sim 2 \times 10^{-3}$ was derived from the input-output characteristics for this VCSEL structure. By oxidizing the AlInN layer in the *n*-type cavity region current micro-apertures were shown to form allowing access to high current densities (> 20 kA/cm^2). Figure 44 (a) shows variation of emission spectra obtained normal to the surface at room temperature (RT) for various pump powers. A clear threshold is observed at an average incident pump power of ~ 1.4 mW. The spectral width of the emission below threshold is about 3.1 nm [Figure 44 (b)], which is essentially due to cavity thickness disorder leading to a decrease of the effective Q factor with increasing spot size and with the measured cavity mode revealing the contributions of several narrow modes. Above threshold, the narrowest mode is about 0.37 nm wide, close to the spectral

resolution limit of the system. As a promising step towards realization of VCSELs under electrical injection, InGaN/GaN LEDs using oxidized $Al_{0.82}In_{0.12}N$ layers as current confining apertures was reported. [238] Figure 45 shows the details and the electroluminescence image of the LED structures. A current density in the order of 20 kA/cm^2 has been achieved, a value which should fulfill the injection requirements on nitride-based VCSELs.

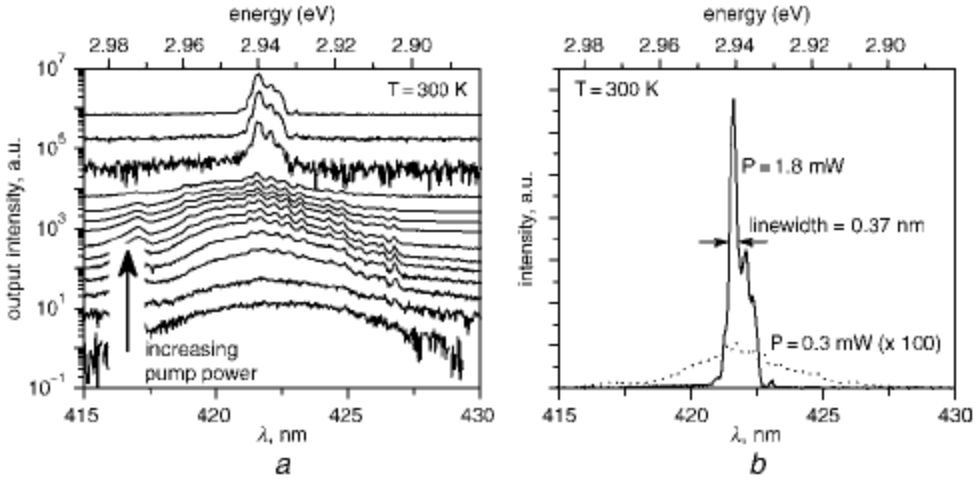

Figure 44
(a) Semi-logarithmic plot displaying RT emission spectra at pump powers ranging from 50 mW to 2mW at 0°, shifted for clarity, and (b) linear plot showing two emission spectra (below and above threshold) of the VCSEL structure (courtesy of E. Feltin of EPLF, Switzerland).

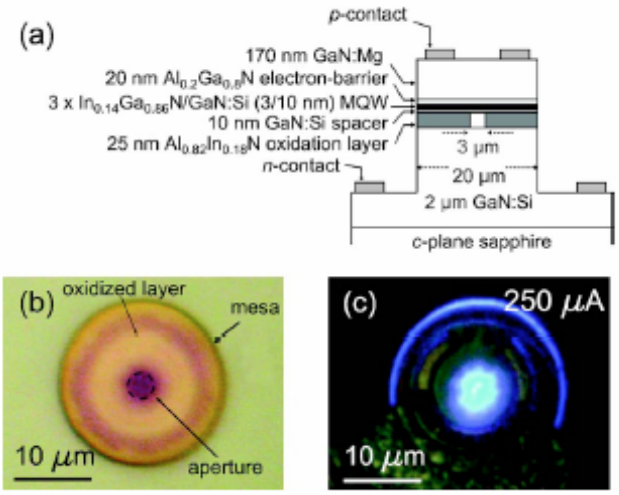

Figure 45
(a) Schematic cross section of the micro LED structures, (b) optical microscope image of a 20 µm mesa with a 3 µm nonoxidized aperture (dark area), and (c) electroluminescence from a micro LED under forward bias (250 µA, 5.8 V) (courtesy of A. Castiglia of EPLF, Switzerland).

Planar semiconductor microcavities (MCs)[239] in strong coupling regime have attracted a good deal of attention owing to their potential to enhance and control the interaction between photons and excitons, which leads to cavity polaritons. The control of the aforementioned interaction is expected to lead to the realization of coherent optical sources such as polariton lasers, which are based on Bose-Einstein condensation, or more strictly non-equilibrium polariton population, due to collective interaction of cavity polaritons with photon modes. In contrast with the bulk polariton, cavity polariton has a quasi two-dimensional nature with a finite energy at zero wave vector, $\boldsymbol{k}$=0, and is characterized by a very small in-plane effective mass. These characteristics lead to bosonic effects in MCs that cannot be achieved in bulk material. In particular, the large occupation number and non-equilibrium polariton population at the lower polariton branch can be accessible at densities well below the onset of exciton bleaching. This can potentially pave the way to ultra low threshold polariton lasers. This feature is markedly different from those governing conventional lasers. Lasing in conventional lasers is predicated upon population inversion which requires substantial pumping/carrier injection. In a microcavity system, however, the lasing condition is uniquely dependent only on the lifetime of the lower polariton ground state. This is expected to lead to extremely low threshold lasers, even when compared to VCSELs.

The experimental observations of these features are prevented in GaAs-based MCs because of the slow relaxation of photoexcited polaritons down to the bottom of the lower polariton branch. Moreover, the needed strong coupling regime is not sustained at RT in the GaAs system due to small exciton binding energy. Consequently, wide-bandgap semiconductors such as GaN and ZnO with their large exciton binding energies must be considered for RT polariton devices. GaN-based MCs are beginning to receive interest in the research community. Several groups have already reported polariton luminescence at RT from bulk[240, 241] and QW[242] GaN-based MCs and vacuum Rabi splitting in these cases were 43 meV and 30 meV, respectively. Recently, polariton lasing at RT in bulk GaN-based MCs in the strong coupling regime was observed under nonresonant pulsed optical pumping.[243] Figure 46 shows (a) the reflectivity from the microcavity, (b) and (c) theoretical angular dispersion from the GaN cavity, and (d) angle-resolved PL spectra at low excitation power up to 60°. The optimum pumping occurred in resonance with the first Bragg mode above the upper DBR stop band, and the system in the strong coupling regime was confirmed by observed anti-crossing behavior from angle-resolved PL. Figure 47 shows the emission spectra at pumped power from 20 μW to 2 mW at 0°. A clear nonlinear behavior is found for the emission at $\lambda \approx 365$ nm, above the critical threshold of $I_{th} = 1.0$ mW. This corresponds to a carrier density of $N_{3D} \sim 2.2 \times 10^{18}$ cm^{-3}, which is an order of magnitude below the Mott density $\approx 1 - 2 \times 10^{19}$ cm^{-3} in GaN at 300 K. The threshold for lasing is one order of magnitude smaller than in previously reported nitride-based VCSELs. Additionally, the emission line was observed to blueshift with increasing pump power and lock at threshold due to polariton-polariton interactions.

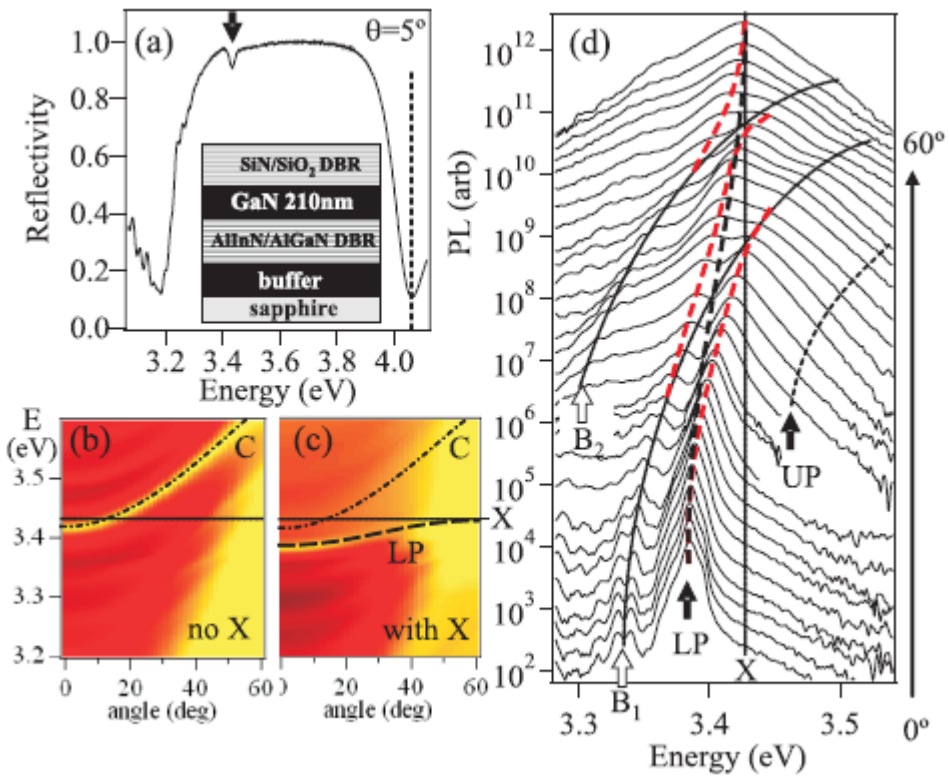

Figure 46. (a) Microcavity reflectivity at 300 K and θ ~ 5°, with lower polariton mode marked by an arrow. Dashed line shows nonresonant pump energy. Inset shows the layer structure. (b), (c) Theoretical angular dispersion both without (b) and with (c) the resonant exciton contribution to the GaN cavity (ω_{LP} dashed line, ω_{cav} dash-dotted line) for a slightly negatively detuned cavity (Δ = -10 meV). (d) Angle-resolved PL at low powers up to 60°, with lower (LP) and upper (UP) polariton, exciton (X), and Bragg (B) modes marked (courtesy of J. J. Baumberg of Cambridge University).

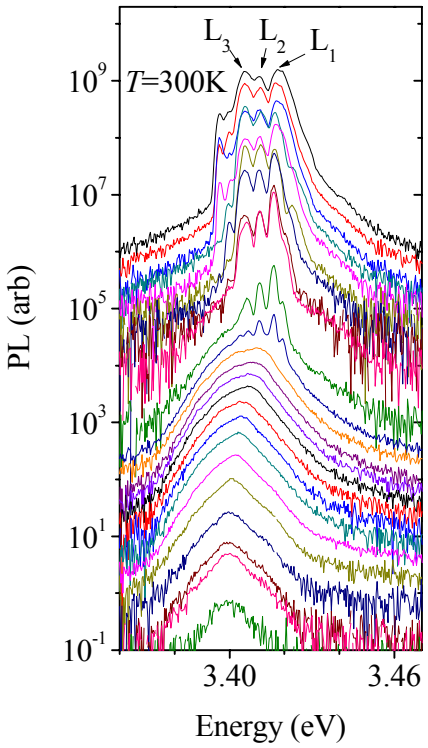

Figure 47. Emission spectra at pump powers from 20 μW to 2 mW at 0°. L_1, L_2 and L_3 indicate different modes (courtesy of J. J. Baumberg of Cambridge University).

Another wide bandgap semiconductor, ZnO is an attractive candidate for ultraviolet (UV) optoelectronics devices. ZnO has an exciton binding energy (60 meV) that is more than twice that of GaN (~ 26 meV). Zamfirescu *et al.*[244] predicted a large Vacuum Rabi splitting Ω_i ~120 meV for cavity polaritons in a model ZnO MC sandwiched between $Mg_{0.3}Zn_{0.7}O$/ZnO DBRs, which projects to an extremely low threshold polariton laser (~2 mW) at RT. A record Ω_i of ~191 meV[245] has been predicted but not yet experimentally observed. On the reflector side, Chichibu *et al.*[246] reported high reflectivity SiO_2/ZrO_2 DBRs for ZnO based MCs owing to a large refractive index contrast between SiO_2 and ZrO_2, giving rise to high reflectivity (> 99 %) and a wide stop band even for an 8 pair SiO_2/ZrO_2 DBR. Recently, ZnO-based MCs were grown by different growth techniques and tested under optical pumping. ZnO based planar resonators which consist of a ZnO cavity layer surrounded with ZrO_2/MgO DBRs were grown by pulsed-laser deposition, and were found to exhibit $\Omega_i \sim$ 50 meV.[247] A vacuum Rabi splitting of the same order (50 meV) was also observed in ZnO-based hybrid MCs using GaN–based bottom DBRs and dielectric (SiO_2/Si_3N_4) top DBRs.[248] Figure 48 (a) shows angle-resolved PL spectra at RT up to 40°. It is clear that the lower polariton mode gets close to the uncoupled exciton mode, and the upper polariton mode is dispersed from the exciton mode to the cavity mode. The experimental cavity polariton dispersion curve shown in Figure 48 (b) exhibits a typical anti-crossing behavior between the cavity mode and exciton mode when the cavity mode energy crosses the exciton mode. These results are promising towards the

realization of RT ZnO-based polariton devices. ZnO-based electrical injection lasers may also be realizable in the near future when reproducible and reliable p-type conductivity in ZnO is achieved.[249,250]

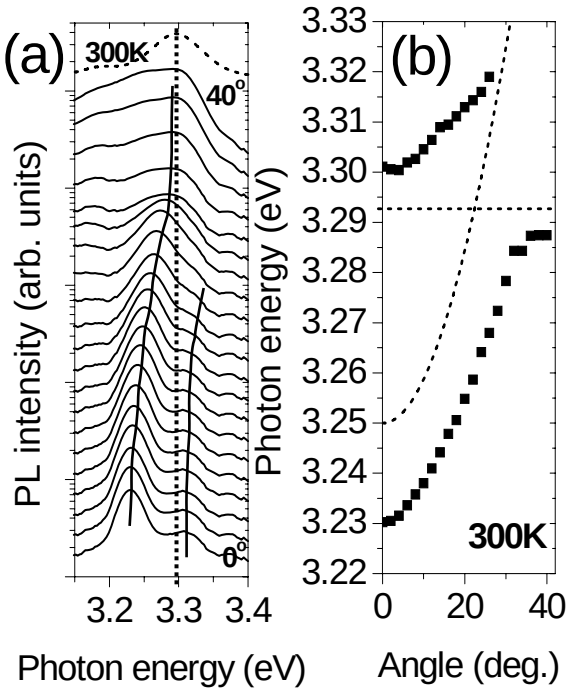

Figure 48. (a) Angle-resolved PL spectra at RT in the range of 0 ° to 40 ° for a λ-thick ZnO hybrid MC. The dotted line is the exciton mode. The solid lines are guides to the eye. (b) Experimental cavity polariton dispersion curve. The dashed lines represent the cavity and exciton modes (courtesy of R. Shimada of Virginia Commonwealth University).

There are plenty of reports on UV lasing from ZnO-based materials and devices under optical pumping, for example, lasing from ZnO photonic crystals[251,252] and random lasing from ZnO powder under certain pumping conditions.[253] A ZnO based optically pumped 3rd order distributed feedback (DFB) laser has also been reported.[254] A single longitudinal mode was observed between 10 and 270 K. Mode selection was accomplished via a third order diffraction grating. As seen from Figure 49 the DFB laser had a spectral linewidth of 0.5 nm, a pump threshold intensity of 0.12 MW/cm^2, and a peak output power of 14 mW. The temperature tuning coefficient of the ZnO refractive index was deduced to be 9×10^{-5} K^{-1} from wavelength vs. temperature measurements. However, none of these methods are promising for device applications, which demand high power and low excitation threshold.

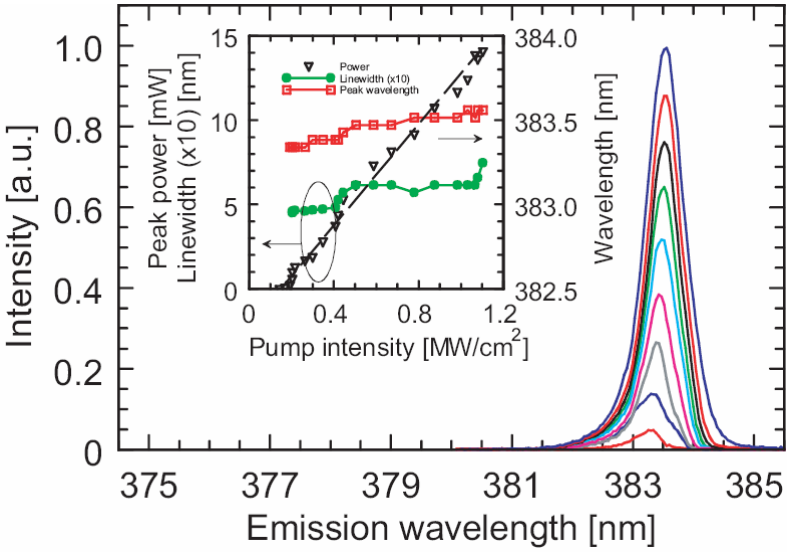

Figure 49. Emission spectra of a ZnO-based DFB laser as a function of optical pump power measured at 0.15, 0.25, 0.35, 0.45, 0.6, 0.8, 0.9, 1.0 and 1.1 MW/cm^2. The inset shows peak power (triangles, left y axis), emission wavelength (squares, right y axis), and linewidth (circles, left y axis, times ten) vs. pump intensity curves (courtesy of D. Hofstetter of Neuchâtel University, Switzerland).

VI.4. Conclusion

In conclusion, semiconductor lasers based on GaN have had a tremendous impact on our lifestyle already; however, reliability issues for the high power laser diodes (having to do with facet damage, electron leakage, and nonradiative recombination center generation) need further investigation and technological effort. Electrically-pumped GaN-based vertical cavity lasers do not seem to be far from realization considering the recent progress in defect reduction and efficient carrier injection. On the ZnO side, unavailability of *p*-type ZnO is the bottleneck. Nevertheless, GaN- and ZnO-based UV lasers are highly attractive candidates for telecommunication and optical storage. In recent years the reliance on internet access has become much more evident, which requires large capacity and high speed communications hardware. It should also be stated that the demand for higher speed and bandwidth will always remain and we must constantly search for materials, devices, and systems that can meet our needs. To satisfy the increasing demands, high density and high speed recordings are also crucially needed. It is therefore imperative for the engineers/scientists to develop blue-green-UV wavelength emitters of high efficiency, such as high-coherence and low-threshold UV lasers which make high density recording/reading possible, for the stated applications. The low threshold or nearly thresholdless VCSELs, in addition to being possible strong light pump sources for white light generation, have applications in ever increasing telecommunications and optical storage. It is clear that this technology has far reaching impact on our lifestyle and the environment in which we live.

VII. Light emitting diodes

VII.1. Preface

The light emitting diodes are poised to launch another revolution in the technology front. They transformed themselves from being indicators to being illuminators. They have advanced to the point that all the portable electronics gadgets sport LEDs for backlighting. Soon large area displays including some TVs will sport them. The biggest catch of all is the indoor illumination helped by inroads in outdoor and special lighting applications first.GaN based LEDs may end up the choice of illumination if the technology can deliver what is needed and if the policy makers and the public see the light. While LEDs are surpassing fluorescent bulb, minus the Hg and the mere size and bulk, in terms of efficiency and lifetime, the goal is to push further. The bottleneck for furthering performance is the internal efficiency of the material. This is dovetailed with the material quality as in any other device. Materials quality also affects, to no one's surprise, degradation rate of the devices. Below, following an introduction to the topic, the state of the field is reviewed followed by concluding comments as to the future.

VII.2. Introduction

Light emitting semiconductor devices have recently been attracting more attention than ever for general solid state lighting and displays. Pushed by the commercial needs and technical advances, the GaN based light emitting diode (LED) devices are approaching to their limit (refer to Table 4 for the performance of status-of-art LEDs). LEDs with a luminous efficacy of 75 lm/W are commercially becoming available in 2006 by Cree, Lumileds and Nichia. Values of 100 lm/W are beginning to appear. However, in order to replace the traditional incandescent or fluorescent light bulb with LEDs as a source of lighting, there are still a few issues to resolve. For example, optical power of the emitter saturates and then decreases as the driving current increases, probably due to the non-optimum quantum well design, leakage current, non-radiative recombination centers, contact degradation, and carrier leakage. This efficiency droop with injection has also been attributed to Auger recombination which is not supposed to be likely in large bandgap semiconductors particularly considering that InGaN based lasers, even wavelengths as long as 480 nm have been achieved. Optimized chip designs, on the other hand, could help to address the issue of internal reflectance loss and enhancement in extraction of generated photons. The drive for shorter wavelength operation is another issue that needs to determine the optimum wavelength for phosphor assisted white light generation.

Table 4. Nitride LED performance for both commercial and developmental devices as of 2007.

High-power LEDs	Wave-length (nm)	Output power (mW)	Flux/ LED (lm)	Luminous efficiency (lm/W)	Drive current (mA)	Drive voltage (V)	Die size (mm^2)	Lifetime (hrs)	Company
UV	365	250			500	3.8	1x1		Nichia
	385	310			500	3.7	1x1	100,000	Nichia
Blue	470		35	9.4	1000	3.72	1x1	50,000	Lumileds
	460	385			700	4.5	0.9x0.9	50,000	Cree
Green	530		55	52.3	300	3.5			Nichia
	530**		100	26.9	1000	3.72	1x1	50,000	Lumileds
White	**Blue + Phosphor		170	69.4	700	3.5	1x1	50,000	Lumileds
			84	75	350	3.2	0.9x0.9	50,000	Cree

* Development, ** commercial

Many applications of these LEDs require that the efficiencies remain high at larger current densities (greater than 50 A cm^{-2}); these include projection displays,[255] automotive headlights,[256] and general lighting.[257] However, InGaN/GaN (0001) quantum well (QW) light-emitting diodes (LEDs) exhibit a maximum external quantum efficiency at very low current densities, typically <10 A cm^{-2}. As the current density is increased beyond that point, a monotonic drop in quantum efficiency is observed in blue and green InGaN/GaN QW LEDs, even under short-pulse, low-duty-factor, constant temperature injection.[258,259,260] The drop in quantum efficiency with increasing current for blue and green InGaN/GaN LEDs has been attributed to many different mechanisms, such as poor injection efficiency,[261, 262] carrier delocalization from quantum dots,[263, 264] exciton dissociation,[265] high plasma carrier temperatures (hot carriers)[266], and Auger recombination[267]. The efficiency droop is discussed in Section VII.5 in more detail.

Another issue with the external quantum efficiency is that the external quantum efficiency drops sharply for wavelengths shorter than 360 nm, as shown in Figure 50. Typically, two reasons are thought to be responsible for the efficiency drop at longer peak wavelength. First of all, a reduced crystal quality is expected for structures with higher In content as is necessary to lower the band gap of $Ga_xIn_{1-x}N$. Moreover, a higher piezoelectric field for $Ga_xIn_{1-x}N$ layers that are more highly strained with higher In content, leads to a stronger separation of the electron and hole wave functions. How to improve the external quantum efficiency without significantly increasing the processing costs is still a challenging problem.

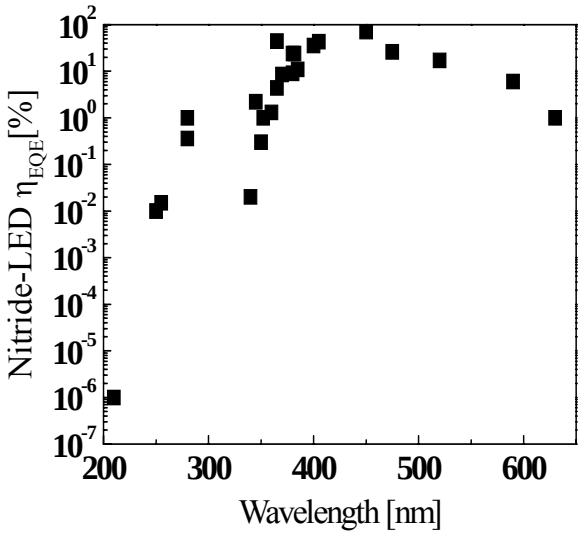

Figure 50: External quantum efficiency of GaN based LEDs (courtesy of H. Amano of Meijo University, Japan[268]).

VII.3. Materials

An LED structure with a metal alloy substrate, which has a very high thermal conductivity of 400 W/m-K, and therefore, allows high-current operation, has been reported. (see Figure 51 for a schematic).[269] The chip has a patterned surface with "photon-injecting nozzle" microstructures to enhance light extraction in the forward direction. 8 LED chips packed together could provide 460 lm white light with a luminous efficacy of 58 lm/W at 470 mA. The Metal Vertical Photon LED (MvpLED) has a p-down epitaxial structure mounted on a reflector layer which is attached to a metal alloy substrate.

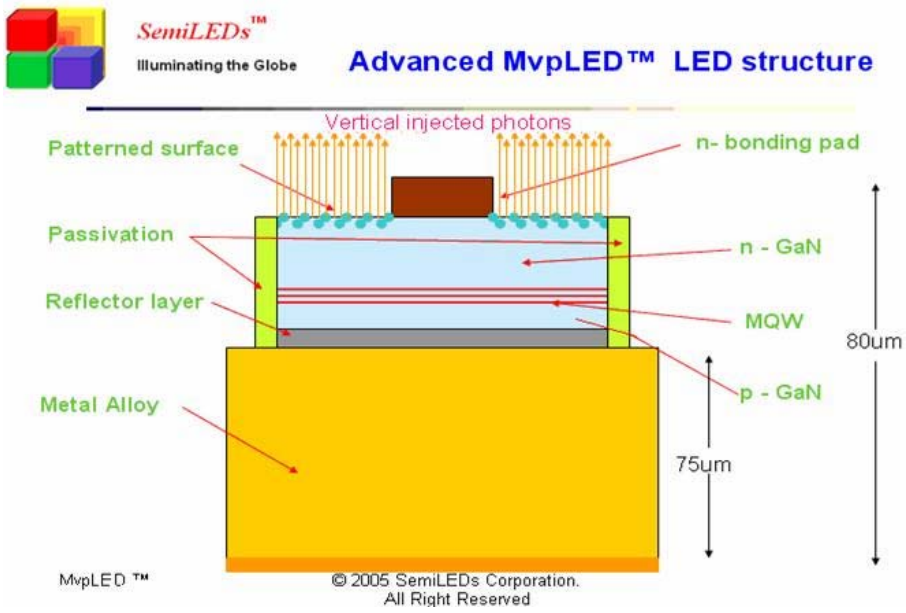

Figure 51. A Metal Vertical Photon LED (MVP-LED) structure from SemiLEDs (courtesy of C. A. Tran of EMCORE Corporation [269]).

LED structures have also been grown by HVPE on bulk GaN and emission at blue (450~480 nm) and green (490~500nm) wavelengths has been demonstrated, as shown in Figure 3.[270] XRD and TEM measurements on HVPE grown InGaN superlattice structures revealed sharp interfaces. The MQW structures were grown by HVPE on p-GaN templates. The acceptor doping level were observed to reach up to 3×19 cm^{-3}, which could be precisely controlled providing uniform doping or abrupt doping profiles with low memory effect. The room-temperature hole mobility of 15-40 cm^2/Vs at a carrier concentration of 4.4×10^{17} – 1.3×10^{18} cm^{-3} was achieved. With the availability of thick crack-free p-GaN templates, HVPE grown GaN substrate may provide user the benefits of high productivity, low cost, and shorter growth cycling.

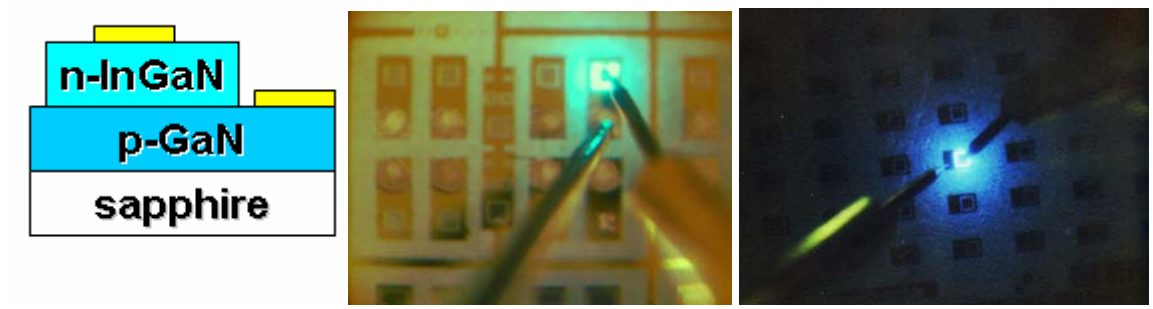

Figure 52. Green and Blue LED structures grown by HVPE (courtesy of A. Usikov of TDI).

VII.4. Device Structure

GaN-based LEDs are commercially used in various areas. However, future demands for these and more advanced applications will still require higher light output with lower power consumption. Nevertheless, only a small fraction of the photons generated inside a GaN LED device can escape because of total internal reflection (TIR) at the interface of GaN and the outer medium.

To eliminate the above-mentioned internal loss issue of GaN LEDs and to extract more light from the device surface, GaN-based photonic crystal (PC)-LEDs fabricated using a laser holography (LH) method have been reported.[271] These structures are suitable for high-throughput and large-area processing. There are two kinds of PC-LEDs reported: top-loaded and bottom-loaded. For the top-loaded PC-LEDs[272], a conventional LED structure was grown first. Then using laser holography method, the photonic crystal pattern was generated, as shown in Figure 53. The resultant LEDs exhibited significant improvements in light extraction, up to 1.5 times that of planar LEDs without PC integration (see Figure 54). Similar results were obtained for the bottom-loaded PC-LEDs, in which the photonic crystal was formed between the substrate and the epilayer (refer to
Figure 55 for a schematic).

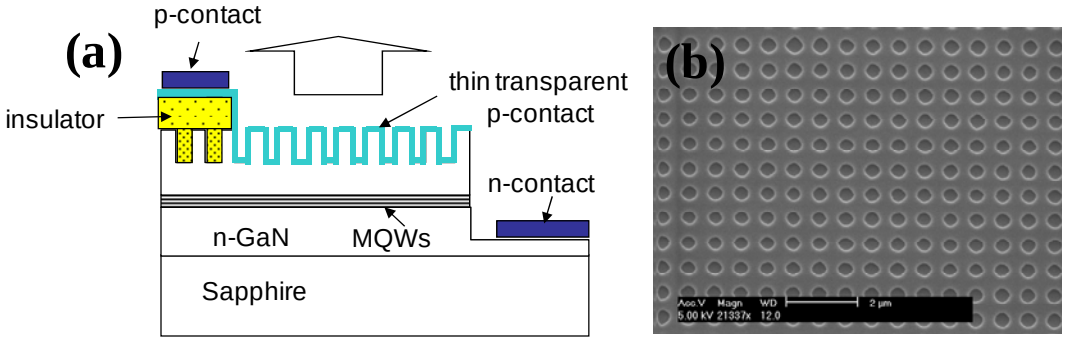

Figure 53: (a) Schematic view of a top-loaded PC-LED, illustrating the vertical layer structure of the device. (b) Scanning electron microscope image for a top-loaded PC-LED device surface. The square-lattice air-hole array pattern was generated by the holographic double-exposure method. The lattice period of this specific example is ~700 nm (courtesy of H. Jeon of Seoul National University, Korea [271]).

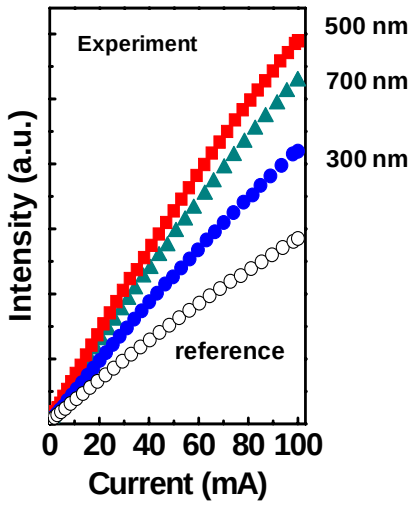

Figure 54: Light output vs. injection current characteristics (L-I) for PC-LED chips with lattice constants of 300 nm ([bullet]), 500 nm ([square, solid]), and 700 nm ([solid triangle]), together with that from a planar reference device ([open circle]) for comparison (courtesy of H. Jeon of Seoul National University, Korea [271]).

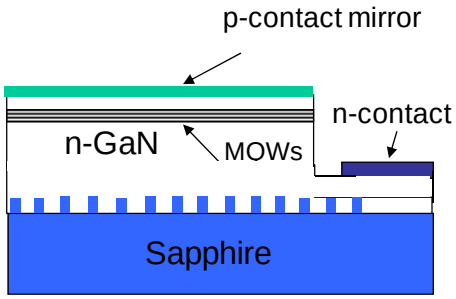

Figure 55: Schematic view of a bottom-loaded PC-LED (courtesy of H. Jeon of Seoul National University, Korea [271]).

Another approach to reduce the internal optical loss is to employ a so-called "side-wall deflector" to reflect out the photons which are trapped between the air-GaN-sapphire waveguide. As shown in Figure 56, typically angles of 20º-40º between the mesa sidewalls and the substrate were achieved by a photoresist reflow method[273]. Experimental results, including photoluminescence and near- and far-field patterns, show a strong additional emission along the sidewall edge (see Figure 57), and the proposed LED structure enhanced the overall surface emission intensity by 2 times for a sidewall angle of 30º. When a combination of photonic crystal and angled sidewall was employed, a 3 times higher emission power was achieved.

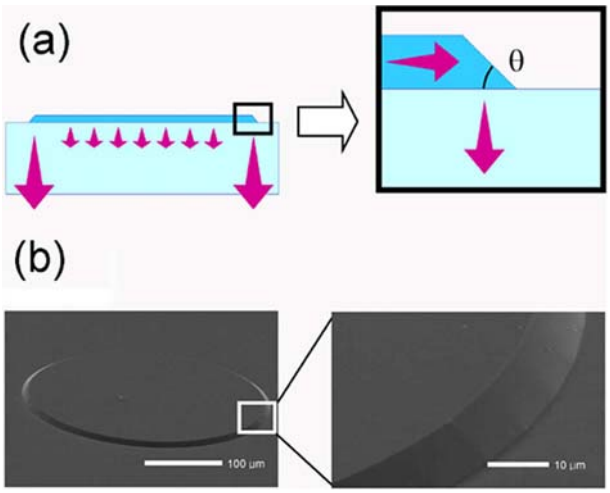

Figure 56: (a) Schematic of the "sidewall-deflector-integrated" LED structure. (b) SEM images of a fabricated "sidewall-deflector-integrated" LED structure (courtesy of H. Jeon of Seoul National University, Korea [273]).

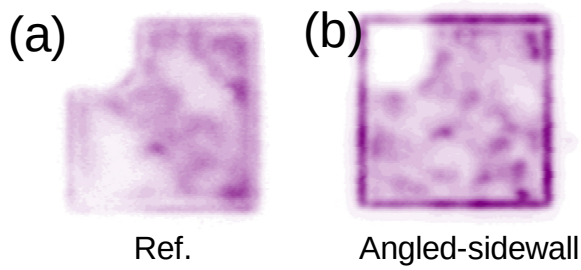

Figure 57: LED emission pattern from a reference LED and a "sidewall-deflector-integrated" LED. Strong additional emission could be observed along the sidewall edge. (courtesy of H. Jeon of Seoul National University, Korea [271]).

VII.5. Efficiency droop at high injection levels

A rather important aspect in GaN LEDs in general is the reduction of output light with increasing injection current. The thermal component o f the problem is reasonably well addressed with very advanced packaging technologies which not only effectively extract the photon generated but also dissipate the heat. However, all GaN LEDs suffer efficiency reduction when pumped at high injection currents, the absolute value of which depends on the layer quality and packaging, among others. Specifically, a good part of the reduction in efficiency in LEDs on c-plane sapphire with increasing injection current is due to reduction in the internal quantum efficiency which in general involves opening up channels for non radiative recombination. Carrier leakage when the band discontinuities in quantum wells region are small can also contribute to such an effect. Consequently, the maximum internal quantum efficiencies are obtained at relatively low injection levels, sometimes as low as 10 A cm^{-2} ([274,275]). This is in contract to the observations made in LEDs based on relatively well developed and high quality conventional III-V semiconductor material systems, such as (In,Al,Ga)As and (Al,Ga)InP. As the current density is increased beyond that point at which the maximum injection efficiency is attained a monotonic drop in quantum efficiency is noted in blue and green

InGaN/GaN QW LEDs, even under short-pulse, low-duty-factor, and constant temperature injection.[274,275] However, just about all the applications of these LEDs require for theme to retain high quantum efficiencies at larger current densities (*e.g.* greater than 50 Acm^{-2}). As mentioned throughout this chapter, these applications include but not limited to projection displays,[276] automotive headlights[277], and general lighting.

The decay in quantum efficiency with increasing current for blue and particularly green InGaN/GaN LEDs has been attributed to many different mechanisms, among which are poor injection efficiency,[278,279] carrier delocalization from quantum dots,[263] exciton dissociation,[265] high plasma carrier temperatures (hot carriers),[266] and polarization effects together with electron blocking layers.[280] Furthermore, the Auger nonradiative recombination[267] as well as methods to mitigate it, [281] has been reported to the cause of the efficiency droop at high injection levels. It should be noted the measurements performed at various laboratories, including that of the author, indicate that the intensity droop is not observed in PL experiments, but rather EL experiments, indicating that reduction in the efficiency is not related to the MQW radiative recombination efficiency but to the loss of carriers such as recombination outside the quantum well region. This is generally terms as carrier leakage. The effect of heating due to increased current at high injection levels has been ruled out. The quantum well layer thickness dependence of the efficiency droop has been investigated which indicate that the droop is not as evident in wider quantum wells which have the down side of reduced overall intensity pointing to some unresolved issues.[282]

In the case of Auger recombination notion, the Auger recombination coefficient pulled out of fitting a 3rd order polynomial is on the order of $1.4x10^{-30}$ to $2.0x10^{-30}$ cm^6s^{-1} which is comparable to that which has been measured for InP that has half the bandgap of InGaN emitting in the blue.[267] This is some 4-5 orders of magnitude larger than what can be expected of the bandgap of the blue of InGaN when extrapolated from the data for more conventional semiconductors ranging from InAsSb on the small bandgap side to GaAs on the relatively large bandgap side.[283] The 4-5 orders of magnitude disparity could in fact increase considering that the dispersion between hole and electron masses in conventional III-V semiconductors is much smaller as compared to InGaN. We should mention that Auger recombination has been studied in the smallest bandgap triad of nitride semiconductors, InN.[284] Regardless, it is clear that the efficiency droops with increasing injection level which points to carrier leakage or loss of some sort, which will take some time sort out.

The theoretical basis for the Auger recombination[285,286,287,288] has been laid years ago. It should be recognized that Auger recombination is an intrinsic property of a given semiconductor and is determined by the conduction and valence bands as well as the bandgap and its type meaning direct or indirect. Further because Auger recombination involve carrier recombination across the band and also carrier excitation to higher energies, the process involves many carriers and as such it becomes more important at high carrier densities. To a first degree, if the Auger recombination, which is more dominant at high injection levels and as in its simplest treatment goes with the third power of the carrier concentration, were to take place in GaN based LEDs at current

densities dwarfed by those in effect in lasers, to be consistent one can surmise that lasers in GaN could not be obtained if the layer qualities were in the same ball park. Because, this is not the case, it is more likely that the efficiency reduction with injection current is related to materials quality/particulars (such as localization which at high injection levels would be not as effective) and heterojunction design (such as thin multiple quantum wells *vs.* one relatively thick active layer considering the large hole effective mass) if the processing and packaging related issues are address effectively. It is likely that the Auger process involving defect levels could enter into the equation. One can then surmise that the current density at which the efficiency peaks would be increased in time as structures addressing carrier leakage aggravated by the large hole mass come into play.

VII.6. Conclusions

The light-emitting diodes (LEDs), which were simple indicator lamps, have become a bright and efficient light source for many applications. They have already begun to displace incandescent lamps for many uses, where their particular characteristics such as efficiency, longevity, durability, compactness, cool operation, and/or directionality are needed. Especially, the advent of nitride based LEDs is poised to revolutionize general lighting. Many technological developments have been made since the first demonstration of GaN LEDs. As a result of the developments, the life time, measured to 70%, lumen maintenance, currently reaches more than 50,000 hours, which is several times longer than other conventional lamps. And sophisticated structures raise the light extraction efficiency of the LED to 80 %. Recently some laboratories showed efficacies over 150 lm/W and high power white LEDs with 100 lm/W or more are commercially available. This number in terms of efficacy surpasses handily that of the incandescent lamps and surpasses that of the fluorescent lamps. In the near future, breakthroughs in LEDs would increase internal and external quantum efficiencies, and result in high-power phosphor-white LEDs with efficiencies reaching 200 lm/W or more (depending on the approach used), which can be achieved by further improvement in the material quality and designing novel structures with enhanced light-extraction efficiency. This new white-light source would change the way we live and the way we consume energy. In the near future when most of current bulbs are changed to very high efficient LEDs, it is predicted that worldwide electricity consumption for lighting decreases by more than 50% and total electricity consumption decreases by more than 10%. LEDs would give us not only the ultimate efficiency but also tremendous opportunities for versatile and smart lighting applications.

While great strides are being made, the internal quantum efficiency and the associated efficiency droop at high injection levels are getting a good deal of attention from the research and development communities. Finally, the prospects for GaN based LEDs are great, but some of the standards, some of which appear somewhat out of touch and or arbitrary, set by the international illumination society may have to be revisited in order to allow LEDs to take their much deserved place in lighting applications. Furthermore, the illumination industry is notorious for being slow in grasping new technologies; particularly a technology like LED which is very different is size and power requirements

from existing technologies. The old cultures which are set in firmly would need to be relaxed some to embrace new and better technologies such as the one provided by the advent of LEDs.

VIII. P-type doping of GaN and ZnO

VIII.1. Introduction

There has been a plethora of papers, no dearth here, on p-type ZnO often times with apparently very high hole concentrations but with low mobilities. In a few cases, the mobilities reported are unreasonably high. Even what is generally known to be n-type dopants have been reported to lead to p-type ZnO. N, which is known to provide the shallowest acceptor impurity, is most likely a genuine p-type dopant. However, N has low solubility on the O lattice sites making it imperative to decrease the background donor concentration and increase the solubility by a co-dopant. Reports are also abound that the purported p-type doping is not stable in ZnO. There have also been p-n junctions reported, but the efficiency of light emission is low considering that one of the selling points of ZnO is supposed to be the efficient light radiative recombination process. The emission width is arguably wide, and the source of emission is controversial and or not well understood. Whether the measurement methods used to determine p-type conductivity to the particular samples are appropriate or not and the resultant pitfalls are discussed. In addition, alternative explanations for the observations as well as new data shedding some light on the topic were presented at the meeting and reviewed here. The discussion on what transpired at the meeting is preceded by the general problem of p-type doping in wide bandgap semiconductors and developments leading to p-type GaN, and followed by the authors' review of the status of p-type doping in ZnO and the likely approaches that might have to be brought to bear to achieve p-type conductivity.

VIII.2. Inherent difficulties associated with p-type doping in wide bandgap semiconductors

Difficulty in controlled bipolar carrier doping (both n- and p-type) in a wide range of concentrations is a major obstacle in wide bandgap semiconductors such as GaN and II-VI compound semiconductors including ZnS, ZnSe, and ZnTe.[289,290,291,292,293,294,295] Prior to the advent of Mg doping, unintentionally doped GaN has, in all cases, been observed to be n-type. The background has been attributed to the presence of intrinsic defects and impurities. Intentional n-type doping is relatively well established through the substitution of group IV elements (Si, Ge) on the Ga sites, producing highly conductive *n*-type GaN. The same intrinsic defects responsible for *n*-type conductivity tend to aggravate the effort for p-type doping by compensating potential acceptors.

Unipolar doping has not been a surprising issue in wide bandgap semiconductors such as GaN, ZnO, CdS, ZnS, and ZnSe are also easily doped to n-type while p-type doping is difficult. The situation is opposite for ZnTe and CdTe where p-type doping is easily obtained while n-type doping is difficult. In general, the asymmetry arises from the fact that wide-gap semiconductors either have a low valence-band maximum or a high conduction-band minimum with respect to the vacuum level.[296,297] As a result, some

materials in which the valence band is relatively close to vacuum level, e.g. ZnTe, CdTe, and diamond, have preferable p-type conductivity. In contrast, materials with a valence band relatively far from the energetic position of the vacuum level, e.g. ZnO, GaN, CdS, ZnS, and ZnSe, have preferable n-type conductivity.

The difficulties can arise from a variety of causes. Attempted p-type dopants may be compensated by low-energy native defects and or background impurities which give rise to propensity to *n*-type doping. To make matters worse, the very attempts to render the semiconductor p-type may in fact create donor like defects which compound the problem. Some centers of compensation are pinned to the same level which hardly depends on the position of valences and conductive bands.[298] This compensation problem is the most challenging phenomenon in wide-gap semiconductors. Low solubility of the dopant in the host materials[299,300] and precipitate formation are also possible causes. We now turn our attention to efforts predating successful p-type doping in GaN.

VIII.3. P-type GaN

VIII.3.1. Pre p-type doping era in GaN LEDs

Owing to its wide bandgap GaN was recognized early on to be a material of considerable importance for short wavelength emitters in the visible, violet and shorter wavelengths of the optical spectrum. However, the roadblock, which turned out to be a formidable one, was the lack of p-type doping which haunted GaN for many decades. To go around what seemed at the time to be somewhat of an intractable problem; structures not relying on p-type doping were developed and used for light emission, albeit with much lower efficiencies that it would be otherwise. Nevertheless, achieving emission in blue by injection electrons from a metal contact in Zn-doped GaN was thrilling.

After the initial report by Pankove et al.[301] of a GaN light emitting diode (LED), numerous workers have fabricated similar structures. Due to the inability to dope GaN p-type, these devices were not conventional p-n junction LED's, but rather metal-insulator-n-type semiconductor (MIN) structures in which a heavily compensated insulating GaN region (compensation was done with Zn doping) was grown on uncompensated n-type GaN. A side contact to the n-type GaN was formed in order to avoid the difficulties related to the chemical etching of GaN. It was theorized by Pankove and Lampert[302] that light emission was obtained when hot electrons impact ionized luminescence centers in the Zn-doped compensated region of GaN. A hot electron model was strongly supported by the observation of antistokes emission in which the electroluminescence was at a higher energy than was being supplied by the applied bias to the electrons.[303,304] Pankove and Levin[305] reported a detailed scanning electron microscopy study of GaN LEDs.

Depending on the compensating impurity, MIN structures have emitted violet[306,307,308,309,310], blue[311,312,313,314,315,316,317,318,319,320,321,322,323], green[311,313,314,320,321,324,325], yellow[311,313, 314,321,324,325,326], orange[311,313], and red[319] light at frequencies up to 50 MHz[327]. By selectively depositing metallic electrodes to form MIN electroluminescent diodes, Pankove[328] demonstrated a blue-green GaN numeric display. Pankove and Norris[329] also reported electroluminescence from Al/Si3N4/GaN structures which exhibited a broad spectrum optical response under electrical pulse stimulus. In these structures, a large electric field was thought to generate holes at the n-type GaN surface which recombined when the field was removed.

VIII.3.2. Doping with Zn

Prior to successful demonstration of p-type GaN, the most investigated[312,315,379,330,331,332,333,334,335,336,337,338,339,340,341,342] potential p-type dopant for GaN has been Zn. Zn impurities effectively compensate GaN resulting in high resistivity material.[312,314,315,330,332,343,344,345] Jacob *et al.*[313] Boulou *et al.*[346,347] and Monemar *et al.*[338]. have published the most complete optical investigations of the properties of Zn-doped GaN. Emission spectra as a function of Zn concentration were taken. Four Zn-related peaks were observed at room temperature. All samples exhibited the commonly observed 2.8 eV emission.[343,344,345,,339,348,349,350,351] In addition, heavily doped samples had additional room temperature peaks at 1.8-1.9 eV, 2.2 eV, and 2.5-2.6 eV which disappeared as the temperature was decreased below 200 K. Samples exhibiting the three midgap Zn-related peaks had weak luminescence compared to the lightly doped samples dominated by the 2.8 eV transition, however their intensity did increase in samples grown under nitrogen poor conditions. From these data, both groups concluded that the 2.8 eV emission corresponds to a Zn_{Ga} center while the three midgap peaks represent a Zn_{As} triple acceptor site. This is in agreement with the photoconductivity results of Pankove and Berkeyheiser[344,345] who observed that Zn, present in sufficient concentrations, favors the substitutional replacement of N vacancies. This is also consistent with the observed lattice expansion at high Zn[352] and Mg[353] doping levels which would result from group II impurities occupying nitrogen lattice sites. Desnica et al.[341] has proposed the incorporation of the ^{67}Ga isotope into GaN. Its subsequent decay into[354] Zn would guarantee that the Zn impurities were in Ga sites and a higher dopant activation and possibly even p-type conduction might result. Pankove [355] has provided an excellent perspective on the GaN doping problem with special attention to Zn doping. A tentative model which is consistent with the observed data was also proposed.

Several groups have investigated the lifetime of the Zn single acceptor transition. Bergman *et al.*[351] measured a decay time of 300 ns at 2 K while Marasina *et al.*[356] reported a sample dependent 150 - 200 ns relaxation time at 100 K which decreased to 70 ns at room temperature. Pankove *et al.* [339,344,345] reported a significantly larger relaxation

time, of the order of microseconds, which was sufficiently long that the authors were led to speculate that the radiative recombination involved a tunneling mechanism. More work is needed to distinguish between these two contradictory results.

VIII.3.3. Doping with Mg: Unsuccessful early efforts

A number of workers [330,342,353,357,358,359,360,361,362] have investigated Mg doping which has also been observed to effectively compensate GaN. Liu *et al.*[363] observed the Mg acceptor luminescence at various doping levels. The Mg peak broadened and shifted to lower energy with increased doping, eventually reaching a minimum energy of 2.95 eV. The intensity of the luminescence remained roughly constant as the Mg content was raised, until the luminescence was abruptly quenched at the same concentration at which the resistivity of the GaN began to increase rapidly. Ilegems and Dingle[342] observed the same 2.95 eV emission. However, a number of groups[364,365,366] have reported the location of the Mg acceptor peak to be 3.2 eV.

VIII.3.4. Doping with Cadmium

There have been several reports[349,351,367 368] which describe attempts to dope GaN with Cd. Bergman et al.[351] were able to dope GaN with a small amount of Cd but a sufficient amount to compensate the electron background concentration could not be incorporated. Three groups[351,364,368] have observed the Cd-related luminescence peak at 2.7 eV while Ilegems *et al.*[349] reported the Cd-related peak at 2.85 eV. Bergman *et al.* [351] measured a 1 μs decay time at 77 K for their 2.7 eV emission.

VIII.3.5. Doping with Calcium

Suggestions have been made that Ca may form a shallow acceptor level in the GaN bandgap.[369] Ca p-type doping of GaN was achieved by ion implantation of Ca^+ ions or by a co-implantation of Ca^+ and P^+ followed by a rapid thermal annealing at temperatures $\geq$ 1100°C. [370] . The ionization energy of 169 meV was found by temperature-dependence measurements of the hole concentration in a sheet, which should be considered with a good deal of caution. Ca acceptors, like those of Mg, can be passivated by atomic hydrogen at low temperatures (250°C); and they can be reactivated by thermal annealing at $\leq$ 500°C for 1 hour. Ca implanted GaN has been investigated in terms of the optical emission spectrum.[364]

VIII.3.6. Doping with Beryllium

Beryllium, if it can be incorporated in a way to replace Ga without creating compensating donor like defects, is a relatively shallow impurity. Two groups[342,364,,371] reported Be-doped GaN without success. Be was observed to effectively compensate the free electrons and high resistivity GaN was obtained. Optical measurements detected a broad Be-related emission at an energy of ~ 2.2 eV. In an experiment with RMBE-grown films, [372] the 380 nm emission peak is the dominant one for low Be-doping levels. In samples with higher doping, 420-430 nm emission is observed.

VIII.3.7. Doping with Mercury

In yet another thread of searching for p-type conductivity, two groups[341,357,367] have investigated Hg doping. No electrical measurements were reported. Pankove and Hutchby[364] observed 2.43 eV emission in Hg-doped samples. Ejder and Grimmeiss[367] observed 2.9 eV emission and estimated the Hg-acceptor level to be 410 meV above the valence band.

VIII.3.8. Doping with Lithium

A number of workers [357.364,371,367] have investigated Li doping. Pankove *et al.*[371] obtained compensated GaN using Li doping. The Li acceptor luminescence was observed at 2.23 eV. Ejder and Grimmeiss[367] estimated the Li-acceptor level to be 750 meV above the valence band.

VIII.3.9. Doping with Carbon

Carbon in both GaN and AlN is amphoteric in nature.[373] Its salient features in both materials are similar: Carbon on a Ga or Al site, C_{cation}, is predicted to be an effective mass donor while carbon on a N site, C_{anion}, is an effective mass acceptor. The ionization energies of the acceptor have been predicted to be equal to 0.2 in GaN and 0.4 eV in AlN. Incorporation of C on a nitrogen site is preferable because the C_N-formation energy is lower under both Ga- and-N rich conditions of growth. Carbon on a cation site, C_{cation}, can also assume a metastable DX-like configuration $C^*_{Ga\ or\ Al}$ which requires a broken bond between C and one neighbor. In this configuration, both the host N and carbon atoms are significantly displaced. $C^*_{Ga\ or\ Al}$ introduces a singlet at approximately 0.4 eV and 0.3 eV above the valence bands of GaN and AlN, respectively, and a singlet occupied by one electron at about 0.3 and 1.0 eV below the conduction bands of GaN and AlN, respectively. Experimental investigations, however, did not lead to credible p-type reports. However, carbon acts as a compensating center in GaN. Unintentional C doping with genesis in organometallic sources used is noted when grown a low pressures.

VIII.3.10. Doping with other impurities

Impurities other than the ones discussed briefly above have also been introduced into GaN for conductivity manipulation. Ion-implantation was used by Pankove and Hutchby[364] to introduce a total of 35 elements into GaN and observed the optical spectra. Al implantation at a very high dose was unsuccessful in producing the alloy shift of the primary 3.45 eV emission to higher energy that was observed by Monemar and Lagerstedt.[374] Monemar and Lagerstedt also reported that high resistivity GaN was obtained when Fe or Cr was incorporated during the growth. Metcalf *et al.*[375] implanted GaN with P and N and measured P-related emission at 2.85 eV and an As-related band at 2.58 eV. A damage induced emission at 2.2 eV was also noted. Ogino *et al.*[376] also reported the PL spectrum of P-doped GaN.

VIII.3.11. Doping with Mg: Successful efforts

Continuing on with the recognizing that harnessing the tremendous potential of GaN hinged on achieving p-type doping, much effort has understandably been aimed at doping GaN p-type by introducing group II (to substitute Ga) and IV (to substitute N) elements. Some impurities have been observed to effectively compensate electrons in GaN leading to highly resistive material. After some two decades of focused effort, Akasaki, Amano and co-workers[357] demonstrated that exposure to low energy electron beam irradiation (LEEBI) enhanced the luminescence efficiency in Zn-doped GaN. Building on the observation that luminescence enhanced by LEEBI treatment, Amano and coworkers,[362, 377, 378, 379, 380] applied the LEEBI technique which converts Mg-compensated GaN into highly p-type material. Optical measurements have shown that the acceptor levels in GaN are several hundred meV above the valence band edge.

Nakamura et al.[381] reported bright, for its time, LEDs by applying the LEEBI method to Mg-doped GaN along with the revelation that the as grown GaN exhibited p-type conductivity, albeit with a meager hole concentration of $2\times10^{15}/cm^3$. LEEBI treatment was reported to enhance the hole concentration to $3\times10^{18}/cm^3$, resulting in a resistivity of 0.2 Ω·cm. The hole mobility remained the same at 9 $cm^2/V\cdot s$. Again using the LEEBI method, In a further development, Nakamura et al.[366] have succeeded in achieving even brighter LEDs. In a subsequent publication, Nakamura *et al.*[382] reported low-resistivity p-type GaN films were obtained by thermal annealing in N_2-ambient at temperatures above 700°C instead of the LEEBI method. Prior to thermal annealing, the resistivity of Mg-doped GaN films was approximately 1×10^6 Ω·cm. In contrast, after thermal annealing the resistivity, hole carrier concentration and hole mobility became 2 Ω·cm, $3\times10^{17}/cm^3$ and 10 $cm^2/V\cdot s$, respectively. In photoluminescence experiments, the intensity of the 750-nm deep-level emission sharply decreased and the 450-nm blue emission intensity increased after thermal annealing.

To elaborate on the successful doping with Mg, Akasaki and coworkers (cited above) have reported the synthesis of p-type GaN and AlGaN Magnesium doping at a concentration of 2 x $10^{20}/cm^3$ was incorporated into GaN resulting in compensated highly resistive material. The sample was then treated with low energy electron beam irradiation (LEEBI) which had the remarkable effect of drastically reducing the resistivity of the sample to ~35 Ωcm. The CL spectrum of the LEEBI GaN:Mg samples was greatly improved. Initially, Hall measurements revealed the GaN to have a hole concentration p ~ 2 x $10^{16}/cm^3$ and a mobility μ_p = 8 cm^2/Vs.

The p-type nature of the LEEBI treated GaN was further demonstrated by the fabrication of a p-n junction LED having rectifying current-voltage characteristics and room temperature emission in the ultraviolet and blue-violet. A similar procedure was performed on Zn-doped samples [379] and a marked increase in the luminescence intensity resulted, however p-type conduction was not achieved. No explanation for this remarkable behavior has been offered.

In GaN:Mg grown by OMVPE, concentration of free holes at room temperature reaches its maximum value of about 10^{18} cm^{-3} for the Mg concentration of about 3×10^{19} cm^{-3}, and it decreases with farther increase of Mg concentration.[383].

VIII.3.12. Role of Hydrogen

Shortly after the discovery that low energy ion irradiation paved the way for Mg activation, it was recognized early on that H played an important role in the form of passivating Mg during growth and leaving the lattice upon post growth irradiation.[384] In this particular reference, Van Vechten et al.[384] discuss defeating compensation due to donor like defects which permanently prevent attaining p-type doping. In fact the abstract stated that "*We propose a general method to obtain high conductivity of either type in wide gap semiconductors where compensation normally limits conductivity of one or both types. We suggest that the successes of Amano et al. and of Nakamura et al. in obtaining more than 10^{18} cm^{-3} holes in GaN are particular examples of the general process that we propose*". Unbeknownst to the GaN community, as it appears, is a very pertinent parallel development in the field of mainly ZnSe, which faced the p-type conundrum as well. Compensating the intentional acceptors with H during growth followed by driving H away after growth was noted in a patent application filed by Rothschild[385] on August 15, 1988 and issues on October 12, 1993. The overall problem of bipolar conductivity problem, i.e. high n-doping but low p-doping along with beneficial aspects of atomic H is eloquently discussed. Also discussed is the increased solubility of the acceptor impurity by presence of H. While this method did not turn out to be practical for ZnSe due to perhaps strong N-H bonds and or possible removal of metals through formation of metal hydrides from the process, it is the process which has

led to achievement of p-type conductivity in GaN.

According to theory developed since then[386,387,388,389], isolated hydrogen may exist as positively charged (H^+), being a shallow donor and located near the N atom, or as negatively charged (H^-), being a deep acceptor and located close to the Ga atom. H^+ prefers the nitrogen antibonding site (1.02 – 1.04 Å from the nearest N atom), whereas for H^- the Ga antibonding site is energetically most stable. H^+ is mobile at room temperature due to small migration barrier (0.7 eV), while H^- is stable (3.4 eV). H^+ is attracted to negatively charged Mg^-, paving the way for passivation until driven out by post growth processes.

Serendipitously, the solubility of hydrogen is considerably higher in p-type than in n-type GaN. This is consistent with high diffusivity of H^+, whereas diffusivity and solubility of H^- is expected low in n-type GaN.[386] In p-type GaN, H^+ and H^- have low and high formation energy, respectively, and the opposite relation is true for n-type GaN. H^0 is never stable in GaN representing a "negative U" system. This terminology is due to Anderson[390] who, in an attempt to account for the lack of observation of paramagnetism for localized intrinsic defects in chalcogenide glasses (amorphous material), proposed a model which relies on existence of an effective negative correlation energy U for electrons localized at a defect site. In this model energy gain associated with electron pairing in dangling bonds of defects which are coupled with large lattice relaxation may be able to overcome the Coulombic repulsion of the spin up and spin down electrons which would end up supplying a net effective attractive interaction between the electrons at the site. This has come to be known as the negative U center. It has also been applied successfully to point defects in Si early on.[391,392]

Hydrogen molecule H_2 is unstable with respect to dissociation into monatomic hydrogen. Besides, it has quite high formation energy. The hydrogen does not form a bond to the Mg atom in p-type GaN, as some investigators argue. Instead it is bound to N atom in p-type GaN, so that the Mg-H complex has a H-N bond with the calculated stretch mode of 3360 cm^{-1} (reference [386]), very close to the stretch mode in NH_3 (3444 cm^{-1}). [386] Hydrogen plays an important role in p-type doping. It passivates Mg during growth and prevents formation of native deep donors due to self-compensation process. After the growth, hydrogen can be removed by annealing, leading to good p-type conductivity. Unlike many other semiconductors, formation of H_2 molecules is very unlikely in GaN. Thus, most reasonable mechanism of H removal during post-growth annealing is diffusion of hydrogen atoms to the surface, interface, or structural defects. Hydrogen is likely to form complexes with point defects. In particular, hydrogenated V_{Ga} is expected to have lower formation energy than the isolated V_{Ga} in n-type GaN, and hydrogenated V_N is predicted to have lower formation energy than the isolated V_N in p-type GaN.[387]

For OMVPE-grown films, it has been argued that H is in its positive charge state, the

H+ proton, and passivates the Mg acceptors which are in their negative charge state during growth; this would prevent the compensating donor-like defects from forming. During post-growth annealing, H^+ is driven out, which results in p-type GaN due to the negatively charged Mg acceptors. Although it has been mentioned frequently that Mg and H form a complex in Mg-doped GaN films, the exact mechanism of formation and the release of H upon a post-growth treatment have not been sufficiently elucidated. In addition, predictions of the position of the H atom from first-principles calculation are not consistent. For example, in the Neugebauer *et al*.[386] calculations, the *anti-bonding site* (i.e., a hydrogen sitting next to a N atom, about 1 Å away from the N site, at the anti-bonding position of the Mg-N bond) is lower in energy than the *bond center (BC) site*. This follows from the argument that the BC position requires an outward motion of the Mg and N atoms, which is very energy consuming in GaN, as GaN is a very hard material. On the other hand, an argued in favor of the BC location for H between substitutional Mg and N nearest neighbors has been provided.[393] In general, H takes the BC position in all other semiconductors.

Also useful is the determination of the *Local Vibrational Modes* (LVMs) of the Mg-H complex in GaN, which provides not only the confirmation of hydrogen in GaN, but also gives significant information on the structure of the complex. At the present time the stretch frequency is, in fact, the only reliably-established physical parameter available from experiment for the Mg-H complex in GaN. To support their spectroscopic identification, Fourier-transform infrared-absorption spectroscopy has been performed on three Mg-doped GaN layers grown by OMVPE.[394] The first sample was as-grown and electrically semi-insulating; the second one was subjected to a thermal anneal and displayed p-type conductivity; and the third sample was exposed to monatomic deuterium at 600^{o}C for 2 h, which increased the resistivity of the material. The as-grown sample displayed a LVM at 3125 cm^{-1} which is in very good agreement with 3360 cm^{-1} predicted by calculations.[386] After thermal activation of Mg, the intensity of this absorption line is reduced. After deuteration, a new absorption line appeared at 2321 cm^{-1}, which disappeared after a thermal activation treatment. The isotopic shift clearly establishes the presence of hydrogen in the complex.

Experimental results on hydrogen in GaN are limited and not well confirmed. High concentrations of hydrogen and carbon have been detected by SIMS and elastic recoil detection analysis (ERDA) in unintentionally doped GaN grown by OMVPE using mixture of triethylgallium (TEG) and ammonia (NH_3) in the presence of nitrogen and/or hydrogen or deuterium.[395] It was established that total hydrogen (carbon) content decreases exponentially from 2×10^{21} to 3×10^{19} cm^{-3} (from 1.4×10^{21} to 2×10^{18} cm^{-3}) when the substrate temperature was increased from 650 to 1100ºC. High concentration of these species is attributed to efficient desorption of hydrocarbons from the GaN surface during growth. Decrease of H and C contamination with increasing temperature is attributed to reduction of effective surface with increasing temperature (increase in crystallite size).

In reactive MBE growth, contamination with H and C is expected to be much smaller due to absence of the metalorganic compounds. However in the MBE growth using ammonia as a source of nitrogen, concentration of hydrogen can be large. Zhang *et al.*[396] reported high concentration of hydrogen in unintentionally doped GaN grown by MBE with ammonia. A remarkable finding of this work is a linear dependence between the background electron concentration and concentration of hydrogen. Hydrogen also has much higher concentration at the surface due to adsorption. The authors of reference[396] suggested that hydrogen sitting near the N site acts as a donor. The activation energy of this donor was estimated as ~120 meV. It is found that hydrogen is present in relatively high concentrations in as-grown GaN samples, and, moreover, it is easily incorporated during plasma etching, solvent boiling, and wet chemical etching.[397]

In summary then, in part owing to the incorporation of a relatively large concentration of shallow-acceptor impurities as compared to the concentration of native donor-like defects in technologically improved GaN, one finds that the Mg acceptor concentration is accomplished primarily through the presence of Mg-H complexes helped by increased H solubility when the Fermi level is closer to the valence band. The ensuing compensation, however, shifts the Fermi level up towards the conduction band. This compensation is lifted (*i*) when samples are irradiated with an electron beam of 5 - 15 keV incident energy for several hours, or (*ii*) when samples are thermally annealed at constant temperature in N environment for about 1/2 hour at temperature greater than 600^{o}C or short rapid thermal annealing at about 850 ^{o}C or even by UV illumination at temperatures above 500ºC.[398] Also, first-principles calculations demonstrate that the same amount of both Mg and H incorporated into the GaN films when they are grown under an H-ambient growth condition, such as that of OMVPE. Furthermore, the calculations predict that more Mg can be incorporated into GaN film when there are more H atoms present.

VIII.4. Towards p-type ZnO

VIII.4.1. Roadblock in achieving p-type ZnO

Fabrication of ZnO-based optical and electronic devices demands high quality n- and p-type ZnO with free-carrier concentrations well in excess of 10^{17} cm^{-3}, preferably in the 10^{18} cm^{-3} range. General prerequisites for "useful" p-type ZnO involves the acceptor concentration to be much higher than the donor concentration (low compensation), large hole disparity between the acceptor and donor concentration in favor of acceptor concentration, and low acceptor ionization energy, preferably below 0.2 eV. In order to achieve high substitutional acceptor concentration, the solid solubility of the particular acceptor impurity used must be high with a low self compensation ratio.

As pointed out above, ZnO, as is the case for other wide-gap semiconductors, suffers from the doping asymmetry problem as well; i.e., it can be doped *n*-type rather easily, but *p*-type proved to be a formidable challenge which from a practical point of view has not been conquered yet. To reiterate, in general, the doping asymmetry arises from the fact that wide-gap semiconductors either have a low valence-band maximum or a high conduction-band minimum which leads to a large bandgap to begin with.[294,297] Some semiconductors such as ZnTe, CdTe, and diamond in which the valence band is relatively close to the vacuum level have preferable p-type conductivity and making them n-type is very difficult, diamond being a case in point. In contrast, ZnO, ZnSe, ZnS, and CdS, which have valence bands relatively far from the vacuum level, have preferable n-type conductivity. Consistent with the aforementioned statement, nominally undoped ZnO has n-type conductivity (high resistivity ZnO has $n \approx 10^{14}$ cm^{-3} and $\mu_n \approx 200$ cm^2/Vs) due to the presence of intrinsic defects such as oxygen vacancies (V_O)[399,400] acting as deep donors, interstitial Zn (Zn_i)[401] and Zn antisites (Zn_O^{2+}) forming shallow donor levels,[400] and background hydrogen acting as a donor at interstitial positions.[402] Zn vacancies (V_{Zn}) have a low formation energy in n-type material. Also they can be created by high-energy (2 MeV) electrons. Zn vacancies are the dominant acceptors in the as-grown n-type ZnO as shown by positron annihilation spectroscopy by Tuomisto *et al.*[403] To date, n-type doping is relatively well established through the substitution of group III elements (Al, Ga, In) on the Zn sites, and highly conductive *n*-type ZnO ($n > 10^{20}$ cm^{-3}) can be produced by intentional doping (e.g., see review by Özgür *et al.*[404] and references therein). Unfortunately, the same intrinsic defects, which are responsible for *n*-type doping, tend to aggravate the efforts to achieve p-type doping by compensating potential acceptors.

Donor centers, both intrinsic defect and impurity induced varieties, which are likely to compensate acceptors in ZnO are as follows:

O vacancies As mentioned above, V_O is a deep donor in ZnO as predicted by theory and determined from EPR experiments.[400,405] Therefore, it is not responsible for n-type conductivity. However, V_O has low formation energy in p-type ZnO, so can compensate acceptors.

Zn interstitials. Zn interstitials are shallow donors. They are probably the ~ 27-meV donors created by electron irradiation. Ionization energy of donors in as-grown ZnO is close to ~35 meV. Zn_I is reported to have a high formation energy in n-type material.

Turning out attention now to impurities**:**

Hydrogen. Hydrogen is not amphoteric in ZnO and it always acts as a donor. Ionization energy of hydrogen donor is ~ 35 – 40 meV. It is typically not the *dominant* donor in the as-grown, bulk ZnO. However, hydrogen is omnipresent in MOVPE-growth and is a fast diffuser; *e.g.* it diffuses at 600 °C. Hydrogen passivates acceptors, such as N_O, by forming H-A complexes. A signature of hydrogen' presence in ZnO is the 3.363 eV D_0X PL line (I_4).

Group III elements (Al, Ga, In) on the Zn sites. Group-III elements can out-diffuse from the foreign substrates (e.g., Al from sapphire or Ga from GaN) on which the

epitaxial layers are grown and could aggravate efforts to achieve p-type conductivity layers.

Group-VII elements (F, Cl, Br) on O-sites (very little is known at the present time).

Some compensating centers are pinned at the same level which hardly depends on the position of valence and conduction bands.[406] This compensation problem is the most challenging phenomenon in wide-gap semiconductors. T make matters worse, the data when scrutinized show instability of p-type conductivity in ZnO, reverting to n-type conductivity within a matter of days.[407] Having said this, we should also be weary about the accuracy of p-type conductivity determination.

As alluded to earlier, in addition to compensation caused by nontrivial mechanism of inter-impurity or impurity-native defects interactions, the limited solubility of p-type impurities,[408] precipitate formation,[409] and relatively deep acceptor levels[410] erect additional obstacles to attaining p-type conductivity. This doping asymmetry problem has been the major obstacle for potential applications of many wide-gap materials, even though they possess excellent properties. In addition to this fundamental problem, some difficulties can be associated with the fact that inhomogeneous impurity incorporation at rough surfaces causes potential fluctuations which in turn makes the determination of the conductivity type is rather difficult via the Hall effect because of the following reasons: Conducting substrates (ZnO, GaN, Si), multilayer systems (ZnO on GaN/Si; ZnO on GaN/sapphire), conversion of, e.g., GaAs to p-GaAs due to Zn-diffusion. Further complications can be introduced due to the fact that metallic zinc shows p-type conductivity and microcrystalline material can show positive Hall coefficient.

As an example, let's discuss the well-known problem of Hall-effect analysis for a material with two-band conduction (co-existing n- and p-type regions).[411] For the ZnO case, this problem has been discussed for ZnO by Claflin *et al.*[412] The Hall coefficient in a material with two-band conduction can be expressed as follows:

$$R_H = \frac{R_p\sigma_p^2 + R_n\sigma_n^2}{(\sigma_p + \sigma_n)^2} = \frac{p\mu_p^2 - n\mu_n^2}{e(p\mu_p + n\mu_n)^2}$$

Equation 4

It is clear that $R_H \rightarrow 0$, when $p\mu_p^2 - n\mu_n^2 = 0$. Singularity appears in the apparent carrier concentration for the single-band analysis of Hall measurements for samples with two-band conduction. Using typical values μ_p = 1 cm^2/Vs, μ_n = 200 cm^2/Vs, and p = 4x10^{18} cm^{-3}, a transition from p-type ($R_H > 0$) to n-type ($R_H < 0$) will be observed when electron concentration in n-type channel for electron concentrations as low as ~1x10^{14} cm^{-3}. The above treatment naturally assumes that the cyclotron motion within the sample is not hindered, except the physical boundaries of the sample. When localization takes place, which is an endemic problem in wide bandgap semiconductors doped with acceptor like impurities particularly at high concentrations, the carriers are really trapped in a sense

and cannot really follow the electric field force and Lorentz force. When and if this happens, the applicability of the conventional Hall measurements would come under question, particularly at low temperatures.

VIII.4.2. Brief review of acceptor impurities in ZnO and current status of p-type doping

One possible approach toward *p*-type ZnO is the introduction of group IA elements, such as Li, Na, and K, on Zn sites which form acceptor levels at 90, 170, and 320 meV, respectively, as predicted by density functional theory.[413] However, doping with group IA elements suffers from their very high diffusivities as well as from self-compensation.[414] For instance, doping with lithium creates semi-insulating ZnO[415] because of additional interstitial Li atoms acting as donors.[413] Therefore, the attention has been turned towards the group V elements, mainly N, P, or As, which generate acceptor states if incorporated substitutionally on the oxygen sites. However, because of their much larger ionic radii than oxygen [N (22%); P (51%); As (59%); Sb (55%)], density functional theory suggests significantly deeper acceptor levels at 0.40, 0.93, and 1.15 eV for N, P, and As, respectively, compared to the group IA elements.[413] For group IB elements on Zn sites, the lowest transition energy level is also deep, e.g. at 0.40 eV for Ag_{Zn}. Intrinsic p-doping via Zn-vacancies is not reliable, because it is difficult to control non-stoichiometry and stability. It is believed that the best candidate for p-type doping in ZnO is N, because it has the smallest ionic radius (relatively close to O ionic radius of 1.38 Å) among the group-V impurities (2.12 Å, 2.22 Å, and 2.45 Å for P^{3-}, As^{3-}, and Sb^{3-}, respectively), and thus should readily substitute for O in ZnO.[410] However, N was found to create a rather deep acceptor level of ~0.2 eV[416] (although the experimental value is lower than the predicted value of 0.4 eV[413]), and its incorporation on the lattice sites is limited to produce high hole concentration.[410] Consistently, many groups reported weak p-type conduction with $p \approx 4x10^{17}$ cm^{-3}, $\mu_p \approx 1$ cm^2/Vs, and $E_A \approx 135$ meV for N-doped ZnO.

It has been shown theoretically[417] that co-doping with acceptor (N) and donor (Al, Ga, In) impurities in the 2:1 ratio in ZnO can stabilize substitution of N at the appropriate lattice site through the formation of N-Ga-N bonds, similar that in co-doping experiments in GaN. Wang and Zunger[418] even proposed the so-called cluster doping, i.e., doping with even more partner atoms than in co-doping, to further optimize the acceptor formation. However, it should be realized that isolated Ga atoms can compensate the N–Ga–N acceptors.[419] Numerous experimental studies based on this approach have revealed discrepancies between theory and experiment and resulted in little or no success in terms of achieving stable *p*-type material with reasonably high free-carrier mobility [reported mobilities typically do not exceed 1-2 $cm^2/(Vs)$].[410,409,420,421,422,423]

While most efforts on p-type doping of ZnO have focused on N doping, considerably fewer studies have considered other group V elements for substitutional doping on the O sites, including P,[424,425,426,427,428,429,430] As,[431,432,433,434,435] and even Sb.[436,437,438] Despite the

fact that ionic radii of these dopants by far exceed that of oxygen, p-type conductivity has been reported with hole concentration above 10^{18} cm^{-3} in P-,[427] As-,[432] and Sb-doped[437,438] ZnO and hole mobility of 20 $cm^2/(V\ s)$ in ZnO:Sb[437] and 11 $cm^2/(V\ s)$ in ZnO:P.[432] Weak *p*-type conductivity in P-doped ZnMgO grown by PLD have also been reported.[439, 440, 441] Hall-effect measurements at RT showed a hole concentration of $2.7x10^{16}$ cm^{-3}, a mobility of 8.2 $cm^2/(V\text{-}s)$, and a resistivity of 35 Ω cm.[440] To explain these findings, Limpijumnong *et al.*[442] proposed a model for large-size-mismatched group-V dopants in ZnO based on first-principles calculations. The model states that dopant atoms do not occupy the O sites as is widely perceived, but rather the Zn sites, each forming a complex with two spontaneously induced Zn vacancies in a process that involves five-fold As coordination. Calculations indicate that the As_{zn}-$2V_{zn}$ defect complex should have an acceptor level at about 150 meV, shallower than that of As_O, and lower formation energy than any of the parent defects.

The same scenario can be applied for Sb and P with the predicted ionization energies of 160 and 180 meV,[443] respectively. The calculated values of the ionization energies are in reasonable agreement with those found experimentally for Sb (0.14 eV[438]) and As (0.12 eV[444]) and much lower than those predicted for direct As and Sb substitution on O sites.[413] Therefore, these data suggest the formation of defect-impurity centers which are responsible for acceptor levels observed in ZnO doped with As or Sb. The implicit assumption here of course is that the experimental values are dependable. We should point out that in systems with high localization, which is very likely to be case here, the Hall measurements do not really apply. Further, when applied, the previous state, temperature and time would lead to changing results. From the viewpoint of device applications, stability of these centers is a very important problem, because heat treatments during device fabrication or device operation in high-injection current regime and electric field can result in different data or complex decomposition, that is, conduction-type inversion.

A new insight into p-type problem has been given by recent studies of local conductivity in acceptor doped ZnO grown by MOCVD[445,446,447] and spray pyrolysis[448] methods using scanning capacitance microscopy (SCM) and scanning surface potential microscopy (SSPM). It has been demonstrated that impurities are preferentially incorporated at or near growth defects.[445] Depending on the growth parameters, largely extended *p*-type domains were observed, surrounded by *n*-type regions. We refer to this as extreme case of localization both in the conduction and valence bands. The differences in local conductivity type were directly correlated to the topography revealing *p*-type for smooth, two-dimensional surfaces and *n*-type signals in the case of three-dimensional island growth or structural defects, such as microcracks or surface pits. For MOCVD-grown ZnO co-doped with As and N, the formation of stable *p*-type ZnO was achieved if

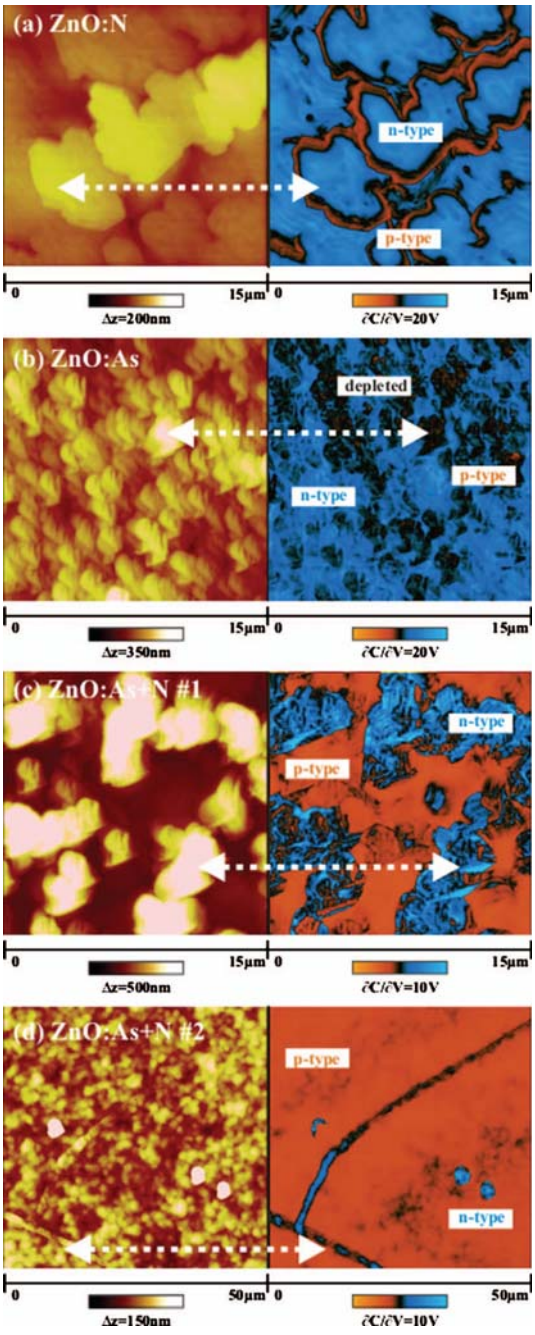

Figure 58. Typical AFM (left) and SCM images (right) of ZnO layers which were conventionally mono-doped with nitrogen (a) or arsenic (b), or co-doped with both acceptor species (c) and (d), respectively. The morphology of the mono-doped samples is not smooth and reveals three-dimensional islands with typical diameters of about 5–8 and 1–2 µm for N and As doping, respectively. The corresponding SCM images show dominant *n*-type regions (bluish) despite the acceptor doping. Moreover, very small *p*-type domains (orange) were found only for ZnO:N, and then exclusively related to island/grain boundaries, whereas ZnO:As revealed no significant *p*-type regions, but a majority of depleted areas (black) due to the smaller grains and the superimposing space charge regions. For the dual-doped layers, (c) shows a typical sample with mixed conductivity, i.e., with dominant three-dimensional islands which are *n*-type in SCM and with smoother, *p*-type regions. In contrast, samples grown under more suitable conditions (d) reveal dominant smooth *p*-type domains which are only partly disturbed by very few microcracks and three-dimensional islands which are all *n*-type (after Krtschil *et al.* [446]).

the growth was two dimensional and yielded smooth surfaces (see Figure 58). In contrast, the acceptor doping completely failed if the growth was three-dimensional.[445,446] These data show again that a deep understanding of impurity-defect interaction is of vital importance for control over the conductivity type in ZnO.

VIII.4.3. Strategies which can be used to overcome p-type problem

Due to the strong bonding, as reflected by the large formation energy of ZnO, intrinsic defect formation energies are relatively large in ZnO. Furthermore, the high acceptor ionization energies make the p-type doping more difficult. Calculated minimum defect formation energy of neutral N_O is rather high: $\Delta H_f\ (N_O)_{min}$ = 1.2 eV (see). For group V on oxygen site acceptor, the lowest transition energy level is for N_O, which is at 0.35 eV above the valence band maximum (VBM). For group IB on Zn site acceptor, the lowest transition energy level is also deep, at 0.40 eV for Ag_{Zn}. Group IA elements (Li, Na, *etc.*) on Zn sites have relatively shallow defect levels, but self compensation limits their use as effective acceptors.

Several approaches can be used to overcome the doping limit:

(1) Increase defect solubility by "defeating" bulk defect thermodynamics using non-equilibrium growth methods (MBE, MOCVD, *etc.*);

(2) Reduce defect ionization energy level by designing shallower dopants or dopant complexes;

(3) Reduce defect compensation and ionization level by modifying the host band structure near the band edges.

VIII.4.3.1. Improving dopant solubility

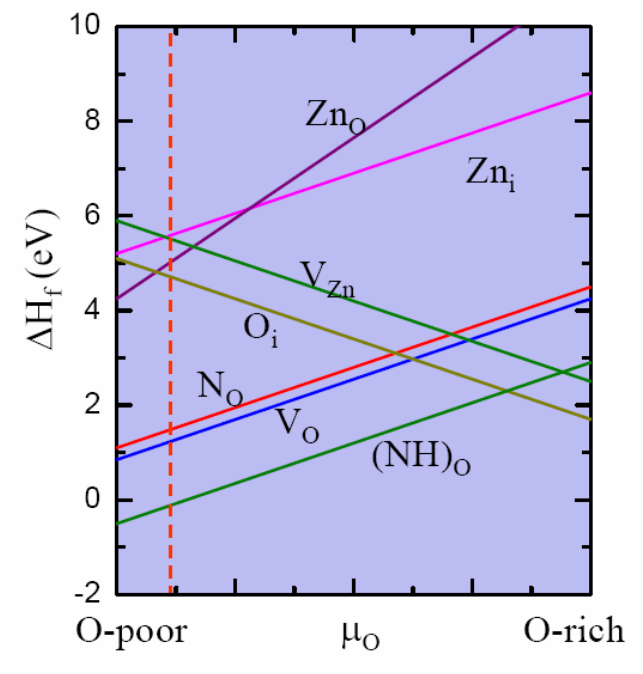

Figure 59. Formation energies, ΔH_f, for intrinsic defects and $(NH)_O$ in ZnO calculated by using first-principles density-functional theory (courtesy of S.H. Wei of National Renewable Energy Laboratory[450]).

Solubility limits can be enhanced above the thermodynamical ones by employing "non-equilibrium" growth techniques, such as MBE and MOCVD. One way to improve the dopant solubility is adjusting dopant chemical potentials. Chemical potential of a dopant in the matrix, μ_A, controls the dopant solubility. Therefore, the key to enhance the solubility of the dopant is to raise the chemical potential and avoid the formation of its precipitates.[449]

As seen from Figure 59, the formation energy of N_O is the lowest under O-poor conditions, whereas V_{Zn} is the lowest under O-rich conditions.[450] Therefore, the O-poor conditions will both increase the concentration of N_O acceptors and decrease the concentration of V_{Zn} compensating donors. It should be noted that the formation energies of other intrinsic defects also depend on the growth conditions. However, the formation energies for other "acceptor-killer" defects, such as Zn interstitials (Zn_i) and O vacancies (V_O), are decreased under O-poor conditions. Therefore, there is an intrinsic problem for enhancing the *p*-type doping using N as the dopant, which can be solved by choosing an appropriate dopant source. Another problem that can arise is associated with a strong relationship between the growth mode and growth conditions for non-equilibrium growth techniques. For instance, high quality Zn-polar ZnO can be grown by MBE only under oxygen rich conditions. The reduction in O/Zn ratio results in three-dimensional material with very rough surface morphology which is a very undesirable scenario because, as mentioned above, impurities are preferentially incorporated at or near growth defects.[445,446] MBE growth of high-quality O-polar ZnO needs roughly 1:1 O/Zn ratio, and deviations towards both O-poor and O-rich conditions deteriorate the material quality. However, adding dopant species to the system can shift the optimum growth windows. This problem needs further theoretical and experimental exploration.

Solubility can also be enhanced by metastable molecular doping. N chemical potential depends on the doping sources (N_2, N_2O, NO, NO_2).[451] As demonstrated by Y.F. Yan *et al.*[452], N solubility in ZnO is much higher if NO or NO_2 is used as a dopant (see Figure 60). Additionally, NO or NO_2 doping also helps to avoid the formation of $(N_2)_O$, which is a compensation donor in ZnO.

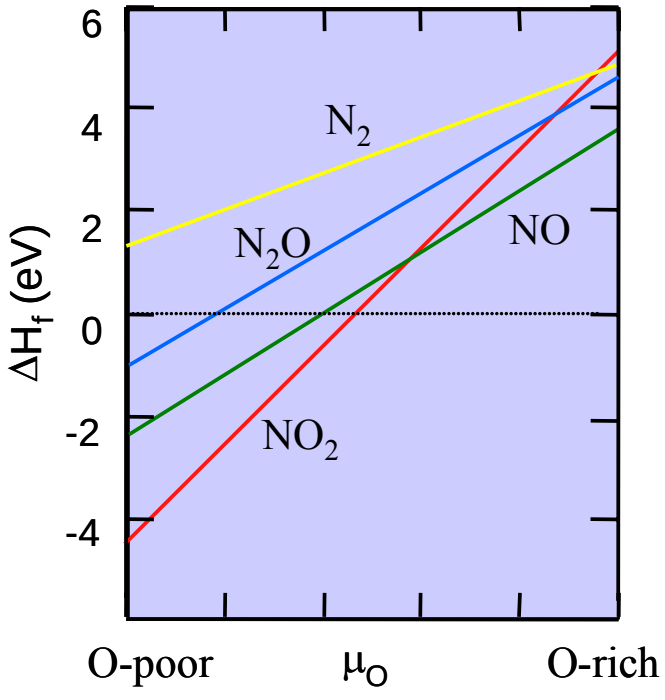

Figure 60. Calculated formation energies of N_O for different N precursors as functions of the O chemical potential (after Y.F. Yan *et al.*[452]).

The solubility of both the dopants and compensating defects depend sensitively on the position of the Fermi level. If we can control the Fermi level at a desirable position, then

we may enhance the solubility of dopants and suppress the formation of compensating defects. One popular approach is passivating the dopants by H atoms. For example, in Mg-doped GaN, the introduction of H can prevent such a shift of the Fermi level. As a result, the concentration of Mg can be enhanced.[453] After film growth, H can be driven out by annealing to achieve *p*-type conductivity. For ZnO:N, the co-doping with H can, in addition to preventing the Fermi level shift, directly passivate N dopants, forming a molecular NH complex on O site [$(NH)_O$]. The binding energy for $(NH)_O$ is 2.9 eV. The $(NH)_O$ complexes electronically mimic O atoms and cause smaller lattice distortion than N_O. Thus, the concentration of $(NH)_O$ in ZnO can be much higher than N_O.[454] Figure 59 shows the calculated formation energy for $(NH)_O$ as a function of O chemical potential. For comparison, the formation energies of N_O and some compensating defects are also shown. It is seen that the formation energy of $(NH)_O$ is lower than any other defects under O-poor conditions. In addition, its existence also pins the Fermi energy level, which also assists to suppress the formation of compensating defects. Therefore, *p*-type doping could be achieved after subsequently driving out the hydrogen atoms from the sample by thermal annealing.

VIII.4.3.2. Designing shallow defect levels in ZnO

A shallow acceptor level above the valence band maximum (VBM) has a wavefunction character similar to the VBM, i.e. it has an anion *p* and cation *d* orbital character. N has the lowest *p* orbital energy, so N_O also has the lowest acceptor level of 0.35 eV among all the group V elements.

For p-type doping, substitution acceptor on cation site is preferred because it leads to a smaller perturbation on the VBM, thus, to a shallow level. It also reduces the self-compensation by anion vacancy (V_O). As mentioned before, group IA elements on Zn sites have relatively shallow defect levels, but self compensation (formation of interstitials) limits their use as effective acceptors. For group IB dopants, the interstitial formation energy is very high, so self compensation is negligible. However, group IB dopants have deeper levels than group IA dopants because of the *p*-*d* coupling. Ag has lower *d* orbital energy, so Ag_{Zn} has lower acceptor energy (0.4 eV) than Cu_{Zn} and Au_{Zn} (0.7 and 0.5eV, respectively).[455]

Due to the large electronegativity of oxygen, the ionization energy of acceptors in ZnO is usually too high. To lower the acceptor ionization energy codoping of ZnO with acceptors and isovalent atoms has been proposed.[456] Using the first-principles bandstructure calculations, it was shown that the acceptor transition energies of V_{Zn}-O_O can be reduced by substituting O with more electronegative F to lower the electronic potential, whereas the acceptor transition energy of N_O-nZn_{Zn} (n=1–4) can be reduced by replacing Zn with isovalent Mg or Be to reduce the anion and cation kinetic *p*-*d* repulsion, as well as the electronic potential.

Table 5. Calculated binding energy E_b of the defect complex and transition energy levels between two different change states (expressed in eV) in ZnO.[456]

Defect	E_b	0 / −	− / 2−
N_O		0.31	
N_O-Mg_{Zn}	0.3	0.29	
N_O-4Mg_{Zn}	1.6	0.23	
N_O-Be_{Zn}	0.1	0.22	
N_O-4Be_{Zn}	1.9	0.12	
V_{Zn}		0.18	0.34
V_{Zn}-F_O	−2.3	0.16	

The calculated defect ionization energy levels suggest that F and Be could be good p-type co-dopant for ZnO (see Table 5). However, the practical implementation of this approach may be not as straightforward as it seems at the first glance, because the isovalent co-doping of ZnO will result also in the increase of band gap which usually gives rise to the increase of ionization energies of donors and acceptors. Therefore, the doping profiles of acceptor and isovalent impurities should be carefully designed. Probably, δ-doping with isovalent atoms can be applied to lower the acceptor ionization energy.

Doping with large atomic size group VB elements, P, As, and Sb may also result in shallow defect levels. For instance, atomic sizes of As and Zn are similar. As_{Zn} has a relatively low formation energy but it is a (triple) donor. V_{Zn} is a native (double) acceptor with low formation energy. However, one As_{Zn} and two V_{Zn} could bind strongly and form a new acceptor complex (As_{Zn}-$2V_{Zn}$). The complex has low formation energy and low ionization energy (~ 150 meV).[442]

Based on defect wavefunction analysis, the following defect complexes have been proposed to reduce the ionization energy of acceptor level in ZnO:

Ag_{Zn} ; $V_{Zn} + F_O$; $V_{Zn} + H$; $Li_{Zn} + H$ (Ref. 455)

$Mg_{Zn} + N_O$; $Be_{Zn} + N_O$; $H + N_O$ (Ref. 456)

$As_{Zn} + 2V_{Zn}$; $P_{Zn} + 2V_{Zn}$ (Ref. 442)

VIII.4.3.3. Modification of the host band structure to reduce ionization energy and compensation

First, through effective doping of mutually passivated defect pairs, a fully compensated defect band can be introduced near the VBM or the CBM of the host. Second, after the fully compensated insulating phase is formed, excess dopants can be used on the passivated system to achieve p-type by ionizing this defect band.[457]

Valence band edge of ZnO can be modified by passivate co-doping with Ga and N. N combined with Ga creates a passivated defect band above the host VBM. Then, shallow acceptor levels can be created by doping the passivated ZnO:(Ga+N) system using excess N. The calculated defect level of N is about 0.1 – 0.2 eV above the defect band. However, one should remember that the introduction of such defect band will result in dramatic degradation of electronic and optical properties of the material.

VIII.4. Conclusions

In contrast to GaN where p-type doping is relatively well-established, the situation with ZnO is still uncertain. One can argue that no credible p-type doping has been reported. The defective nature of the material, localization induced by the candidate p-type impurities, and possibly other complications such as shunting conduction layers, etc., make it very difficult to interpret the Hall measurements. Credible injection structure would lessen the emphasis on Hall measurements, but they are not available. Several issues should be addressed for a successful resolution of p-type problem in ZnO:

(a) Control over point and extended defects which act as either compensation centers for p-type impurities (point defects) or regions of localization for such centers (extended defects).
(b) Control over the impurities many of which act as shallow or deep donors compensating the acceptor impurities by proper designing of growth conditions.
(c) Insight into the nature of acceptor centers in ZnO that will allow the prediction of their behavior, thermal stability and elaboration on techniques for improving p-type impurity incorporation and activation.

The most straightforward way to solve the first problem is by employing homoepitaxy on bulk ZnO substrates which are available now and by optimizing the growth conditions in such a way that the formation energies for compensating donors would increase. The second problem needs to be solved through improving growth techniques that will allow the density of impurities to be reduced both in thin films and bulk material. The approach to solving the third problem can be through a combination of modern techniques giving insight into the nature of defect complexes and development of theoretical models predicting such centers.

IX. Nitride-based resonant tunneling diode, superlattice, and intersubband transition structures

IX.1. Preface

The resonant tunneling diode (RTD) structures in many ways represent the ultimate in terms of the demands placed on the quality of the heterostructures in that any defect induced current leakage path would shunt any tunneling current. In a different way, but ultimately similar, is the requirement of high quality imposed by structures exploring intersubband transitions (ISBT). Furthermore, realization of Bloch oscillations in short period nitride superlattices relies critically on the material quality including the heterojunction interfaces. RTD structures, which for the purpose of this discussion will also represent other vertical structures with potential of negative differential resistance (NDR), have been reported in the literature. However, a close examination indicates that it is most likely that all the observed NDR is related to trapping effects. This simply implies that much better materials quality is needed to achieve intrinsic NDR. The driving force from a device point of view is to achieve THz oscillations to be used for sources. As for ISB devices, the goal is to achieve high speed variable wavelength devices. In a general sense, achievement of the above mentioned structures which function as expected would hark the era of high quality GaN based heterostructures, particularly the vertical varieties.

The intrinsic high speed operation of RTD could pave the way for a wide range of applications such as THz sources. As for and ISBTs, they too can operate at relatively higher frequencies as compared to their conventional III-V cousins because of the very short (on the order of 100 fs) electron lifetime in excited states. In addition, the III-nitrides have high breakdown voltages and large band discontinuities which are essential for achieving high power and room temperature operation. Somewhat relates is the fact that the capability of high power operation has been successfully demonstrated by heterojunction field effect transistors due to the intrinsic properties of nitrides.

The topics provided below will pave the way to the discussion of vexing issues in regard to vertical heterostructure based GaN devices, namely the resonant tunneling devices and intersubband transition based structures, and what is needed for ultimate success.

IX.2. Introduction

In addition to the heterojunction field effect transistors and commercialized light emitting diodes in the visible and UV regions, nitride based resonant tunneling diodes and intersubband transition based emitters and detectors are expected to have advantages over GaAs material varieties such as high power capability owing to the larger conduction band discontinuities as well as being environmentally friendlier.

Although a negative differential resistance (NDR) in nitrides was first reported in 2002 by *Kikuchi et al.,*[458] and negative differential resistance with a peak-to-valley-current ratio of 32 was claimed, the mechanism of the observed NDR has been under debate.[459] Current instabilities in AlN/GaN double barrier structures were also observed which have

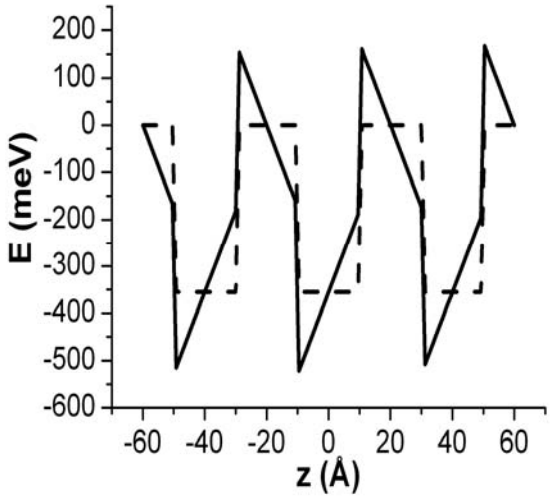

Figure 61. Conduction band profile in AlGaN/GaN SL (eV) in the direction of growth (angstrom): solid line includes polarization fields; dashed line corresponds to flat-band approximation; x=0.18, d_b=d_w=20 Å (after Litvinov *et al.*[475]).

been attributed to either the resonant tunneling processes or charging processes of defects.[460,461]

As for the intersubband related activity, ISBTs from 1.3 μm to ~ 3 μm in AlN/GaN or AlGaN/GaN short-period superlattice (SL) have been reported by different groups.[462,463,464,465] There is also an issue whether the intersubband transitions can be observed as readily as it can be in GaN based systems. To overcome this issue, Hofstatter et al.[466] employed the photovoltaic mode to exploit the intersubband transitions for photodetectors. From a technological point of view, when the number of AlN/GaN pairs increases on GaN buffer layers or substrates, severe cracking develops. To overcome this issue, the SL should be grown on either Al(Ga)N buffers[467] or with lattice matched AlInGaN barriers.[468] For the former case, the high dislocation density is an issue when the samples were grown on sapphire substrates.

IX.3. Resonant tunneling structures and short-period superlattices

Although several groups[458,469,470] have so far claimed observation of tunneling related NDR in the nitride system, none of them demonstrated high frequency oscillations of any kind. Let us first delve into the simulated results first followed by experimental observations and interpretation.

IX.3.1. Simulations

There have been quite a few reports on the topic already.[471,472,473,474,475] In an AlGaN/GaN SL, to obtain the miniband in SL, Litvinov (Waveband) *et al.*[474,475] simulated the band diagram shown in Figure 61, with the consideration of polarization field. During their

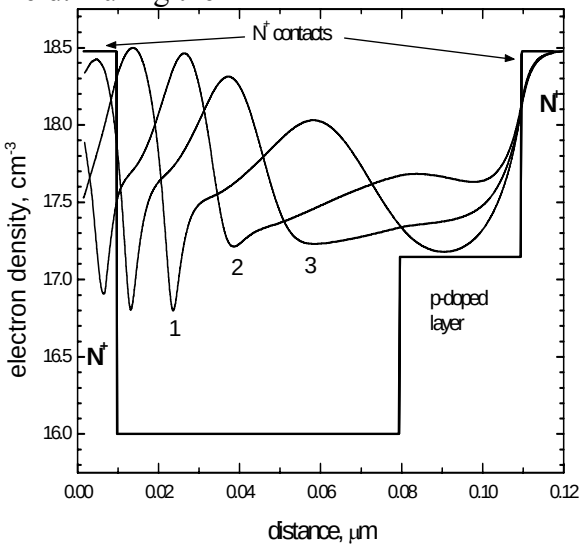

Figure 62. Spatial distribution of the electron (solid) and doping (dashed) concentration at consecutive times:1-3T/8, 2 – T/2, 3-3T/4, 4-7T/8, where T is the period of oscillations (courtesy of V. Litvinov of WaveBand/Sierra Nevada Corporation).

calculation, 1 eV bowing was used to get the bandgap of AlGaN, and the conduction band offset was given by the following equation:

$$\Delta E_c(x) = E_g(x) - E_g^{GaN} - \Delta E_v(x) \approx 0.603x + 0.99x^2 \text{ [eV]}$$

Equation 5

Numerical calculations[471] with the help of the Poisson-Schrödinger solver[476] confirmed the conduction band offsets were calculated using the first-principle valence band offsets between binary alloys.[477] In solver based calculations the polarization charge is modeled as delta-doped regions at the interfaces. Simulations showed that when Al composition (x) and SL periods (d) are in the range of $0.18<x< 0.4$ and $d<50$ Å, respectively, the miniband energy dispersion required more than the first nearest neighbor term in the dispersion law in which case the simple cosine-law was normally used in the kinetic equation to study the electron dynamics in a narrow band.

As the result of the simulation optimum, the Al content (x), superlattice period (d), and the parameters of the external circuit were determined and a representative equivalent circuit defined. In the optimized structure, the AlGaN/GaN SL contains 50

pair d_b= 9Å and d_w = 15Å, and Al%=42%. Complete screening of the polarization fields (flat-band SL) leads to a 10% decrease in the miniband width (low-field mobility). That slow change allows neglecting the carrier concentration dependence of the SL parameters. Both sides of the sample are straddled by highly n-type doped (10^{19} cm^{-3}) 0.01 μm-thick layers to provide good ohmic contact. Additional p-doped layer (p = 1.5×10^{17} cm^{-3} in Figure 62) prevents spillover of electrons from the metal contact. The lattice temperature is assumed to be 300 K. The spatial electron density and evolution of the electrical domains in a 4.7 V biased SL is shown in Figure 62.

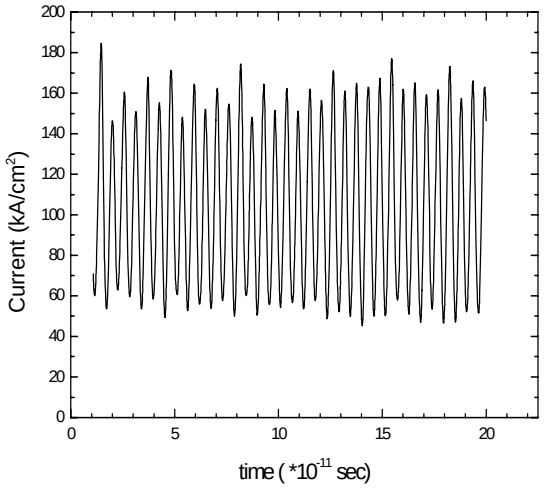

Figure 63. Current oscillations (courtesy of V. Litvinov of WaveBand/Sierra Nevada Corporation).

To start the oscillations the bias was increased from zero to a value higher than $2LF_{crit}$, where L is the total SL thickness, the F_{crit}=100 kV/cm for x=0.42 Al. Usually, the higher mobility results the higher frequency of oscillations. However, considering that a high current through the structure could damage the ohmic contacts, the practical simulations were kept at an average current near 100 kA/cm^2, which is shown in Figure 63.

Output power P_f and intrinsic efficiency η were also calculated based on the simulation results with harmonic oscillations at 200 GHz. For a typical mesa area of 100 μm^2, the output power is about 12.5 mW with an (3-6) % intrinsic efficiency.

IX.3.2. Experimental

For vertical carrier transport, IV characteristics are very sensitive to the dislocations and traps, much more so that the devices relying on lateral carrier transport. RTD and superlattice structures have both been studied experimentally, and the typical DC IV measured at 10K in a 10 pair AlN/GaN SL.[478] The sample was cooled down to 10 K in the dark (covered with Al foil). Before shinning the light, the IV was measured, and

no NDR was observed (dot line in Figure 64). After shining with the Xe lamp, immediately, the NDR appeared under reverse bias but peak to valley ratio depending on the sweeping directions. The main difference of this particular sample from the RTD structures, in which NDR was only observed during sweeping up,[479,480] is that the NDR features are more pronounced during the sweep-down. Moreover, the NDR features are reproducible no matter the scanning times. For a comparison, in the GaN/AlGaN

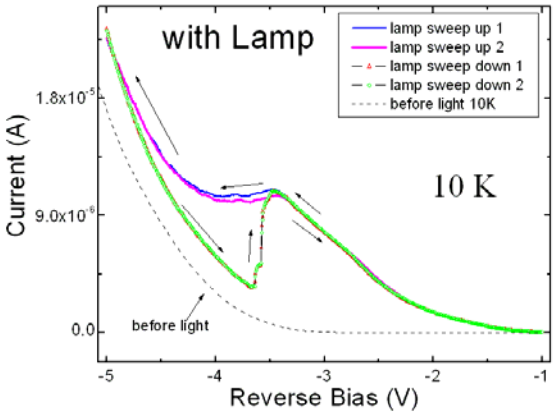

Figure 64. Reverse bias IV of 10 pair AlN/GaN superlattice at 10 K with a Xe lamp (courtesy of J. Xie of Virginia Commonwealth University).

double-barrier RTD grown on the single crystal GaN substrates, the NDR disappeared after several scans, and was partially contributed by electron traps.[479]

IX.3.3. Points deserving further attention

The main issue for this application is the material quality. As we can see that the experimental IV is very sensitive to the light which indicated that the NDR may be related to charging process due to the defects in the SL. After the sample was covered by Al foil, the NDR slowly disappeared. In addition, the strong polarization field causes the complexity in the simulation, and asymmetry of the tunneling condition. To solve this problem, investigation of structures grown on non-polar templates would be preferred. Closing the discussion related to the quality, it seems imperative that the layers be grown on GaN substrates.

IX.4. Inter-subband transitions

The technical difficulties associated with the epitaxial growth, doping, and the inherent large dislocation densities in nitride materials hinder the production of good quality materials and impede progress in device performance. Despite these technical

issues, some progress has indeed been made in fabricating photovoltaic detectors based on the intersubband transitions in the nitride system.

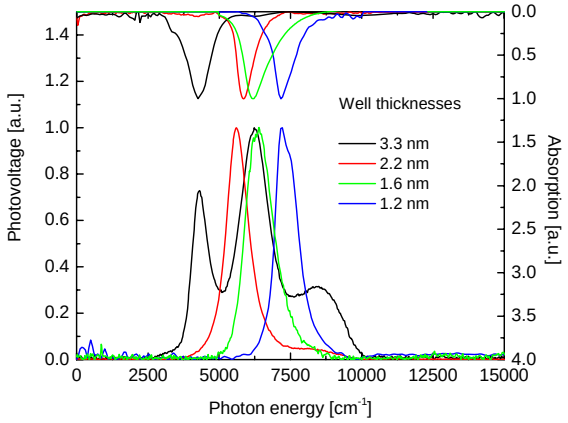

Figure 65. Measured photovoltage response of 4 different samples (after Baumann *et al.* [481]).

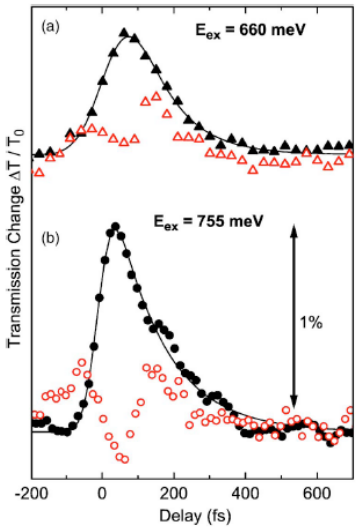

Figure 66. Time dependent change of transmission measured with pump pulses centered at (a) E_{ex}=660 meV and at (b) E_{ex}=755 meV (after Wang *et al.* [482]).

IX.4.1. Experimental

Baumann *et al.*[481] studied one set of samples with different well thickness grown on c-face sapphire by MBE. ~ 500-nm-thick *n*-type AlGaN buffer layer (Si, 5×10^{19} cm^{-3}) with a high Al content between 67 % and 100%. The active region consists of a regular 20 period superlattice with undoped AlN barriers and degenerately doped GaN quantum wells (Si, $5–10\times10^{19}$ cm^{-3}) and is typically about 50% relaxed. The well thickness ranges from 17 to 38 Å, while the barrier widths are between 18 and 34 Å. Both optical intersubband absorption and photovoltage (PV) spectra responses were measured for all samples and the PV responses for four different samples are plotted in Figure 65.

Absorption measurement was obtained by dividing the *p*-polarized sample transmission spectrum by the *p*-polarized spectrum of the internal white light source, followed by the normalization. As clearly seen from Figure 65, a transition energy increases with decreasing well width due to the stronger quantum confinement. Furthermore, according to the selection rule, only TM polarization was observed. However, for barrier thicknesses larger than about 25 Å, the optical intersubband absorption peaks at a considerably smaller energy than the photovoltage spectrum. To explain this difference, the authors proposed a model with taking into account the oscillator strength of the involved transitions.

Further studies [482] by using femtosecond two-color pump-probe in the near infrared range show spectral holes separated by the longitudinal optical (LO) phonon frequency and a homogeneous line broadening of approximately 50 meV. The nonlinear bleaching signal decays with a time constant of 160 fs due to intersubband scattering of delocalized electrons, followed by a weak picosecond component attributed to the relaxation of electrons from longer-lived localized states (see Figure 66).

Based on ISBT in AlN/GaN superlattice, the infrared detector ~1.55 μm was fabricated and measured at room temperature, and the detection of a sinusoidally modulated laser beam up to 2.37 GHz was achieved.[483] This particular sample was grown by plasma assisted molecular beam epitaxy, and the active region consisted of a 40 period AlN/GaN SL. Both wells and barriers have a nominal thickness of 1.5 nm and the wells are n-doped to 1×10^{20} cm^{-3}. This active region is sandwiched between a 1.1 μm-thick AlN buffer layer deposited on c-sapphire and a 50 nm AlN cap. For high frequency measurement, a 1.55 μm NEL NLK1554STB DFB laser diode was sinusoidally modulated. The PV signal was amplified by a lock-in amplifier and an additional low noise preamplifier. Acquisition was performed with a spectrum analyzer. The obtained frequency response of the sample at room temperature was shown in Figure 67. At 10 MHz, the response signal reaches a maximum at 10 MHz and then drops with a slope of 20 dB/decade. From the inset of Figure 67, the maximum frequency at which frequency the detector still works was 2.94 GHz.

IX.4.2. Issues

On the experimental side, the ISBT in nitride SL has been indeed observed and the detector working at room temperature has been demonstrated. However, some basic issues are still needed to be carefully addressed. For example, polarization induced electrical field in the SL requires a very thin GaN well (~10 Å) which makes growth difficult and the large conduction band discontinuity wasn't fully utilized. Unlike the LEDs, the studies of ISBT on non-polar substrates are limited. Furthermore, can nitride based ISBT devices beat the well established GaAs technology in the real application?

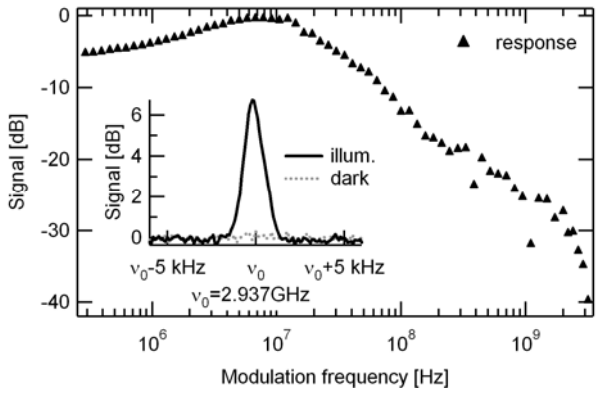

Figure 67. Measured room temperature frequency response together with fit consisting of one high pass and two low passes. The Inset shows spectrum analyzer trace at 2.94 GHz (after Giorgetta *et al.*[483]).

IX.5. Conclusions

The NDR based on real resonant tunneling or Bloch oscillation still hasn't be demonstrated in nitride materials, most probably, due to the high density of the defects in GaN. Furthermore, the polarization field introduces the additional complexity in simulation and experiment. To fully realize the potential of nitrides for the THz application, the high quality GaN templates with low density of defects (line and point defects) must be used. On the side, although the ISBT has been achieved in AlN/GaN SL, the material quality is still the limitation for real application, and GaN or AlN bulk substrates (discussed in another report) should be used.

X. ZnO devices and applications

X.1. Introduction

In many respects ZnO competes with GaN for device applications. It is clear that GaN has demonstrated itself well beyond any credible doubt that it is indeed capable of producing very high performance electronic and optical devices. The issues such as reliability, efficiency, etc., are being explored which by and in of itself is indicative of a success story. Power field effect transistors (FETs) are capable of producing over 500 W of CW power in the communication band, light emitting diodes (LEDs) have taken world like a storm with emphasis being on the efficiency while they are already more efficient than the mighty fluorescent bulbs, and blue lasers are already in Sony Play Station III. The same, however, cannot necessarily be said about ZnO at this point. The applications of ZnO overlap a good deal with those of GaN. On the electronic side, the relatively low mobility of ZnO as compared to GaN and stronger electron-phonon coupling together with relatively low thermal conductivity are serious shortcomings for ZnO. However, transparent thin film transistors built in poly-ZnO appear to hold some potential. It remains to be seen, however, as to how competitive ZnO would be with the existing technologies. On the optical device front, ZnO needs desperately to show high p-type conductivity along with heterojunctions for competitive devices to be built. Again the competition is GaN, which is well on its way to really dominate the optical device development arena in the short wavelength end of the visible spectrum and UV. One advantage that ZnO has over GaN is the 60 meV, compared to 25 meV for GaN, exciton binding energy. In addition, ZnO appears to be a more efficient light emitter as compared to GaN. If lasers utilizing excitonic transitions were to be built, ZnO would have an advantage over GaN provided that p-type conductivity is obtained and other necessary processing capabilities are developed for ZnO. Further, electromechanical coupling of ZnO, particularly along the c-direction is higher than that of GaN, which could pave the way for applications such as acoustic wave devices.[484] Further yet, if and when the highly hyped and touted nanostructures were someday to be of some use, ZnO appears to be well suited for producing those structures. In fact nano structures in ZnO have been done well before the current crop of nano aficionados knew what nano meant. The worldwide shortage of In in the face of expanding demand for ITO seems to be opening the door for ZnO based transparent oxides to be explored. If successful, this application area is huge. The participants of the workshop were challenged to address the above discussed issues and delved into the present and potential device applications of ZnO including the hybrid varieties utilizing both GaN and ZnO.

Speakers reviewed progress made in the field of ZnO devices and applications during the past several years. Research in this field dealt mostly with ZnO nanostructures (nanowires, nanorods, nanobelts, nanotips) and their integration with the mainstream semiconductor materials – e.g. with Si, GaN, and organic semiconductors. One-dimensional (1D) nanostructures, such as nanowires (NW), have attracted a great deal of

attention due to their advantages, such as good charge carrier transport properties and high crystalline quality.[485,486,487] 1D systems have unique properties that make them potentially attractive for nanoscale devices (light-emitting diodes, lasers, photodetectors, chemical/bio sensors, and SAW devices), which have been intensively investigated.[488,489,490,491] Below we summarize the discussions that took place as well as progress made in ZnO but not covered at the workshop.

X.2. Devices utilizing ZnO nanostructures

Heterojunction light emitters based on p-n junctions formed between n-ZnO nanotips and p-GaN film are of interest and have been investigated. [492] The diodes demonstrated threshold and breakdown voltages of ~ 3V and ~–8V, respectively, and a reverse leakage current of ~ 54 μA at –5V. Blue light emission was observed under a forward bias with a dominant EL wavelength at 406 nm attributed to recombination of electrons injected from ZnO nanotips and the holes in p-GaN where the emission took place because n-doping in ZnO is higher than p-doping in GaN. N-ZnO Nanotip/p-Si p-n diodes were also fabricated by the same group exhibiting low threshold voltage (< 2V) and sharp breakdown voltage at ~ -17V, and a relatively small reverse leakage current ~50μA at -10V. Such type of p-n diodes are thought to have potential applications in Si IC interconnects.

ZnO nanotips have also been used to increase the outcoupling as an improved passive light extraction layer in GaN light emitters.[493] The cross-sectional schematic of an integrated ZnO nanotip/GZO/GaN LED is shown in Figure 68(a). InGaN/GaN multiple quantum well LED structures were grown on *c*-plane sapphire by MOCVD. Ga-doped ZnO (GZO) layer, which is used as a contact to *p*-GaN and also as an optically transparent window, was deposited on top of these conventional GaN LED structures. Then ZnO

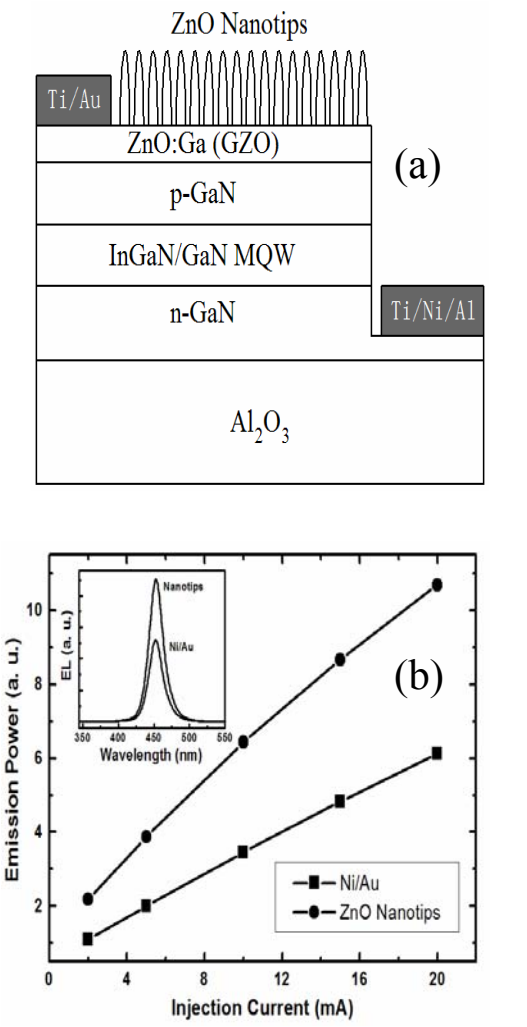

Figure 68. (a) Schematic of an integrated ZnO nanotip/GZO/GaN LED; (b) Light output power vs. forward injection current for Ni/Au and ZnO nanotip/GZO/GaN LED; inset is EL spectra of Ni/Au *p*-contact GaN LED and ZnO nanotip/GZO/GaN LED at a forward current of 20 mA (courtesy of Y. Lu of Rutgers University[493]).

nanotips were grown on GZO coated GaN as a light extraction layer for the LED. In comparison with a conventional Ni/Au *p*-electrode GaN LED, light emission efficiency enhanced by a factor of ~1.7 [Figure 68(b)]. The enhancement in light extraction efficiency was explained by the interaction between the spontaneous emission from the GaN LED and ZnO nanostructures. With an optimized GZO layer on *p*-GaN, significantly higher light emission efficiency is expected from the integrated ZnO nanotip/GZO/GaN LED structure. The results represent one of the ways of the integration of ZnO nanotips with GaN-based optoelectronic devices. This method for enhancing light extraction is very suitable for low cost and large scale fabrication since as-grown nanotips do not require e-beam lithography or etching and can be integrated with GaN-based optoelectronic devices using epitaxial growth technology. With or without the nanotips and fuelled by worldwide shortage of In, transparent conductor GZO or ZnO:Al (AZO) in place of indium tin oxide (ITO), which is used in all GaN based LEDs, might turn out to be very lucrative as will be discussed below.

Nanowires (NWs) are often configured also as field effect transistor (FET) structures with a back gate for current transport studies [see Figure 69(a)]. Employing the coupled piezoelectric and semiconducting dual properties of ZnO a piezoelectric field effect transistor (PE-FET) composed of a ZnO NW bridging across two ohmic contacts was demonstrated by Wang *et al*.[494] for measuring forces in the nanonewton range. In such a PE-FET the source to drain current is controlled by the bending of the NW. The mechanism for the PE-FET operation has been attributed to the carrier trapping effect and the creation of a charge depletion region under elastic deformation. The linear relationship between the bending force and the conductance was found at small bent regions, demonstrating the principle of nanowire-based nanoforce and nanopressure sensors. To improve the electrical characteristics of ZnO nanorod FETs different treatments were employed. Park *et al*.[486] reported significant improvement by coating ZnO nanorods with polyimide. The I_{sd}–V_g curves of ZnO nanorod FET after the polyimide coating fully turned off at Vg=−5 V and exhibited a large current ON/OFF ratio of 10^4–10^5 and a transconductance as high as 1.9 μS at V_g=2.3 V (when V_{sd} =1.0 V) that was an order of magnitude higher than that for as-grown ZnO nanorod FETs without polyimide coating [Figure 69(c)]. The electron mobility estimated from transconductance showed a maximum value of 1000–1200 cm^2/Vs. A significant improvement of ZnO NW FET device performance was also observed in another report[485] after surface passivation.

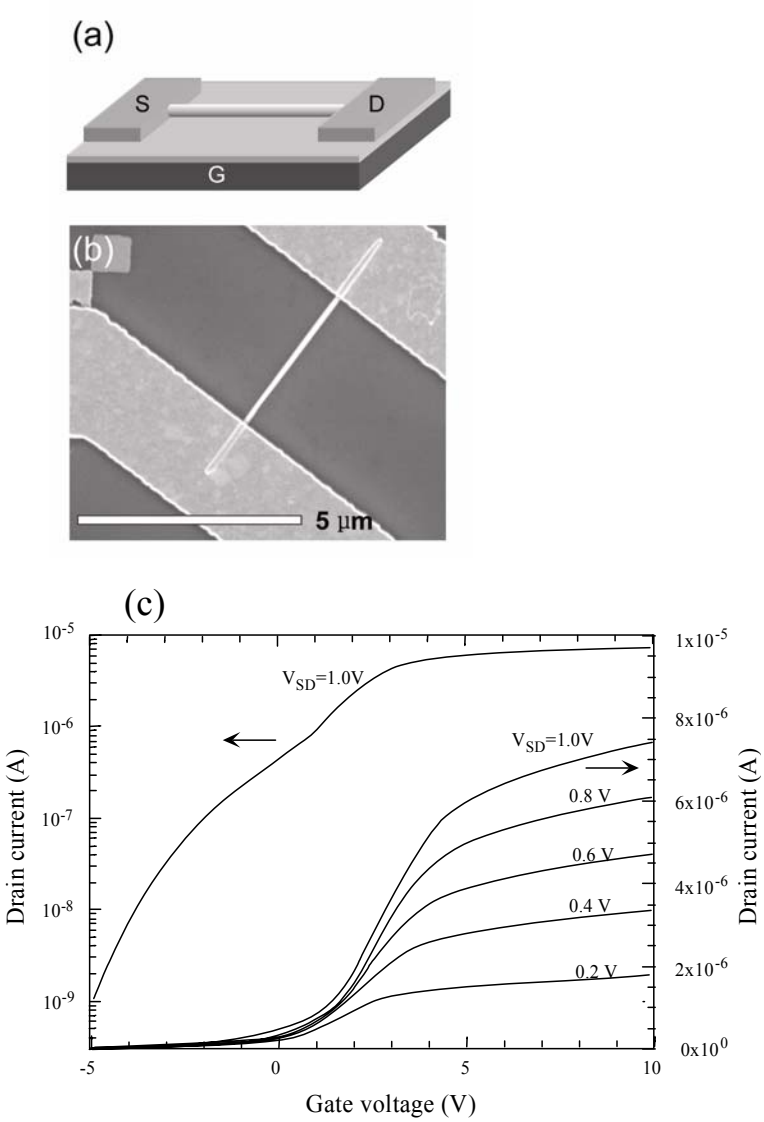

Figure 69. (a) Schematic side view and (b) field-emission scanning electron microscopy image of a ZnO nanorod FET device. (c) I_{sd}–V_g curves (solid line) as a function of V_{sd} and log scale plot (open circles) of I_{sd}–V_g (V_{sd}=1.0 V) for a ZnO single nanorod FET after polyimide coating on the device (after Park *et al.*[486]).

X.3. Transparent conducting oxides and thin-film transistors

Unlike the conventional FET or thin film transistor (TFT) structures, transparent TFTs (TTFTs) require all device components (channel, gate, electrodes, substrate) to be transparent. Such invisible TTFT can be used in wide range of applications where transparency is required for some commercial and military applications. For instance, automobile windshields could transmit visual information so that glass could also serve as an electronic device improving security systems. The military is interested in research of this type thin film transistors because of possible uses in sophisticated technology for

fighting equipment. Also being insensitive to visible light TTFTs do not require device protection from illumination, unlike the commercial amorphous silicon transistors in which visible light generates excess carriers and, therefore, need to be shielded. In this vein, there has been an increased interest in transparent thin-film transistors (TTFT) based on ZnO as an active channel layer for use in the field of transparent applications.[495,496,497,498,499,500,501,502,503,504,505,506]

Before delving into the discussion of transparent transistor structures let us spend a little more time to discuss the transparent oxides based on ZnO in their own merits. As mentioned briefly, in most optoelectronic devices such as flat panel displays, LEDs, and solar cells, it is essential to use a transparent electrode such as a thin film transparent conducting oxide (TCO). Although tin-doped indium oxide (ITO) thin films deposited by magnetron sputtering are widely used today for most transparent electrode applications, there are many reports on other TCO semiconductors such as aluminum zinc oxide (AZO), gallium zinc oxide (GZO), indium zinc oxide (IZO), tin zinc oxide (TZO) in large part due to expected worldwide shortage of In. The growing demand for ITO thin-film transparent electrodes is the impetus for looking at alternative TCO materials since a stable supply of ITO may be difficult to achieve for the expanding market because of the cost and, as mentioned, limited amount of indium available. The ZnO based TCOs have attracted significant attention due to their good conductivity, high optical transparency (in the 90% range), excellent surface smoothness, low deposition temperature, good etchability for patterning, and good reproducibility.[507,508,509,510] Candidates for transparent amorphous oxides having large electron mobilities must be constituted of heavy post transition metal cations with an electronic configuration $(n-1)d^{10}ns^0$, where $n \geq 5$.[511] Oxide semiconductor XZO films, where X=Al,Ga,In,Sn, are prepared from the target made of homogeneous $Al_2O_3(ZnO)_n$, $Ga_2O_3(ZnO)_n$, $In_2O_3(ZnO)_n$, $SnO_2(ZnO)_n$ compounds. Although various dopants have been used to fabricate ZnO TCO films, minimum resistivity (below 2×10^{-4} Ω·cm) and the maximum carrier concentration (about 10^{20} cm^{-3}) have only been obtained in AZO and GZO films, as can be seen from Table 6.[512] For example, resistivities as low as $0.85\text{x}10^{-4}$ Ω-cm and $0.81\text{x}10^{-4}$ Ω-cm have been obtained for ZnO:Al[513] and ZnO:Ga[514] thin films grown by pulsed laser deposition, comparable to values obtained for ITO (e.g. $0.72\text{x}10^{-4}$ Ω-cm [515]). In general, the electrical properties of the TCO films strongly depend on the deposition methods and conditions. AZO and GZO films with resistivities in the order of 10^{-5} Ω-cm have been grown by PLD, for which preparing films on large substrates with a high deposition rate is very difficult to achieve.

Table 6. Resistivity, carrier concentration, and dopant content for typical ZnO films doped with various impurities. After Minami.[512]

Dopant	Dopant content (Wt %)	Resistivity, $\times 10^{-4}$ Ω·cm	Carrier concentration, $\times 10^{20}$ cm^{-3}
Al_2O_3	1-2	0.85	15.4
Ga_2O_3	2-7	1.2	14.5
B_2O_3	2	2.0	5.4
Sc_2O_3	2	3.1	6.7
SiO_2	6	4.8	8.8
V_2O_5	0.5-3	5.0	4.9
F	0.5	4.0	5.0
Undoped	0	4.5	2.0

Coming back to TTFTs, although Si has shown it supremacy in the field of thin film transistor (TFT) technology with amorphous Si (*a-Si*) and polycrystalline-Si (*poly-Si*), an interest is developing for the optically transparent analogue, the TTFT technology.[495,496,498] To date TTFTs have been fabricated using different transparent oxide semiconductors such as SnO_2, Ga_2O_3, ZnO, etc.[498] Among these transparent oxides is the semiconductor ZnO with a band gap (~3.3 eV), making it optically transparent in the visible region. Also it should be noted that such invisible thin film transistors using ZnO as an active channel achieve much higher field effect mobility than amorphous silicon transistors (0.5 cm^2/V-s) – the major material of today's FET technology. As in the case of overall renewal of interest in ZnO, interest in TTFT technology was reborn due to reports of p-type conductivity in several wide bandgap oxide semiconductors.[516,517]

Song *et al*.[509] reported on TTFT using amorphous IZO for the active channel layer and gate-source-drain electrodes fabricated by rf magnetron sputtering at room temperature while amorphous AlO_x served as the gate dielectric. The devices exhibited threshold voltages of 1.1 V, on/off ratios of ~10^6, saturation currents of 1.41 μA at 5 V, and optical transmittance of about 80% in the visible range. Nomura *et al*.[518] proposed to use a novel semiconducting material, amorphous oxide semiconductor In-Ga-Zn-O (a-IGZO), for the active channel in TTFTs. They deposited *a*-IGZO on polyethylene terephthalate (PET) at room temperature that exhibited a Hall effect mobility more than 10 cm^2 V^{-1} s^{-1}. TTFTs fabricated on such PET sheets showed saturation mobilities of 6–9 cm^2 $V^{-1}s^{-1}$, and device characteristics were stable during repetitive bending of the TTFT sheet. The transfer characteristics showed a low off-current, of the order of 10^{-7} A, and a ~10^3 on-to-off current ratio. Studies on the effect of bending on the TTFT characteristics showed that the performance of the TTFT after repetitive bending remained unaffected. Only a slight decrease in the saturation current was observed. The TTFT was stable at temperatures up to 120 °C, but became inoperative at higher temperatures, probably owing to the softening of the PET substrate. Hoffman *et al*.[496] reported a bottom-gate-type TTFT fabricated using undoped ZnO as an active channel deposited via ion beam sputtering. Their device operated as an *n*-channel enhancement-mode TFT and its

effective channel mobility and threshold voltages were found to be 0.35–0.45 $cm^2/V{\cdot}s$ and 10–15 V, respectively.

A key issue for ZnO TTFTs is the selection of gate insulators. Various gate dielectric materials have been tested for ZnO-based TFTs, such as SiO_2,[499] HfO_2,[503] PbZrTiO,[519] ZnMgO,[520] and Y_2O_3.[521] As an example, TTFTs with transparent oxide semiconductor ZnO serving as the electron channel and 200 nm-thick high dielectric constant $Bi_{1.5}Zn_{1.0}Nb_{1.5}O_7$ (BZN) as the gate insulator have been reported.[522] The devices were shown to have very low operation voltages (<4 V) afforded by the high capacitance of the BZN dielectric. At an operating voltage of 4 V the devices exhibited a field effect mobility (drift mobility) and a current on/off ratio of 0.024 cm^2/V-s and $2x10^4$, respectively, and the threshold voltage was 2 V. High optical transparency (>80% for wavelengths above 400 nm), low-temperature processing, and low operation voltage of ZnO-based thin-film transistors with integrated BZN dielectric are promising for transparent device technology. Masuda *et al*.[499] fabricated *n*-channel depletion-mode TTFTs with undoped ZnO grown by PLD on glass for the channel and a double-layer gate insulator consisting of SiN_x (250 nm) and SiO_2 (50 nm) to suppress the leakage current, where ITO was used as the gate electrode and IZO as the source and drain electrodes. Even though the TFTs operated successfully with an optical transmittance of more than 80%, the on-to-off ratio was only ~ 10^5.

High performance thin TTFTs with nitrogen doped ZnO as an active layer grown by atomic layer deposition have been demonstrated by Lim *et al*.[505] By nitrogen doping the electron concentration in ZnO was lowered to $6x10^{14}$ cm^{-3}, which is crucial for lowering the leakage current. Consequently, the enhancement-mode TTFT devices (40 μm channel width, 20 μm channel length) exhibited off-currents as low as 2 pA, with a threshold (turn-on) voltage of 4.7 V, an on-to-off drain current ratio of $9.5x10^7$, and a saturation mobility of 6.7 cm^2/V-s at 35 V drain bias. The entire TFT fabrication process was carried out below 150 °C including the Al_2O_3 gate insulator deposition before the ZnO channel growth.

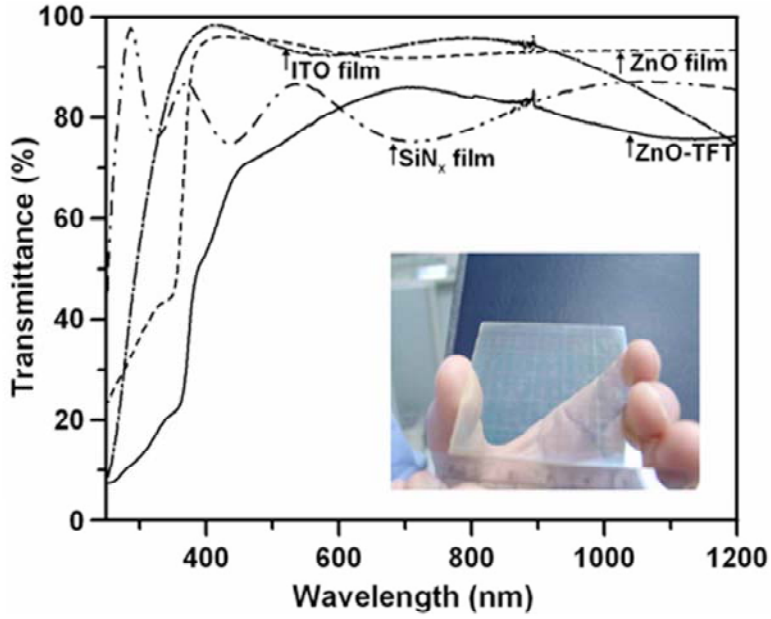

Figure 70. Optical transmission spectra for the top-gate structure of ZnO-TFT (except substrate) through the ITO film (gate), SiN_x (gate insulator), and (ZnO film) channel region, and the thicknesses are 100, 300, and 200 nm, respectively. The inserted photo shows a 5×5 cm^2 substrate with 75 devices of ZnO-TFT on Corning 1737 glass substrate (After Cheng *et al*.[506]).

ZnO-based TTFTs with high on-to-off ratios have been fabricated also by using simpler deposition techniques such as sol-gel and chemical bath deposition on glass substrates with a maximum process temperature of 230 °C.[506] Figure 70 shows the optical transmission spectra through the ZnO TTFT excluding the glass substrate. The structure consists of a 100 nm-thick ITO film gate, a 300 nm-thick SiN_x gate insulator, and a 200 nm-thick ZnO film channel region. The transmittance transistors were highly transparent in the visible range, with transmittance as high as 75% to approximately 85% at wavelengths from 500 to 700 nm. The I_D-V_G curve revealed a drain current with on to off ratio of more than 10^7, while the device had field-effect mobility of 0.67 cm^2 /V s.

X.4. Sensors and Solar Cells based on ZnO nanostructures

ZnO nanorod FET sensors may open up opportunities to create highly sensitive and selective real-time detection of a wide variety of gas and bio molecules. The principle of gas sensor operation depends on the nature of gas molecules and is based on the modification of NW FET channel conductivity. The oxygen vacancies in ZnO function as n-type donors on oxide surfaces and are electrically and chemically active. Upon adsorption of charge accepting gas molecules, for example NO_2 and O_2, electrons are depleted from the conduction band resulting in a reduced conductivity of the n-type oxide. On the other hand, molecules that chemically react with surface oxygen (for example, CO and H_2) react with surface adsorbed oxygen on ZnO and remove it leading to an increase in conductivity. ZnO exhibits strong adsorption of molecules on the surface, which

affects the electrical characteristics of ZnO-based devices, dependent on surface-mediated phenomena. Thanks to the large surface-to-volume ratio of the nanostructures, the detection sensitivity of FET biosensors may be increased to a single-molecular detection level by measuring the small conductance changes caused by binding of biomolecular species on a nanorod conduction channel.

X.4.1. Gas Sensors

There is strong current interest in the development of lightweight gas sensors capable of ppm sensitivity and extended operation at low-power levels. All experimental results demonstrate that ZnO nanowires, owing to the large surface area, have a potential for detecting NO_2[523,524], NH_3,[525] NH_4,[526] CO,[526] H_2,[527,528,529] H_2O,[530] O_3,[529,531,532] H_2S,[533] C_2H_5OH,[534]. Detection of gas molecules is usually achieved either by measuring resistivity change of nanocrystalline ZnO films or the NW channel of FET.

Cho *et al.*[523] reported 1.8 fold decrease in resistance of well-dispersed ZnO nanorods at 1 ppm NO_2, while there was no significant change in resistance at 50 ppm CO. Sputtered nano-crystallite Cu-doped ZnO films of columnar structure with average grain size of 5 nm exhibited very high sensitivity (2.7–20 ppm) to CO at 350 ^oC.[526] A substantial change in resistance of the ZnO films was also observed at a low operating temperature of 150 ^oC when the sensor was exposed to 6 ppm CO. The sensitivity of room temperature detection of hydrogen by ZnO nanaorods was shown to be greatly enhanced by sputter-depositing clusters of Pd on the surface.[528] An increase in the resistivity by a factor of 5 was observed upon exposure to hydrogen concentrations of 10-500 ppm compared to the one without Pd. Pd-coated ZnO nanorods showed sensitivities lower than 10 ppm, with 95% recovery of the initial conductance after 20 s.

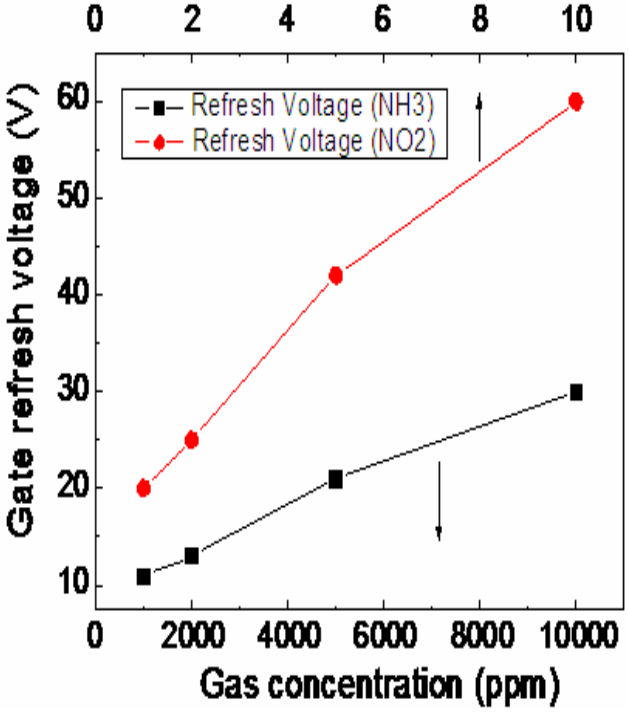

Figure 71. Gate refresh voltages for NH_3 and NO_2 gas molecules as a function of gas concentration (After Ref 535).

ZnO nanorods are also a promising candidates for detecting extremely low concentrations of H_2S. High response and good selectivity properties of ZnO nanorods to low concentrations of H_2S was observed by Wang *et al.*[533] The ratio of the

electrical resistance in air to that in 0.05 ppm H_2S was measured to be 1.7 at room temperature.

One of the most important parameters of gas sensors is their selectivity. The selectivity is achieved by applying different voltages to the gate of a nanowire FET or by performing measurements at different temperatures since different gas molecules have different activation energies. Figure 71 shows an example of such selectivity for NH_3 and NO_2 gas molecules, where the refresh (erase) voltages, negative gate voltages required for electrical desorption of adsorbed gas molecules, for the two gas molecules are significantly different making it possible to distinguish different gas species.[535]

X.4.2. Bio Sensors

The potential of ZnO nanostructures as nanosized biosensors has also been explored for detecting different biological molecules. Development of 1D ZnO nanostructures as bio sensors is in the state of infancy and only a limited number of reports are available.[536,537,538,539,540,541] The 1D ZnO biosensors have advantages such as stability to in air, nontoxicity, chemical stability, electrochemical activity, ease of synthesis, and the bio-safe characteristics. As in the case of gas sensors, the principle of operation is that the conductance of ZnO nanorod FETs drastically changes when bio molecules are adsorbed on the ZnO surface.

The key parameter in most biological processes is the need for a small change of the *p*H concentration created by the release of H^+ ions during biochemical reactions, and its determination is a prerequisite for many processes. The sensing mechanism for pH is the polarization-induced bound surface charge by interaction with the polar molecules in the liquids. Application of ZnO nanorods as *p*H sensors for intracellular chemical sensing is under development and a room temperature sensitivity (change in surface potential) as high as ~59 mV per decade change in the pH value has been reported.[541]

Kim *et al.*[536] reported on the fabrication of electrical biosensors based on functionalized ZnO nanorod surfaces with biotin for highly sensitive detection of a biomolecule streptavidin. The biotin-modified ZnO nanorod FET exhibited drastic conductance increase to 17 μS after exposition to a 250 nM streptavidin solution, presumably due to the biotin-streptavidin binding.

X.4.3. Solar sells

Solar cells are the most promising renewable energy technologies because they provide clean and renewable energy reducing our dependence on fossil oil and reducing our impact on the environment. Dye-sensitized solar cells (DSSCs), using inorganic semiconductors, are being studied now as novel devices for very efficient, inexpensive, large-scale solar energy conversion. DSSCs have been explored as possible substitutes for conventional silicon cells, but they suffer from possible dye agglomeration or electrolyte leakage.[542,543,544,545,546] During its traversal to the photoelectrode an electron in a polycrystalline solar cell usually crosses about 10^3 to 10^6 nanoparticles, and disorder

structure of the nanoparticles film leads to enhanced scattering of free electrons, thus reducing the electron mobility and increasing electron recombination rate. Replacement of the nanoparticle film with an array of oriented single-crystalline nanorods must result in the rapid collection of carriers generated throughout the device as the nanorods provide a direct path from the point of photogeneration to the conducting substrate, thus effectively reducing the electron recombination losses. Moreover, electron transport in the single crystalline rod is expected to be several orders of magnitude faster than that in a random polycrystalline network. As shown in Figure 72,[547] a DSSC has three main components: *i*) A thick (~10 μm) film of wide band gap semiconductor nanostructures (TiO_2, SnO_2, or ZnO), *ii*) a monolayer of organic dye molecules absorbed onto the semiconductor nanostructures, and *iii*) a liquid electrolyte containing the redox couple I^-/I_3^- that penetrates in between the dye-coated nanostructures.

ZnO is obviously one of the best candidate semiconductors for DSSC applications as it can be synthesized easily and inexpensively into different shapes and sizes using various methods, and is environment friendly and stable indefinitely. Photomodulation experiments with dye-sensitized ZnO solar cells have shown tens to hundreds of times faster electron transport in nanorod array electrodes than in nanocrystalline particulate electrodes, with electron lifetimes being only slightly smaller.[548]

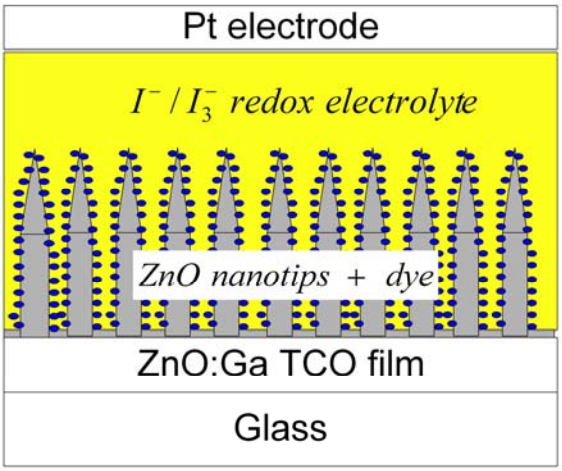

Figure 72. A schematic of nanotip ZnO based DSSCs (Courtesy of Y. Lu of Rutgers University).

X.5. Conclusions

ZnO offers some potential in providing electronic, photonic, and spin-based devices, and encouraging progress has been made in the research phase. Despite this progress there is still a number of important issues that are in need of further investigation before

this material can be transitioned to commercial use. The task is made more difficult by the highly successful GaN which competes for similar applications. However, there are some niche applications of ZnO which are not addressed by GaN which if explored fully might pave the way for ZnO. Transparent thin film transistors, ZnO-based transparent oxides, laser structures exploiting the large exciton binding energy of ZnO (see the report on lasers wherein ZnO active layers are explored for potential polariton lasers) are among these applications.

In case of TTFTs, the critical issues are the mobility in non crystalline or polycrystalline ZnO, the choice of gate oxide, the choice of substrate, and the methods to deal with high electron concentrations encountered in the ZnO channel layer. For the electrical characteristics the on-to-off ratio as well as the transconductance is important to hone in on.

ZnO also lends itself to applications in sensing, in part due to ease with which ZnO can be produced in the form of nanostructures. There is still much to be understood in terms of the mechanism of ZnO gas and bio sensors. Although a number of ZnO sensors have been reported on detecting different gas and bio molecules, the selectivity remains to be the main issue since identification of the nature of the absorbed molecules is very important. Although several approaches have been proposed, which employ different activation energies of different gas molecules, this field is still in a state of infancy, as the others really, and much more effort needs to be expended to pave the way for improved selectivity of ZnO sensors and increase the lifetime of the devices.

Regarding the solar sells, which received some attention although the competition is very stiff, further studies are required to improve the current density. This could be achieved by application of various electrolytes and doping the ZnO films to improve its conductivity. There is also the control of the properties of individual building blocks which at this point is inadequate and device-to-device reproducibility is low.

As for the nanostructures, ZnO nanostructures (nanowires, nanorods, etc.) provide a way for a new generation of devices, but a deliberate effort has to be expended for ZnO nanostructures to be taken seriously for large scale device applications, and to achieving high device density with accessibility to individual nanodevices. Reliable methods for assembling and integrating building blocks into circuits need to be developed.

Finally, ZnO as a semiconductor is going to have very stiff competition from GaN which is much more mature in terms of devices (also has acceptable p-type dopant unlike the case in ZnO). Lack of a credible p-type doping hampers, to put it lightly, any thought of optical emitters in ZnO. Furthermore, highly ionic nature of ZnO with large electron phonon coupling and low thermal conductivity do not bode well for ZnO-based electronic devices. Nanostructures seem a little easier to produce with ZnO, but it remains to be seen whether nanostructures in general as hyped would really make inroads in the area of devices.

REFERENCES

[1] A. Van Vechten, "Quantum dielectric theory of electronegativity in covalent systems. III. Pressure–temperature phase diagrams, heats of mixing, and distribution coefficients", Phys. Rev. B **7**, (1973) 1479.

[2] J. Karpinski, J. Jun, S. Porowski, Equilibrium pressure of N_2 over GaN and high pressure solution growth of GaN, J.Cryst. Growth **66** (1984) 1.

[3] W. Utsumi, H. Saitoh, H. Kaneko, T. Watanuki, K. Aoki, O. Shimomura, Congruent melting of gallium nitride at 6 GPa an its application to single crystal growth, Nat. Mater. **2,** (2003) 735.

[4] [12] S. Porowski, "High pressure crystallization of III-V nitrides", Acta Physica Polonica. **87** (1995) 295.

[5] M. Leszczynski, I. Grzegory, H. Teisseyre, T. Suski, M. Bockowski, J. Jun, J.M. Baranowski, S. Porowski, J. Dodmagala, "The microstructure of gallium nitride monocrystals grown at high pressure", J. Cryst. Growth **169,** (1996) 235.

[6] K. Saarinen, T. Laine, S. Kuisma, J. NissilS, P. Hautoja¨ri, L. Dobrzynski, J.M. Baranowski, K. Pakula, R. Stepniewski, M.Wojdak, A.Wysmolek, T. Suski, M. Leszczynski, I. Grzegory, and S. Porowski, "Observation of native Ga vacancies in GaN by positron annihilation", Phys. Rev. Lett. **79** (1997), 3030.

[7] M. Lefeld, I. Frymark, "Extended defects in GaN single crystals", J. Phys. D Appl. Phys. **34**, (2001) A148.

[8] Z. Liliental-Weber, J. Jasinski, and J. Washburn, "Comparison between structural properties of bulk GaN grown in liquid Ga under N_2 pressure and GaN grown by other methods", J. Cryst. Growth **246**, (2002) 259.

[9] J.L. Weyher, I. Match, G. Kamler, J. Borysiuk, and I. Grzegory, "Characterization of GaN single crystals by defect selective etching", Phys. Stat. Sol. C **3**, (2003) 821.

[10] I. Grzegory, "High pressure crystallization of GaN for electronic applications", J. Phys. Condens. Matter. **14**, (2002) 11055.

[11] I. Grzegory, "High nitrogen pressure growth of GaN crystal and their applications for epitaxy of GaN-based structures", Mater. Sci. Eng. B 82 (2001) 30.

[12] T. Fukuda and D. Ehrentraut, "Prospects for the ammonothermal growth of large GaN crystal", J. Cryst. Growth **305,** (2007) 304.

[13] D. Ehrentraut, Y. Kagamitani, C. Yokoyama, and T. Fukuda, "Physico-chemical features of the acid ammonothermal growth of GaN", J. Cryst. Growth 310, (2008) 891.

[14] M. Callahan, B.G. Wang, K. Rakes, D. Bliss, L. Bouchillette, M. Suscavage, and S.Q. Wang, "GaN single crystals grown on HVPE seeds in alkaline supercritical ammonia", J. Mat. Sci. **41**, (2006) 1399.

[15] J.H. Edgar (Kansas State University, Dept. Chem. Engineering), private communication (2008).

[16] F. Iwasaki and H. Iwasaki, "Historical review of quartz crystal growth", J. Cryst. Growth 237–339 (2002) 820.

[17] H. Yamane, M. Shimada, S.J. Clarke, and F.J. Disalvo, "Preparation of GaN single crystals using a Na flux", Chem. Mater. **9**, (1997) 413.

[18] J.K. Jian, G. Wang, C. Wang, W.X. Yuan, and X.L. Chen, "GaN single crystals grown under moderate nitrogen pressure by a new flux: Ca3N2", J. Crystal Growth **291**, (2006) 72.

[19] T. Iwahashi, F. Kawamura, M. Morishita, Y. Kai, M. Yoshimura,Y. Mori, and T. Sasaki, "Effects of ammonia gas on threshold pressure and seed growth for bulk GaN single crystals by Na flux method", J. Crystal Growth **253**, (2003) 1.

[20] M. Morishita, F. Kawamura, M. Kawahara, M. Yoshimura,Y. Mori, and T. Sasaki, "Promoted nitrogen dissolution due to the addition of Li or Ca to Ga-Na melt; some effects of additives on the growth of GaN single crystals using the sodium flux method," J. Crystal Growth **284**, (2005) 91.

[21] T. Yamada and H. Yamane, "Seeded growth of GaN single crystals by Na flux method using Na vapor", Jpn. J. Appl. Phys. **45,** (2006) L898.

[22] F. Kawamura, H. Umeda, M. Kawahara, M. Yoshimura, Y. Mori,T. Sasaki, H. Okado, K. Arakawa, and H. Mori; "Drastic decrease in dislocations during liquid phase epitaxy growth of GaN single crystals using Na flux method without any artificial processes"; Jpn. J. Appl. Phys.; **45**, 2528, (2006).

[23] T. Yamada, H. Yamane, H. Iwata and S. Sarayama, "The process of GaN single crystal growth by the Na flux method with Na vapor"; J. Cryst. Growth; **286**, 494, (2006)

[24] B.N. Feigelson and R.L. Henry; "Growth of GaN crystals from molten solution with Ga free solvent using a temperature gradient"; J. Cryst. Growth; **281**, 5, (2005) (in the special issue on bulk AlN and GaN substrates).

[25] B.N. Feigelson, R.M. Frazier, and M. Twigg; "III-nitride crystal growth from nitride salt solution"; J. Cryst. Growth; **305**, 399, (2007)**.**

[26] G.A. Slack and T.F. McNelly; "Growth of high-purity AlN crystals"; J. Crystal Growth; **34**, (1976) 263; G.A. Slack and T.F. McNelly; "AlN single-crystals"; J. Crystal Growth; **42**, 560, (1977).

[27] Z. Gu, L.Du J.H. Edgar, N.,Nepal, J.Y. Lin, H.X. Jiang, and R. Witt; "Sublimation growth of aluminum nitride crystals"; J. Crystal Growth **297**; 105, (2006).

[28] B. Raghothamachar, M. Dudley, J.C. Rojo, K. Morgan, and L.J. Schowalter; "X-ray characterization of bulk AlN single crystals grown by the sublimation technique"; J. Crystal Growth; **250**, 244, (2003).

[29] S.B. Schujman, L.J. Schowalter, R.T. Bondokov, K.E. Morgan, W. Liu, J.A. Smart, and T. Bettles; "Structural and surface characterization of large diameter, crystalline AlN substrates for device fabrication"; J. Cryst. Growth; **310**, 887, (2008) .

[30] D. Gogova, D. Siche, R. Fornari, B. Monemar, P. Gibart, L. Dobos,B. Pe´cz, F. Tuomisto, R. Bayazitov, and G. Zollo; "Optical and structural studies of high-quality bulk-like GaN grown by HVPE on a MOVPE AIN buffer layer"; Semicond. Sci. Technol.; **21,** 702, (2006).

[31] B. Łucznik, B. Pastuszka, I. Grzegory, M. Boc´kowski, G. Kamler, E. Litwin-Staszewska, S. Porowski; "Deposition of thick GaN layers by HVPE on the pressure grown GaN substrates"; J. Crystal Growth; **281**, (2005) 38.

[32] R.P. Vaudo, X. Xu, A. Salant, J. Malcarne, and G.R. Brandes; "Characteristics of semi-insulating, Fe-doped GaN substrates"; Phys. Status Solidi (a); **200**, (2003) 18.

[33] J.A. Freitas Jr., J.G. Tischler, J.-H. Kim, Y. Kumagai, and A. Koukitu; "Properties of Fe-doped semi-insulating GaN substrates for high-frequency device fabrication"; J. Cryst. Growth; **305**, (2007) 403.

[34] T. Sekiguchi, S. Miyashita, K. Obara, T. Shishido, and N. Sakagami; "Hydrothermal growth of ZnO single crystals and their optical characterization"; J. Cryst. Growth; **214-15**, 72, (2000).

[35] M. Sakagami, M. Yamashita, T. Sekiguchi, S. Miyashita, K. Obara, and T. Shishido; "Variation of electrical properties on growth sectors of ZnO single crystals"; J. Cryst. Growth; **229**, 98, (2001).

[36] W.-J. Li, E.-W. Shi, W.-Z. Zhong, and Z.-W. Yin; "Growth mechanism and growth habit of oxide crystals"; J. Cryst. Growth; **203**, 186, (1999).

[37] M. Shiloh and J. Gutman; "Growth of ZnO single crystals by chemical vapour transport"; J. Cryst. Growth; **11**, 105, (1971).

[38] K. Matsumoto and K. Noda; "Crystal growth of ZnO by chemical transport using $HgCl_2$ as a transport agent"; J. Cryst. Growth; **102**, 137, (1990).

[39] J.-M. Ntep, S. Said Hassani, A. Lusson, A. Tromson-Carli, D. Ballutaud, G. Didier, and R. Tribou1et; "ZnO growth by chemical vapour transport"; J. Cryst. Growth; **207,** 30, (1999).

[40] J. Nause; "ZnO broadens the spectrum"; III-Vs Review; **12**, 28, (1999).

[41] J. Nause and B. Nemeth; "Pressurized melt growth of ZnO boules"; Semicon. Sci. Technol.; **20**, S45, (2005).

[42] J. Nause (Cermet, Inc.), private communication (2008).

[43] T. Fukuda and D. Ehrentraut; "Prospects for the ammonothermal growth of large GaN crystal"; J. Cryst. Growth; **305,** 304, (2007).

[44] K. Maeda, M. Sato, I. Niikura, and T. Fukuda, "Growth of 2 inch ZnO bulk single crystal by the hydrothermal method"; Semicon. Sci. Technol.; **20**, S49, (2005).

[45] "The 3rd International Workshop on ZnO and Related Materials"; Sendai City War, Reconstruction Memorial Hall, Sendai, Japan; October 5-8, 2004.

[46] E. Ohshima, H. Ogino, I. Niikura, K. Maeda, M. Sato, M. Ito, and T. Fukuda; "Growth of the 2-in-size bulk ZnO single crystals by the hydrothermal method"; J. Cryst. Growth; **260**, 166, (2004).

[47] C. G. Van de Walle and J. Neugebauer; " First-principles calculations for defects and impurities: Applications to III-nitrides"; J. Appl. Phys.; **95**, 3851, (2004).

[48] J. Neugebauer and C. Van de Walle; "Atomic geometry and electronic structure of native defects in GaN"; Phys. Rev. B; **50**, 8067, (1994).

[49] P. Boguslawski, E. L. Briggs, and J. Bernholc; " Native defects in gallium nitride"; Phys. Rev. B; **51**, 17255, (1995).

[50] T. Mattila and R.M. Nieminen; " Point-defect complexes and broadband luminescence in GaN and AlN"; Phys. Rev.B.; **55**, 9571, (1997).

[51] A. Janotti and C. Van de Walle; "Oxygen Vacancies in ZnO", Appl.Phys.Lett. 87, 122102 (2005); ibid, "Native point defects in ZnO"; Phys. Rev. B; **76**, 165202, (2007).

[52] S. B. Zhang, S.-H. Wei, and Alex Zunger; "Intrinsic *n*-type versus *p*-type doping symmetry and the defect physics of ZnO"; Phys. Rev. B; **63**, 75205, (2001).

[53] Fumiyasu Oba, Shigeto R. Nishitani, Seiji Isotani, and Hirohiko Adachi; "Energetics of native defects in ZnO"; J. Appl. Phys.; **90**, 824, (2001).

[54] Eun-Cheol Lee, Y.-S. Kim, Y.-G. Jin, and K. J. Chang; "Compensation mechanism for N acceptors in ZnO"; Phys. Rev. B; **64,** 85120, (2001).

[55] J. M. Smith and W. E. Vehse; "ESR of electron irradiated ZnO, Confirmation of the F^+ centre"; Phys. Lett.; **31A**, 147, (1970).

[56] V. Soriano and D. Galland; "Photosensitivity of the EPR spectrum of the F^+ center in ZnO"; phys. stat. sol. (b); **77**, 739 (1976).

[57] L.S. Vlasenko and G. W. Watkins; "Optical detection of electron paramagnetic resonance in room-temperature electron-irradiated ZnO"; Phys. Rev. B; **71**, 125210, (2005).

[58] Ü. Özgür, Ya. I. Alivov, C. Liu, A. Teke, M. Reshchikov, S. Doğan, V. Avrutin, S. –J. Cho, and H. Morkoç; "A comprehensive review of ZnO and related devices"; J. Appl. Phys. R; **98**, 041301, (2005).

[59] H. Morkoç and Ü. Özgür , "Zinc Oxide: Fundamentals, and Materials and Device Technology ", Wiley-VCH, Berlin, in press.

[60] C. G. Van de Walle; "Hydrogen as a Cause of Doping in Zinc Oxide"; Phys. Rev. Lett.; **85**, 1012 (2000).

[61] A. Janotti and C. G. Van de Walle; "Hydrogen multicentre bonds"; Nature Mat.; **6**, 44 (2007).

[62] O. Schmidt, P. Kiesel, C. G. Van De Walle, Chris, N. M. Johnson, J. Nause, and G. H. Dohler; "Effects of an electrically conducting layer at the zinc oxide surface"; Jp. J. Appl. Phys.; **44**, 7271 (2005).

[63] D. C. Look, H. L. Mosbacker, Y. M. Strzhemechny, and L. J. Brillson; "Effects of surface conduction on Hall-effect measurements in ZnO"; Superl. Microstr.; **38**, 406 (2005).

[64] M. A. Reshchikov and H. Morkoç; "Luminescence properties of defects in GaN"; J. Appl. Phys.; **97**, 061301, (2005).

[65] K. Vanheusden, C. H. Seager, W. L. Warren, D. R. Tallant, and J. A. Voigt; "Correlation between photoluminescence and oxygen vacancies in ZnO phosphors"; Appl. Phys. Lett. 68, 403, (1996); ibid; "Mechanisms behind green photoluminescence in ZnO phosphor powders"; J. Appl. Phys.; **79**, 7983, (1996).

[66] M. A. Reshchikov, H. Morkoç, B. Nemeth, J. Nause, J. Xie, B. Hertog, and A. Osinsky; "Luminescence properties of defects in ZnO"; Physica B; **401-402**, 358, (2007).

[67] R. Dingle; "Luminescent Transitions Associated With Divalent Copper Impurities and the Green Emission from Semiconducting Zinc Oxide"; Phys. Rev. Lett.; **23**, 579, (1969).

[68] M. A. Reshchikov, H. Morkoç, S. S. Park, and K. Y. Lee; "Two charge states of dominant acceptor in unintentionally doped GaN: Evidence from photoluminescence study"; Appl. Phys. Lett.; **81**, 4970, (2002).

[69] M. A. Reshchikov, R. H. Patillo, and K. C. Travis, ; "Photoluminescence in wurtzite GaN containing carbon", Mat. Res. Soc. Symp. Proc. **892**, FF23.12 (2006).

[70] M. Zafar Iqbal, M. A. Reshchikov, L. He, and H. Morkoç, "Effect of ambient on photoluminescence from GaN grown by molecular-beam epitaxy", J. of Electronic Materials, Vol. **32**, p. 346-349, (2003),

[71] M. A. Reshchikov, M. Zafar Iqbal, D. Huang, L. He, and H. Morkoç, "Surface-Related Photoluminescence Effects in GaN", Proceedings of MRS Fall 2002 Meeting, November 2002 Boston USA. AFOSR, ONR. NSF. *Materials Research Society Symposium - Proceedings*, v **743**, p 635-640, (2002).

[72] S. Sabuktagin, M. A. Reshchikov, D.K.Johnstone and H. Morkoç, "Band bending near the surface in GaN as detected by a charge sensitive probe" presented at the 2003 Fall MRS meeting, Boston MA Nov. – Dec 2003, Mat. Res. Soc. Symp. Proc. **798**, Y5.39 (2004); *Mater. Res. Soc. Symposium Proceedings Vol.798). Mater. Res. Soc. 2004, pp.793-798. Warrendale, PA, USA.*

[73] M. A. Reshchikov, S. Sabuktagin, D. K. Johnstone, and H. Morkoç; "Transient photovoltage in GaN as measured by atomic force microscope tip"; J. Appl. Phys.; **96**, 2556, (2004).

[74] S. Chevtchenko, X. Ni, Q. Fan, A.A. Baski, and H. Morkoç, "Surface band bending of *a*-plane GaN studied by surface potential electric force microscopy", Appl. Phys. Lett. **88**, 122104, (2006)

[75] D. Zwingel; "Trapping and recombination processes in the thermoluminescence of Li-doped ZnO single crystals"; J. Luminescence; **5**, 385 (1972).

[76] J. K. Furdyna; "Diluted magnetic semiconductors"; J. Appl. Phys.; **64,** R29, (1988).

[77] T. Dietl, H. Ohno, F . Matsukura, J . Cibert, and D. Ferrand; "Zener Model Description of Ferromagnetism in Zinc-Blende Magnetic Semiconductors"; Science; **287,** 1019, (2000).

[78] K. Sato and H. Katayama-Yoshida; "Stabilization of ferromagnetic states by electron doping in Fe-, Co- or Ni-doped ZnO"; Jpn. J. Appl. Phys.; **40,** L334, (2001).

[79] G.P. Das, B. K. Rao, and P . Jena; "Ferromagnetism in Cr-doped GaN: A first-principles calculation"; Phys. Rev. B; **69,** 214422, (2004).

[80] C. Liu, F. Yun, and H. Morkoc; "Ferromagnetism of ZnO and GaN: A Review"; J. Mat. Sci.; **16,** 555, (2005).

[81] G. Prinz; "Magnetoelectronics"; Science; **282,** 1660, (1998).

[82] T. Story, R. R. Galazka, R. B. Frankel, and P . A. Wolff; "Carrier-concentration–induced ferromagnetism in PbSnMnTe"; Phys. Rev. Lett.; **56,** 777, (1986).

[83] C. Zener; "Interaction Between the d Shells in the Transition Metals"; Phys. Rev.; **81,** 440, (1951).

[84] K. Sato and H. Katayama-Yoshida; "Material Design for Transparent Ferromagnets with ZnO-Based Magnetic Semiconductors"; Jpn J. Appl. Phys.; **39,** L555, (2000).

[85] H. Akai and P .H. Dederichs; "Local moment disorder in ferromagnetic alloys"; Phys. Rev. B **47,** 8739, (1993). & H. Akai; "Ferromagnetism and Its Stability in the Diluted Magnetic Semiconductor (In, Mn)As"; Phys. Rev. Lett.; **81,** 3002, (1998).

[86] C. Zener; "Interaction between the d-Shells in the Transition Metals. II. Ferromagnetic Compounds of Manganese with Perovskite Structure"; Phys. Rev.; **82,** 403, (1951).

[87] M. Toyoda, H. Akai, K. Sato, and H. Katayama-Yoshida; "Electronic structures of (Zn,TM)O (TM: V, Cr, Mn, Fe, Co, and Ni) in the self-interaction-corrected calculations"; Physica B; **376–377**, 647, (2006).

[88] K. Sato and H. Katayama-Yoshida; "Electronic structure and ferromagnetism of transition-metal-impurity-doped zinc oxide"; Physica B; **308,** 904 (2001).

[89] M. Bercui and R. N. Bhatt; "Effects of Disorder on Ferromagnetism in Diluted Magnetic Semiconductors"; Phys. Rev. Lett.; **87,** 107203, (2001).

[90] A. Kaminski and S . Das Sarma; "Coordination-Number Dependence of Magnetic Hyperfine Fields at Cd on Ni Surfaces"; Phys. Rev. Lett. **88,** 247201 (2001).

[91] T. Dietl, F . Matsukura and H. Ohno; "Temperature-dependent magnetization in diluted magnetic semiconductors"; Phys. Rev. B; **66,** 033203, (2002).

[92] S. Das Sarma, E. H. Hwang, and A. Kaminski; "Temperature-dependent magnetization in diluted magnetic semiconductors"; Phys. Rev. B; **67,** 155201, (2003).

[93] J. Warnock and P . A. Wolff; "Spherical model of acceptor-associated bound magnetic polarons"; Phys. Rev. B; **31,** 6579, (1985).

[94] M. Sawicki, T. Dietl, J. Kossut, J . Igalson, T. Wojtowicz, and W. Plesiewicz; "Influence of s-d exchange interaction on the conductivity of Cd1-xMnxSe:In in the weakly localized regime"; Phys. Rev. Lett.; **56,** 508, (1986).

[95] J . M. D. Coey, M. Venkatesan, and C. B. Fitzgerald, Nat. Mater; "Donor impurity band exchange in dilute ferromagnetic oxides"; **4,** 173, (2005).

[96] T. Dietl and J . Spalek; "Effect of Fluctuations of Magnetization on the Bound Magnetic Polaron: Comparison with Experiment"; Phys. Rev. Lett.; **48,** 355, (1982).

[97] N. Theodoropoulou, A.F . Hebard, M.E.Overberg, C.R. Abernathy, S. J. Pearton, S .N.G. Chu, and R.G. WIilson; "Magnetic and structural properties of Mn-implanted GaN"; Appl. Phys. Lett.; **78,** 3475, (2001).

[98] G. T. Thaler, M. E. Overberg, B. Gil, R. Frazier, C. R. Abernathy, S . J . Pearton, J . S . Lee, S . Y. Lee, Y. D. Park, Z. G. Khim, J . Kim and F . Ren; "Magnetic properties of n-GaMnN thin films"; Appl. Phys. Lett.; **80,** 3964, (2002).

[99] M.E. Overberg, C.R. Abernathy, S .J . Pearton, N. A. Theodoropoulou, K.T. Mccarthy, and A. F . Herard; "Indication of ferromagnetism in molecular-beam-epitaxy-derived N-type GaMnN"; Appl. Phys. Lett.; **79,** 1312, (2001).

[100] K.H. Kim, K. J. Lee, D. J. Kim, H. J. Kim, Y. E. Ihm, D. Djayaprawira, M. Takashi, C.S . Kim, C.G. Kim, and S . H. Yoo; "Magnetotransport of p-type GaMnN assisted by highly conductive precipitates"; Appl. Phys. Lett.; **82,** 1775, (2003).

[101] M.C. Park, K.S . Kuh, J .M. Myong, J .M. Lee, J .Y. Chang, K.I . Lee, S .H. Han, and W.Y. Lee; "Room temperature ferromagnetic (Ga,Mn)N epitaxial films with low Mn

concentration grown by plasma-enhanced molecular beam epitaxy"; Solid State Commun.; **124,** 11, (2002).

[102] J .Y. Chang, G.H. Kim, J .M. Lee, S .H. Han, W.Y. Lee, M.H. Han, K. S . Huh, and J .M. Myong; "Transmission electron microscopy study on ferromagnetic (Ga,Mn)N epitaxial films"; J. Appl. Phys.; **93,** 7858, (2003).

[103] S. Sonoda, S . Shimizu, T. Sasaki, Y. Yamamoto, and H. Hori; "Molecular beam epitaxy of wurtzite (Ga,Mn)N films on sapphire(0 0 0 1) showing the ferromagnetic behaviour at room temperature"; J. Cryst. Growth; **237,** 1358, (2002).

[104] D.S. Han, J . Park, K.W. Rhie, S . Kim, and J . Chang; "Ferromagnetic Mn-doped GaN nanowires"; Appl. Phys. Lett.; **86,** 032506, (2005).

[105] M.L. Reed, N.A. El-Masry, H.H. Stadelmaier, M.E. Ritums, M.J . Reed, C.A. Parker, J .C. Roberts, and S . M. Bedair; "Room temperature ferromagnetic properties of (Ga, Mn)N"; Appl. Phys. Lett.; **79,** 3473, (2001).

[106] M. Zajac, J . Gosk, E. Grzanka, M. Kamin'ska, A. Twardowski, B. Strojek, T. Szyszko, and S . Podsiadlo; "Possible origin of ferromagnetism in (Ga,Mn)N"; J. Appl. Phys. **93,** 4715, (2003).

[107] M.B. Haider, C.L. Constantin, H. Albrithen, H. Yang, E. Trifan, D. Ingram, A. R. Smith, C. V. Kelly, and Y. I jiri; "Ga/N flux ratio influence on Mn incorporation, surface morphology, and lattice polarity during radio frequency molecular beam epitaxy of (Ga,Mn)N"; J. Appl. Phys. **93,** 5274, (2003).

[108] R. Frazier, G. Thaler, M. Overberg, B. Gila, C. R. Albernathy, and S . J . Pearton; "Indication of hysteresis in AlMnN"; Appl. Phys. Lett.; **83,** 1758, (2003).

[109] H.X. Liu, S .Y. Wu, R.K. Singh, L. Gu, D.J . Smith, N. Newman, M.R. Dilley, L. Montes, and M. B. Simmonds; "Observation of ferromagnetism above 900 K in Cr–GaN and Cr–AlN"; Appl. Phys. Lett.; **85,** 4076, (2004).

[110] S .E. Park, H.- J . Lee, Y. C. Cho, S .-Y. Jeong, C. R. Cho, and S. Cho; "Room-temperature ferromagnetism in Cr-doped GaN single crystals"; Appl. Phys. Lett.; **80,** 4187, (2002).

[111] M. Hashimoto, Y.-K. Zhou, M. Kanakura, and H. Asahi; "High temperature (>400 K) ferromagnetism in III–V-based diluted magnetic semiconductor GaCrN grown by ECR molecular-beam epitaxy"; *Solid State Commun*.; **122,** 37 (2002).

[112] S. Y. Wu, H. X. Liu, L. Gu, R.K. Singh, L. Budd, M.M. Van Schilfgaarde, M. R. Mccartney, D. J . Smith, and N. Newman; "Synthesis, characterization, and modeling of high quality ferromagnetic Cr-doped AlN thin films"; Appl. Phys. Lett.; **82,** 3047, (2003).

[113] S .Y. Wu, H. X. Liu, L. Gu, R. K. Singh, M. Van Schilfgaarde, D.J . Smith, M. Dilley, L. Montes, M. B. Simmonds, and N. Newman, "Synthesis and characterization of high quality ferromagnetic Cr-doped GaN and AlN thin films with Curie temperatures above 900K ",*GaN and Related Alloys - 2003 Symposium (Mater. Res. Soc. Symposium Proceedings Vol.798)*, p 551-5 (2004).

[114] J .S. Lee, J. D. Lim, Z. G. Khim, Y.D. Park, S .J . Pearton and S .N.G. Chu; "Magnetic and structural properties of Co, Cr, V ion-implanted GaN"; J. Appl. Phys.; **93,** 4512, (2003).

[115] Y. Shon, Y. H. Kwon, Y. S. Park, SH. U. Yuldashev, S .J . Lee, C. S. Park, K. J. Chung, S. J. Yoon, H. J . Kim, W. C. Lee, D. J . Fu, T. W. Kang, X. J . Fan, Y. J. Park and H. T. Oh; "Ferromagnetic behavior of p-type GaN epilayer implanted with Fe+ ions"; J. Appl. Phys.; **95,** 761, (2004).

[116] Nobuaki Teraguchi, Akira Suzuki, Yasushi Nanishi, Yi-Kai Zhou, Masahiko Hashimoto, and Hajime Asahi; "Room-temperature observation of ferromagnetism in diluted magnetic semiconductor GaGdN grown by RF-molecular beam epitaxy";Solid State Communications; **122**, 651, (2002).

[117] S. Dhar, O.Brandt. M. Ramsteiner, V. E. Sapega and K. H. Ploog; "Colossal Magnetic Moment of Gd in GaN"; Phys. Rev. Lett.; **94**, 037205, (2005).

[118] K. Sato and H. Katayama-Yoshida; "Material Design of GaN-Based Ferromagnetic Diluted Magnetic Semiconductors"; Jpn. J. Appl.Phys.; **40,** L485, (2001).

[119] V. Avrutin, Ü. Özgür, J. Xie, Y. Fu, F. Yun, H. Morkoç, and V.I. Litvinov," "Gd-implanted GaN as a candidate for spin injector", SPIE", *Proceedings of SPIE - The International Society for Optical Engineering*, v 6121, *Gallium Nitride Materials and Devices*, 2006, p 61210U.

[120] G. M. Dalpian and S.H. Wei; "Electron-induced stabilization of ferromagnetism in Ga1–xGdxN"; Phys. Rev. B; **72**,115201, (2005).

[121] G. M. Dalpian, S.-H. Wei, X. G. Gong, A. J. R. da Silva, and A. Fazzio; "Phenomenological band structure model of magnetic coupling in semiconductors"; Solid State Commun.; **138**, 353, (2006).

[122] T. Dietl, H. Ohno, F. Matsukura, J. Cibert, and D. Ferrand; "Zener Model Description of Ferromagnetism in Zinc-Blende Magnetic Semiconductors"; Science; **287**, 1019 (2000).

[123] K. Sato, H. Katayama-Yoshida; "Material Design for Transparent Ferromagnets with ZnO-Based Magnetic Semiconductors"; Jpn. J. Phys., Part 2; **39**, L555, (2000).

[124] G. Lawes, A. S. Risbud, A. P. Ramirez, and R. Seshadri; "Absence of ferromagnetism in Co and Mn substituted polycrystalline ZnO"; Phys. Rev. B; **71**, 045201, (2005);

C. N. R. Rao and F. L. Deepak; "Absence of ferromagnetism in Mn- and Co-doped ZnO"; J. Mater. Chem.; **15**, 573, (2005).

[125] Y. D. Park, A.T. Hanbicki, S.C. Erwin, C.S. Hellberg, J.M. Sullivan, J.E. Mattson, T.F. Ambrose, A. Wilson, G. Spanos, and B.T. Jonker; "A Group-IV Ferromagnetic Semiconductor: Mn_xGe_{1-x}"; Science; **295**, 651, (2002).

[126] K. Ando, "Magneto-optical studies of s,p-d exchange interactions in GaN : Mn with room-temperature ferromagnetism", Appl. Phys. Lett. **82**, 100 (2003).

[127] D. P. Norton, M. E. Overberg, S. J. Pearton, K. Pruessner, J. D. Budai, L. A. Boatner, M. F. Chisholm, J. S. Lee, Z. G. Khim, Y. D. Park, and R. G. Wilson; "Magneto-optical studies of s, p-d exchange interactions in GaN:Mn with room-temperature ferromagnetism"; Appl. Phys. Lett.; **83**, 5488, (2003).

[128] T. Fukumura, Z. W. Jin, M. Kawasaki, T. Shono, T. Hasegawa, S. Koshihara, and H. Koinuma; "Magnetic properties of Mn-doped ZnO"; Appl. Phys. Lett.; **78**, 958, (2001).

[129] A. S. Risbud, N. A. Spaldin, Z. Q. Chen, S. Stemmer, and R. Seshadri; "Magnetism in polycrystalline cobalt-substituted zinc oxide"; Phys. Rev. B; 68, 205202, (2003).

[130] K. Ueda, H. Tabata, and T. Kawai, "Magnetic and electric properties of transition-metal-doped ZnO films"; "Magnetic and electric properties of transition-metal-doped ZnO films"; Appl. Phys. Lett.; **79**, 988, (2001).

[131] H.-J. Lee, S.-Y. Jeong, C. R. Cho, and C. H. Park; "Study of diluted magnetic semiconductor: Co-doped ZnO"; Appl. Phys. Lett.; **81**, 4020, (2002).

[132] W. Prellier, A. Fouchet, B. Mercey, Ch. Simon, and B. Raveau; "Laser ablation of Co:ZnO films deposited from Zn and Co metal targets on (0001) Al_2O_3 substrates"; Appl. Phys. Lett.; **82**, 3490, (2003).

[133] H. Saeki, H. N. Tabata, and T. Kawai; "Magnetic and electric properties of vanadium doped ZnO films"; Solid State Commun.; **120**, 439, (2001).

[134] V. Avrutin, Ü. Özgür, S. Chevtchenko, C. Litton, and H. Morkoç, "Optical and magnetic properties of ZnO:V prepared by ion implantation", J. Electron. Mat. **36** 483 (2007).

[135] P. Sharma, A. Gupta, K.V. Rao, F.J. Owens, R. Sharma, R. Ahuja, J.M.O. Guillen, B. Johansson, and G.A. Gehring; "Ferromagnetism above room temperature in bulk and transparent thin films of Mn-doped ZnO"; Nat. Mater.; **2**, 673, (2003).

[136] A. Che Mofor, A. El-Shaer, A. Bakin, A. Waag, H. Ahlers, U. Siegner, S. Sievers, M. Albrecht, W. Schoch, N. Izyumskaya, V. Avrutin, S. Sorokin, S. Ivanov, and J. Stoimenos; "Magnetic property investigations on Mn-doped ZnO Layers on sapphire"; Appl. Phys. Lett.; **87**, 062501, (2005).

[137] J. H. Park, M. G. Kim, H. M. Jang, and S. Ryu; “Co-metal clustering as the origin of ferromagnetism in Co-doped ZnO thin films”; Appl. Phys. Lett.; **84**, 1338, (2004).

[138] D. Chakraborti, J. Narayan, and J. Prater; “Room temperature ferromagnetism in $Zn_{1-x}Cu_xO$ thin films”; Appl. Phys. Lett. **90**, 062504, (2007).

[139] T. Dietl; “Origin and control of ferromagnetism in dilute magnetic semiconductors and oxides (invited)”; J. Appl. Phys.; **103**, 07D111, (2008).

[140] T. Dietl, Nat. Mat; “From our readers: Self-organized growth controlled by charge states of magnetic impurities”; **5,** 673, (2006).

[141] K. Sato, H. Katayama-Yoshida, P. Dederichs; "High Curie Temperature and Nano-Scale Spinodal Decomposition Phase in Dilute Magnetic Semiconductors"; Jap. J. Appl. Phys. Pt. 2; **44,** L948, (2005).

[142] S. Kuroda, N. Nishizawa, K.Takita, M. Mitomo, Y. Bando, K. Osuch, and T. Dietl; “Origin and control of high-temperature ferromagnetism in semiconductors”; Nat. Mat. **6,** 440 (2007).

[143] H. Saito, V. Zayets, S. Yamagata, and K. Ando; “Magneto-optical studies of ferromagnetism in the II-VI diluted magnetic semiconductor $Zn_{1-x}Cr_xTe$”; Phys. Rev. B **66**, 081201(R), (2002).

[144] H. Saito, V. Zayets, S. Yamagata, and K. Ando; “Magneto-optical studies of ferromagnetism in the II-VI diluted magnetic semiconductor $Zn_{1-x}Cr_xTe$”; Phys. Rev. Lett. **90**, 207202-1, (2003).

[145] G. Martinez-Criado, A. Somogyi, S. Ramos, J. Campo, R. Tucoulou, M. Salome, J. Susini, M. Hermann, M. Eickhoff, and M. Stutzmann; "Room-Temperature Ferromagnetism in a II-VI Diluted Magnetic Semiconductor $Zn_{1-x}Cr_xTe$"; Appl. Phys. Lett.; **86,** 131927, (2005)**.**

[146] A. Bonanni, M. Kiecana, C. Simbrunner, T. Li,, M. Sawicki, M. Wegscheider, M. Quast, H. Przybylinska, A. Navarro-Quezada, R. Jakiela, A. Wolos, W. Jantsch, and T. Dietl; "Paramagnetic GaN:Fe and ferromagnetic (Ga,Fe)N: The relationship between structural, electronic, and magnetic properties"; Phys. Rev. B; **75**, 125210, (2007).

[147] G. Springholz, V. Holy, M. Pinczolits, and G. Bauer; “Self-Organized Growth of Three- Dimensional Quantum-Dot Crystals with fcc-Like Stacking and a Tunable Lattice Constant”; Science; **282**, 734, (1998).

[148] L.-H. Ye, A.J. Freeman, and B. Delley; “Half-metallic ferromagnetism in Cu-doped ZnO: Density functional calculations”; Phys. Rev. B; **73**, 033203, (2006).

[149] F. Reuss, S. Frank , C. Kirchner, R. Kling, T. Gruber, and A. Waag; "Magnetoresistance in epitaxially grown degenerate ZnO thin films"; Appl. Phys. Lett.; **87,** 112104, (2005).

[150] M. Johnson, B.R. Bennett, M.J. Yang , M.M. Miller, and B.V. Shanabrook; "Hybrid Hall effect device"; Appl.Phys.Lett.; **71**, 974, (1997).

[151] K. Ando, H. Saito, V. Zayets, and M. C. Debnath, "Optical properties and functions of dilute magnetic semiconductors", J. Phys.: Condens. Matter. **16**, S5541 (2004).

[152] K. Ando, H. Saito, Z.W. Jin, T. Fukumura, M. Kawasaki, Y. Matsumoto, and H. Koinuma; "Magneto-optical properties of ZnO-based diluted magnetic semiconductors"; J. Appl. Phys.; **89,** 7284, (2001).

[153] K. Ando, H. Saito, Z. Jin, T. Fukumura, M. Kawasaki, Y. Matsumoto, and H. Koinuma; "Large magneto-optical effect in an oxide diluted magnetic semiconductor $Zn_{1-x}Co_xO$"; Appl. Phys.Lett.; **78,** 2700, (2001).

[154] K. Ando, T. Hayashimi, M. Tanaka, and A. Twardowski; "Magneto-optic effect of the ferromagnetic diluted magnetic semiconductor $Ga_{1-x}Mn_xAs$"; J. Appl. Phys.; **83,** 6548, (1998).

[155] K. Ando, "Magneto-optics (Springer Series in Solid-State Science)",edited by S. Sugano and N.Kojima (Springer, Berlin, 2000) vol. **128**, p. 211.

[156] K. Ando and H. Munekata, "Magneto-optical study of spin-carrier interactions in (In,Mn)As**",** J. Magn. Magn. Mater. **272–276**, 2004 **(**2004).

[157] K. Ando, "Magneto-optical studies of s, p–d exchange interactions in GaN:Mn with room-temperature ferromagnetism"; Appl. Phys. Lett, **82,** 100 (2003).

[158] W. Pacuski, D. Ferrand, J. Cibert, C. Deparis, J. A. Gaj, P. Kossacki, and C. Morhain; "Effect of the *s ,p-d* exchange interaction on the excitons in $Zn_{1-x}Co_xO$ epilayers"; Phys. Rev. B; **73**, 035214, (2006).

[159] W. Pacuski, D. Ferrand, J. Cibert, J. A. Gaj, A. Golnik, P. Kossacki, S. Marcet, H. Mariette, and E. Sarigiannidou; "Excitonic giant Zeeman effect in GaN:Mn^{3+}"; Phys. Rev. B; **76**, 165304, (2007).

[160] W. Pacuski, P. Kossacki, D. Ferrand, A. Golnik, J. Cibert, M. Wegscheider, A. Navarro-Quezada, A. Bonanni, M. Kiecana, M. Sawicki, and T. Dietl; "Observation of Strong-Coupling Effects in a Diluted Magnetic Semiconductor $Ga_{1-x}Fe_xN$"; Phys. Rev. Lett.; **100,** 037204, (2008).

[161] S. Datta and B. Das; "Electronic analog of the electro-optic modulator"; Appl. Phys. Lett.; **56,** 665, (1990).

[162] W. M. Chen, I. A. Buyanova, K. Nishibayashi, K. Kayanuma, K. Seo, A. Murayama, Y. Oka, G. Thaler, R. Frazier, C. R. Abernathy, F. Ren, S. J. Pearton, C.-C. Pan, G.-T. Chen, and J.-I. Chyi; "Efficient spin relaxation in InGaN/GaN and InGaN/GaMnN quantum wells: An obstacle to spin detection", Appl. Phys. Lett.; **87**, 192107, (2005).

[163] I. A. Buyanova, M. Izadifard, W. M. Chen, J. Kim, F. Ren, G. Thaler, C. R. Abernathy, S. J. Pearton, C.-C. Pan, G.-T. Chen, J.-I. Chyi, and J. M. Zavada; "On the origin of spin loss in GaMnN/InGaN light-emitting diodes"; Appl. Phys. Lett.; **84**, 2599, (2004).

[164] R. Stępniewski, M. Potemski, A. Wysmołek, K. Pakuła, J. M. Baranowski, J. Łusakowski, I. Grzegory, S. Porowski, G. Martinez, P. Wyder; "Symmetry of excitons in GaN"; Phys. Rev. B; **60**, 4438, (1999).

[165] A. Tackeuchi, T. Kuroda, A. Shikanai, T. Sota, A. Kuramata, and K. Domen; "No spin polarization of carriers in InGaN"; Physica E; **7**, 1011, (2000).

[166] J. Campo, M. Julier, D. Coquillat, J. P. Lascaray, D. Scalbert, and O. Briot; "Zeeman splittings of excitonic transitions at the Γ point in wurtzite GaN: A magnetoreflectance investigation"; Phys. Rev. B; **56**, R7108, (1997).

[167] C. K. Choi, J. B. Lam, G. H. Gainer, S. K. Shee, J. S. Krasinski, and J. J. Song, Yia-Chung Chang; "Polarization dependence of the excitonic optical Stark effect in GaN"; Phys. Rev. B; **65**, 155206, (2002).

[168] J. Akerman *et al*.; Chapter 5 in "Magnetoelectronics," ed. M. Johnson; (Elsevier Ltd. Oxford, 2004).

[169] S.S.P. Parkin, C. Kaiser, A. Panchula, P.M. Rice, B. Hughes, M. Samant, and Yang, Nat. Mat.; "Giant tunnelling magnetoresistance at room temperature with MgO (100) tunnel barriers"; **3**, 862, (2004).

[170] S. Yuasa, T. Nagahama, A. Fukushima, Y. Suzuki, and K. Ando; "Giant room-temperature magnetoresistance in single-crystal Fe/MgO/Fe magnetic tunnel junctions"; Nat. Mater.; **3**, 868, (2004).

[171] Weifeng Shen, Dipanjan Mazumdar, and Xiaojing Zou, Xiaoyong Liu, B. D. Schrag, and Gang Xiao; "Effect of film roughness in MgO-based magnetic tunnel junctions"; Appl. Phys. Lett.; **88**, 182508, (2006).

[172] H. Morkoç; "*Handbook of Nitride Semiconductors and Devices*"; Wiley-VCH, 2008, in press.

[173] Nitronex; "Reliability Summary"; Challenges facing ZnO and GaN: Facts and Myths, Virginia Crossing Resort October 18-19, 2007.

[174] Qualification reports for this and other devices from Nitronex were accessed on January 3, 2008 at: http://www.nitronex.com/design_support.html

[175] A. Christou; "The Main Degradation Mechanisms of GaN-based Transistors: A Short Summary"; Challenges facing ZnO and GaN: Facts and Myths, Virginia Crossing Resort October 18-19, 2007.

[176] S.C. Binari, J. Mittereder, D. Via, and E. Viveiros; "Tri-Service Reliability Observations of DARPA WBGS-RF Deliverables"; Challenges facing ZnO and GaN: Facts and Myths, Virginia Crossing Resort October 18-19, 2007.

[177] T. J. Drummond, R. J. Fischer, W. F. Kopp, H. Morkoç, K. Lee, and M. S. Shur; "Bias dependence and light sensitivity of (Al,Ga)As/GaAs MODFETs at 77K"; IEEE Trans. Electron Devices; **30**, 1806, (1983).

[178] C.H. Lin, W.K. Wang, P.C. Lin, C.K. Lin, Y.J. Chang, and Y.J. Chan; "Transient pulsed analysis on GaNHEMTs at cryogenic temperatures"; IEEE Elec. Dev. Lett.; **26**, 710, (2005).

[179] H.F. Sun and C.R. Bolognesi; "Anomalous behavior of AlGaN/GaN heterostructure field-effect transistors at cryogenic temperatures: From current collapse to current enhancement with cooling"; Appl. Phys. Lett.; **90**, 123505, (2007).

[180] Hinoki *et al.*; "Correlation between the leakage current and the thickness of GaN-layer of AlGaN/GaN-HFET"; Phys. Stat. Sol. (c); **4**, 2728, (2007).

[181] Y. Nanishi; Challenges facing ZnO and GaN: Facts and Myths; Virginia Crossing Resort; October 18-19, 2007.

[182] J.Q. Xie, X.F. Ni, M. Wu, J.H. Leach, Ü. Özgür, and H. Morkoç, "High electron mobility in nearly lattice-matched AlInN/GaN heterostructure field effect transistors", Appl. Phys. Lett. **91**, 132116 (2007).

[183] Nitronex, Inc; "Reliability Physics"; Challenges facing ZnO and GaN: Facts and Myths, Virginia Crossing Resort October 18-19, 2007.

[184] R. Coffie, Y. C. Chen, I. Smorchkova, M. Wojtowicz, Y. C. Chou, B. Heying, and A. Oki; "Impact of AlN interlayer on reliability of AlGaN/GaN HFETs"; IEEE 06CH37728 44th Annual International Reliability Physics Symposium, San Jose, pp. 99, 2006

[185] S. Sabuktagin, S. Dogan, A. Baski, H. Morkoç, "Surface charging and current collapse in an AlGaN/GaN HFET", Appl. Phys. Lett. Appl. Phys. Lett. **86**, 083506 (2005).

[186] Shahriar Sabuktagin, Yong-Tae Moon, Seydi Dogan, A. A. Baski, and Hadis Morkoç," Observation of Surface charging at the edge of a Schottky contact", IEEE Electron. Dev. Lett., Vol. **EDL 27**, No. 4, pp. 211-213, (2005).

[187] R.J. Trew, Y. Liu, W.W. Kuang, and G.L. Bilbro, "The Physics of Reliability for High Voltage AlGaN/GaN HFETs", *Compound Semiconductor Integrated Circuits Symposium Digest*, San Antonio, TX, pp. 103-106, Nov. 2006.

[188] G. L. Bilbro, "Gate Leakage Mechanisms", presented at Challenges facing ZnO and GaN: Facts and Myths, Virginia Crossing Resort October 18-19, 2007.

[189] D. Mahaveer Sathaiya and Shreepad Karmalkar, "Edge Effects on Gate Tunneling Current in HEMTs", IEEE Trans. Electron Devices; **54**, 2614, (2007).

[190] Zhifang Fan, S. Noor Mohammad, Wook Kim, Özgür Aktas, Andrei E. Botchkarev, and Hadis Morkoç, "Very low Resistance Multi-layer Ohmic Contact to n-GaN", Appl. Phys. Lett.; **68**, 1672, (1996).

[191] J. Vatus, J. Chevrier, P. Delescluse, and J.-F Rochette, "Highly selective reactive ion etching applied to the fabrication of low-noise AlGaAs GaAs FET's", IEEE Trans on Electron Devices; **33**, 934, (1986).

[192] Wen-Kai Wang, Yu-Jen Li, Cheng-Kuo Lin, Yi-Jen Chan, Guan-Ting Chen, and Jen-Inn Chyi; **"**Low damage, Cl_2 based gate recess etching for 0.3-μm gate-length AlGaN/GaN MODFET fabrication"; IEEE Electron Dev. Lett.; **25**, 52, (2004).

[193] A. Matulionis, Seminar given at VCU, Wednesday, October 17, 2007.

[194] J. Liberis, M. Ramonas, O. Kiprijanovic, A. Matulionis, N. Goel, J. Simon, K. Wang, H. Xing, and D. Jena; "Hot phonons in Si-doped GaN"; Appl. Phys. Lett.; **89**, 202117, (2006).

[195] L. K. J. Vandamme; "Noise as a Diagnostic Tool for Quality and Reliability of Electronic Devices"; IEEE Trans. Electron Devices; **41**, 2176, (1994).

[196] J.-M. Peransin, P. Vignaud, D. Rigaud, and L. J. Vandamme; "l/f Noise in MODFET's at Low Drain Bias"; IEEE Trans. Electron Devices; **37**, 2250, (1990).

[197] A. Sozza, A. Curutchet, C. Dua, N. Malbert, N. Labat and A. Touboul; "AlGaN/GaN HEMT Reliability Assessment by means of Low Frequency Noise Measurements"; Microelectronics Reliability; **46**, 1725, (2006).

[198] N. Maeda, M. Hiroki, N. Watanabe, Y. Oda, H. Yokoyama, T. Yagi, T. Makimoto, T. Enoki, and T. Kobayashi; "Systematic Study of Insulator Deposition Effect (Si_3N_4, SiO_2, AlN, and Al_2O_3) on Electrical Properties in AlGaN/GaN Heterostructures"; Jpn. J. Appl. Phys.; **46**, 547, (2007).

[199] B.M. Green, K.K. Chu, E.M. Chumbes, J.A. Smart, J.R. Shealy, and L.F. Eastman; "The effect of surface passivation on the microwave characteristics of undoped AlGaN/GaN HEMT's"; IEEE Elec. Dev. Lett.; **21**, 268, (2001).

[200] A. Hierro, S. A. Ringel, M. Hansen, J. S. Speck, U. K. Mishra, and S. P. DenBaars; "Hydrogen passivation of deep levels in n-GaN"; Appl. Phys. Lett.; **77**, 1499, (2000).

[201] J. Kikawa, T. Yamada, T. Tsuchiya, S. Kamiya, K. Kosaka, A. Hinoki, T. Araki, A. Suzuki and Y. Nanishi; "An Analysis of the Increase in Sheet Resistance with the Lapse of Time of AlGaN/GaN HEMT Structure Wafer"; Phys. Stat. Sol. (c); **4**, 2678, (2007).

[202] S. Elhamri, A. Saxler, W. C. Mitchel et al.; "Study of deleterious aging effects in GaN/AlGaN heterostructures"; J. Appl. Phys.; **93**, 1079, (2003).

[203] S. C. Binari, P. B. Klein, and T. E. Kazior; "Trapping effects in GaN and SiC microwave FETs"; Proc. IEEE; **90**, 1048, (2002).

[204] S.C. Binari, K. Ikossi, J.A. Roussos, W. Kruppa, D. Park, H.B. Dietrich, D.D. Koleske, A.E. Wickenden, and R.L. Henry; "Trapping effects and microwave power performance in AlGan/GaN HEMTs"; IEEE Trans. Elec. Dev.; **48**, 465, (2001).

[205] A. Kastalsky and R. A. Kiehl; "On the low-temperature degradation of (AlGa)As/GaAs modulation-doped field-effect transistors"; IEEE Trans. Electron Devices; **33**, 414 (1986).

[206] J.A. Mittereder, S.C. Binari, P.B. Klein, J.A. Roussos, D.S. Katzer, D.F. Storm, D.D. Koleske, A.E. Wickenden, and R.L. Henry; "Current collapse induced in AlGaN/GaN high-electron-mobility transistors by bias stress"; Appl. Phys. Lett.; **83**, 1650, (2003).

[207] S.C. Binari, K. Ikossi-Anastasiou, W. Kruppa, H.B. Dietrich, G. Kelner, R.L. Henry, D.D. Koleske, and A.E. Wickenden; "Correlation of drain current pulsed response with microwave power output in AlGaN/GaN HEMTs"; Mat. Res. Soc. Symp. Proc.; **572**, 541, (1999).

[208] G. Meneghesso, G. Verzellesi, R. Pierobon, F. Rampazzo, A. Chini, U.K. Mishra, C. Canali, and E. Zanoni; "Surface-Related Drain Current Dispersion Effects in AlGaN–GaN HEMTs"; IEEE, Trans. Elec. Dev.; **51**, 1554, (2004).

[209] P. Handel; Challenges facing ZnO and GaN: Facts and Myths, Virginia Crossing Resort October 18-19, 2007.

[210] D.V. Lang; "Deep-level transient spectroscopy: A new method to characterize traps in semiconductors"; J. Appl. Phys.; **45**, 3023, (1974).

[211] P.B. Klein and S.C. Binari; "Photoionization spectroscopy of deep defects responsible for current collapse in nitride-based field effect transistors"; J. Phys: Condens. Mattter; **15**, R1641, (2003).

[212] P. B. Klein, J. A. Freitas, Jr., S. C. Binari, and A. E. Wickenden; "Observation of deep traps responsible for current collapse in GaN metal semiconductor field effect transistors"; Appl. Phys. Lett.; **75**, 4016, (1999).

[213] P. B. Klein, S. C. Binari, K. Ikossi, A. E.Wickenden, D. D. Koleske, and R. L. Henry; "Current collapse and the role of carbon in AlGaN/GaN high electron mobility transistors grown by metalorganic vapor-phase epitaxy"; Appl. Phys. Lett.; **79**, 3527, (2001).

[214] M. Ramonas, A. Matulionis, J. Liberis, L.F. Eastman, X. Chen, Y.-J. Sun; "Hot-phonon effect on power dissipation in a biased $Al_xGa_{1-x}N$/AlN/GaN channel"; Phys. Rev. B; **71**, 075324, (2005).

[215] C.-K. Sun, F. F. Vallée, S. Keller, J. E. Bowers, S. P. Den Baars, "Femtosecond studies of carrier dynamics in InGaN", Appl. Phys. Lett.70(15)**,** pp. 2004-2006 (1997).

[216] K. T. Tsen, D. K. Ferry, A. Botchkarev, B. Sverdlov *et al*.; "Time-resolved Raman studies of the decay of the longitudinal optical phonons in wurtzite GaN"; Appl. Phys. Lett.; **72**, 2132, (1998).

[217] RFMD Corporation; Challenges facing ZnO and GaN: Facts and Myths, Virginia Crossing Resort October 18-19, 2007.

[218] A. Christou; "*Reliability of GaAs Monolithic Integrated Circuits*"; John Wiley and Sons, October 1992, second edition 1995.

[219] Y. Inoue, S. Masuda, M. Kanamura, T. Ohki, K. Makiyama, N. Okamoto, K. Imanishi, T. Kikkawa, N. Hara, H. Shigematsu, and K. Joshin; "Degradation-Mode Analysis for Highly Reliable GaN-HEMT"; IEEE MTT-S International Microwave Symposium Digest, 639-642, (2007).

[220] S. Nakamura, M. Senoh, S. Nagahama, N. Iwasa, T. Yamana, T. Matsushita, Y. Sugimoto, H. Kiyoku; "Optical gain and carrier lifetime of InGaN multi-quantum well structure laser diodes"; Appl. Phys. Lett.; **69** (26), 1568, (1996).

[221] S. Tomiya, O. Goto, M. Ikeda; "Structural defects and degradation of high power pure-blueGaN-based laser diodes"; SPIE Photonic West- OPTO 07, GaN Material and Devices III, 19-24 January 2008 San Jose, CA. *Proceedings of SPIE - The International Society for Optical Engineering* V. **6894** , *Gallium Nitride Materials and Devices III, art no. 6894-22.*

[222] N. Sharma, P. Thomas, D. Tricker, and C. Humphreys, "Chemical mapping and formation of V-defects in InGaN multiple quantum wells"; Appl. Phys. Lett.; **77**, 1274, (2000).

[223] Y. Chen, T. Takeuchi, H. Amano, I. Akasaki, N. Yamada, Y. Kaneko, and S. Y. Wang; "Pit formation in GaInN quantum wells"; Appl. Phys. Lett.; **72**, 710, (1998).

[224] Mitsuo Fukuda; "Reliability and Degradation of Semiconductor Lasers and LEDs"; Artech House; 1991.

[225] Osamu Ueda; "Reliability and Degradation of III-V Optical Devices"; Artech House; 1996.

[226] M. Takeya, T. Mizuno, T. Sasaki, S. Ikeda, T. Fujimoto, Y. Ohfuji, K. Oikawa, Y. Yabuki, S. Uchida, M. Ikeda; "Degradation in AlGaInN lasers"; *Phys. Stat. Sol*. (c); **0** (7), 2292-2295, (2003).

[227] N. Kuroda, Ch. Sasaoka, A. Kimura, A. Usui, Y. Mochizuki; "Precise control of pn-junction proþles for GaN-based LD structures using GaN substrates with low dislocation densities"; *J. of Cryst. Growth*; **189/190,** 551-555, (1998).

[228] M. Ikeda, T.Mizuno, m. Takeya, S. Goto, S. Ikeda, T. Fujimoto, Y. Ohfuji; "High-power GaN-based semiconductor lasers"; *Phys. Stat. Sol*. (c); **1** (6), 1461-1467, (2004).

[229] Michael Kneissl, David P. Bour, Linda Romano, Chris. G. Van de Walle, John E. Northrup, William S. Wong, David W. Treat, Mark Teepe, Tanya Schmidt, Noble M. Johnson; "Performance and degradation of continuous-wave InGaN multiple-quantum-well laser diodes on epitaxially laterally overgrown GaN substrates"; *Appl. Phys. Lett.*; **77**, 1931, (2000).

[230] C. C. Kim, Y. Choi, Y. H. Jang, M. K. Kang, Minho Joo, and M. S. Noh.; "Degradation modes of highpower InGaN/GaN laser diodes on low-defect GaN substrates"; SPIE Photonic West- OPTO 07 GaN Material and Devices III; 19-24 January 2008 San Jose, CA. *Proceedings of SPIE - The International Society for Optical Engineering* V. *6894* , *Gallium Nitride Materials and Devices III, art no. 6894-23.*

[231] L. Marona, P. Wiśniewski, L. Leszczyński, I. Grzegory, T. Suski, S. Porowski, R. Czernecki, A. Czerwinski, M. Pluska, J. Ratajczak, and P. Perlin; "Why InGaN lasder-diode degradation is accompanied by the improvement of its thermal stability"; SPIE Photonic West- OPTO 08 GaN Material and Devices III, 19-24 January 2008 San Jose, CA. *Proceedings of SPIE - The International Society for Optical Engineering* V. **6894** , *Gallium Nitride Materials and Devices III, art no. 6894-26* .

[232] T. Schoedl, U.T. Schwartz, V. Kummler, M. Furitch, A. Leber, A. Miler, A. Lell, V. Harle; "Facet degradation of GaN heterostructure laser diodes"; *J.* Appl. Phys.; **97**, 123102, (2005).

[233] S. Uchida, M. Takeya, S. Ikeda, T. Mizuno, T. Fujimoto, O. Matsumoto, S. Goto, T. Tojyo, M. Ikeda; "Recent progress in high-power blue-violet lasers"; IEEE Journal of Selected Topics in Quantum Electronics; **9** (5), 1252-1259, (2003).

[234] T. Swietlik, G. Franssen, P. Winiewski, S. Krukowski, S. P. epkowski, L. Marona, M. Leszczyski, P. Prystawko, I. Grzegory, T. Suski, S. Porowski,, P. Perlin; "Anomalous temperature characteristics of single wide quantum well InGaN laser diode"; Appl. Phys. Lett.; **88**, 071121, (2006).

[235] H. Y. Ryu, K. H. Ha, S. N. Lee, T. Jang, H. K. Kim, J. H. Chae, K. S. Kim, K. K. Choi, J. K. Son, H. S. Paek, Y. J. Sung, T. Sakong, O. H. Nam, and Y. J. Park; "Highly stable temperature characteristics of InGaN blue laser diodes"; Appl. Phys. Lett.; **89**, 031122, (2006).

[236] H. Morkoç, "Handbook of *Nitride Semiconductors and Devices*" (Wiley, 2008).

[237] E. Feltin, G. Christmann, J. Dorsaz, A. Castiglia, J. –F. Carlin, R. Butté, N. Grandjean, S. Christopoulos, G. Baldassarri Höger von Högersthal, A. J. D. Grundy, P. G. Lagoudakis and J. J. Baumberg; "Blue lasing at room temperature in an optically pumped lattice-matched AlInN/GaN VCSEL structure"; Electron lett., **43**, 924, (2007).

[238] A. Castiglia, D. Simeonov, H. J. Buehlmann, J. –F. Carlin, E. Feltin, J. Dorsaz, R. Butté, N. Grandjean; "Efficient current injection scheme for nitride vertical cavity surface emitting lasers"; Appl. Phys. Lett.; **90**, 033514, (2007).

[239] For a review see, e.g, M. S. Skolnick, T. A. Fisher and D. M. Whittaker; "Strong coupling phenonena in quantum microcavity structures"; Semicond. Sci. Technol.; **13**, 645, (1998).

[240] R. Butté, G. Christmann, E. Feltin, J. –F. Carlin, M. Mosca, M. Ilegems and N. Grandjean; "Room-temperature polariton luminescence from a bulk microcavity"; Phys. Rev. B; **73**, 033315, (2006).

[241] A. Alyamani, D. Sanvitto, A. A. Khalifa, M. S. Skolnick, T. Wang, F. Ranalli, P. J. Parbrook, A. Tahraoui and R. Airey; "GaN hybrid microcavities in the strong coupling regime grown by metal-organic chemical vapor deposition on sapphire substrates"; J. Appl. Phys.; **101**, 093110, (2007).

[242] E. Feltin, G. Christmann, R. Butté, J. –F Carlin, M. Mosca and N. Grandjean; "Room temperature polariton luminescence from a GaN/AlGaN quantum well microcavity"; Appl. Phys. Lett.; **89**, 071107, (2006).

[243] S. Christopoulos, G. Baldassarri Höger von Högersthal, A. J. D. Grundy, P. G. Lagoudakis, A. V. Kavokin, J. J. Baumberg, G. Christmann, R. Butté, E. Feltin, J. –F. Carlin and N. Grandjean, "Room-temperature polariton lasing in semiconductor microcavities"; Phys. Rev. Lett.; **98**, 126405, (2007).

[244] M. Zamfirescu, A. Kavokin, B. Gil, G. Malpuech and M. Kaliteevski; "ZnO as a material mostly adapted for the realization of room-temperature polariton lasers"; Phys. Rev. B; **65**, 161205, (2002).

[245] S.F. Chichibu, A. Uedono, A. Tsukazaki, T. Onuma, M. Zamfirescu, A. Ohtomo, A. Kavokin, G. Cantwell, C. W. Litton, T. Sota and M. Kawasaki; "Exciton-polariton spectra and limiting factors for the room-temperature photoluminescence efficiency in ZnO"; Semicond. Sci. Technol.; **20**, S67, (2005).

[246] S. F. Chichibu, T. Ohmori, N. Shibat and T. Koyama; "Dielectric SiO_2/ZrO_2 distributed Bragg reflectors for ZnO microcavities prepared by the reactive helicon-wave-excited-plasma sputtering method"; Appl. Phys. Lett.; **88**, 161914, (2006).

[247] R. Schmidt-Grund, B. Rheinländer, C. Czekalla, G. Benndorf, H. Hochmut, A. Rahm, M. Lorenz, and M. Grundmann; "ZnO based planar and micropillar resonators"; Superlattices and microstructures; **41**, 360, (2007).

[248] R. Shimada, J. Xie, V. Avrutin, Ü. Özgür, and H. Morkoç; "Cavity polaritons in ZnO-based hybrid microcavities"; Appl. Phys. Lett.; **92**, 011127, (2008).

[249] A. Tsukazaki, A. Ohtomo, T. Onuma, M. Ohtani, T. Makino, M. Sumiya, K. Ohtani, S. F. Chichibu, S. Fuke, Y. Segawa, H. Ohno, H. Koinuma and M. Kawasaki; "Repeated temperature modulation epitaxy for p-type doping and light-emitting diode based on ZnO"; Nature Materials; **4**, 42, (2005).

[250] Y. R. Ryu, J. A. Lubguban, T. S. Lee, H. W. White, T. S. Jeong, C. J. Youn and B. J. Kim; "Excitonic ultraviolet lasing in ZnO-based light emitting devices"; Appy. Phys. lett.; **90**, 131115, (2007).

[251] X. Wu, A. Yamilov, X. Liu, S. Li, V. P. Dravid, R. P. H. Chang and H. Cao; "Ultraviolet photonic crystal laser"; Appl. Phys. lett.; **85**, 3657, (2004).

[252] M. Scharrer, A. Yamilov, X. Wu, H. Cao, and R. P. H. Chang; "Ultraviolet lasing in high-order bands of three dimentional; ZnO photonic crystals"; Appl. Phys. Lett.; **88**, 201103, (2006).

[253] H. Cao, Y. G. Zhao, S. T. Ho, E. W. Seeling, Q. H. Wang and R. P. H. Chang; "Random laser action in semiconductor powder"; Phys. Rev. Lett.; 82, 2278, (1999).

[254] D. Hofstetter, Y. Bonetti, F. R. Giorgetta, A. –H El-Chaer, A. Bakin, A. Wagg, R. Schmidt-Grund, M Schubert and M. Grundmann; "Demonstration of an ultraviolet ZnO-based optically pumped third order distributed feedback laser"; Appl. Phys. Lett.; **91**, 111108, (2007).

[255] G. Harbers and S. Bierhuizen; "Performance of High Power Light Emitting Diodes in Projection Applications"; SID Int. Symp. Digest Tech. Papers; 37, 2007, (2006).

[256] M. R. Krames, O. B. Shchekin, R. Mueller-Mach, G. O. Mueller, L. Zhou, G. Harbers, and M. G. Craford; "Status and Future of High-Power Light-Emitting Diodes for Solid-State Lighting"; IEEE J. Disp. Technol.; 3, 160, (2007).

[257] M. G. Craford, N. Holonyak, Jr., and F. A. Kish; "In pursuit of the ultimate lamp"; Sci. Am. (2001).

[258] M. R. Krames, O. B. Shchekin, R. Mueller-Mach, G. O. Mueller, L. Zhou, G. Harbers, and M. G. Craford; "High-brightness AlGaInN light-emitting diodes"; Proc. SPIE; 3938, 2, (2000).

[259] A. Y. Kim, W. Goetz, D. A. Steigerwald, J. J. Wierer, N. F. Gardner, J. Sun, S. A. Stockman, P. S. Martin, M. R. Krames, R. S. Kern, and F. M. Steranka;" Performance of High-Power AlInGaN Light Emitting Diodes Phys "; Status Solidi A; 188, 15, (2001).

[260] S. Nakamura and G. Fosol; "The Blue Laser Diodes"; (Springer, Berlin, 1998).

[261] I. A. Pope, P. M. Smowton, P. Blood, J. D. Thomson, M. J. Kappers, and C. J. Humphreys; "Carrier leakage in InGaN quantum well light-emitting diodes emitting at 480 nm"; Appl. Phys. Lett.; 82, 2755, (2003).

[262] I. V. Rozhansky and D. A. Zakheim; "Analysis of processes limiting quantum efficiency of AlGaInN LEDs at high pumping"; Phys. Status Solidi A; 204, 227, (2007).

[263] K. Okamoto, A. Kaneta, Y. Kawakami, S. Fujita, J. Choi, M. Terazima, and T. Mukai; "Confocal microphotoluminescence of InGaN-based light-emitting diodes"; J. Appl. Phys.; 98, 064503, (2005).

[264] S. F. Chichibu, A. Uedono, T. Onuma, B. A. Haskell, A. Chakraborty, T. Koyama, P. T. Fini, S. Keller, S. P. Denbaars, J. S. Speck, U. K. Mishra, S. Nakamura, S. Yamaguchi, S. Kamiyama, H. Amano, I. Akasaki, J. Han, and T. Sota; "Origin of defect-insensitive emission probability in In-containing (Al,In,Ga)N alloy semiconductors"; Nat. Mater. **5**, 810, (2006).

[265] S. F. Chichibu, T. Sota, K. Wada, and S. Nakamura; "Exciton localization in InGaN quantum well devices"; J. Vac. Sci. Technol. B; 16, 2204, (1998).

[266] A. R. Vasconcellos, R. Luzzi, C. G. Rodrigues, and V. N. Freire; "Hot-phonon bottleneck in the photoinjected plasma in GaN"; Appl. Phys. Lett.; **82**, 2455, (2003).

[267] Y. C. Shen, G. O. Mueller, S. Watanabe, N. F. Gardner, A. Munkholm, and M. R. Krames, "Auger recombination in InGaN measured by photoluminescence"; Appl. Phys. Lett.; **91**, 141101, (2007)

[268] H. Amano, Meijo University; Challenges facing ZnO and GaN: Facts and Myths, Virginia Crossing Resort October 18-19, 2007.

[269] C. A. Tran, SemiLEDs; Challenges facing ZnO and GaN: Facts and Myths, Virginia Crossing Resort October 18-19, 2007.

[270] Alexander Usikov, TDI; Challenges facing ZnO and GaN: Facts and Myths, Virginia Crossing Resort October 18-19, 2007.

[271] Heonsu Jeon, Seoul National University; Challenges facing ZnO and GaN: Facts and Myths, Virginia Crossing Resort October 18-19, 2007.

[272] Dong-Ho Kim, Chi-O Cho, Yeong-Geun Roh, Heonsu Jeon, and Yoon Soo Park; "Enhanced light extraction from GaN-based light-emitting diodes with holographically generated two-dimensional photonic crystal patterns"; Appl. Phys. Lett.; 87, 203508, (2005)

[273] Jae-Soong Lee, Joonhee Lee, Sunghwan Kim, and Heonsu Jeon; "GaN-based light-emitting diode structure with monolithically integrated sidewall deflectors for enhanced surface emission"; IEEE Photonics Technology Letters; **18**, 1588, (2006).

[274] M. R. Krames, O. B. Shchekin, R. Mueller-Mach, G. O. Mueller, L. Zhou, G. Harbers, and M. G. Craford; "Light-Emitting Diodes: Research, Manufacturing, and Applications IV"; Proc. SPIE; **3938**, 2, (2000).

[275] T. Mukai, M. Yamada, and S. Nakamura; "Characteristics of InGaN-Based UV/Blue/Green/Amber/Red Light-Emitting Diodes"; Jpn. J. Appl. Phys.; Part 1, **38**, 3976, (1999).

[276] G, Harbers and S. Bierhuizen; "Performance of High Power Light Emitting Diodes in Projection Applications"; Society for information display (SID) Int. Symp. Digest Tech. Papers; **37**, 2007 (2006).

[277] Michael R. Krames, Oleg B. Shchekin, Regina Mueller-Mach, Gerd O. Mueller, Ling Zhou, Gerard Harbers, and M. George Craford, "Status and Future of High-Power Light-Emitting Diodes for Solid-State Lighting", J. Display Technol, **3**, 160 (2007)

[278] I. A. Pope, P. M. Smowton, P. Blood, J. D. Thomson, M. J. Kappers, and C. J. Humphreys; "Carrier leakage in InGaN quantum well light-emitting diodes emitting at 480 nm"; Appl. Phys. Lett.; **82**, 2755, (2003).

[279] I. V. Rozhansky and D. A. Zakheim; "Analysis of processes limiting quantum efficiency of AlGaInN LEDs at high pumping"; Phys. Status Solidi A; **204**, 227, (2007).

[280] Min-Ho Kim, Martin F. Schubert, Qi Dai, Jong Kyu Kim, and E. Fred Schubert, Joachim Piprek and Yongjo Park; "Origin of efficiency droop in GaN-based light-emitting diodes"; Appl. Phys. Lett. **91**, 183507 (2007)

[281] N. F. Gardner, G. O. Müller, Y. C. Shen, G. Chen, S. Watanabe, W. Götz, and M. R. Krames; "Blue-emitting InGaN–GaN double-heterostructure light-emitting diodes reaching maximum quantum efficiency above 200 A/cm^2"; Appl. Phys. Lett.; 91, 243506, (2007)

[282] Y.-L. Li, Y.-R. Huang, and Y.-H. Lai; "Efficiency droop behaviors of InGaN/GaN multiple-quantum-well light-emitting diodes with varying quantum well thickness"; Appl. Phys. Lett.; **91**, 181113, (2007)

[283] J. Piprek; "Semiconductor Optoelectronic Devices: Introduction to Physics and Simulations"; Academic Press, San Diego, 2003.

[284] D.-J. Jang, G.-T. Lin, C.-L. Hsiao, and L. W. Tu and M.-E. Lee; "Auger recombination in InN thin films"; Appl. Phys. Lett; **92**, 042101, (2008)

[285] A. R. Beattie and P. T. Landsberg; "Auger Effect in Semiconductors"; *Proc. R. Soc. Lond. A.;* 249, 16, (1958)

[286] A. R. Beattie and P. T. Landsberg; "One-Dimensional Overlap Functions and Their Application to Auger Recombination in Semiconductors"; *Proc. R. Soc. Lond. A.;* 258, 486, (1960)

[287] P. T. Landsberg; "On detailed balance between Auger recombination and impact ionization in semiconductors"; *Proc. R. Soc. Lond. A.;* 331, 103, (1972)

[288] P. T. Landsberg and M. J. Adams; "Theory of donor-acceptor radiative and Auger recombination in simple semiconductors"; *Proc. R. Soc. Lond. A.;* 334, 523, (1973)

[289] W. Walukiewicz, "Intrinsic limitations to the doping of wide-gap semiconductors", Physica B Vol. **302-303**, 123–134 (2001).

[290] G. F. Neumark, Phys. Rev. Lett. Vol. **62**, 1800 (1989).

[291] D. J. Chadi, Phys. Rev. Lett. Vol. **72**, 534 (1994).

[292] S. B. Zhang, S.-H. Wei, and A. Zunger, Phys. Rev. Lett. Vol. **84**, 1232 (2000).

[293] T. Minami, H. Sato, H. Nanto, and S. Takata, Jpn. J. Appl. Phys. Vol. **24**, L781 (1985).

[294] S. B. Zhang, S.-H. Wei, and A. Zunger, J. Appl. Phys. Vol. **83**, 3192 (1998).

[295] D. B. Laks, C. G. Van de Walle, G. F. Neumark, and S. T. Pantelides, Appl. Phys. Lett. Vol. **63**, 1375 (1993).

[296] S. B. Zhang, S.-H. Wei, and A. Zunger, "A phenomenological model for systematization and prediction of doping limits in II-VI and I-III-VI2 compounds", J. Appl. Phys. **83**, 3192 (1998).

[297] S. B. Zhang, S.-H. Wei, and A. Zunger, "Overcoming doping bottlenecks in semiconductors and wide-gap materials", Physica B **273–274**, 976 (1999).

[298] A. Kvit and S. Oktyabrsky, "Defects in CdTe and Related Compounds" in "Encyclopedia of Materials: Science and Technology. Ed. by S. Mahajan, Elsevier (2001).

[299] C. G. Van de Walle, D. B. Laks, G. F. Neumark, and S. T. Pantelides, Phys. Rev. B Vol. **47**, 9425 (1993).

[300] T. Yamamoto and H. Katayama-Yoshida, "Solution using a codoping method to unipolarity for the fabrication of p-type ZnO", Jpn. J. Appl. Phys., Part 2 **38**, L166 (1999).

[301] J.I. Pankove, E.A. Miller and J. E. Berkeyheiser, RCA Rev., **32**, 383, (1971).

[302] J.I. Pankove and M.A. Lampert, Phys. Rev. Lett., **33**, 361, (1974);

[303] J.I. Pankove, IEEE Trans. Electron Devices, **22**, 721, (1975);

[304] J.I. Pankove, Phys. Rev. Lett., **34**, 809, (1975).

[305] J.I. Pankove and E.R. Levin, J. Appl. Phys., **46**, 1647, (1975).

[306] H.P. Maruska, W.C. Rhines and D.A. Stevenson, Mater. Res. Bull., **7**, 777, (1972).

[307] H.P. Maruska, D.A. Stevenson and J.I. Pankove, Appl. Phys. Lett., **22**, 303, (1973);

[308] H.P. Maruska and D.A. Stevenson, Solid State Electronics, **17**, 1171, (1974).

[309] A.N. Vasilishchev, L.N. Mikhailov, V.G. Sidorov, M.D. Shagalov and Yu.K. Shalabutov, Sov. Phys. Semicond., **9**, 1189, (1976).

[310] H. Amano, K. Hiramatsu, M. Kito, N. Sawaki and I. Akasaki, J. Cryst. Growth, **93**, 79, (1988).

[311] G. Jacob, R. Madar and J. Hallais, Mater. Res. Bull., **11**, 445, (1976).

[312] T. Kawabata, T. Matsuda and S. Koike, J. Appl. Phys., **56**, 2367, (1984).

[313] G. Jacob, M. Boulou and M. Furtado, J. Cryst. Growth, **42**, 136, (1977).

[314] G. Jacob, M. Boulou and D. Bois, J. Luminescence, **17**, 263, (1978).

[315] G. Jacob, M. Boulou, M. Furtado and D. Bois, J. Electron. Mater., **7**, 499, (1978).

[316] J.I. Pankove, IEEE Trans. Electron Devices, **22**, 721, (1975);

[317] J.I. Pankove, Phys. Rev. Lett., **34**, 809, (1975).

[318] A.N. Vasilishchev, L.N. Mikhailov, V.G. Sidorov, M.D. Shagalov and Yu.K. Shalabutov, Sov. Phys. Semicond., **9**, 1189, (1976).

[319] H. Amano, K. Hiramatsu, M. Kito, N. Sawaki and I. Akasaki, J. Cryst. Growth, **93**, 79, (1988).

[320] J I. Pankove, E.A. Miller and J.E. Berkeyheiser, J. Luminescence, **5**, 84, (1972).

[321] A. Shintani and S. Minagawa, J. Electrochem. Soc., **123**, 1725, (1976).

[322] Y. Ohki, Y. Toyoda, H. Kobayashi and I. Akasaki, Inst. Phys. Conf. Ser., **63**, 479, (1982).

[323] I. Akasaki, H. Amano, K. Hiramatsu and N. Sawaki, Inst. Phys. Conf. Ser., **91**, 633, (1988).

[324] A. Shintani and S. Minagawa, J. Appl. Phys., **48**, 1522, (1977).

[325] G. Jacob and D. Bois, Appl. Phys. Lett., **30**, 412, (1977).

[326] J.I. Pankove, E.A. Miller and J.E. Berkeyheiser, J. Luminescence, **6**, 54, (1973).

[327] J.I. Pankove and J.E. Berkeyheiser, Proc. IEEE, **60**, 1456, (1972).

[328] J.I. Pankove, RCA Rev., **34**, 336, (1973).

[329] J.I. Pankove and R.E. Norris, RCA Rev., **33**, 377, (1972).

[330] H.P. Maruska and J.J. Tietjen, Appl. Phys. Lett., 15, 327, (1969).

[331] T. Matsumoto, M. Sano and M. Aoki, Jpn. J. Appl. Phys., **13**, 373, (1974).

[332] E. Ejder and P.O. Fagerström, J. Phys. Chem. Solids, **36**, 289, (1975).

[333] A.S. Adonin, V.A. Evmenenko, L.N. Mikhailov and N.G. Ryabtsev, Inorg. Mater., **17**, 1187, (1982).

[334] J.J. Nickl, W. Jus and R. Bertinger, Mater. Res. Bull., **10**, 1097, (1975).

[335] L.A. Marasina, A.N. Pikhtin, I.G. Pichugin and A.V. Solomonov, Phys. Status Solidi A, **38**, 753, (1976).

[336] T. Sasaki and S. Zembutsu, J. Appl. Phys., **61**, 2533, (1987).

[337] V.G. Sidorov, M.D. Shagolov, Y.K. Shalabutov and I.G. Pichugin, Sov. Phys. Semicond., **11**, 94, (1977).

[338] B. Monemar, O. Lagerstedt and H. P. Gislason, J. Appl. Phys., **51**, 625, (1980).

[339] J.I. Pankove, E.A. Miller, D. Richman and J.E. Berkeyheiser, J. Luminescence, **4**, 63, (1971).

[340] K. Hiramatsu, H. Amano and I. Akasaki, J. Cryst. Growth, **99**, 375, (1990).

[341] U.V. Desnica, N.B. Urli and B. Etlinger, Phys. Rev. B, **15**, 4119, (1977).

[342] M. Ilegems and R. Dingle, J. Appl. Phys., **44**, 4234, (1973).

[343] R.K. Crouch, W.J. Debnam and A.L. Fripp, J. Mater. Sci., **13**, 2358, (1978).

[344] J.I. Pankove, J.E. Berkeyheiser and E.A. Miller, J. Appl. Phys., **45**, 1280, (1974).

[345] J.I. Pankove and J.E. Berkeyheiser, J. Appl. Phys., **45**, 3892, (1974).

[346] M. Boulou, G. Jacob and D. Bois, Rev. Phys. Appl., **13**, 555, (1978).

[347] M. Boulou, M. Furtado, G. Jacob and D. Bois, J. Luminescence, **18/19**, 767, (1979).

[348] L.A. Marasina, A.N. Pikhtin, I.G. Pichugin and A.V. Solomonov, Phys. Status Solidi A, **38**, 753, (1976).

[349] M. Ilegems, R. Dingle and R.A. Logan, J. Appl. Phys., **43**, 3797, (1972).

[350] J.I. Pankove and J.A. Hutchby, Appl. Phys. Lett., **24**, 281, (1974).

[351] P. Bergman, G. Ying, B. Monemar and P.O. Holtz, J. Appl. Phys., **61**, 4589, (1987).

[352] O. Lagerstedt and B. Monemar, Phys. Rev. B, **19**, 3064, (1979).

[353] H.P. Maruska, L.J. Anderson and D.A. Stevenson, J. Electrochem. Soc., **121**, 1202, (1974).

[354] M. Ilegems, J. Cryst. Growth, **13/14**, 360, (1972).

[355] J.I. Pankove, Europian Mater. Res. Soc. Symp. Proc., Strasbourg (1991)

[356] L.A. Marasina, A.N. Pikhtin, I.G. Pichugin and A.V. Solomonov, Phys. Status Solidi A, **38**, 753, (1976).

[357] H. Amano, I. Akasaki, T. Kozawa, K. Hiramatsu, N. Sawaki, K. Ikeda and Y. Ishii, "Electron beam effects on blue luminescence of zinc-doped GaN",J. Lumin., **40/41**, 121, (1988).

[358] H.G. Grimmeiss and B. Monemar, J. Appl. Phys., **41**, 4054, (1970).

[359] M. Sano and M. Aoki, Jpn. J. Appl. Phys., **15**, 1943, (1976).

[360] S.S. Liu, T.R. Cass and D.A. Stevenson, J. Electronic Mater., **6**, 237, (1977).

[361] I. Akasaki and H. Amano, Mater. Res. Soc. Fall Meeting, Boston, MA, 1991.

[362] I. Akasaki, H. Amano, M. Kitoh and K. Hiramatsu," Photoluminescence of Mg-doped p-type GaN and electroluminescence of GaN p-n junction LED", J. Luminescence, **48/49**, 666-670, (1991)

[363] S.S. Liu, T.R. Cass and D.A. Stevenson, J. Electronic Mater., **6**, 237, (1977).

[364] J.I. Pankove and J.A. Hutchby, J. Appl. Phys., **47**, 5387, (1976).

[365] S. Nakamura, M. Senoh, and T. Mukai, Jpn. J. Appl. Phys. Pt. 2 Vol. **30**, L1708 (1991).

[366] S. Nakamura, T. Mukai and M. Senoh, "High-power GaN P-N junction blue-light-emitting diodes", Jpn. J. Appl. Phys., **30**, L1998-L2001, (1991).

[367] E. Ejder and H. G. Grimmeiss, J. Appl. Phys., **5**, 275, (1974).

[368] O. Lagerstedt and B. Monemar, J. Appl. Phys., **45**, 2266, (1974).

[369] S. Strite, Jpn. J. Appl. Phys. Vol. 33, L699 (1994)

[370] J. W. Lee, S.J. Pearton, J.C. Zolper, and R. A. Stall, Appl. Phys. Lett. Vol. 68, 2102 (1996)

[371] J.I. Pankove, M.T. Duffy, E.A. Miller and J.E. Berkeyheiser, J. Luminescence, **8**, 89, (1973).

[372] A. Salvador, W. Kim, O. Aktas, A. Botchkarev, Z. Fan, H. Morkoç: Appl. Phys. Lett. Vol. 69, 2692 (1996)

[373] P. Boguslawski, E.L. Brigs. J. Bernholc: Appl. Phys. Lett. 69, 233 (1996)

[374] B. Monemar and O. Lagerstedt, J. Appl. Phys., **50**, 6480, (1979).

[375] R. D. Metcalfe, D. Wickenden and W.C. Clark, J. Luminescence, **16**, 405, (1978).

[376] T. Ogino and M. Aoki, Jpn. J. Appl. Phys., **18**, 1049, (1979).

[377] H. Amano, M. Kito, K. Hiramatsu and I. Akasaki, Jpn. "p-type conduction in Mg-doped GaN treated with low-energy electron beam irradiation (LEEBI)", Jpn. J. Appl. Phys., **28**, L2112, (1989).

[378] H. Amano, M. Kitoh, K. Hiramatsu and I. Akasaki, "UV and blue electroluminescence from Al/GaN:Mg/GaN LED treated with low-energy electron beam irradiation (LEEBI)", Inst. Phys. Conf. Ser., **106**, 725-730, (1990); H. Amano, M. Kitoh, K. Hiramatsu and I. Akasaki, "UV and blue electroluminescence from Al/GaN:Mg/GaN LED treated with low-energy electron beam irradiation (LEEBI)", Inst. Phys. Conf. Ser., **106**, 725-730, (1990).

[379] H. Amano, M. Kitoh, K. Hiramatsu and I. Akasaki, "Growth and luminescence properties of Mg-doped GaN prepared by MOVPE", *Journal of the Electrochemical Society*, v 137, n 5, May 1990, p 1639-41

[380] I. Akasaki and H. Amano, Mater. Res. Soc. Fall Meeting, Boston, MA, 1991.

[381] S. Nakamura, M. Senoh and T. Mukai, "Highly P-typed Mg-doped GaN films grown with GaN buffer layers", Jpn. J. Appl. Phys., **30**, L1708-L1711, (1991)

[382] S. Nakamura, T. Mukai, M. Senoh, and N. Iwasa, "Thermal annealing effects on p-type Mg-doped GaN films**",** *Japanese Journal of Applied Physics, Part 2 (Letters)*, v 31, n 2B, L139-42, 15 Feb. 1992.

[383] H. Obloh, K. H. Bachem, U. Kaufmann, M. Kunzer, M. Maier, A. Ramakrishnan, and P. Schlotter, "Self-compensation in Mg doped p-type GaN grown by MOCVD", J. Cryst. Growth, Vol. **195**, 270 (1998).

[384] J. A. Van Vechten, J. D. Zook, R. D. Horning, and B. Goldenberg, "Defeating Compensation in Wide Gap Semiconductors by Growing in H that is Removed by Low Temperature De-Ionizing Radiation", Jpn. J. Appl. Phys. Vol. 31, pp. 3662-3663, (1992)

[385] G. F. Neumark Rothschild, "Wide bandgap semiconductors having low bipolar resistivity and method of formation", US patent 5,252,499 issued on October 12, 1993

[386] J. Neugebauer, C. G. Van de Walle, "Hydrogen in GaN:Novel Aspects of a Common Impurity", Phys. Rev. Lett. **75**, 4452 (1995).

[387] C. G. Van de Walle, "Interaction of hydrogen with native defects in GaN", Phys. Rev.B **56**, R10020-R10023 (1997).

[388] Chris G. Van de Walle, and Jorg Neugebauer, "First-principles calculations for defects and impurities: Applications to III-nitrides", J. Appl. Phys., Vol. 95, No. 8, pp. 3851-3879, 15 April 2004

[389] J. Neugebauer and Chris G. Van de Walle, in *Hydrogen in Semiconductors II*, edited by N. H. Nickel, *Semiconductors and Semimetals* Vol. 61, Treatise editors R. K. Willardson and E. R. Weber , Academic Press, Boston, (1999), p. 479.

[390] P. W. Anderson, "Model for the Electronic Structure of Amorphous Semiconductors", Phy. Rev. Letts. Vol. 34. No. 15. pp.953-955, 4 April 1975.

[391] G. D. Watkins and J. R. Troxell, "Negative-U properties of Point Defects in Silicon", Phy. Rev. Lett., Vol. 44. No.9, pp. 593-596, 3 March 1980

[392] J. R. Troxell, and G. D. Watkins, "Interstitial boron in silicon: A negative U center", Phy. Rev. B, Vol. 22. No. 1, pp.921-931, July 15, 1980

[393] Y. Okamoto, M. Saito, A. Oshiyama, Jpn. J . Appl. Phys. Vol. 35, L807 (1996)

[394] W. Götz, N. M. Johnson, J. Walker, D. P. Bour, and R. A. Street, Appl. Phys. Lett. Vol. **68**, 667 (1996).

[395] O. Ambacher, H. Angerer, R. Dimitrov, W. Rieger, M. Stutzmann, G. Dollinger, and A. Bergmaier, Phys. Stat. Sol. (a) Vol. **159**, 105 (1997).

[396] J. P. Zhang, D.-Z. Sun, X.-L. Wang, M.-Y. Kong, Y.-P. Zeng, J. M. Li, and L. Y. Lin, "Hydrogen contaminant and its correlation with background electrons in GaN", Semicond. Sci. Technol. Vol. 14, 403 (1999).

[397] S. J. Pearton, in GaN and Related Materials, Vol. 2 of Optoelectronic Properties of Semiconductors and Superlattices, Ed. By M. O. Manasreh (Gordon and Breach, New York, 1997).

[398] Y. Kamiura, Y. Yamashita, and S. Nakamura, Physica B Vol. **273-274**, 54 (1999).

[399] W. Walukiewicz; "Defect formation and diffusion in heavily doped semiconductors"; Phys. Rev. B.; **50**, 5221, (1994).

[400] A. Janotti and C.G. Van de Walle; "Oxygen vacancies in ZnO"; Appl. Phys. Lett.; **87**, 122102, (2005).

[401] D. C. Look, J. W. Hemsky, and J. R. Sizelove, "Residual Native Shallow Donor in ZnO", Phys. Rev. Lett. **82**, 2552 (1999).

[402] C.G. Van de Walle; "Hydrogen as a Cause of Doping in Zinc Oxide"; Phys. Rev. Lett.; **85**, 1012, (2000).

[403] F. Tuomisto, V. Ranki, K. Saarinen, and D.C. Look; "Evidence of the Zn Vacancy Acting as the Dominant Acceptor in n-Type ZnO"; Phys. Rev. B.; **91,** 205502, (2003).

[404] Ü. Özgür, Ya. I. Alivov, C. Liu, A. Teke, M. A. Reshchikov, S. Doğan, V. Avrutin, S.-J. Cho, and H. Morkoç; "A comprehensive review of ZnO materials and devices"; J. Appl. Phys.; **98**, 041301, (2005).

[405] K. Vanheusden, C.H. Seager, W.L. Warren, D.R. Tallant, and J.A. Voight; "Correlation between photoluminescence and oxygen vacancies in ZnO phosphors"; Appl. Phys. Lett.; **68** 403-405, (1996).

[406] A. Kvit and S. Oktyabrsky; "Defects in CdTe and Related Compounds" in Encyclopedia of Materials: Science and Technology. Ed. by S. Mahajan, Elsevier (2001).

[407] T. M. Barnes, K. Olson, and C.A. Wolden; "On the formation and stability of p-type conductivity in nitrogen-doped zinc oxide"; Appl. Phys. Lett.; **86**, 112112, (2005).

[408] T. Yamamoto and H. Katayama-Yoshida; "Solution using a codoping method to unipolarity for the fabrication of p-type ZnO"; Jpn. J. Appl. Phys., Part 2; **38**, L166, (1999).

[409] K. Nakahara, H. Takasu, P. Fons, A. Yamada, K. Iwata, K. Matsubara, R. Hunger, and S. Niki; "Interactions between gallium and nitrogen dopants in ZnO films grown by radical-source molecular-beam epitaxy"; Appl. Phys. Lett.; **79**, 4139, (2001).

[410] S. J. Pearton, D. P. Norton, K. Ip, Y. W. Heo, and T. Steiner; "Recent advances in processing of ZnO"; J. Vac. Sci. Technol. B; **22,** 932, (2004).

[411] M. Keever, T.J. Drummond, H. Morkoç, K. Hess, B.G. Streetman, and M. Ludowise; "Hall-effect and mobility in heterojunction layers"; J. Appl. Phys. **53,** 1034, (1982).

[412] B. Claflin, D. C. Look, S. J. Park, and G. Cantwell; "Persistent n-type photoconductivity in p-type ZnO "; J. Crystal Growth **287**, 16, (2006).

[413] C. H. Park, S. B. Zhang, and S. H. Wei; "Origin of p-type doping difficulty in ZnO: The impurity perspective"; Phys. Rev. B; **66**, 073202, (2002).

[414] D. C. Look and B. Claflin; "High-quality, melt-grown ZnO single crystals"; Phys. Status Solidi B; **241**, 624, (2004).

[415] M. G. Wardle, J. P. Goss, and P. R. Briddon; "Theory of Li in ZnO: A limitation for Li-based p-type doping"; Phys. Rev. B, **71,** 155205, (2005).

[416] D. C. Look, D. C. Reynolds, C. W. Litton, R. L. Jones, D. B. Eason, and G. Cantwell; "Characterization of homoepitaxial p-type ZnO grown by molecular beam epitaxy"; Appl. Phys. Lett.; **81**, 1830, (2002).

[417] T. Yamamoto and H. Katayama-Yoshida; "Solution using a codoping method to unipolarity for the fabrication of p-type ZnO"; Jpn. J. Appl. Phys. Pt. 2; **38**, L166, (1999).

[418] L. G. Wang and A. Zunger; "Dilute nonisovalent (II-VI)-(III-V) semiconductor alloys: Monodoping, codoping, and cluster doping in ZnSe-GaAs"; Phys. Rev. Lett.; **90**, 256401, (2003).

[419] E.-C. Lee, Y.-S. Kim, Y.-G. Jin, and K.-J. Chang; "First-principles study of p-type doping and codoping in ZnO"; J. Korean Phys. Soc.; **39**, S23, (2001).

[420] M. Sanmyo, Y. Tomita, and K. Kobayashi; "Preparation of zinc oxide films containing Be and N atoms by radio frequency magnetron sputtering"; Thin Solid Films, **472**, 189, (2005).

[421] A. Tsukazaki, H. Saito, K. Tamura, M. Ohtani, H. Koinuma, M. Sumiya, S. Fuke. T. Fukumura, and M. Kawasaki; "Systematic examination of carrier polarity in composition spread ZnO thin films codoped with Ga and N"; Appl. Phys. Lett.; **81**, 235, (2002).

[422] K. Nakahara, H. Takasu, P. Fons, A. Yamada, K. Iwata, K Matsubara, R. Hunger, and S. Niki; "Growth of N-doped and Ga+N-codoped ZnO films by radical source molecular beam epitaxy"; J. Crystal Growth; **237-239**, 503, (2002).

[423] M. Sumiya, A. Tsukazaki, S. Fuke, A. Ohtomo, H. Koinuma, and M. Kawasaki; "SIMS analysis of ZnO films co-doped with N and Ga by temperature gradient pulsed laser deposition"; Appl. Surf. Sci.; **223**, 206, (2004).

[424] S. H. Lim, J. W. Kim, H. S. Kang, G. H. Kim, H. W. Chang, and S. Y. Lee; "Characterizations of phosphorus doped ZnO multi-layer thin films to control carrier concentration"; Superlattices and Microstructures; **38**, 377, (2005).

[425] C.-C. Lin, S.-Y. Chen, and S.-Y. Cheng; "Physical characteristics and photoluminescence properties of phosphorous-implanted ZnO thin films"; Appl. Surf. Sci.; **238**, 405, (2004).

[426] Y. W. Heo, Y. W. Kwon, Y. Li, S. J. Pearton, and D. P. Norton; "Properties of Phosphorus-Doped (Zn,Mg)O Thin Films and Device Structures"; J. Electron. Mater.; **34**, 409, (2005).

[427] F. Chen, Z. Ye, W. Xu, B. Zhao, L. Zhu, and J. Lv; "Fabrication of p-typeZnO thin films via MOCVD method by using phosphorus as dopant source"; J. Cryst. Growth; **281**, 458, (2005).

[428] V. Vaithianathan, B.-T. Lee, and S. S. Kim; "Pulsed-laser-deposited p-type ZnO films with phosphorus doping"; J. Appl. Phys.; **98**, 043519, (2005).

[429] D.-K. Hwang, H.-S. Kim, J.-H. Lim, J.-Y. Oh, J.-H. Yang, S.-J. Park, K.-K. Kim, D. C. Look, and Y. S. Park; "Study of the photoluminescence of phosphorus-doped p-type ZnO thin films grown by radio-frequency magnetron sputtering"; Appl. Phys. Lett.; **86**, 151917, (2005).

[430] S.-H. Kang, D.-K. Hwang, and S.-J. Park; "Low-resistance and highly transparent Ni/indium-tin oxide ohmic contacts to phosphorous-doped p-type ZnO"; Appl. Phys. Lett.; **86**, 211902, (2005).

[431] D. C. Look, G. M. Renlund, R. H. Burgener, II, and J. R. Sizelove; "As-doped p-type ZnO produced by an evaporation/sputtering process"; Appl. Phys. Lett.; **85**, 5269, (2004).

[432] V. Vaithianathan, B.-T. Lee, and S. S. Kim; "Preparation of As-doped p-type ZnO films using a Zn3As2 /ZnO target with pulsed laser deposition"; Appl. Phys. Lett.; **86**, 062101, (2005).

[433] U. Wahl, E. Rita, J. G. Correia, A. C. Marques, E. Alves, and J. C. Soares; "Direct Evidence for As as a Zn-Site Impurity in ZnO"; Phys. Rev. Lett.; **95**, 215503, (2005).

[434] T. S. Jeonga, M. S. Hana, J. H. Kima, C. J. Youna, Y. R. Ryub, H. W. White; "Crystallinity-damage recovery and optical property of As-implanted ZnO crystals by post-implantation annealing"; J. Cryst. Growth; **275**, 541, (2005).

[435] S.-J. So and C.-B. Park; "Diffusion of phosphorus and arsenic using ampoule-tube method on undoped ZnO thin films and electrical and optical properties of P-type ZnO thin films"; J. Cryst. Growth; **285**, 606, (2005).

[436] T. Aoki, Y. Shimizu, A. Miyake, A. Nakamura, Y. Nakanishi, and Y. Hatanaka; "p-Type ZnO Layer Formation by Excimer Laser Doping"; Phys. Stat. Sol. (b); **229**, 911, (2002).

[437] F. X. Xiu, Z. Yang, L. J. Mandalapu, D. T. Zhao, and J. L. Liu; "High-mobility Sb-doped p-type ZnO by molecular-beam epitaxy"; Appl. Phys. Lett.; **87**, 152101, (2005).

[438] F. X. Xiu, Z. Yang, L. J. Mandalapu, D. T. Zhao, and J. L. Liu; "Photoluminescence study of Sb-doped p-type ZnO films by molecular-beam epitaxy "; Appl. Phys. Lett.; **87**, 252102, (2005).

[439] Y. W. Heo, Y. W. Kwon, Y. Li, S. J. Pearton, and D. P. Norton; "P-type behavior in phosphorus-doped (Zn,Mg)O device structures"; Appl. Phys. Lett.; **84**, 3474, (2004).

[440] Y. J. Li, Y. W. Heo, Y. Kwon, K. Ip , S. J. Pearton, and D. P. Norton; "Transport properties of p-type phosphorus-doped (Zn,Mg)O grown by pulsed-laser deposition"; Appl. Phys. Lett.; **87**, 072101, (2005).

[441] D. P. Norton, M. Ivill, Y. Li, Y. W. Kwon, J. M. Erie, H. S. Kim, K. Ip, S. J. Pearton, Y. W. Heo, S. Kim, B. S. Kang, F. Ren, A. F. Hebard, and J. Kelly; "Charge carrier and spin doping in ZnO thin films"; Thin Solid Films; **496**, 160, (2006).

[442] S. Limpijumnong, S. B. Zhang, S.-H. Wei, and C. H. Park; "Doping by Large-Size-Mismatched Impurities: The Microscopic Origin of Arsenic or Antimony-Doped p-Type Zinc Oxide"; Phys. Rev. Lett.; **92**, 155504, (2004).

[443] Woo-Jin Lee, Joongoo Kang, K.J. Chang; "Electronic structure of phosphorus dopants in ZnO"; Physica B; **376,** 699, (2006).

[444] Y.R. Ryu, T.S. Lee, and H.M. White; "Properties of arsenic-doped p-type ZnO grown by hybrid beam deposition"; Appl. Phys. Lett.; **83**, 87, (2003).

[445] A. Dadgar, A. Krtschil, F. Bertram, S. Giemsch, T. Hempel, P. Veit, A. Diez, N. Oleynik, R. Clos, J. Christen, and A. Krost; "ZnO MOVPE growth: From local impurity incorporation towards p-type doping"; Superlattices Microstructures; **38**, 245, (2005).

[446] A. Krtschil, A. Dadgar, N. Oleynik, J. Bläsing, A. Diez, and A. Krost; "Local p-type conductivity in zinc oxide dual-doped with nitrogen and arsenic"; Appl. Phys. Lett.; **87**, 262105, (2005).

[447] A. Krtschil, A. Dadgar, A. Diez, and A. Krost; "Electrical characterization of defect states in local conductivity domains in ZnO:NAs layers"; J. Mat. Res.; **22,** 1775, (2007).

[448] J.-L. Zhao, X.M. Li, A. Krtschil, A. Krost, W.D. Yu, Y.-W. Zhang, Y.-F. Gu, and X.-D. Gao; "Study on anomalous high p-type conductivity in ZnO films on silicon substrate prepared by ultrasonic spray pyrolysis"; Appl. Phys. Lett.; **90**, 062118, (2007).

[449] S.-H. Wei; "Overcoming the doping bottleneck in semiconductors"; Computational Materials Science; **30**, 337, (2004)

[450] S.H. Wei, Challenges facing ZnO and GaN: Facts and Myths; Oct, 2007.

[451] S. Limpijumnong, X. Li, S.-H. Wei, and S. B. Zhang; "Substitutional diatomic molecules NO, NC, CO, N-2, and O-2: Their vibrational frequencies and effects on p doping of ZnO"; Appl. Phys. Lett.; **86**, 211910, (2005).

[452] . Y.F. Yan, S.B. Zhang, and S.T. Pantelides**; "**Control of doping by impurity chemical potentials: Predictions for p-type ZnO"; Phys. Rev. Lett.; **86**, 5723, (2001).

[453] J. Neugebauer and C. G. van de Walle; "Hydrogen in GaN – novel aspects of a common impurity"; Phys. Rev. Lett.; **75**, 4452, (1995).

[454] Y. Yan, S.B. Zhang, S.J. Pennycook, and S.T. Pantelides; "A theoretical study of p-type doping of ZnO: problems and solutions"; *Mater. Res. Soc. Symp. Proc.;* **666**, F2.6, (2001).

[455] Y. Yan, M. M. Al-Jassim, and S.-H. Wei; "Doping of ZnO by group-IB elements"; Appl. Phys. Lett.; **89**, 181912, (2006).

[456] J. Li, S.-H. Wei, S.-S. Li, and J.-B. Xia; "Design of shallow acceptors in ZnO: First-principles band-structure calculations"; Phys. Rev. B; **74**, 081201R, (2006).

[457] Y. Yan, J. Li, S.-H. Wei, and M. M. Al-Jassim; "Possible approach to overcome the doping asymmetry in wideband gap semiconductors"; Phys. Rev. Lett.; **98**, 135506, (2007).

[458] A. Kikuchi, R. Banai, K. Kishino, C.-M. Lee, and J.-I. Chyi; "AlN/GaN double-barrier resonant tunneling diodes grown by rf-plasma-assisted molecular-beam epitaxy"; Appl. Phys. Lett.; **81**, 1729, (2002).

[459] A. E. Belyaev, C. T. Foxon, S. V. Novikov, O. Makarovsky, L. Eaves, M. J. Kappers, and C. J. Humphreys; "Design, fabrication, and characterization of coupling-strength-controlled directional coupler based on two-dimensional photonic-crystal slab waveguides"; Appl. Phys. Lett.; **83**, 3626, (2003).

[460] C. T. Foxon, S. V. Novikov, A. E. Belyaev, L. X. Zhao, O. Makarovsky, D. J. Walker, L. Eaves, R. I. Dykeman, S. V. Danylyuk, S. A. Vitusevich, M. J. Kappers, J. S. Barnard, and C. J. Humphreys; "Current-voltage instabilities in GaN/AlGaN resonant tunnelling structures"; Phys. stat. sol. (c); **0**, 2389, (2003).

[461] A.E. Belyaeva, O. Makarovskya, D.J. Walkera, L. Eavesa, C.T. Foxona, S.V. Novikova; L.X. Zhaoa, R.I. Dykemanc, S.V. Danylyukd, S.A. Vitusevichd, M.J. Kapperse, J.S. Barnarde, and C.J. Humphreyse; "Resonance and current instabilities in AlN/GaN resonant tunnelling diodes"; Physica E; **21,** 752, (2004).

[462] K. Kishino, A. Kikuchi, H. Kanazawa, and T. Tachibana; "Intersubband transition in (GaN)m/(AlN)n superlattices in the wavelength range from 1.08 to 1.61 μm"; Appl. Phys. Lett.; **81**, 1234, (2002).

[463] I.Waki, C. Kumtornkittikul, Y. Shimogaki, and Y. Nakano; "Shortest intersubband transition wavelength (1.68 μm) achieved in AlN/GaN multiple quantum wells by metalorganic vapor phase epitaxy"; Appl. Phys. Lett.; **82**, 4465, (2003).

[464] K. Driscoll, A. Bhattacharyya, T. D. Moustakas, R. Paiella, L. Zhou and D. J. Smith; "Intersubband absorption in AlN/GaN/AlGaN coupled quantum wells"; Appl. Phys. Lett.; **91**, 141104, (2007).

[465] A. Vardi, N. Akopian, and G. Bahir, L. Doyennette, M. Tchernycheva, L. Nevou, and F. H. Julien, F. Guillot and E. Monroy; "Room temperature demonstration of GaN/AlN quantum dot intraband infrared photodetector at fiber-optics communication wavelength"; Appl. Phys. Lett.; **88**, 143101, (2006).

[466] Daniel Hofstetter, Esther Baumann, Fabrizio R. Giorgetta, Fabien Guillot, and Eva Monroy; "High frequency operation of a GaN/AlN based intersubband photodetector in the telecommunication wavelength range", SPIE Photonic West- Opto 07 GaN Material and Devices III, 19-24 January 2008 San Jose, CA. *Proceedings of SPIE - The International Society for Optical Engineering* V. ????? , *Gallium Nitride Materials and Devices III, art no ????? 2008* (in press).

[467] E. Baumann, F. R. Giorgetta,a_ and D. Hofstetter, H. Lu, X. Chen, W. J. Schaff, L. F. Eastman, S. Golka, W. Schrenk, and G. Strasser; "Intersubband photoconductivity at 1.6 μm using a strain-compensated AlN/GaN superlattice"; Appl. Phys. Lett.; **87**, 191102, (2005).

[468] M. Motyka and R. Kudrawiec, G. Cywiński, M. Siekacz, and C. Skierbiszewski, J. Misiewicz; "Energy difference between electron subbands in AlInN/GaInN quantum wells studied by contactless electroreflectance spectroscopy"; Appl. Phys. Lett.; **89**, 251908, (2006).

[469] S. N. Grinyaev and A. N. Razzhuvalov; "Resonant electron tunneling in GaN / $Ga_{1-x}Al_xN$ (0001) strained structures with spontaneous polarization and piezoeffect"; Phys. Solid State; **43**, 549, (2001).

470 S. Golka, C. Pflügl, W. Schrenk, and G. Strasser, C. Skierbiszewski, M. Siekacz, I. Grzegory, and S. Porowski; "Negative differential resistance in dislocation-free GaN/AlGaN double-barrier diodes grown on bulk GaN"; Appl. Phys. Lett.; **88**, 172106, (2006)

[471] V.I. Litvinov; "Challenges facing ZnO and GaN"; Facts and Myths, Oct, 2007.

[472] I. Gordion, A. Manasson, and V.I. Litvinov "Electrical Domains and Submillimeter Signal Generation in AlGaN/GaN Superlattices"; IEEE Trans. Electr. Devices; **53**, 1294, (2006);

[473] V. I. Litvinov, and A. Manasson; "Superlattice in an interminiband resonance ac field"; J. Appl. Phys.; **98**, 043505, (2005)

[474] V.I. Litvinov, and A. Manasson; "Large-signal negative dynamic conductivity and high-harmonic oscillations in a superlattice"; Phys.Rev. B; **70**, 195323, (2004).

[475] V.I. Litvinov, A. Manasson, and D. Pavlidis; "Short-period intrinsic Stark GaN/AlGaN superlattice as a Bloch oscillator"; Appl. Phys. Lett.; **85**, 600, (2004)

[476] Available online at: http://www.nd.edu/~gsnider/

[477] H. Wei and A. Zunger; "Calculated natural band offsets of all II–VI and III–V semiconductors: Chemical trends and the role of cation d orbitals"; Appl. Phys. Lett.; **72**, 2011, (1998).

[478] J.Xie, Ü. Özgür and H. Morkoç; *Challenges facing ZnO and GaN: Facts and Myths*; Oct, 2007.

[479] S. Golka, C. Pflügl, W. Schrenk, G. Strasser, C. Skierbiszewski, M. Siekacz, I. Grzegory, and S. Porowski; "Negative differential resistance in dislocation-free GaN/AlGaN double-barrier diodes grown on bulk GaN"; Appl. Phys. Lett.; **88**, 172106, (2006)

[480] J. Xie, Ph.D thesis, Chapter Three, Virginia Commonwealth University, (2007)

[481] E. Baumann, F. R. Giorgetta, D. Hofstetter, H. Wu, W. J. Schaff, L. F. Eastman, and L. Kirste; " Tunneling effects and intersubband absorption in AlN/GaN superlattices"; Appl. Phys. Lett.; **86**, 032110, (2005)

[482] Z. Wang, K. Reimann, M. Woerner, T. Elsaesser, D. Hofstetter, E. Baumann, F. R. Giorgetta, H. Wu, W. J. Schaff, and L. F. Eastman; "Ultrafast hole burning in intersubband absorption lines of GaN/AlN superlattices"; Appl. Phys. Lett.; **89**, 151103, (2006)

[483] F.R. Giorgetta, E. Baumann, F. Guillot, E. Monroy and D. Hofstetter; "High frequency (f=2.37 GHz) room temperature operation of 1.55 μm AlN/GaN-based intersubband detector"; Electronics Lett. **43**, 185, (2007).

[484] Y. Lu, N. W. Emanetoglu, and Y. Chen; "ZnO piezoelectric devices", in "Zinc Oxide Bulk, Thin Films and Nanostructures: Processing, Properties and Applications"; edited by Chennupati Jagadish and Stephen J. Pearton, ISBN: 0-0804-4722-8.

[485] P. C. Chang, Zh. Fan, Ch. J. Chien, D. Stichtenoth, C. Ronning, and J. G. Lu, "High-performance ZnO nanowire field effect transistors"; Appl. Phys. Lett.; **89**, 133113, (2006).

[486] W. Park, J. S. Kim, and G. C. Yi, M. H. Bae and H.-J. Le; "Fabrication and electrical characteristics of high-performance ZnO nanorod field-effect transistors"; Appl. Phys. Lett.; **85**, 5052, (2006).

[487] Zh. Fan and Jia G. Lu; "Electrical properties of ZnO nanowire field effect transistors characterized with scanning probes"; Appl. Phys. Lett.; **86**, 032111, (2005).

[488] P. Yang, H. Yan, S. Mao, R. Russo, J. Johnson, R. Saykally, N. Morris, J. Pham, R. He, and H.-J. Choi; "Controlled Growth of ZnO Nanowires and Their Optical Properties"; Advanced Functional Materials; **12**, 323, (2002).

[489] Q. Wan, Q. H. Li, Y. J. Chen, T. H. Wang, X. L. He, J. P. Li, and C. L. Lin; "Fabrication and ethanol sensing characteristics of ZnO nanowire gas sensors"; Appl. Phys. Lett.; **84**, 3654, (2004).

[490] C. H. Liu, J. A. Zapien, Y. Yao, X. M. Meng, C. S. Lee, S. S. Fan, Y. Lifshitz, and S. T. Lee; "High-Density, Ordered Ultraviolet Light-Emitting ZnO Nanowire Arrays"; Advanced Materials; **15**, 838, (2003).

[491] H. Kind, H. Yan, B. Messer, M. Law, and P. Yang; "Nanowire Ultraviolet Photodetectors and Optical Switches"; Advanced Materials **14**, 158, (2002).

[492] Y. Lu, presented at "Challenges facing ZnO and GaN: Facts and Myths", Virginia Crossing Resort October 18-19, 2007.

[493]J. Zhong, H. Chen, G. Saraf, Y. Lu, C. K. Choi, and J.J. Song; "Integrated ZnO nanotips on GaN light emitting diodes for enhanced emission efficiency"; Appl. Phys. Lett.; **90**, 203515, (2007).

[494] X. D. Wang, J. Zhou, J. H. Song, J. Liu, N. S. Xu, and Z. L. Wang; "Piezoelectric Field Effect Transistor and Nanoforce Sensor Based on a Single ZnO Nanowire"; Nano Letters; **6**, 2768, (2006).

[495] J. F.Wager; "Transparent electronics"; Science **300**, 1245, (2003).

[496] R. Hoffman; "ZnO thin-film transistors"; in **"**Zinc Oxide Bulk, Thin Films and Nanostructures: Processing, Properties and Applications", edited by Chennupati Jagadish and Stephen J. Pearton, ISBN: 0-0804-4722-8.

[497]R. L. Hoffman, B. J. Norris, and J. F. Wager; "ZnO-based transparent thin-film transistors"; Appl. Phys. Lett.; **82**, 733, (2003).

[498] H. Ohta and H. Hosono; "Transparent oxide optoelectronics"; Materials Today; **7**, 42, (2004).

[499] S. Masuda, K. Kitamura, Y. Okumura, and S. Miyatake; "Transparent thin film transistors using ZnO as an active channel layer and their electrical properties"; J. Appl. Phys.; **93**, 1624, (2003).

[500] P. F. Carcia, R. S. McLean, M. H. Reilly, and G. Nunes, Jr.; "Transparent ZnO thin-film transistor fabricated by rf magnetron sputtering"; Appl. Phys. Lett.; **82**, 1117, (2003).

[501] S. Sasa, M. Ozaki, K. Koike, M. Yano, and M. Inoue; "High-performance ZnO/ZnMgO field-effect transistors using a hetero-metal-insulator-semiconductor structure"; Appl. Phys. Lett.; **89**, 053502, (2006).

[502] Y. Ohya, T. Niwa, T. Ban, and Y. Takahashi; "Thin Film Transistor of ZnO Fabricated by Chemical Solution Deposition"; Jpn. J. Appl. Phys.; Part 1 **40**, 297, (2001).

[503] Y. Kwon, Y. Li, Y. W. Heo, M. Jones, P. H. Holloway, D. P. Norton, Z. V. Park, and S. Li; "Enhancement-mode thin-film field-effect transistor using phosphorus-doped (Zn,Mg)O channel"; Appl. Phys. Lett.; **84**, 2685, (2004).

[504] Y. W. Heo, L. C. Tien, Y. Kwon, D. P. Norton, S. J. Pearton, B. S. Kang, and F. Ren; "Depletion-mode ZnO nanowire field-effect transistor"; Appl. Phys. Lett.; **85**, 2274, (2004).

[505] S. J. Lim, S.-J. Kwon, H. Kim, and J.-S. Park; "High performance thin film transistor with low temperature atomic layer deposition nitrogen-doped ZnO"; Appl. Phys. Lett.; **91**, 183517, (2007).

[506] H.-C. Cheng, C.- F. Chen, and C.-Y. Tsay; "Transparent ZnO thin film transistor fabricated by sol-gel and chemical bath deposition combination method"; Appl. Phys. Lett.; **90**, 012113, (2007).

[507] Toshihiro Miyata, and Tadatsugu Minami; "Present status of transparent conducting oxide thin-film development for transparent electrode applications", Presented at SPIE Photonic West- Opto 07 GaN Material and Devices III, 19-24 January 2008 San Jose, CA.

[508] N. L. Dehuff, E. S. Kettenring, D. Hong, H. Q. Chiang, J. F. Wager, R. L. Hoffman, C.-H. Park, and D. A. Keszler; "Transparent thin-film transistors with zinc indium oxide channel layer"; J. Appl. Phys.; **97**, 064505, (2005).

[509] J.-I. Song, J.-S. Park, H. Kim, Y.-W. Heo, J.-H. Lee, and J.-J. Kim, and B. D. Choi; "Transparent amorphous indium zinc oxide thin-film transistors fabricated at room temperature"; Appl. Phys. Lett.; **90**, 022106, (2007).

[510] N. Ito, Y. Sato, P. K. Song, A. Kaijio, K. Inoue, and Y. Shigesato; "Electrical and optical properties of amorphous indium zinc oxide films"; Thin Solid Films; **496**, 99, (2006).

[511] H. Hosono; "Ionic amorphous oxide semiconductors: Material design, carrier transport, and device application"; J. Non-Crystalline Solids; **352**, 851, (2006).

[512] T. Minami; "Transparent conducting oxide semiconductors for transparent electrodes"; Semicond. Sci. Technol.; **20**, S35, (2005).

[513] H. Agura, A. Suzuki, T. Matsushita, T. Aoki, and M. Okuda; "Low resistivity transparent conducting Al-doped ZnO films prepared by pulsed laser deposition"; Thin Solid Films; **445**, 263, (2003).

[514] S.-M. Park, T. Ikegami, and K. Ebihara; "Effects of substrate temperature on the properties of Ga-doped ZnO by pulsed laser deposition"; Thin Solid Films; **513**, 90, (2006).

[515] A. Suzuki, T. Matsushita, T. Aoki, and Y. Yoneyama; "Pulsed laser deposition of transparent conducting indium tin oxide films in magnetic field perpendicular to plume"; Jpn. J. Appl. Phys.; **40**, L401, (2001).

[516] H. Kawazoe, M. Yasukawa, H. Hyodo, M. Kurita, H. Yanagi, and H. Hosono; "P-type electrical conduction in transparent thin films of $CuAlO_2$"; Nature; **389**, 939, (1997).

[517] A. Kudo, H. Yanagi, H. Hosono, and H. Kawazoe; "$SrCu_2O_2$: A p-type conductive oxide with wide band gap"; Appl. Phys. Lett.; **73**, 220, (1998).

[518] K. Nomura, H. Ohta, A. Takagi, T. Kamiya, M. Hirano, and H. Hosono; "Room-temperature fabrication of transparent flexible thin-film transistors using amorphous oxide semiconductors"; Nature; **432**, 488, (2004).

[519] N. Izyumskaya, Y.-I Alivov, H. Lee, Y. -S. Kang, S-J Cho, and Hadis Morkoç; "Multi-functional perovskite oxides and their applications: the case of PZT"; Critical Reviews in Solid State and Materials Sciences; **32**, 111, (2007).

[520] H. Wu, J. Liang, G. Jin, Y. Lao, and T. Xu; "Transparent Thin-Film Transistors Using ZnMgO as Dielectrics and Channel"; IEEE Transactions on Electron Devices; **54**, 2856, (2007).

[521] K. Nomura, H. Ohta, A. Takagi, T. Kamiya, M. Hirano, and H. Hosono; "Room temperature fabrication of transparent flexible thin-film transistors using amorphous oxide semiconductors"; Nature; **432**, 488, (2004).

[522] I.-D. Kim, Y.-W. Choi, and H. L. Tuller; "Low-voltage ZnO thin-film transistors with high-κ $Bi_{1.5}Zn_{1.0}Nb_{1.5}O_7$ gate insulator for transparent and flexible electronics"; Appl. Phys. Lett.; **87**, 043509, (2005).

[523] P.S. Cho, K.W. Kim, and J.H. Lee; "NO_2 sensing characteristics of ZnO nanorods prepared by hydrothermal method"; Journal of Electroceramics; **17**, 975, (2006).

[524] C. Baratto, G. Sberveglieri, A. Onischuk, B. Caruso, and S. Stasio; "Low temperature selective NO_2 sensors by nanostructured fibers of ZnO"; Sensors and Actuators B-Chemical; **100**, 261, (2004).

[525] G. S. Devi, V. B. Subrahmanyam, S. C. Gadkari, and S. K Gupta; "NH_3 gas sensing properties of nanocrystalline ZnO based thick films"; Analytica Chimica Acta; **568**, 41, (2006).

[526] H. Gong, J. Q. Hu, J.H. Wang, C.H. Ong, and F.R. Zhu; "Nano-crystalline Cu-doped ZnO thin film gas sensor for CO"; Sensors and Actuators B-Chemical; **115**, 247, (2006).

[527] C. S. Rout, A. R. Raju, A. Govindaraj, and C. N. R. Rao; "Hydrogen sensors based on ZnO nanoparticles"; Solid State Communications; **138**, 136, (2006).

[528] H. T Wang, B. S. Kang, F. Ren, L. C. Tien, P. W. Sadik, D. P. Norton, S. J. Pearton, and J. Lin; "Hydrogen-selective sensing at room temperature with ZnO nanorods"; Appl. Phys. Lett.; **86**, 243503, (2005).

[529] B. S. Kang, Y. W. Heo, L. C. Tien, D. P. Norton, F. Ren, B. P. Gila, and S. J. Pearton; "Hydrogen and ozone gas sensing using multiple ZnO nanorods"; Appl. Phys. A-Materials Science & Procedures; **80**, 1029, (2005).

[530] X. H. Wang, Y. F. Ding, J. Zhang, Z. Q. Zhu, S. Z. You, S. Q. Chen, and J. Z. Zhu; "Humidity sensitive properties of ZnO nanotetrapods investigated by a quartz crystal microbalance"; Sensors and Actuators B-Chemical; **115**, 421, (2006).

[531] S. Christoulakis, M. Suchea, E. Koudoumas, M. Katharakis, N. Katsarakis, and G. Kiriakidis; "Thickness influence on surface morphology and ozone sensing properties of nanostructured ZnO transparent thin films grown by PLD"; Appl. Surface Science; **252**, 5351, (2006).

[532] R. Martins, E. Fortunato, P. Nunes, I. Ferreira, A. Marques, M. Bender, N. Katsarakis, V. Cimalla, and G. Kiriakidis; "Zinc oxide as an ozone sensor"; J. Appl. Phys.; **96**, 1398, (2004).

[533] C. H. Wang, X. F. Chu, and M. W. Wu; "Detection of H_2S down to ppb levels at room temperature using sensors based on ZnO nanorods"; Sensors and Actuators B-Chemical; **113**, 320, (2006).

[534] T. F. Xue, J. F. Hu, H. W. Qin, Y. Zhou, K. An, L. Zhang, T. Han, Y. X. Li; "Sensing properties of the ZnO based composite oxide (Al,Sb)/ZnO to C_2H_5OH gas"; Rare Metal Materials and Engineering; **33**, 1006, (2004).

[535] Z. Fan and J. G. Lu, Appl. Phys. Lett **86**, 123510 (2005).

[536] J. S. Kim, W. I. Park, C.-H. Lee, and G.-C. Yi; "ZnO Nanorod Biosensor for Highly Sensitive Detection of Specific Protein Binding"; J. Korean Physical Society; **49**, 1635, (2006).

[537] P. D. Batista and M. Mulato; "ZnO extended-gate field-effect transistors as pH sensors"; Appl. Phys. Lett.; **87**, 143508, (2005).

[538] B. S. Kang, F. Ren, Y. W. Heo, L. C. Tien, D. P. Norton, and S. J. Pearton; "pH measurements with single ZnO nanorods integrated with a microchannel"; Appl. Phys.ics Lett.; **86**, 112105, (2005).

[539] O. Dulub, B. Meyer, and U. Diebold; "Observation of the Dynamical Change in a Water Monolayer Adsorbed on a ZnO Surface"; Phys. Rev. Lett.; **95**, 136101, (2005).

[540] S. M. Al-Hillia, M. Willander, A. Öst, and P. Strålfors; "ZnO nanorods as an intracellular sensor for pH measurements"; J. Appl. Phys.; **102**, 084304, (2007).

[541] S. M. Al-Hilli, R. T. Al-Mofarji, and M. Willander; "Zinc oxide nanorod for intracellular pH sensing"; Appl. Phys. Lett.; **89**, 173119, (2006).

[542] W. J. E. Beek, M. M. Wienk, and R. A. J. Janssen; "Efficient Hybrid Solar Cell from Zinc Oxide Nanoparticles and a Conjugated Polymer"; Advanced Materials; **16**, 1009, (2004).

[543] M. Law, L. Greene, J. C. Johnson, R. Saykally, and P. Yang; "Nanowire dye-sensitized solar cells"; Nature; **4**, 455, (2005).

[544] A. Du Pasquier, H. Chen, and Y. Lu; "Dye sensitized solar cells using well-aligned zinc oxide nanotip arrays"; Appl. Phys. Lett.; **89**, 253513, (2006).

[545] J. B. Baxter and E. S. Aydil; "Nanowire-based dye-sensitized solar cells"; Appl. Phys. Lett.; **86**, 053114, (2005).

[546] C. Y. Jiang, X. W. Sun, G. Q. Lo, D. L. Kwong, and J. X. Wang; "Improved dye-sensitized solar cells with a ZnO-nanoflower photoanode"; Appl. Phys. Lett.; **90**, 263501, (2007).

[547] J.Lu; *Challenges facing ZnO and GaN: Facts and Myths*; Oct, 2007.

[548] A. B. F. Martinson, J. E. McGarrah, M. O. K. Parpia, and J. T. Hupp, Phys. Chem. Chem. Phys. **8**, 4655 (2006).